Forced Symmetry-Breaking as a Mechanism for Bursting

by

Jeffrey Michael Moehlis

B.S. (Iowa State University) 1993

A dissertation submitted in partial satisfaction of the
requirements for the degree of
Doctor of Philosophy

in

Physics

in the

GRADUATE DIVISION
of the
UNIVERSITY of CALIFORNIA at BERKELEY

Committee in charge:

Professor Edgar Knobloch, Chair
Professor Jonathan Wurtele
Professor Oliver O'Reilly

Spring 2000

The dissertation of Jeffrey Michael Moehlis is approved:

Chair Date

Date

Date

University of California at Berkeley

Spring 2000

Forced Symmetry-Breaking as a Mechanism for Bursting

Copyright Spring 2000

by

Jeffrey Michael Moehlis

Abstract

Forced Symmetry-Breaking as a Mechanism for Bursting

by

Jeffrey Michael Moehlis

Doctor of Philosophy in Physics

University of California at Berkeley

Professor Edgar Knobloch, Chair

Forced symmetry-breaking, or the introduction of small perturbations that reduce the symmetry of a system, can be responsible for complex dynamics in a system that would otherwise behave in a regular manner. This observation is of particular interest because in real physical systems symmetries are rarely exact and symmetry-breaking imperfections must be assumed to be present. This dissertation shows that forced symmetry-breaking can lead to periodic or irregular bursts of very large dynamic range. The results are applied to relevant hydrodynamical systems.

First, a model of large aspect-ratio binary fluid convection which considers the competition between two nearly degenerate modes of opposite parity is studied. The model corresponds to a Hopf bifurcation with broken D_4 symmetry, where the "interchange" symmetry between the two modes is weakly broken because of the large but finite aspect-ratio. For open parameter regimes, it is shown that periodic or irregular bursting with very

large dynamic range may occur close to threshold. The bursts are found to be associated with global bifurcations involving fixed points and periodic orbits "at infinity". Global connections involving finite amplitude states are also present. The intricate sequence of bifurcations that take place is described in several cases, and the robustness of the results to small higher order terms in the amplitude equations is demonstrated.

Second, the effect of resonant temporal forcing on a system undergoing a Hopf bifurcation with D_4 symmetry is studied. The forcing breaks the continuous normal form symmetry of the amplitude equations. For the example which is considered, a type of gluing bifurcation (called a "supergluing bifurcation") is found and described. It is also shown that the attracting quasiperiodic solution which exists in the absence of forcing "wrinkles" into chaos as the amplitude of the forcing is increased, with the overall behavior governed by the approach of the attractor to solutions at infinity. Windows in which stable periodic solutions exist are also found and are associated with the traversal in parameter space through Arnol'd tongues. In addition, it is shown that bursts related to those found in the model of large aspect-ratio binary fluid convection may arise due to the forcing. Here the onset of bursting can be via an interior crisis or Type I intermittency.

Finally, other mechanisms that lead to behavior that has been called bursting are reviewed and compared to the new mechanism described in this dissertation.

Professor Edgar Knobloch
Dissertation Committee Chair

To my parents

and to my wife Allison

for all of their love and support.

Contents

List of Figures **vii**

List of Tables **xi**

1 Ordinary Differential Equation Models for Hydrodynamical Systems **1**
1.1 Equations of Hydrodynamics 3
1.2 An Example: Rayleigh-Bénard Convection 5
1.3 Derivation of Ordinary Differential Equation Models 10
1.4 Derivation of Ordinary Differential Equation Models by Symmetry Arguments 15

2 Dynamical Systems Theory and Bifurcation Theory **19**
2.1 Types of Solutions and the Calculation of their Stability 21
2.1.1 Fixed Points 22
2.1.2 Periodic Orbits 23
2.1.3 Quasiperiodic Orbits 25
2.1.4 Strange Attractor 25
2.2 Invariant Manifolds 29
2.3 Normal Forms 33
2.4 Local Bifurcations for Vector Fields 35
2.5 Bifurcations for Maps 40
2.6 Global Bifurcations 44
2.6.1 Planar Homoclinic Bifurcation 44
2.6.2 Homoclinic Explosion 45
2.6.3 Orbit Homoclinic to a Saddle-Focus: Shil'nikov Bifurcation 47
2.7 Bifurcations with Symmetry 50
2.7.1 The Hopf Bifurcation with O(2) Symmetry 52
2.7.2 The Hopf Bifurcation with D_4 Symmetry 55
2.8 Forced Symmetry-Breaking: A Preview 58

3 Bursts in a Model of Large Aspect-Ratio Binary Fluid Convection **61**
3.1 The Model 61
3.2 Basic Equations and their Symmetries 72

3.3 The Perfect System ($\Delta\lambda = \Delta\omega = 0$): The Hopf Bifurcation with D_4 Symmetry 75
3.4 Bursts in the Imperfect System ($\Delta\lambda \neq 0$, $\Delta\omega \neq 0$) 83
3.4.1 Burst Mechanism 83
3.4.2 Codimension One Heteroclinic Cycles Involving Infinite Amplitude Solutions 85
3.4.3 Numerical Studies of the Imperfect System 90
3.5 Robustness of Results 123
3.5.1 Symmetry-Breaking Parameters 123
3.5.2 Higher Order Terms 127
3.6 Concluding Remarks 132
3.6.1 Summary 132
3.6.2 An Alternative Model 134
3.6.3 Comparison with the Experiments 138

4 Wrinkled Tori and Bursts due to Resonant Temporal Forcing of the Hopf Bifurcation with D_4 Symmetry 139
4.1 Normal Forms For Nonautonomous Equations 140
4.2 Equations for the Hopf Bifurcation with D_4 Symmetry with Resonant Temporal Forcing 143
4.3 An Example 147
4.3.1 The Effect of Forcing on the w and v Solutions and the Supergluing Bifurcation 148
4.3.2 Attractors: Wrinkled Tori and Bursts 153
4.4 Concluding Remarks 160
4.4.1 Summary 160
4.4.2 Further Remarks on the Supergluing Bifurcation 165

5 Other Burst Mechanisms for Hydrodynamical Systems 168
5.1 Bursts in the Wall Region of a Turbulent Boundary Layer 169
5.2 Bursts in Shear Flows Undergoing Subcritical Transition to Turbulence . . 171
5.3 Heteroclinic Connections to Infinity 173
5.4 Bursts in the Kolmogorov Flow 175
5.5 Bursts in the Taylor-Couette System 178
5.6 Intermittency 181
5.6.1 Low-dimensional Intermittency 181
5.6.2 Crisis-induced Intermittency 182
5.6.3 Intermittency Involving an Invariant Manifold 183
5.7 Bursts in Neural Systems 184
5.8 Discussion 185

6 Conclusion 189

A Parameter Symmetries for the Hopf Bifurcation with D_4 Symmetry 198

B Heteroclinic Orbits in the Hopf Bifurcation with D_4 Symmetry 201

C Radial Stability of *ns* and *qp* Solutions for the Hopf Bifurcation with D_4 Symmetry **204**

D Proof that Heteroclinic Cycles Involving Infinite Amplitude Solutions are Traced Out in Finite Time **210**

E Perturbation of a Hopf Bifurcation by Resonant Temporal Forcing **215**
E.1 Local Bifurcations 216
E.2 Numerical Results 219
E.3 Codimension Two Bifurcations 221
E.3.1 Double Zero Bifurcations 223
E.3.2 Other Codimension Two Bifurcations 226
E.4 Relation to a Codimension Three Bifurcation 228

Index **231**

Bibliography **233**

List of Figures

1.1 Rayleigh-Bénard convection setup. 6
1.2 Neutral stability curve for Rayleigh-Bénard convection. 9
1.3 Chaotic behavior for the Lorenz equations. 12

2.1 The Poincaré map for a three-dimensional autonomous system. 24
2.2 The horseshoe map. 27
2.3 Center and stable manifolds for a fixed point. 30
2.4 Bifurcation diagrams for the (a) saddle-node, (b) transcritical, and (c) pitchfork bifurcations. 37
2.5 (a) Bifurcation diagram and (b) phase space portrait for the supercritical Hopf bifurcation. 38
2.6 Attractor for the logistic map. 41
2.7 (a) Stable and unstable periodic orbits on the invariant circle. (b) Arnol'd tongues. 42
2.8 Phase portraits and bifurcation diagram for a planar homoclinic bifurcation. 46
2.9 Example phase portraits for planar global bifurcations in the presence of Z_2 symmetry. 46
2.10 Two homoclinic orbits to the origin related by reflection symmetry in $\mathbb{R}^3$. . 47
2.11 The dependence of the unstable manifold of the origin on λ for a homoclinic orbit to a saddle-focus. 49
2.12 Bifurcation diagrams associated with a homoclinic orbit to a saddle-focus. . 49
2.13 Possible bifurcation diagrams for the Hopf bifurcation with O(2) symmetry. 56
2.14 Bifurcation diagrams associated with the universal unfolding of the supercritical pitchfork bifurcation. 59

3.1 Mechanism by which the Soret effect can lead to oscillations at the onset of convection for a binary fluid with negative separation ratio. 63
3.2 Critical Rayleigh number R_c versus separation ratio S (schematic). 64
3.3 Bursts in binary fluid convection experiments. 66
3.4 Onset of convection in ^{3}He/^{4}He mixtures ($P = 0.6$, $\tau = 0.03$) in large aspect-ratio containers. 68

3.5 The first even and odd temperature eigenfunctions when $P = 0.6$, $\tau = 0.03$, $\Gamma = 34.0$ and $S = -0.021$ in the form of a space-time plot. 71
3.6 Space-time plots showing the perturbation Ψ from the trivial state for fixed point solutions of the associated spherical system. 78
3.7 Distinct regions of parameter space with $B_R = -2.8$ and $C_R = -1$. 80
3.8 Possible bifurcation diagrams for $-3 < B_R < -1$, $C_R = -1$ showing radial stability for u, v, and w solutions. 82
3.9 All bifurcation diagrams for the perfect system with the connections B $\to$ A of the type required for the existence of heteroclinic cycles involving infinite amplitude solutions. 87
3.10 Invariant manifolds for the case that A is an infinite amplitude periodic orbit and B is an infinite amplitude fixed point. 89
3.11 Partial bifurcation diagram for Example 1(a). 95
3.12 Detailed bifurcation diagram for Example 1(a). 96
3.13 Stable periodic rotation. 97
3.14 The perturbation Ψ from the trivial state represented in a space-time plot showing (a) the periodic blinking state and (b) the periodic winking state. . 98
3.15 Stable periodic libration. 99
3.16 Heteroclinic cycles involving infinite amplitude solutions for Example 1(a). . 101
3.17 Bifurcation diagram showing global bifurcations involving the finite amplitude u/v fixed points. 102
3.18 The RS heteroclinic orbit connecting two κ_1-related u/v fixed points. 103
3.19 Eigenvalues of the u/v fixed points. 103
3.20 (a) Stable g^1 solution and (b) bifurcation diagram for the g^1 branch. 104
3.21 The two κ_1-related homoclinic orbits to the κ_1-related u/v fixed points. . . 104
3.22 Chaotic rotation. 106
3.23 Detail of the bifurcation diagram for Example 1(a). 107
3.24 (a) Two stable κ_1-related NRS w_e^2 solutions. (b) Stable NRS period 6 orbit and burst sequence. 109
3.25 (a,b) Two κ_1-related NRS strange attractors. These attractors merge in a symmetry-increasing bifurcation. (c) The resulting RS strange attractor. . . 109
3.26 Maps for the symmetry-increasing bifurcation. 110
3.27 Bifurcation diagram for Example 1(b). 112
3.28 Bifurcation diagram and approximate heteroclinic cycles involving infinite amplitude solutions for Example 1(b). 113
3.29 Bifurcation diagram for Example 2. 115
3.30 Heteroclinic cycles involving the infinite amplitude solutions for Example 2. 115
3.31 Bifurcation diagrams for (a) the u/v^1 and (b) the w_e^1 solution branches. (c,d) Two basic units of the heteroclinic network. 116
3.31 *Continued.* 117
3.31 *Continued.* 118
3.32 Sketches of several subsidiary heteroclinic cycles. 119
3.33 The eigenvalues of the u/v fixed points. 120
3.34 Bifurcation diagram for the s^1 solution branch, and related solutions. 121

3.35 Bifurcation diagram for Example 3. 122
3.36 Bifurcation diagram for Example 4. 123
3.37 Bifurcation diagrams showing robustness to changes in $\Delta\omega$. 125
3.38 The perturbation Ψ from the trivial state showing stable periodic solution for increasing $\Delta\omega$. The bursts fade away with increasing $\Delta\omega$ and are replaced by smaller amplitude, higher frequency states. 126
3.39 Bursts with large dynamic range at $\lambda = 15$ and $A = 1 - 1.5i$, $B = -2.8 + 5i$, $C = 1 + i$, $\Delta\lambda = 0.03$ and $\Delta\omega = 10$. 128
3.40 Bifurcation diagram for the parameters $A = 1 - 1.5i$, $B = -2.8 + 5i$, $C = 1 + i$, $\Delta\lambda = 0.03$, $\Delta\omega = -0.02$. 128
3.41 Stable chaotic states with successive visits to the vicinity of the same and/or different infinite amplitude states. 129
3.42 Bursts with extremely large dynamic range. 129
3.43 Robustness of the bursts to the addition of small fifth order terms. 131
3.44 Bifurcation diagrams showing robustness to the addition of small fifth order terms. 132
3.45 Possible schematic bifurcation diagrams for the O(2)-equivariant Hopf bifurcation (a) in the absence of symmetry-breaking, (b) with broken translation symmetry. 135
3.46 Space-time plots which provide an interpretation of the traveling-wave coordinates. 136
3.47 Phase portraits for the Hopf bifurcation with O(2) symmetry. 137

4.1 Bifurcation diagram and sketches of phase portraits for the dynamics in the two-dimensional invariant subspaces $z_+ = 0$ and $z_- = 0$. 149
4.2 At the supergluing bifurcation there are four symmetry-related orbits forming homoclinic connections to the trivial state. 150
4.3 Bifurcation diagrams showing the effect of forcing on the v and w periodic solutions. The supergluing bifurcation occurs at point SG. 152
4.4 Quasiperiodic solutions for (a) $f = 0$ and (b) $f = 0.5$. 154
4.5 Trajectory and time series for attractors for (a) $f = 0.8$, (b) $f = 0.91$, (c) $f = 0.98$, and (d) $f = 0.995$. As f increases, the attractors are being "dragged" toward the u_∞ solutions which are denoted by the dots. 155
4.6 Stable periodic solutions for (a) $f = 0.94$ and (b) $f = 0.968$. Notice that different periodic solutions may have different symmetry properties. 156
4.7 Poincaré maps constructed by intersecting the flow with the hyperplane $\psi = 10$ (from smaller to larger values) for (a) $f = 0$, (b) $f = 0.8$, (c,d) $f = 0.91$, (e) $f = 0.94$, (f) $f = 0.968$, (g) $f = 0.98$, (h) $f = 0.995$. 157
4.8 Bifurcation diagram showing the instantaneous value of ρ whenever the trajectory pierces the Poincaré section defined by $\psi = 10$ (from smaller to greater values) after the transients have died out. The attractor which is shown corresponds to adiabatically increasing the value of f from $f = 0$. . . 159
4.9 Symmetry-related stable, periodic J solutions for $f = 1$. 159

4.10 Poincaré maps constructed by intersecting the flow with the hyperplane $\psi = 10$ for (a) $f = 1.2$ showing the attracting quasiperiodic solution which lies on a torus, and (b) $f = 1.28$ showing the wrinkled torus. 161
4.11 Attractor for $f = 1.5$ giving bursts when the trajectory makes visits near the u_∞ solutions. 161
4.12 Poincaré maps constructed by intersecting the flow with the hyperplane $\psi = 10$ for (a) $f = 2.25$ showing the attracting quasiperiodic solution which lies on a torus, (b) $f = 2$ showing a stable periodic orbit, and (c) $f = 1.9$ showing how the torus has become wrinkled. 162
4.13 Attractors for (a) $f = 2.4283$ and (b) $f = 2.4284$. The onset of bursting as f increases through 2.42837 is via Type I intermittency. 163
4.14 Time series showing that bursts persist for (a) $f = 5$ and (b) $f = 10$. . . . 164

5.1 Sample bifurcation diagram for the interaction of an odd and even mode for the Kolmogorov flow. 177
5.2 Azimuthal component of vorticity in the laminar interpenetrating spiral state, just before a burst, and in the turbulent state. 179
5.3 The solid line shows the inner cylinder reduced Reynolds number ϵ_b for the onset of bursts obtained from data in [176]. The dashed line shows the estimate $\epsilon = \Gamma^{-2}$ near and below which the asymptotic bursting mechanism described in Chapter 3 is expected to apply. 181

6.1 Attractor for the Hopf bifurcation with D_4 symmetry with broken reflection symmetry κ_1. 192
6.2 Trajectory and time series for attractors when both the interchange symmetry κ_2 and the normal form symmetry are broken. 194

A.1 Parameter symmetries. 199

B.1 Region in parameter space with a heteroclinic orbit connecting symmetry-related v solutions when $B_R = C_R = -1$ for the Hopf bifurcation with exact D_4 symmetry. 203

C.1 Radial stability of ns and qp solutions. 205
C.2 The dependence of A_R^* on B_I for different fixed values of C_I. 207
C.3 Possible bifurcation diagrams for $-3 < B_R < -1$, $C_R = -1$, including ns and qp solutions in addition to u, v, and w solutions. 209

D.1 Heteroclinic cycle involving the A and B infinite amplitude fixed points. . . 211

E.1 Bifurcation sets for the perturbation of a Hopf bifurcation by resonant temporal forcing. 220
E.1 *Continued.* 221
E.2 Sketches of representative phase portraits for each region. 222
E.3 Sketches of representative phase portraits on the bifurcation sets which do not correspond to local bifurcations. 224

List of Tables

2.1 Symmetries of solutions for the Hopf bifurcation with O(2) symmetry. . . . 54
2.2 Fixed point solutions to equations (2.11,2.12). 55
2.3 Symmetries of solutions for the Hopf bifurcation with D_4 symmetry. 57

3.1 Fixed point solutions in the associated spherical system for the perfect system ($\Delta\lambda = \Delta\omega = 0$). 76
3.2 Eigenvalues for fixed point solutions of the three-dimensional system for the perfect problem. 79
3.3 Existence and angular stability properties of all solutions for $-3 < B_R < -1$ and $C_R = -1$. 81
3.4 Eigenvalues and Floquet multipliers for the infinite amplitude solutions involved in heteroclinic cycles for the examples of §3.4.3. 94
3.5 Maximum burst amplitude and time between bursts for stable periodic solutions. 124

5.1 The different mechanisms for bursting discussed in this dissertation. 188

B.1 Conditions for existence and stability of heteroclinic orbits in the associated spherical system connecting pairs of u, v and w fixed points. 202

E.1 Approximate numerical values at which codimension two bifurcations occur in Figure E.1. 223

Acknowledgements

It is a pleasure to thank Edgar Knobloch for the guidance he provided throughout the preparation of this work. His enthusiasm, deep insight, and generosity of ideas have had a great impact on me as a scientist, and are hopefully reflected in this dissertation. I also thank Professors Jonathan Wurtele and Oliver O'Reilly for their prompt and valuable comments on this dissertation.

I feel fortunate to have attended many interesting and challenging courses here at UC Berkeley. Courses (in roughly chronological order) by the following professors have been particularly useful: Allan Kaufman, Edgar Knobloch, Jerry Marsden, Eugene Commins, Philip Marcus, Eyvind Wichmann, Stephen Morris, Stanley Berger, Andrew Szeri, and Oliver O'Reilly.

Also, I thank my parents for their love, support, and encouragement. They are responsible for fostering a love of learning which I will always carry with me. Finally, I extend my deepest gratitude to my wife, Allison, who has made my last years of graduate school much more exciting and for whom my love knows no bound.

Chapter 1

Ordinary Differential Equation Models for Hydrodynamical Systems

Forced symmetry-breaking, or the introduction of perturbations that reduce the symmetry of a system, can be responsible for complex dynamics in a system that would otherwise behave in a regular manner. Effects of forced symmetry-breaking include the appearance of new solutions which have no analog in the fully symmetric system, and the introduction of global bifurcations which may be responsible for chaotic dynamics [1, 2, 3, 4, 5, 6]. From a physics perspective this observation is of particular interest. In physical systems symmetries are rarely exact and some symmetry-breaking imperfections must be assumed to be present. If these imperfections have a dramatic effect on the observed dynamics then studies of idealized symmetric systems may have little relevance to the real

world. However, the problem studied in this dissertation shows that even if this is the case, the symmetric system still holds the key for understanding the dynamics in the imperfect system. Specifically, this dissertation considers the effect of forced symmetry-breaking for the Hopf bifurcation in systems with square symmetry. New types of periodic and chaotic solutions are found to be associated with global bifurcations introduced by forced symmetry-breaking, including bursts of very large dynamic range. The results are applied to relevant hydrodynamical systems including binary fluid convection in a large aspect-ratio container.

The study of the effect of forced symmetry-breaking is undertaken by analyzing appropriate ordinary differential equation models. In this chapter, the derivation of such models is illustrated. First, the fluid flow equations are reviewed, with special attention paid to Rayleigh-Bénard convection. A linear stability analysis is performed for the simplest case of stress-free boundary conditions at the top and bottom of the convection cell. Then, in an attempt to understand nonlinear effects, a set of nonlinear ordinary differential equations (the Lorenz equations) is derived. It is pointed out that the chaotic behavior of the Lorenz equations is not relevant to the actual convection problem, and an asymptotically exact model which *is* relevant is derived. Finally, an identical model is derived using symmetry principles. The derivations of ordinary differential equation models for Rayleigh-Bénard convection are illustrative of general procedures for deriving ordinary differential equation models for hydrodynamical systems. Such models may then be analyzed using dynamical systems theory and bifurcation theory, as described in Chapter 2. In Chapter 3, a model for binary fluid convection in a large aspect-ratio container is derived using symmetry principles. The equations correspond to a Hopf bifurcation with broken square symmetry

(because of broken "interchange" symmetry between the two modes), and they are studied in detail using a forced symmetry-breaking perspective. In particular, it is shown that periodic and chaotic bursts of very large dynamic range can occur; the bursts are associated with heteroclinic cycles involving infinite amplitude solutions, and repeated bursts can occur because of the broken square symmetry of the equations. Chapter 4 shows that related bursts may arise due to resonant temporal forcing of a system undergoing a Hopf bifurcation with square symmetry. Chapter 5 reviews other burst mechanisms which have been proposed for hydrodynamical systems and compares them to the new mechanism presented in this dissertation. Finally, Chapter 6 discusses the results.

1.1 Equations of Hydrodynamics

The equations describing fluid flow are [7]

$$\frac{\partial \mathbf{u}}{\partial t} + (\mathbf{u} \cdot \nabla)\mathbf{u} = \frac{1}{\rho} \nabla \cdot \sigma + \mathbf{F}$$

$$\frac{\partial \rho}{\partial t} + \nabla \cdot (\rho \mathbf{u}) = 0,$$

$$\frac{\partial}{\partial t}\left(\frac{1}{2}u^2 + E\right) + (\mathbf{u} \cdot \nabla)\left(\frac{1}{2}u^2 + E\right) = -\frac{1}{\rho} \nabla \cdot \mathbf{q} + \frac{1}{\rho} \nabla \cdot (\sigma \cdot \mathbf{u}) + \mathbf{u} \cdot \mathbf{F},$$

where $\mathbf{u} = (u_1, u_2, u_3)$ is the fluid velocity, ρ is the fluid density, $\mathbf{F} = (F_1, F_2, F_3)$ is the external body force per unit mass, σ is the stress tensor, E is the internal energy per unit mass, and $\mathbf{q}$ is the heat flux vector. All of these quantities are functions of the spatial variable $\mathbf{x} = (x_1, x_2, x_3)$ and time t. σ is a second rank, symmetric tensor; the vector $\mathbf{n} \cdot \sigma$ has magnitude equal to stress (force per unit area) and points in the direction of the force across the plane with unit normal $\mathbf{n}$.

As given, the above fluid flow equations cannot be solved because there are more unknowns than equations. It is necessary to specify equations of state relating the density ρ and internal energy E to the pressure p and the temperature T, and also constitutive relations for $\mathbf{q}$ and σ. The Fourier heat conduction law gives

$$\mathbf{q} = -k_T \nabla T,$$

where k_T is the heat conductivity which is assumed to be a scalar (corresponding to an isotropic fluid). For Newtonian fluids, the components of the stress tensor are

$$\sigma_{ij} = -p\delta_{ij} + 2\mu e_{ij} + \lambda \delta_{ij} \nabla \cdot \mathbf{u},$$

where e is the rate of strain tensor with Cartesian components

$$e_{ij} \equiv \frac{1}{2}\left(\frac{\partial u_i}{\partial x_j} + \frac{\partial u_j}{\partial x_i}\right),$$

and μ and λ are the first and second coefficients of viscosity, respectively. Assuming equivalence between mechanical and thermodynamic pressure[1], $\lambda = -2\mu/3$. Then, the fluid flow equations become

$$\frac{\partial u_i}{\partial t} + u_j \frac{\partial u_i}{\partial x_j} = -\frac{1}{\rho}\frac{\partial p}{\partial x_i} + \frac{1}{\rho}\frac{\partial}{\partial x_j}\left\{2\mu\left(e_{ij} - \frac{1}{3}(\nabla \cdot \mathbf{u})\delta_{ij}\right)\right\} + F_i, \tag{1.1}$$

$$\frac{\partial \rho}{\partial t} + \nabla \cdot (\rho \mathbf{u}) = 0, \tag{1.2}$$

$$\rho\left(\frac{\partial E}{\partial t} + (\mathbf{u} \cdot \nabla)E\right) = -p\, \nabla \cdot \mathbf{u} + \Phi + \nabla \cdot (k \nabla T), \tag{1.3}$$

where

$$\Phi \equiv 2\mu\left(e_{ij}e_{ij} - \frac{1}{3}(\nabla \cdot \mathbf{u})^2\right)$$

[1] This is known as Stokes' assumption. It is supported by kinetic theory for monatomic gases, and is valid in practice for all Newtonian fluids [8].

is the rate of viscous dissipation. The usual summation over repeated indices is taken. Equation (1.1) is known as the Navier-Stokes equation; it is a nonlinear partial differential equation in $\mathbf{u}$, and its nonlinearity is responsible for much of the mathematical difficulty and physical complexity of fluid dynamics. Equations (1.1-1.3) together with appropriate equations of state are generally believed to describe the full range of phenomena for (Newtonian) fluids, from laminar to turbulent flow.

1.2 An Example: Rayleigh-Bénard Convection

As an example, consider Rayleigh-Bénard convection in which an unbounded layer of fluid is heated from below. The basic phenomenology of this system is as follows. For a given fluid and setup, if the temperature difference across the layer (ΔT) is below a critical value (ΔT_c), the fluid is motionless with heat transferred by conduction. This is called the conduction or trivial state. At $\Delta T = \Delta T_c$, the buoyancy forces overcome the stabilizing effects of thermal diffusion and viscous damping, and the motionless conduction state loses stability to a convecting state characterized by fluid motion. In the classic setup, for ΔT just above ΔT_c the fluid establishes a steady symmetric pattern of motion in which the rising hot plumes are arranged in parallel convection rolls or as a square or hexagonal pattern; the type of pattern which actually forms in an experiment depends upon the geometry and boundary conditions (top, bottom, and lateral) of the convection cell and the properties of the fluid. If ΔT is increased further, the motion becomes increasingly complex, ultimately displaying spatio-temporal chaos. Useful references on Rayleigh-Bénard convection include [9, 10, 11, 12, 13].

The first quantitative experiments in convection were done by Bénard [14]. He found that for a thin horizontal layer of melted spermaceti heated from below and with a free upper surface, convection could be established in a steady hexagonal pattern of flow cells. Rayleigh [15] modeled Bénard's experiments by considering the setup shown in Figure 1.1. A layer of viscous fluid is contained between rigid horizontal plates separated by a distance H, where the top and bottom plates are maintained at fixed temperatures T_1 and T_0, respectively. Gravity acts in the negative z-direction with acceleration g. Rayleigh considered fluids which satisfy the Boussinesq approximation [16]: the constitutive relation for the density is assumed to be

$$\rho = \rho_0[1 - \alpha(T - T_0)],$$

where ρ_0 is the density at $z = 0$, and α is called the coefficient of thermal expansion; however, this variation in density with temperature is neglected everywhere except in the "buoyancy" term of the resulting equations. Also, α and μ are assumed to be independent of temperature. The main conditions for the applicability of the Boussinesq approximation

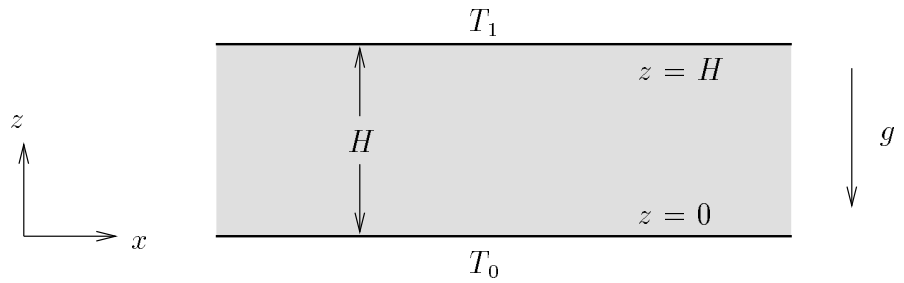

Figure 1.1: Rayleigh-Bénard convection setup.

are

$$U \ll c, \qquad H \ll H_\rho \equiv \left(\frac{1}{\rho}\,\frac{\partial \rho}{\partial z}\right)^{-1},$$

where U is a typical flow speed, c is the speed of sound in the fluid, and H_ρ is called the density scale height (see [17, 18, 19]). In particular, it is an appropriate approximation for many laboratory convection systems.

The conduction state is characterized by the lack of fluid motion and a linear vertical temperature profile:

$$\mathbf{u}_{cond} = 0, \qquad T_{cond} = T_0 - \frac{T_0 - T_1}{H}\, z.$$

Let $T = T_{cond} + \theta$, where θ is the departure from the conduction state temperature profile. Assuming two-dimensional motion, and nondimensionalizing spatial variables by H, time by H^2/κ, velocities by κ/H, and temperature by $T_0 - T_1$, equations (1.1-1.3) with the Boussinesq approximation become [10]

$$\frac{\partial\, \nabla^2 \psi}{\partial t} + \frac{\partial(\psi, \nabla^2 \psi)}{\partial(x,z)} = RP\frac{\partial \theta}{\partial x} + P\nabla^4 \psi, \tag{1.4}$$

$$\frac{\partial \theta}{\partial t} + \frac{\partial(\psi, \theta)}{\partial(x,z)} = \frac{\partial \psi}{\partial x} + \nabla^2 \theta. \tag{1.5}$$

Here ψ is the stream function defined so that for $\mathbf{u} \equiv u\hat{\mathbf{x}} + w\hat{\mathbf{z}}$,

$$u = -\frac{\partial \psi}{\partial z}, \qquad w = \frac{\partial \psi}{\partial x},$$

and

$$\frac{\partial(f,g)}{\partial(x,z)} \equiv \frac{\partial f}{\partial x}\frac{\partial g}{\partial z} - \frac{\partial f}{\partial z}\frac{\partial g}{\partial x}$$

is called the Jacobian of f and g. R and P are nondimensional parameters known as the Rayleigh number and the Prandtl number, respectively, and are defined as

$$R \equiv \frac{g\alpha(T_0 - T_1)H^3}{\kappa\nu}, \qquad P \equiv \frac{\nu}{\kappa}. \tag{1.6}$$

Finally, $\kappa = k/\rho_0 C_V$ is the thermal diffusivity where C_V is the specific heat of the fluid at constant volume, and $\nu = \mu/\rho_0$ is the coefficient of kinetic viscosity.

A complete specification of the problem also requires a choice of boundary conditions. Following Rayleigh, consider the case where the temperature is fixed and there is no tangential stress at the top and bottom plate. Then,

$$\psi = \frac{\partial^2 \psi}{\partial z^2} = \theta = 0 \qquad z = 0, 1. \tag{1.7}$$

Rayleigh performed a linear stability analysis of the conduction state $\theta = \psi = 0$. Such an analysis determines when the conduction state is unstable to the infinitesimal disturbances that are always present, even in the most carefully controlled experiment. Linearizing equations (1.4,1.5) about the conduction state,

$$\frac{\partial \nabla^2 \psi}{\partial t} = RP \frac{\partial \theta}{\partial x} + P \nabla^4 \psi, \tag{1.8}$$

$$\frac{\partial \theta}{\partial t} = \frac{\partial \psi}{\partial x} + \nabla^2 \theta. \tag{1.9}$$

Applying $(\frac{\partial}{\partial t} - \nabla^2)$ to (1.8) and using (1.9) implies that

$$\left(\frac{\partial}{\partial t} - \nabla^2 \right) \frac{\partial \nabla^2 \psi}{\partial t} = RP \frac{\partial^2 \psi}{\partial x^2} + P \left(\frac{\partial}{\partial t} - \nabla^2 \right) \nabla^4 \psi.$$

This equation subject to boundary conditions (1.7) is solved by separation of variables to give solutions of the form $\psi \sim e^{st} e^{ikx} \sin n\pi z$, where k is real, and $n = 1, 2, \cdots$. If $\mathrm{Re}(s) < 0$ for all values of k and n, the conduction state is linearly stable. If $\mathrm{Re}(s) > 0$ for some values of k and n, then such perturbations will grow in time, giving an instability of the conduction state. The condition $\mathrm{Re}(s) = 0$ corresponds to marginal stability. It is readily shown for this problem that marginal stability will only occur with $\mathrm{Im}(s) = 0$, and for given

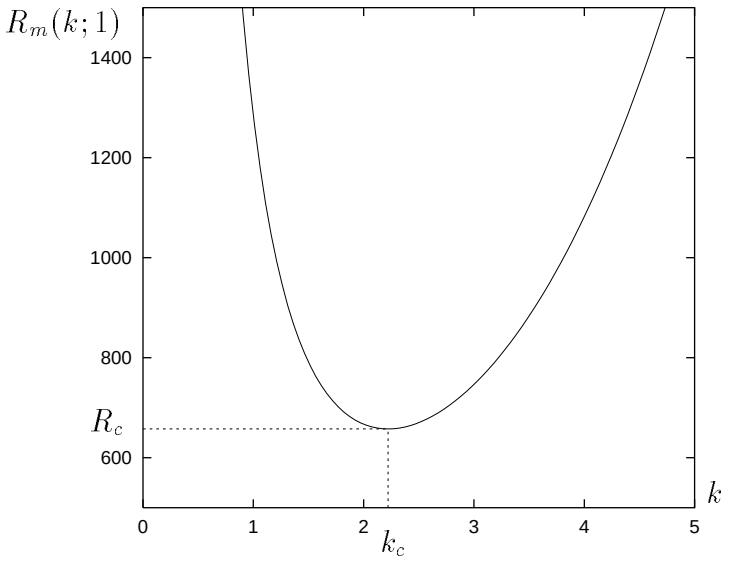

Figure 1.2: Neutral stability curve $R_m(k,1)$ for Rayleigh-Bénard convection. The conduction state is stable (unstable) for values of k and R below (above) the curve.

k and n occurs at Rayleigh number

$$R_m(k;n) \equiv \frac{(k^2+n^2\pi^2)^3}{k^2}.$$

For fixed k, R_m takes its smallest value for $n=1$. The neutral stability curve $R_m(k;1)$ is shown in Figure 1.2. The minimum of $R_m(k;1)$ is

$$(k_c, R_c) \equiv \left(\frac{\pi}{\sqrt{2}}, \frac{27\pi^4}{4}\right).$$

For $R < R_c$ the conduction state is stable to all infinitesimal disturbances. At $R = R_c$ the conduction state loses stability to a pattern with wavenumber k_c. If R is increased further, various types of secondary instabilities may occur [20, 21, 12]; the analysis of these secondary instabilities typically requires a partial differential equation model, and is outside the scope of this dissertation.

Ironically, it was shown experimentally [22] and theoretically [23] that for Bénard's experimental setup, convection was likely driven by the variation of surface tension with temperature rather than the thermal instability of the heavier fluid being on top of lighter fluid. However, Rayleigh's model is still applicable to a variety of convection systems, and convection in a horizontal layer of fluid heated from below is still typically called Rayleigh-Bénard convection. Convection driven by surface tension effects (often called Marangoni convection) has also been studied theoretically and experimentally (see [11] and references therein), although not in as much detail as Rayleigh-Bénard convection.

1.3 Derivation of Ordinary Differential Equation Models

The linearized equations considered by Rayleigh cannot give a full account of Rayleigh-Bénard convection. For example, they predict that for R just above R_c the perturbation to the conduction state will continue to grow exponentially without bound. This clearly cannot be the case. Eventually, the nonlinear terms which were excluded from the analysis will grow large enough that they cannot be ignored. In principle, one can solve the full partial differential equations (1.4,1.5) to determine how the linear stability analysis is modified by the presence of nonlinearity. However, the mathematical complexity of the full equations makes such analysis very difficult, and led Lorenz [24] to consider the following nonlinear ordinary differential equation model for Rayleigh-Bénard convection.

The Lorenz equations are important both for historical and instructive reasons. They are derived by a Galerkin truncation, that is, the variables that describe the state of the fluid are expanded in terms of a finite number of modes. Lorenz only included

the modes that are necessary for a consistent and nontrivial nonlinear model, as follows. Rayleigh's linear stability analysis predicts that the perturbation $\psi_R \sim \sin k_c x \sin \pi z$ will be unstable for R just above R_c. From (1.8), the corresponding temperature perturbation is $\theta_R \sim \cos k_c x \sin \pi z$. The nonlinear terms in equations (1.4,1.5) for these perturbations are

$$\frac{\partial(\psi_R, \nabla^2 \psi_R)}{\partial(x,z)} = 0, \qquad \frac{\partial(\psi_R, \theta_R)}{\partial(x,z)} \sim \sin 2\pi z.$$

Thus, for a consistent nonlinear model, the mode $\theta \sim \sin 2\pi z$ must also be included. Therefore, consider the Galerkin truncation[2]

$$\psi(x,z,t) = 3X(t) \sin k_c x \sin \pi z,$$

$$\theta(x,z,t) = \frac{27}{2\sqrt{2}} \frac{\pi^3}{R} Y(t) \cos k_c x \sin \pi z - \frac{1}{\pi R} Z(t) \sin 2\pi z.$$

Plugging this into (1.4), multiplying the resulting equation by $\sin k_c x \sin \pi z$, and integrating from $z = 0$ to $z = 1$ and from $x = 0$ to $x = 2\pi/k_c$ gives an ordinary differential equation for $X(t)$. Similarly, equations for $Y(t)$ and $Z(t)$ are obtained from (1.5). Specifically, one obtains the Lorenz equations

$$\begin{aligned} \dot{X} &= -PX + PY, \\ \dot{Y} &= -XZ + rX - Y, \\ \dot{Z} &= XY - bZ, \end{aligned} \tag{1.10}$$

where the dot refers to differentiation with respect to $3\pi^2 t/2$, $r \equiv R/R_c$, and $b = 8/3$. The nonlinearity of these equations comes ultimately from the nonlinearity of the hydrodynamical equations. When Lorenz numerically solved these equations, he found that "two states

[2]The coefficients of the modes are chosen to give agreement with the equations derived in [24], but otherwise have no significance.

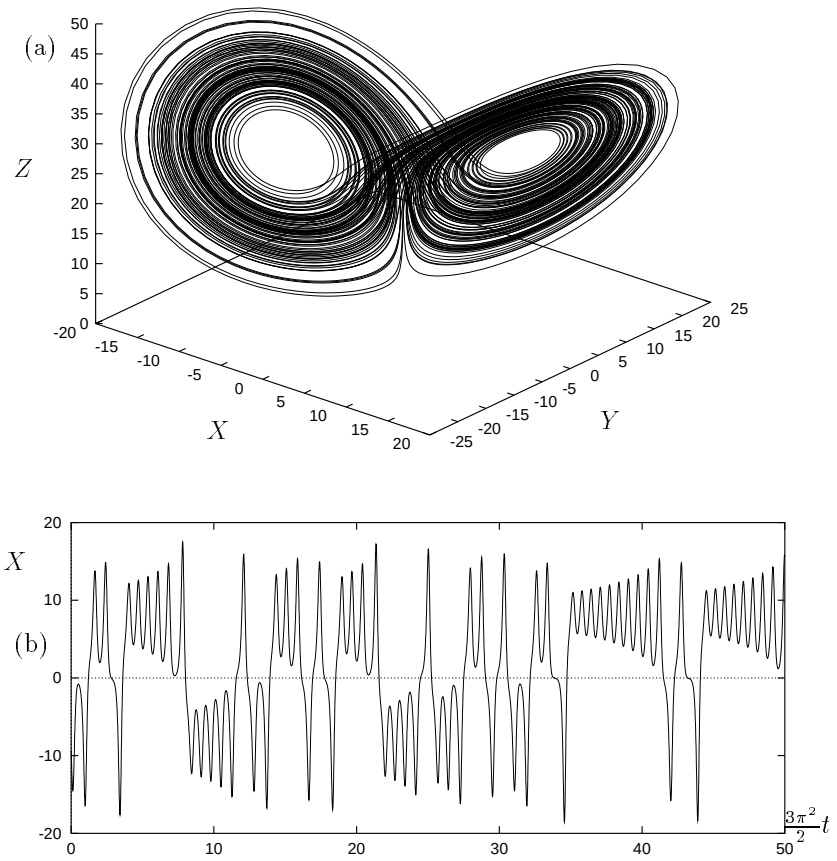

Figure 1.3: Chaotic behavior for the Lorenz equations for $R = 28, P = 10, b = 8/3$. (a) Lorenz attractor in the (X, Y, Z) phase space, and (b) time series for X.

differing by imperceptible amounts may eventually evolve into two considerably different states. If, then, there is any error whatever in observing the present state - and in any real system such errors seem inevitable - an acceptable prediction of an instantaneous state in the distant future may well be impossible" [24]. In today's language, for certain parameter values these equations exhibit chaotic solutions as shown in Figure 1.3 (see §2.1.4 for a precise definition of chaos). The Lorenz equations have now become probably the most widely studied system of nonlinear ordinary differential equations. It is therefore perhaps a disappointment that, except for $r \approx 1$ (see the discussion of the center manifold reduction in

§2.2), the Lorenz equations do not accurately describe Rayleigh-Bénard convection. In particular, more modes are necessary to adequately resolve the solution to equations (1.4,1.5) for the range of Rayleigh numbers for which the Lorenz equations predict chaos, and the chaotic behavior disappears as more modes are included in the truncation [25].[3] This is an important lesson: care must be used in order to derive ordinary differential equation models whose solutions are relevant to the solutions of the fluid flow equations.

For contrast, the model derived next describes the behavior of equations (1.4,1.5) exactly, provided R is asymptotically close to R_c. Suppose that the system is confined to a box of horizontal length $2\pi/k_c$ with stress-free and perfectly insulating lateral boundary conditions:

$$\psi = \frac{\partial^2 \psi}{\partial x^2} = \frac{\partial \theta}{\partial x} = 0, \qquad x = 0, \frac{2\pi}{k_c}. \tag{1.11}$$

Taking ∇^2 of equation (1.4) and subtracting RP times $\partial/\partial x$ of equation (1.5),

$$\frac{\partial}{\partial t}\left[\nabla^4 \psi - RP\frac{\partial \theta}{\partial x}\right] = P\nabla^6 \psi - RP\frac{\partial^2 \psi}{\partial x^2} - \nabla^2 \frac{\partial(\psi, \nabla^2 \psi)}{\partial(x,z)} + RP\frac{\partial}{\partial x}\frac{\partial(\psi,\theta)}{\partial(x,z)}. \tag{1.12}$$

Now, let

$$\begin{aligned} R &= R_c(1+\epsilon^2\gamma), \qquad \tau = \epsilon^2 t, \\ \psi &= \epsilon\psi_1 + \epsilon^2\psi_2 + \epsilon^3\psi_3 + \cdots, \\ \theta &= \epsilon\theta_1 + \epsilon^2\theta_2 + \epsilon^3\theta_3 + \cdots, \end{aligned}$$

where $\epsilon \ll 1$. At $\mathcal{O}(\epsilon)$, (1.12) becomes

$$\nabla^6 \psi_1 - R_c \frac{\partial^2 \psi_1}{\partial x^2} = 0$$

[3] The expansion used by [25] imposed symmetries which restricted the dynamics to an invariant subspace, thereby preventing some types of symmetry-breaking bifurcations. Later work by [26] corrected this, but while different results were obtained, chaos was still not found.

with solution $\psi_1 = A(\tau)\sin k_c x \sin \pi z$, where A is a real amplitude. Now, from (1.5) at $\mathcal{O}(\epsilon)$,

$$R_c \frac{\partial \theta_1}{\partial x} + \nabla^4 \psi_1 = 0,$$

so

$$\theta_1 = \frac{\sqrt{2}}{3\pi} A(\tau) \cos k_c x \sin \pi z.$$

With these expressions for ψ_1 and θ_1, equation (1.12) at $\mathcal{O}(\epsilon^2)$ gives

$$\nabla^6 \psi_2 - R_c \frac{\partial^2 \psi_2}{\partial x^2} = 0.$$

Without loss of generality, ψ_2 may be taken to be zero: it may be absorbed into ψ_1 which satisfied an equation of the same form. Equation (1.4) at $\mathcal{O}(\epsilon^2)$ implies that θ_2 is independent of x. Thus, from equation (1.5) at $\mathcal{O}(\epsilon^2)$,

$$\frac{\partial^2 \theta_2}{\partial z^2} = \frac{\partial \psi_1}{\partial x}\frac{\partial \theta_1}{\partial z} - \frac{\partial \psi_1}{\partial z}\frac{\partial \theta_1}{\partial x}$$

with solution

$$\theta_2 = -\frac{[A(\tau)]^2}{24\pi} \sin 2\pi z.$$

Finally, at $\mathcal{O}(\epsilon^3)$, equation (1.12) implies that

$$\nabla^6 \psi_3 - R_c \frac{\partial^2 \psi_3}{\partial x^2} = R_c \gamma \frac{\partial^2 \psi_1}{\partial x^2} - R_c \frac{\partial}{\partial x}\frac{\partial(\psi_1, \theta_2)}{\partial(x, z)} + \frac{1}{P}\frac{\partial}{\partial \tau}\left(\nabla^4 \psi_1 - R_c P \frac{\partial \theta_1}{\partial x}\right). \qquad (1.13)$$

It is not necessary to solve for ψ_3; instead, to maintain the asymptoticness of the expansion, a solvability condition is imposed (e.g. [27]). Here, the right hand side of (1.13) multiplied by $\sin k_c x \sin \pi z$ and integrated from $x = 0$ to $x = 2\pi/k_c$ and from $z = 0$ to $z = 1$ must vanish. Thus,

$$\frac{dA}{d\tau} = \frac{3\pi^2}{2}\,\frac{P}{1+P}\,\gamma A - \frac{\pi^2}{16}\,\frac{P}{1+P}\,A^3. \qquad (1.14)$$

This equation describes a supercritical pitchfork bifurcation at $\gamma = 0$ (see §2.4), and does not have chaotic solutions.[4] Notice that ψ_1, θ_1, and θ_2 have the same spatial form as the modes used by Lorenz; however, because of appropriate scaling, (1.14) gives an asymptotically correct description of Rayleigh-Bénard convection while the Lorenz equations do not.

Although chaos does not appear in the asymptotically exact equation for Rayleigh-Bénard convection, this does not mean that chaos is irrelevant to convection problems. Experimentally, chaotic behavior in Rayleigh-Bénard convection was first found by [28], and the first few bifurcations in the well-known period-doubling cascade to chaos (see §2.5) was observed, for example, by [29]. Also, numerical simulation of equations equivalent to (1.4,1.5) with the more realistic no-slip boundary conditions (zero velocity on all walls) instead of stress-free boundary conditions (as assumed by Lorenz) has shown the possibility of chaotic solutions [30, 31]. Finally, generalizations of two-dimensional Rayleigh-Bénard convection (for example, also imposing a horizontal magnetic field for an electrically conducting fluid) can have chaotic solutions near onset, as is confirmed both by asymptotically exact ordinary differential equation models and by numerical solution of the governing partial differential equations; this is nicely summarized in [32].

1.4 Derivation of Ordinary Differential Equation Models by Symmetry Arguments

Consider two-dimensional Rayleigh-Bénard convection with identical boundary conditions at rigid sidewalls $x = \pm\frac{L}{2}$. Equations (1.4,1.5) with these boundary conditions

[4] For N first-order autonomous ordinary differential equations for real variables, the existence of chaos requires $N \geq 3$. Equation (1.14) has $N = 1$.

have a reflection symmetry about $x = 0$; specifically, if $(\psi(x,z,t), \theta(x,z,t))$ is a solution, then so is $(-\psi(-x,z,t), \theta(-x,z,t))$. We suppose that there is a single primary mode with a zero eigenvalue at onset. Then, near onset the deviation of the temperature from pure conduction takes the form

$$\theta(x,z,t) = A(t)f(x,z) + \text{h.o.t.}$$

This primary mode will be either even or odd with respect to reflection about $x = 0$. If it is odd under reflection, i.e., $f(-x,z) = -f(x,z)$, then

$$\begin{aligned} \theta(-x,z,t) &= A(t)f(-x,z) + \text{h.o.t.} \\ &= -A(t)f(x,z) + \text{h.o.t} \end{aligned}$$

should also describe a solution. Thus, if $A(t)$ is a solution to the amplitude equation, $-A(t)$ should also be a solution. In other words,

$$\frac{dA}{dt} = f(A) \Rightarrow \frac{d(-A)}{dt} = f(-A).$$

In the Taylor expansion

$$f(A) = \sum_{j=1}^{\infty} a_j A^j,$$

it is therefore necessary that $(-1)^j = -1$, that is, that j is odd. Thus,

$$f(A) = h(A^2)A$$

for some function h. Truncating at cubic order,

$$\frac{dA}{dt} = a_1 A + a_3 A^3, \tag{1.15}$$

where a_1 and a_3 are real. Equation (1.15) has the same form as equation (1.14), and can be derived with much less effort. However, this approach has a major drawback, namely

that values of a_1 and a_3 (including the Prandtl number dependence) cannot be determined by symmetry arguments alone. In the absence of other symmetries, if the primary mode is even under reflection, i.e., $f(-x,z) = f(x,z)$, A will satisfy the equation

$$\frac{dA}{dt} = a_1 A + a_2 A^2 + \text{h.o.t.}$$

In general, the appropriate ordinary differential equation model for weakly nonlinear Rayleigh-Bénard convection depends somewhat subtly on the vertical and lateral boundary conditions and the parity properties of the neutral mode at onset; see [33, 34] for more details.

The derivation of equation (1.15) is an example of a general technique for deriving ordinary differential equation models using symmetry principles [35, 34]. Suppose that

$$\dot{\mathbf{v}} = f(\mathbf{v}; \lambda), \tag{1.16}$$

where $\mathbf{v} \in \mathbb{R}^n$ and $\lambda \in \mathbb{R}^m$ represent dependent variables and system parameters, respectively. Let G describe a linear group acting on the dependent variables.[5] We say that if

$$f(\gamma \mathbf{v}; \lambda) = \gamma f(\mathbf{v}; \lambda) \tag{1.17}$$

for all $\gamma \in G$, then (1.16) is *equivariant* with respect to the group G. This is equivalent to the statement that if $\mathbf{v}(t)$ is a solution to (1.16) then so is $\gamma\mathbf{v}(t)$ for all $\gamma \in G$.[6] For example, if a system is equivariant under left-right reflections and a right-moving wave exists as a solution, then a reflection-related left-moving wave will also exist as a solution.

There is a systematic way to derive amplitude equations (1.16) which are equiv-

[5] See [36] and [35] for the background on group theory necessary for this dissertation.

[6] Acting on equation (1.16) with γ gives $\gamma\dot{\mathbf{v}} = \gamma f(\mathbf{v}; \lambda)$. But $\gamma\dot{\mathbf{v}} = d(\gamma\mathbf{v})/dt$; also equivariance of f gives $\gamma f(\mathbf{v}; \lambda) = f(\gamma\mathbf{v}; \lambda)$. Thus, $d(\gamma\mathbf{v})/dt = f(\gamma\mathbf{v}; \lambda)$, so $\gamma\mathbf{v}$ is also a solution.

ariant with respect to G, as follows. An *invariant* function $g(\mathbf{v};\lambda)$ satisfies

$$g(\mathbf{v};\lambda) = g(\gamma\mathbf{v};\lambda) \tag{1.18}$$

for all $\gamma \in G$. For a given representation of a compact Lie group G, there exists a finite set of invariant polynomials $\mathcal{H}(G) \equiv \{u_1(\mathbf{v}), u_2(\mathbf{v}), \cdots, u_k(\mathbf{v})\}$ (called a Hilbert basis) such that any invariant polynomial may be expressed as a polynomial function of elements of $\mathcal{H}(G)$. Similarly, there is a finite set of equivariant vector field generators $\{f_1(\mathbf{v}), f_2(\mathbf{v}), \cdots, f_n(\mathbf{v})\}$ such that for the n invariant functions $\{g_1(\mathbf{v};\lambda), g_2(\mathbf{v};\lambda), \cdots, g_n(\mathbf{v};\lambda)\}$,

$$f(\mathbf{v};\lambda) = \sum_{j=1}^{n} g_j(\mathbf{v};\lambda) f_j(\mathbf{v}).$$

Depending on the group G, the actual computation of $\mathcal{H}(G)$ and the equivariant generators can be difficult, but they can be obtained by direct calculation (see the examples in [35]). Alternatively, a sophisticated method using Gröbner bases has been presented in Appendix A of [37]. For the Rayleigh-Bénard system considered above with Boussinesq symmetry, $G = Z_2$, $n = 1$, $\mathcal{H}(G) = \{A^2\}$, $g_1(A) = h(A^2)$, and $f_1(A) = A$.

In Chapter 3, a model for binary fluid convection in a large aspect-ratio container is derived using symmetry principles. The equations correspond to a Hopf bifurcation with weakly broken square symmetry, and the analysis of these equations will show that they allow the possibility of periodic or chaotic bursts of very large dynamic range. Chapter 4 shows that related bursts can occur due to resonant temporal forcing of a system undergoing a Hopf bifurcation with square symmetry.

Chapter 2

Dynamical Systems Theory and Bifurcation Theory

Having obtained ordinary differential equation models, for example by the methods described in Chapter 1, it is now possible to use the well-developed techniques of dynamical systems theory and bifurcation theory to study the behavior of such models. For our purposes, a dynamical system is defined by the system of differential equations

$$\dot{\mathbf{x}} \equiv \frac{d\mathbf{x}}{dt} = f(\mathbf{x}; \lambda), \tag{2.1}$$

where $\mathbf{x} = \mathbf{x}(t) \in \mathbb{R}^n$ is the state at time t, $\lambda \in \mathbb{R}^m$ describes system parameters, and $f : \mathbb{R}^n \times \mathbb{R}^m \to \mathbb{R}^n$ is a smooth function.[1] The vector field f generates a *flow* $\phi(\mathbf{x}, t)$ which satisfies (2.1) in the sense that

$$\frac{d}{dt}(\phi(\mathbf{x}, t))|_{t=\tau} = f(\phi(\mathbf{x}, \tau); \lambda).$$

[1] For n even, it is often convenient to associate f with an equivalent vector field $\tilde{f} : \mathbb{C}^{n/2} \times \mathbb{R}^m \to \mathbb{C}^{n/2}$. It will be apparent from the context how the vector field is defined.

For notational simplicity, the λ dependence of $\phi(\mathbf{x}, t)$ is suppressed. Equation (2.1) is called *autonomous* because the vector field f is independent of t. Note that the n-th order nonautonomous dynamical system $\dot{\mathbf{x}} = f(\mathbf{x}, t; \lambda)$ may be written as an $(n+1)$-th order autonomous system for $(\mathbf{x}, x_{n+1})$

$$\dot{\mathbf{x}} = f(\mathbf{x}, x_{n+1}; \lambda), \qquad \dot{x}_{n+1} = 1.$$

Fundamental results regarding existence and uniqueness of solutions of (2.1) can be found in [38, 39], and will be assumed in the following.

It is often of interest to study how the behavior of (2.1) depends on the parameters λ, which is the subject of bifurcation theory. The definition of a bifurcation point is as follows. The vector fields f and g are *topologically equivalent* if there exists a homeomorphism q such that for any t_1, there is a t_2 which preserves the sense but not necessarily the parametrization of time such that

$$q(\phi^f(\mathbf{x}, t_1)) = \phi^g(q(\mathbf{x}), t_2),$$

where ϕ^f is the flow for $\dot{\mathbf{x}} = f(\mathbf{x}; \lambda)$, and ϕ^g is the flow for $\dot{\mathbf{y}} = g(\mathbf{y}; \lambda)$. Recall that a homeomorphism q is an invertible map for which both q and q^{-1} are continuous. A vector field f on a compact manifold M is *structurally stable* if there exists an $\epsilon > 0$ such that f is topologically equivalent to all vector fields g on M which satisfy 1) f and g differ only on the compact set K, and 2) on K, f, g and their first derivatives differ by less than ϵ at each point. The parameter λ_0 is defined to be a *bifurcation value* if $f(\mathbf{x}; \lambda_0)$ is not structurally stable [40]. This definition is quite technical; it is typically sufficient to think of a bifurcation as a qualitative change in the behavior of a dynamical system as a system

parameter is varied. Examples of such qualitative changes include a change in the number and/or stability of fixed point solutions and the creation or destruction of a limit cycle, as discussed below.

Important results from dynamical systems theory and bifurcation theory are now discussed, with emphasis on those which will be useful for the remainder of the dissertation. More detail may be found, for example, in [40, 41, 42, 43, 44].

2.1 Types of Solutions and the Calculation of their Stability

Although transient behavior may be important for physical systems[2], we will typically be interested in attractors, which are states that the system can eventually settle down to. Precisely, the closed invariant set $A \in \mathbb{R}^n$ is called an *attractor* if the following two conditions hold [41]:

- A is an *attracting set*, that is, there is some neighborhood U of A such that for all $x \in U$ and all $t \geq 0$, $\phi(x,t) \in U$ and $\phi(x,t) \to A$ as $t \to \infty$. In words, A is an attracting set if all states near A stay near A and approach A under the evolution of the flow.

- A is *topologically transitive*, that is, for any two open sets $U, V \subset A$ there exists a $t \in \mathbb{R}$ such that $\phi(U,t) \cap V \neq \emptyset$. In words, A is topologically transitive if all points in A eventually come arbitrarily close to every other point in A under the evolution of the flow.

[2]Indeed, [45] points out that "everything we observe in nature is transient," even if a system is asymptotically approaching some state.

It is often difficult to rigorously prove that a solution to (2.1) is an attractor. This dissertation often makes use of the "numerical proof" that if numerically calculated stability properties of A are appropriate, or if the numerically calculated solution settles down to a set A as $t \to \infty$, then A is an attractor. Attractors cannot exist for Hamiltonian systems; they require the system to be dissipative. There are often coexisting attractors, each with its own basin of attraction. Despite the primary focus on attractors, it should be noted that solutions which are not attractors may be important in order to understand the origins of certain types of interesting behavior, including many global bifurcations.

For our purposes, the important classes of solutions to equation (2.1) are fixed points, periodic orbits, quasiperiodic orbits, and strange attractors.

2.1.1 Fixed Points

A *fixed point* $\mathbf{x_f}$ of (2.1) satisfies $f(\mathbf{x_f}; \lambda) = 0$. Thus, if the state starts at $\mathbf{x_f}$, it will remain at $\mathbf{x_f}$ forever. There are two important definitions for stability of a fixed point:

- $\mathbf{x_f}$ is *Liapunov stable* if for all $\epsilon > 0$ there exists a $\delta(\epsilon) > 0$ such that if $|\mathbf{x} - \mathbf{y}| < \delta$, then $|\phi(\mathbf{x}, t) - \phi(\mathbf{y}, t)| < \epsilon$. In words, $\mathbf{x_f}$ is Liapunov stable if solutions starting close to it remain close to it for all time.

- $\mathbf{x_f}$ is said to be *asymptotically stable* if it is Liapunov stable and there exists a constant $b > 0$ such that if $|\mathbf{x} - \mathbf{y}| < b$, then $|\phi(\mathbf{x}, t) - \phi(\mathbf{y}, t)| \to 0$ as $t \to \infty$. In words, $\mathbf{x_f}$ is asymptotically stable if solutions starting close to it tend to it under the evolution of the flow.

The concept of asymptotic stability is more useful for the problems considered in this dissertation, and "stable" will be used to mean "asymptotically stable" throughout. If $\mathbf{x_f}$ is not stable, it is called *unstable*. If the fixed point $\mathbf{x_f}$ is stable, then it is an attractor.

In practice, the stability of a fixed point $\mathbf{x_f}$ is determined by the linearization of equation (2.1) about $\mathbf{x_f}$ given by

$$\dot{\xi} = \mathrm{D}f(\mathbf{x_f}; \lambda)\xi,$$

where $\mathrm{D}f$ is the Jacobian matrix with elements

$$(\mathrm{D}f)_{ij} = \frac{\partial f_i}{\partial x_j}.$$

If all eigenvalues of $\mathrm{D}f$ have negative real parts, then $\mathbf{x_f}$ is stable. If any eigenvalues of $\mathrm{D}f$ have positive real part, then $\mathbf{x_f}$ is unstable.

2.1.2 Periodic Orbits

A *periodic orbit* is a solution for which there exists a T with $0 < T < \infty$ such that $\mathbf{x}(t) = \mathbf{x}(t+T)$ for all t. The period of the orbit is defined to be the minimum such T. A periodic orbit is also called a *limit cycle* if it is isolated in the sense that there exists a neighborhood of the periodic orbit that contains no other periodic orbit.

The stability of a periodic orbit is calculated by considering the *Poincaré map* which replaces the flow of the n-th order continuous time dynamical system with an $(n-1)$-th order discrete time dynamical system. Specifically, an $(n-1)$-dimensional *surface of section* Σ is chosen such that the flow under f is always transverse to Σ (see Figure 2.1). Let the successive intersections in a given direction of the solution $\mathbf{x}(t)$ with Σ be denoted by $\mathbf{x_i}$.

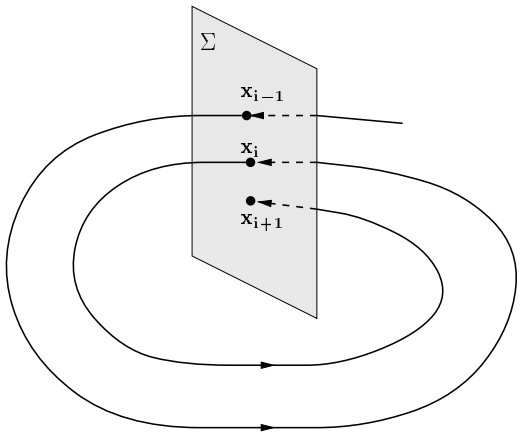

Figure 2.1: The Poincaré map for a three-dimensional autonomous system.

The Poincaré map

$$\mathbf{x_{i+1}} = g(\mathbf{x_i}; \lambda) \tag{2.2}$$

determines the $(i+1)$-st intersection of the trajectory with Σ from the i-th intersection. A periodic orbit of (2.1) corresponds to a fixed point $\mathbf{x_f}$ of (2.2) characterized by $g(\mathbf{x_f}; \lambda) = \mathbf{x_f}$. The linearization of (2.2) about $\mathbf{x_f}$ is

$$\xi_{i+1} = \mathrm{D}g(\mathbf{x_f}; \lambda)\xi.$$

If all eigenvalues of $\mathrm{D}g$ have modulus less than unity, then $\mathbf{x_f}$ (and thus the corresponding periodic orbit) is stable. If any eigenvalues of $\mathrm{D}g$ have modulus greater than unity, then $\mathbf{x_f}$ (and thus the corresponding periodic orbit) is unstable. If $\mathbf{x_f}$ is stable then it is an attractor of (2.2) and the corresponding periodic orbit is an attractor of (2.1).

An alternative way to determine the stability of a periodic orbit is to use Floquet theory. It can be shown that the $(n-1)$ eigenvalues of $\mathrm{D}g$ are equal to the $(n-1)$

nontrivial Floquet multipliers of the periodic orbit; the remaining Floquet multiplier is equal to unity and corresponds to perturbations along the periodic orbit [40]. The determination of Floquet multipliers or the eigenvalues of Dg typically must be done numerically.

2.1.3 Quasiperiodic Orbits

A *quasiperiodic orbit* is a solution which can be written as

$$\phi(\mathbf{x}, t) = g(\omega_1 t, \omega_2 t, \cdots, \omega_p t),$$

where p is finite, g is periodic with period 1 in each of its arguments, and all of the frequencies ω_i are rationally independent. Such a solution defines an p-torus. For dynamical systems (2.1) with phase-shift symmetry,[3] it is possible to remove one frequency from a quasiperiodic orbit by transformation of variables. Thus, a two-frequency quasiperiodic orbit in the original variables will be a periodic orbit in the new variables, and Floquet multipliers may be calculated numerically to determine stability. A stable periodic orbit in the new variables corresponds to the quasiperiodic orbit being an attractor in the original variables. This method of determining the stability of quasiperiodic orbits will be used extensively in Chapter 3.

2.1.4 Strange Attractor

In order to define a strange attractor, it is first necessary to define what is meant by chaos. A compact set Λ which is invariant under the flow $\phi(\mathbf{x}, t)$ is said to be *chaotic* if the following two conditions hold [41]:

[3] The phase-shift symmetry might arise from the normal form symmetry (see §2.3).

- $\phi(\mathbf{x}, t)$ has *sensitive dependence on initial conditions* on Λ, that is, there exists $\epsilon > 0$ such that for any $\mathbf{x} \in \Lambda$ and any neighborhood U of $\mathbf{x}$, there exists $\mathbf{y} \in U$ and $t > 0$ such that $|\phi(\mathbf{x}, t) - \phi(\mathbf{y}, t)| > \epsilon$. In words, solutions which are close to each other at a given time will eventually diverge from each other.

- Λ is topologically transitive under the flow $\phi(\mathbf{x}, t)$. The meaning of this was given in the definition of an attractor.

The additional condition that periodic orbits of $\phi(\mathbf{x}, t)$ are dense in Λ is sometimes added to the definition of "chaotic" (e.g. [46]), but will not be done so here. For N first-order autonomous ordinary differential equations for real variables, the existence of chaos requires $N \geq 3$. An analogous definition of chaos for maps is taken, where the continuous flow ϕ is replaced by successive iterations of the map. For invertible maps (such as the Poincaré map), the existence of chaos requires that the map be at least two-dimensional. It is possible to have chaos for noninvertible one-dimensional maps.

The "prototypical map possessing a chaotic invariant set" [41] is the horseshoe map introduced by S. Smale [47]. Given its importance, a brief discussion is included here. The horseshoe map M_h stretches and folds the unit square (see Figure 2.2). Under repeated iteration of the map, almost every initial condition eventually leaves the square; there is no attractor. Let Λ be the invariant set of points which never leave the square:

$$\Lambda = \cap_{n=-\infty}^{\infty} = M_h^n(S).$$

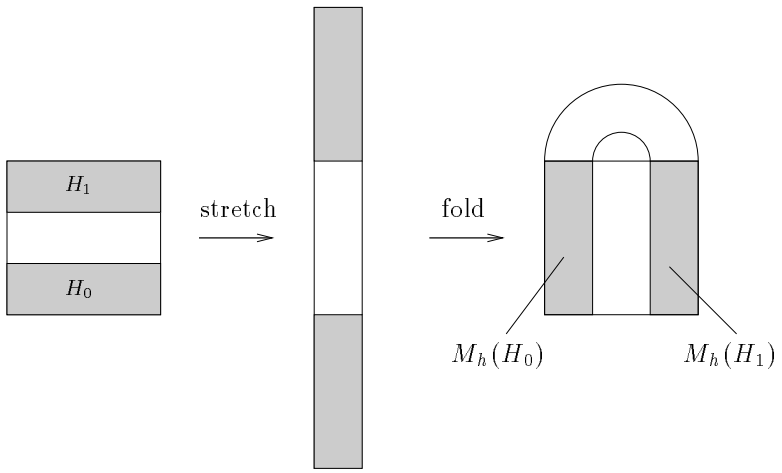

Figure 2.2: The horseshoe map first uniformly stretches the unit square vertically by a factor greater than two and uniformly compresses it horizontally by a factor less than two. Then, the long strip is folded into a horseshoe shape, with all of the bending occurring in the unshaded region. The horseshoe shape is placed on top of the original square.

Λ is a Cantor set, that is, it is a set which is closed, perfect (every point is a limit point), and is totally disconnected. A point $x \in \Lambda$ can be specified by a bi-infinite symbol sequence

$$a = \cdots a_{-3}a_{-2}a_{-1}.a_0a_1a_2\cdots$$

where $a_i = 0$ if $M_h^i(x)$ is in H_0, and $a_i = 1$ if $M_h^i(x)$ is in H_1, the horizontal strips H_0 and H_1 being shown in Figure 2.2. The symbol immediately to the right of the decimal point states whether the orbit is presently in H_0 or H_1. The distance between two symbol sequences s and $\bar{s}$ is defined to be

$$d(s,\bar{s}) = \sum_{i=-\infty}^{\infty} \frac{|s_i - \bar{s}_i|}{2^{|i|}}.$$

Defining σ to be the shift map which moves the decimal one place to the right, it can be shown that there is a homeomorphism h such that $\sigma \circ h = h \circ M_h$. Thus, the shift

on the bi-infinite symbol space is equivalent to the horseshoe map applied to the invariant set Λ. There are thus a countable number of periodic orbits in Λ corresponding to the set of repeating sequences, and the periodic orbits are dense on Λ (that is, arbitrarily close to any point in Λ there is a periodic orbit). There are an uncountable number of aperiodic orbits in Λ corresponding to the set of nonrepeating sequences. There is also a dense orbit (which comes arbitrarily close to every point) in Λ, namely the orbit $\cdots 0, 1, 00, 01, 10, 11, 000, 001, \cdots$. The existence of the dense orbit implies that Λ is topologically transitive under successive iterations of the map. Finally, the dynamics on Λ display sensitive dependence on initial conditions. For example, consider the two sequences $s = \cdots 01.010101 \cdots$ and $\bar{s} = \cdots 01.010100 \cdots$. s and $\bar{s}$ are at present very close to each other, but after five iterations of the shift map they will be very far apart. In terms of the unit square, after five iterations of the shift map the orbit corresponding to the sequence s will be in H_1, while the orbit corresponding to the sequence $\bar{s}$ will be in H_0.

In practice, chaotic behavior is often demonstrated by numerically showing that an attractor has a positive Liapunov exponent. There are as many Liapunov exponents as there are dimensions in the state space of the system, but the largest is usually the most important. Liapunov exponents are defined as follows. Suppose that $\mathbf{x}(t)$ is the orbit on an attractor with initial condition x_0. Consider an infinitesimal perturbation $\delta\mathbf{x_0}$ from this orbit. Then, defining $\mathbf{u_0} = \delta\mathbf{x_0}/|\delta\mathbf{x_0}|$, the Liapunov exponent corresponding to $\mathbf{x_0}$ and $\mathbf{u_0}$ is

$$q(\mathbf{x_0}, \mathbf{u_0}) = \lim_{t\to\infty} \frac{1}{t} \ln\left(\frac{|\delta\mathbf{x}(t)|}{|\delta\mathbf{x_0}|}\right).$$

In words, the Liapunov exponent measures the rate of divergence of the nearby orbits. If $\mathbf{u_0}$ is chosen arbitrarily, then the largest Liapunov exponent will typically be found by this procedure. To get the other exponents, the original perturbation direction $\mathbf{u_0}$ must be chosen to lie in the appropriate orthogonal subspace. Alternatively, consider the evolution of an infinitesimal sphere of perturbed initial conditions. During its evolution the sphere will be distorted into an infinitesimal ellipsoid. Letting $\delta_k(t)$ for $k = 1, \cdots, n$ denote the length of the k^{th} principal axis of the ellipsoid, $\delta_k(t) \sim \delta_k(0)e^{\lambda_k t}$, where $\{\lambda_k\}$ are the Liapunov exponents.

A *strange attractor* is defined to be an attractor that is chaotic. As with the definition of "chaotic," this definition is not universally taken: sometimes a strange attractor is defined to be an attractor with a fractal structure (e.g. [48]). These definitions are not equivalent, because attractors that are chaotic need not have a fractal structure, and attractors with a fractal structure need not be chaotic [49]. It is very difficult to rigorously prove the existence of a strange attractor for a specific dynamical system, and only numerical evidence for the systems under consideration in this dissertation will be presented.

2.2 Invariant Manifolds

A useful result from the theory of dynamical systems is the following [41, 43]:

> **Center Manifold Theorem**: Let f be C^r, that is f and its partial derivatives up to order r are continuous, with $f(\mathbf{x_f}) = 0$. Divide the eigenvalues μ of $\mathrm{D}f(\mathbf{x_f})$ into three sets, $\sigma_u, \sigma_s, \sigma_c$, where $\mu \in \sigma_u$ if $\mathrm{Re}(\mu) > 0$, $\mu \in \sigma_s$ if $\mathrm{Re}(\mu) < 0$, and $\mu \in \sigma_c$ if $\mathrm{Re}(\mu) = 0$. Let E^u, E^s and E^c be the corresponding generalized eigenspaces. Then there exist C^r unstable and stable manifolds W^u and W^s tangential to E^u and E^s respectively at $\mathbf{x} = \mathbf{x_f}$, and a C^r center manifold W^c tangential to E^c at $\mathbf{x} = \mathbf{x_f}$. All are invariant, but W^c is not necessarily unique.

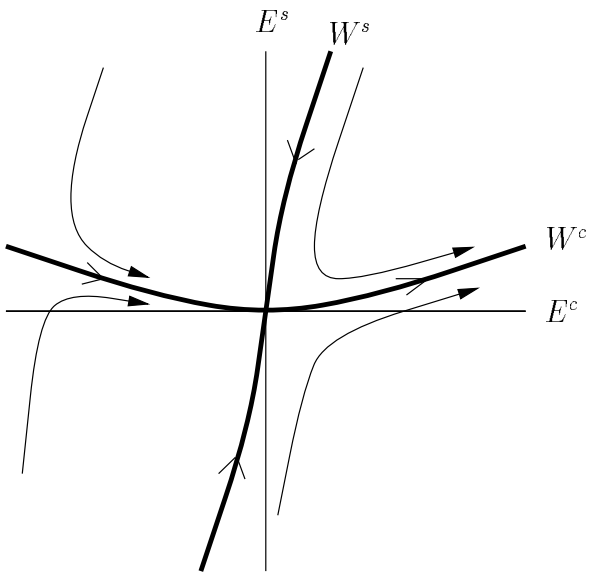

Figure 2.3: Center and stable manifolds of a fixed point. For $t \to \infty$, the system evolution asymptotically approaches the evolution on the center manifold.

Here invariance means that every initial condition on one of the manifolds remains on that manifold under evolution of the flow. Trajectories in W^u and W^s have simple dynamical properties: if $\mathbf{x}(t) \in W^s$ then $\mathbf{x}(t) \to \mathbf{x_f}$ as $t \to \infty$, and if $\mathbf{x}(t) \in W^u$ then $\mathbf{x}(t) \to \mathbf{x_f}$ as $t \to -\infty$. That is, points on the stable (unstable) manifold approach the fixed point $\mathbf{x_f}$ asymptotically as $t \to \infty$ $(-\infty)$.

Now consider the center manifold. In the neighborhood of $\mathbf{x_f}$, the evolution in W^s and W^u is fast, while the evolution in W^c is slow. If $\sigma_u = \emptyset$ and $\sigma_s \neq \emptyset$, then trajectories near $\mathbf{x_f}$ collapse toward W^c on a timescale determined by the eigenvalue in σ_s whose real part has smallest magnitude. Thus, the asymptotic behavior as $t \to \infty$ is determined by the dynamics on W^c, leading to a lower dimensional (and therefore simpler!) system of equations to analyze (see Figure 2.3). Specifically, split up equation (2.1) as

$$\frac{d\mathbf{U}}{dt} = A\mathbf{U} + f_1(\mathbf{U}, \mathbf{V}),$$

$$\frac{d\mathbf{V}}{dt} = B\mathbf{V} + f_2(\mathbf{U}, \mathbf{V}),$$

where A is a matrix with eigenvalues with zero real part, B is a matrix with eigenvalues with negative real part, and f_1 and f_2 are nonlinear functions of $\mathbf{U}$ and $\mathbf{V}$. Since W^c is tangential to $E^c = \{(\mathbf{U}, \mathbf{V}) : \mathbf{V} = 0\}$, it can be represented as

$$W^c(\mathbf{x_f}) = \{(\mathbf{U}, \mathbf{V}) | \mathbf{V} = h(\mathbf{U}), h(\mathbf{x_f}) = 0, \mathrm{D}h(\mathbf{x_f}) = 0\},$$

where h is defined on some neighborhood of $\mathbf{x_f}$. Then on W^c,

$$\frac{d\mathbf{U}}{dt} = A\mathbf{U} + f_1(\mathbf{U}, h(\mathbf{U})). \tag{2.3}$$

This procedure is called a center manifold reduction. Although the center manifold is not unique, the dynamics are the same on all center manifolds of a given fixed point.

The center manifold reduction is illustrated for the Lorenz equations (1.10) for the fixed point $\mathbf{x_f} = (X_f, Y_f, Z_f) = (0, 0, 0)$, following [40]. It is readily shown that at $r = 1$, the eigenvalues of $\mathbf{x_f}$ are $\sigma_c = \{0\}$ and $\sigma_s = \{-(1 + P), -b\}$. The linear part of the equations may be diagonalized by letting

$$\begin{pmatrix} X \\ Y \\ Z \end{pmatrix} = \begin{pmatrix} 1 & P & 0 \\ 1 & -1 & 0 \\ 0 & 0 & 1 \end{pmatrix} \begin{pmatrix} u \\ v \\ w \end{pmatrix},$$

giving

$$\begin{pmatrix} \dot{u} \\ \dot{v} \\ \dot{w} \end{pmatrix} = \begin{pmatrix} 0 & 0 & 0 \\ 0 & -(1+P) & 0 \\ 0 & 0 & -b \end{pmatrix} \begin{pmatrix} u \\ v \\ w \end{pmatrix} + \begin{pmatrix} -\frac{P}{1+P}(u + Pv)w \\ \frac{1}{1+P}(u + Pv)w \\ (u + Pv)(u - v) \end{pmatrix}. \tag{2.4}$$

Thus, u gives the coordinates on E^c, while v and w give the coordinates on E^s. Now, let

$$v = h_1(u) = a_2u^2 + a_3u^3 + \cdots, \tag{2.5}$$

$$w = h_2(u) = b_2u^2 + b_3u^3 + \cdots. \tag{2.6}$$

Plugging these into the $\dot{u}$ equation from (2.4) gives

$$\dot{u} = -\frac{P}{1+P}b_2u^3 + \mathcal{O}(u^4).$$

The coefficient b_2 may be determined by differentiating (2.6) and equating the result to the $\dot{w}$ equation from (2.4) with the substitution of (2.5,2.6):

$$\begin{aligned} 2b_2u\dot{u} + 3b_3u^2\dot{u} + \cdots = & -b(b_2u^2 + b_3u^3 + \cdots) \\ & +[u + P(b_2u^2 + b_3u^3 + \cdots)][u - (b_2u^2 + b_3u^3 + \cdots)]. \end{aligned}$$

Now, using $\dot{u} \sim \mathcal{O}(u^3)$ and equating coefficients at $\mathcal{O}(u^2)$ gives $b_2 = 1/b$. Thus, the dynamics on W^c are

$$\dot{u} = -\frac{P}{1+P}\,\frac{1}{b}u^3 + \mathcal{O}(u^4)$$

To determine the dynamics up to $\mathcal{O}(u^3)$ it is not necessary to determine a_2, a_3, or b_3.

The transition from $r < 1$ to $r > 1$ may be captured by defining $r = 1 + \mu$ and treating μ as an additional independent variable with $\dot{\mu} = 0$. By a similar center manifold reduction treating both u and μ as coordinates on the center eigenspace (see [41]),

$$\dot{u} = \frac{P}{1+P}\,\mu u - \frac{P}{1+P}\,\frac{1}{b}\,u^3 + \cdots, \tag{2.7}$$

an equation of the same form as (1.14) and (1.15).

While the center manifold theory has been illustrated for a system of ordinary differential equations, it may also be applied directly to infinite dimensional systems such as

the partial differential equations describing Rayleigh-Bénard convection. A useful theorem regarding the center manifold for infinite dimensional systems is given in [50]; the hypotheses for this theorem are quite technical, but the following two conditions are typically the most important for fluid dynamical applications: 1) the eigenvalue spectrum must be bounded away from the imaginary axis, and 2) the dimension of the center eigenspace must be finite. Then, a local center manifold exists, and the asymptotic behavior for $t \to \infty$ is determined by the dynamics on the center manifold [50].

It is also possible to define stable, unstable, and center manifolds for periodic orbits. For the periodic orbit γ, trajectories in $W^u(\gamma)$ and $W^s(\gamma)$ have simple dynamical properties: if $x(t) \in W^s(\gamma)$ then $x(t) \to \gamma$ as $t \to \infty$, and if $x(t) \in W^u(\gamma)$ then $x(t) \to \gamma$ as $t \to -\infty$.

2.3 Normal Forms

Equation (2.3) may be simplified putting it into *normal form*, a process which preserves the qualitative dynamics of the original system and simplifies the subsequent bifurcation analysis. In practice, normal forms are found by successive "near identity" transformations. Specifically, let

$$\mathbf{U} = \mathbf{z} + g(\mathbf{z}), \qquad g(\mathbf{z}) = \sum_{j \geq 2} g_j(\mathbf{z}),$$

where g_j is a homogeneous polynolmial of order j, that is, a polynomial function with terms only of order j. Substituting this into (2.3),

$$\frac{d\mathbf{z}}{dt} = (\mathrm{Id} + \mathrm{D}g)^{-1}[A\mathbf{z} + Ag(\mathbf{z}) + f(\mathbf{z} + g(\mathbf{z}), h(\mathbf{z} + g(\mathbf{z})))],$$

where Id is the identity matrix. This is expanded order by order, and the g_j's are chosen successively to eliminate as many terms as possible. Such transformations can remove all "nonresonant" terms, as discussed in [40, 41]. Note that maps may also be put into normal form by a similar procedure.

The resulting normal form is not unique because there may be a choice of which terms to remove, a fact which may sometimes be exploited to also remove some "resonant" terms [51, 52]. Also, since the procedure of putting the equation into normal form is done order by order, it must be terminated at some point, giving a truncated normal form. While formally the normal form preserves the dynamics of the original system, it is not known precisely which qualitative features of the dynamics are preserved in a *truncated* normal form. Parametric dependence may be included in the normal form by treating both $\mathbf{U}$ and system parameters λ as coordinates on the center eigenspace, similar to what can be done for the center manifold reduction.

Normal forms can have greater symmetry than the original equation [53] (see also [35, 42]). Specifically, the normal form is equivariant with respect to the one-parameter group

$$\Gamma \equiv \{\exp(sA^\dagger) : s \in \mathbb{R}\},$$

where $A^\dagger$ is the adjoint (transpose and complex conjugate) of the matrix A in equation (2.3). For example, suppose that W^c is two-dimensional, and the evolution on W^c has linearization

$$\begin{pmatrix} \dot{u}_1 \\ \dot{u}_2 \end{pmatrix} = \begin{pmatrix} 0 & \omega_0 \\ -\omega_0 & 0 \end{pmatrix} \begin{pmatrix} u_1 \\ u_2 \end{pmatrix}.$$

Letting $z = (u_1 + iu_2)/2$,

$$\begin{pmatrix} \dot{z} \\ \dot{\bar{z}} \end{pmatrix} = \begin{pmatrix} i\omega_0 & 0 \\ 0 & -i\omega_0 \end{pmatrix} \begin{pmatrix} z \\ \bar{z} \end{pmatrix},$$

where $\bar{z}$ is the complex conjugate of z. Then, the normal form for the $(\dot{z}, \dot{\bar{z}})$ equations is equivariant with respect to

$$\exp(sA^\dagger) = \begin{pmatrix} e^{i\phi} & 0 \\ 0 & e^{-i\phi} \end{pmatrix}, \qquad \phi \equiv -s\omega_0,$$

or equivalently, the normal form for the $\dot{z}$ equation is equivariant with respect to the group

$$S^1 : z \to e^{i\phi} z, \qquad \phi \in [0, 2\pi).$$

It is then readily shown (see §1.4) that

$$\frac{dz}{dt} = g_1(|z|^2)z. \tag{2.8}$$

This S^1 symmetry arises from coordinate transformations, and does not represent a true symmetry of the system. Here the normal form symmetry corresponds to a phase-shift symmetry, and since the solution to (2.8) is to leading order $z \sim e^{i\omega_0 t}$, it may be interpreted as a time translation symmetry. The coordinate transformations extend the symmetry of the vector field evaluated *on* the periodic orbit to a *neighborhood* of the periodic orbit.

2.4 Local Bifurcations for Vector Fields

Suppose $\mathbf{x_f}$ is a fixed point of (2.1). A *local bifurcation* occurs at $\lambda = \lambda_0$ when at least one of the eigenvalues of $\mathrm{D}f(\mathbf{x_f}; \lambda)$ crosses the imaginary axis as λ is varied through $\lambda = \lambda_0$. Without loss of generality, let $\mathbf{x_f}$ be at the origin, and let $\lambda_0 = 0$.

A *steady bifurcation* is a local bifurcation which occurs when a single real eigenvalue crosses the imaginary axis. At the crossing, the eigenvalue is equal to zero. Common steady bifurcations with their normal forms (which are one-dimensional because a single eigenvalue crosses the imaginary axis, and are suitably rescaled) are:

- *Saddle-node bifurcation* with normal form $\dot{x} = \lambda + ax^2$, where $a = \pm 1$.

  For example, for $a = -1$ no fixed points exist for $\lambda < 0$, but the fixed points $x_{f\pm} = \pm\sqrt{\lambda}$ exist for $\lambda \geq 0$. x_{f+} is stable, while x_{f-} is unstable.

- *Transcritical bifurcation* with normal form $\dot{x} = \lambda x + ax^2$, where $a = \pm 1$.

  For example, for $a = -1$ the fixed points $x_{f1} = 0$ and $x_{f2} = \lambda$ exist for all λ. However, x_{f1} is stable (unstable) for $x < 0$ (> 0), while x_{f2} is stable (unstable) for $x > 0$ (< 0). There is an *exchange of stability* at $\lambda = 0$.

- *Pitchfork bifurcation* with normal form $\dot{x} = \lambda x + ax^3$, where $a = \pm 1$.

  For example, for the *supercritical* case ($a = -1$), the fixed point $x_{f0} = 0$ is the only fixed point for $\lambda < 0$; it is stable. For $\lambda > 0$, three fixed points exist: the now unstable fixed point $x_{f0} = 0$, and two stable fixed points $x_{f\pm} = \pm\sqrt{\lambda}$. Note that the normal form for the pitchfork bifurcation is equivariant under the group Z_2 generated by $x \to -x$. Equations (1.14,1.15, 2.7) describe the onset of convection via a supercritical pitchfork bifurcation. A *subcritical* pitchfork bifurcation has $a = 1$ in the normal form.

Figure 2.4 shows *bifurcation diagrams* for these normal forms, in which the loci of the invariant sets (here, fixed points) are shown in the (x, λ) product space. In these and other bifurcation diagrams, solid (dashed) lines correspond to stable (unstable) solutions.

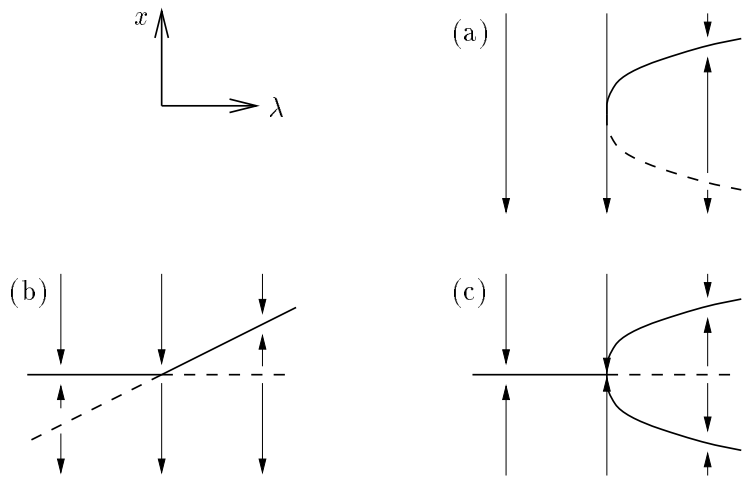

Figure 2.4: Bifurcation diagrams for the (a) saddle-node, (b) transcritical, and (c) pitchfork bifurcations with $a = -1$ in the normal forms. The vector fields are indicated by arrows.

A *Hopf bifurcation* is a local bifurcation which occurs when a complex conjugate pair of eigenvalues crosses the imaginary axis at $\pm i\omega_0$, where $\omega_0 > 0$. The normal form for the Hopf bifurcation is two-dimensional and is most conveniently expressed in terms of the complex variable z:

$$\dot{z} = (\gamma(\lambda) + i\omega(\lambda))z + (a + ib)|z|^2 z + \cdots,$$

where $\gamma(\lambda) \pm i\omega(\lambda)$ is the complex conjugate pair of eigenvalues. Note that this has the same form as equation (2.8), which was derived using the appropriate normal form symmetry. The eigenvalues are assumed to cross the imaginary axis in a nondegenerate manner, that is,

$$\gamma(0) = 0, \qquad \omega(0) \equiv \omega_0 \neq 0, \qquad \frac{d\gamma}{d\lambda}(0) > 0.$$

Also, it is assumed that $a \neq 0$. Then near this bifurcation point, $\gamma(\lambda) = d\lambda + \cdots$ and

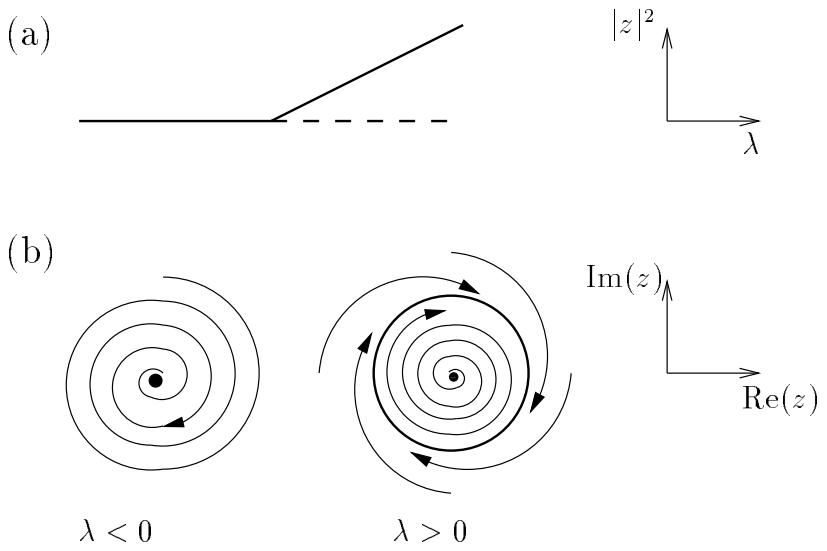

Figure 2.5: (a) Bifurcation diagram and (b) phase space portrait for the supercritical Hopf bifurcation with $a < 0$, $d > 0$. Only a stable fixed point exists for $\lambda < 0$, while an unstable fixed point and a stable periodic orbit exist for $\lambda > 0$.

$\omega = \omega_0 + c\lambda + \cdots$, where c and d are real constants. Thus, in polar coordinates $z \equiv re^{i\phi}$,

$$\begin{aligned} \dot{r} &= d\lambda r + ar^3 + \cdots, \\ \dot{\theta} &= \omega_0 + c\lambda + br^2 + \cdots. \end{aligned}$$

The system behavior can be deduced by recognizing that the r equation is equivalent to the normal form for the pitchfork bifurcation, except that only solutions with $r \geq 0$ are defined. For example, suppose $a < 0$. Then, only the $r = 0$ fixed point exists for $d\lambda < 0$, and it is stable. For $d\lambda > 0$, the $r = 0$ fixed point is unstable, and a constant amplitude solution $r = \sqrt{-d\lambda/a}$ exists. From the θ equation, this corresponds to a limit cycle which is readily shown to be stable. A bifurcation diagram and corresponding phase space portraits for the Hopf bifurcation are shown in Figure 2.5. This case is called *supercritical* because the periodic orbit branch bifurcates into the region of parameter space (here $d\lambda > 0$) for

which the origin is unstable. A Hopf bifurcation is called *subcritical* when the periodic orbit branch bifurcates into the region of parameter space (here $d\lambda < 0$) for which the origin is stable.

Finally, a *multiple bifurcation* occurs when several eigenvalues cross the imaginary axis simultaneously.[4] Multiple bifurcations often provide an organizing center for a system's dynamics, and may imply the occurrence of *global* bifurcations which are described in §2.6. For example, the double zero bifurcation in which real eigenvalues cross the imaginary axis at zero with multiplicity two is well understood [54, 55, 40, 41, 56]; this is often called a Takens-Bogdanov bifurcation, and it is an example of a codimension two bifurcation because generically two parameters must be varied in order to reach the bifurcation point. Other well-studied codimension two multiple bifurcations include a pure imaginary pair and a simple zero eigenvalue simultaneously crossing the imaginary axis, and two pure imaginary nonresonant pairs of eigenvalues simultaneously crossing the imaginary axis [40, 41, 44]. Bifurcations of higher codimension have also been studied: for example, a codimension three bifurcation (the "triple zero bifurcation") in which a real eigenvalue with multiplicity three crosses the imaginary axis at zero is of particular interest in systems with reflection symmetry because it implies the possibility of chaotic behavior [57].[5]

[4] By convention, the Hopf bifurcation is not considered a multiple bifurcation.

[5] Reference [58] shows that chaotic direction-reversing waves may also occur for the triple zero bifurcation with O(2) symmetry.

2.5 Bifurcations for Maps

Suppose $\mathbf{x_f}$ is a fixed point of the map

$$\mathbf{x_{n+1}} = g(\mathbf{x_n}; \lambda).$$

That is, $g(\mathbf{x_f}; \lambda) = \mathbf{x_f}$. Such a map may or may not be a Poincaré map. A bifurcation occurs at $\lambda = \lambda_0$ when at least one of the eigenvalues of $\mathrm{D}g(\mathbf{x_f}; \lambda)$ crosses the unit circle as λ is varied through $\lambda = \lambda_0$. Without loss of generality, let $\mathbf{x_f}$ be at the origin, and let $\lambda_0 = 0$.

When a single eigenvalue crosses through $+1$, the following bifurcations are possible:

- *Saddle-node bifurcation* with normal form $x_{n+1} = x_n + \lambda \pm x_n^2$.
- *Transcritical bifurcation* with normal form $x_{n+1} = x_n + \lambda x_n \pm x_n^2$.
- *Pitchfork bifurcation* with normal form $x_{n+1} = x_n + \lambda x_n \pm x_n^3$.

These normal forms are all one-dimensional because a single eigenvalue crosses the unit circle. The analysis of the branches of fixed points for these bifurcations is completely analogous to that for their vector field counterparts discussed above.

A *period-doubling* bifurcation occurs when a single eigenvalue crosses through -1. The normal form for this bifurcation is one-dimensional and is given by

$$x_{n+1} = -(1 + \lambda)x_n + ax_n^3, \qquad a = \pm 1.$$

For example for $a = 1$, as λ is increased through zero the fixed point at the origin loses stability to an orbit with period equal to two iterations of the map (or equivalently, a fixed

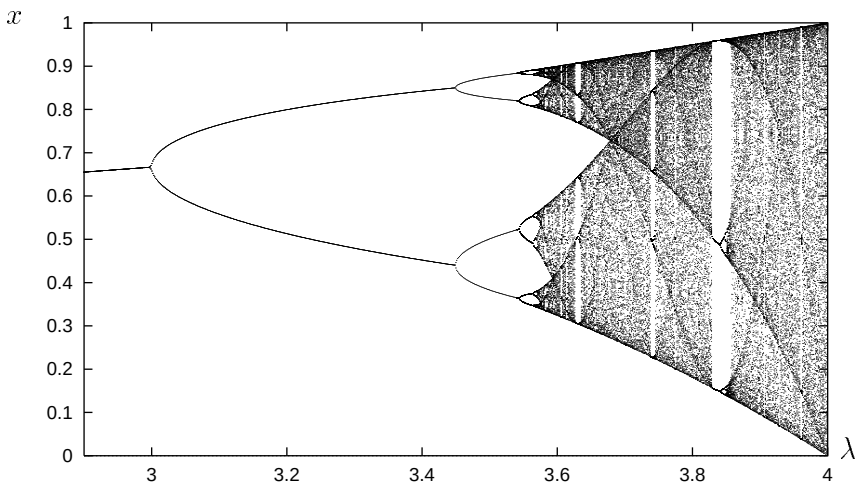

Figure 2.6: Attractor for the logistic map $x_{n+1} = \lambda x_n(1-x_n)$. For $\lambda < \lambda_1 \equiv 3$ the attractor is a fixed point. As λ is increased through λ_1, a period-doubling bifurcation occurs, giving a stable orbit with period equal to two iterations of the map. This orbit then undergoes a period-doubling bifurcation at $\lambda_2 \approx 3.45$, etc. This period-doubling cascade accumulates at $\lambda \approx 3.57$. Unstable solutions are not shown.

point of the map composed with itself). This bifurcation has no analog for vector fields. If the map is a Poincaré map, the new orbit corresponds to a period-doubled periodic orbit, that is, a periodic orbit with approximately twice the period of the original orbit. A common route to chaos is an infinite cascade of such period-doublings, shown for the logistic map in Figure 2.6. Such cascades have a number of universal properties: for example, the period-doublings accumulate according to

$$\frac{\lambda_j - \lambda_{j-1}}{\lambda_{j+1} - \lambda_j} \to 4.66920\cdots$$

as $j \to \infty$, where λ_j is the λ value at which the j-th period-doubling occurs [59, 60].

Finally, a *Naimark-Sacker* bifurcation occurs when a complex conjugate pair of eigenvalues $\mu(\lambda)$ and $\bar{\mu}(\lambda)$ cross the unit circle at $\lambda = \lambda_0 \equiv 0$. Under the condition that $[\mu(0)]^m \neq 1$ for $m = 1, 2, 3, 4$, the normal form for this bifurcation is most conveniently

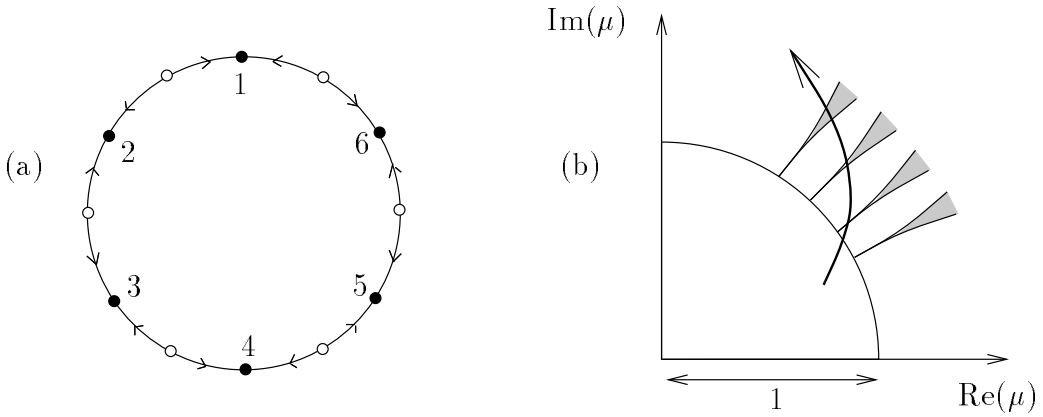

Figure 2.7: (a) Stable (solid dots) and unstable (open dots) periodic orbits on the invariant circle. The numbers label the successive iterations of the map for the stable periodic orbit. The rotation number of this orbit is 1/6. (b) Arnol'd tongues emanating from the unit circle showing the domains of existence of periodic orbits. The periodic orbits are born and die in saddle-node bifurcations at the edge of a tongue. The thick line shows a typical path traced out when λ is varied; such a path crosses an infinite number of tongues.

expressed in terms of the complex variable z:

$$z_{n+1} = \mu(\lambda) z_n + c(\lambda)|z_n|^2 z_n + \cdots .$$

Under the nondegeneracy conditions

$$\frac{d\mu}{d\lambda}(0) \neq 0, \qquad \mathrm{Re}[c(0)] \neq 0$$

an invariant circle bifurcates from the origin at $\lambda = 0$. This bifurcation thus resembles a "Hopf bifurcation for maps".[6] However, the dynamics on the invariant circle near a Naimark-Sacker bifurcation are quite complicated. For open intervals in λ, there are two periodic orbits with the same period on the circle, one stable and the other unstable (see Figure 2.7(a)). These periodic orbits are born and die in saddle-node bifurcations which

[6] If the map is a Poincaré map for a vector field, this bifurcation is sometimes called a torus bifurcation because the resulting invariant circle corresponds to motion on a torus.

occur at the end of the intervals. This behavior is understood by considering the system behavior in terms of two parameters. In practice, these parameters might be λ and some other system parameter; for convenience, we can think of the two parameters as $\mathrm{Re}(\mu)$ and $\mathrm{Im}(\mu)$. Figure 2.7(b) shows the domains of existence, called Arnol'd tongues, for such periodic solutions. There is an infinite number of tongues, one touching the unit circle at each $e^{2\pi ip/q}$ where p and q are relatively prime integers. The number p/q gives the average angle (normalized by 2π) around the invariant circle that the solution on the corresponding periodic orbit moves under one iteration of the map; it is called the rotation number of the periodic orbit. A generic curve in parameter space will intersect an infinite number of tongues, giving an infinite number of intervals for which different periodic orbits exist. Far from the "tip" of the tongue, that is, far from the unit circle in Figure 2.7(b), tongues can overlap, and the system behavior can become even more complicated (see [61] and Chapter 4).

There are four distinct strong resonances for the Naimark-Sacker bifurcation corresponding to $[\mu(\lambda_0)]^m = 1$ for $m = 1, 2, 3, 4$. These may be partially studied by interpolation of the appropriate maps to obtain an associated vector field. Letting $\mu(0) = e^{2\pi ip/q}$ where p and q are relatively prime integers, the associated vector fields for the strong resonances are [62, 44]:

- $q = 1$: $\quad \dot{x} = y, \qquad \dot{y} = \mu_1 + \mu_2 y + ax^2 + bxy,$
- $q = 2$: $\quad \dot{x} = y, \qquad \dot{y} = \mu_1 x + \mu_2 y + ax^3 + bx^2 y,$
- $q = 3$: $\quad \dot{z} = \gamma z + A\bar{z}^2 + Bz^2\bar{z},$
- $q = 4$: $\quad \dot{z} = \gamma z + A\bar{z}^3 + Bz^2\bar{z}.$

For $q = 1, 2$ all variables and coefficients are real, while for $q = 3, 4$ all variables and coefficients are complex. These vector fields correspond to the normal forms for double zero bifurcations with Z_q symmetry, and their dynamics are discussed in detail in [62, 56] (see also [40] for $q = 1, 2$). For $q = 3, 4$, the vector fields also correspond to the normal forms for Hopf bifurcations in the presence of resonant $1 : q$ forcing (c.f. §4.1).

2.6 Global Bifurcations

A *global bifurcation* is a bifurcation in which the qualitative changes in the system behavior cannot be captured by a local analysis of fixed points of the dynamical system or the Poincaré map. A detailed treatment of global bifurcations is given in [63]; also see [40, 64, 41, 43]. Global bifurcations are often associated with the creation or destruction of periodic orbits. In this dissertation, evidence for global bifurcations is found numerically, often by following periodic orbits to very high period.

2.6.1 Planar Homoclinic Bifurcation

Suppose $\mathbf{x_f}$ is a fixed point of a dynamical system. A *homoclinic orbit* is an orbit $\phi(\mathbf{x}, t)$ such that $\phi(\mathbf{x}, t) \to \mathbf{x_f}$ as $t \to \infty$ and $t \to -\infty$. This is distinguished from a *heteroclinic orbit* in which $\phi(\mathbf{x}, t) \to \mathbf{x_f}$ as $t \to \infty$ and $\phi(\mathbf{x}, t) \to \mathbf{x_{f2}}$ as $t \to -\infty$, where $\mathbf{x_{f2}}$ is a distinct fixed point from $\mathbf{x_f}$.

Consider the dynamical system $\dot{\mathbf{x}} = f(\mathbf{x}; \lambda)$ where $f : \mathbb{R}^2 \times \mathbb{R} \to \mathbb{R}^2$, $\lambda \in \mathbb{R}$. Suppose that a homoclinic orbit exists at, without loss of generality, $\lambda_0 = 0$, with the stable manifold inside (outside) the unstable manifold for $\lambda < 0$ (> 0). Let σ be the sum of the

eigenvalues of $\mathbf{x_f}$. Then [41]

> For λ sufficiently small: i) If $\sigma < 0$, there exists a unique stable periodic orbit on one side of $\lambda = 0$; on the opposite side, there are no periodic orbits. ii) If $\sigma > 0$, the same conclusion holds as in i), except that the periodic orbit is unstable.

Phase portraits for $\sigma < 0$ and a bifurcation diagram for the planar homoclinic bifurcation are shown in Figure 2.8. In the presence of Z_2 symmetry, the global bifurcations shown in Figure 2.9 can occur.

2.6.2 Homoclinic Explosion

Consider $\dot{\mathbf{x}} = f(\mathbf{x}; \lambda)$ where $\mathbf{x} = (x, y, z) \in \mathbb{R}^3, \lambda \in \mathbb{R}$, and suppose that f is equivariant under the reflection $(x, y, z) \to (-x, -y, z)$. Furthermore, suppose that $\mathbf{x_f} = (0, 0, 0)$ is a fixed point with linearization

$$\dot{x} = \mu_1 x, \qquad \dot{y} = \mu_2 y, \qquad \dot{z} = \mu_3 z,$$

where the eigenvalues μ_1, μ_2, μ_3 satisfy $\mu_2 < \mu_3 < 0 < \mu_1$, and $|\mu_3/\mu_1| < 1$. Finally, suppose that at $\lambda = \lambda_0 \equiv 0$ there is a pair of homoclinic orbits to the origin related by the reflection symmetry as shown in Figure 2.10. Consider the Poincaré map P with surface of section $\Sigma = \{(x, y, z) | z = \epsilon, |x| < \epsilon, |y| < \epsilon\}$, where $\epsilon > 0$ is small. Then [65, 41]

> On one side of the bifurcation, (say, $\lambda < 0$) all trajectories leave Σ under the evolution of P. On the other side (say, $\lambda > 0$) Σ possesses an invariant Cantor set Λ on which the Poincaré map P is homeomorphic to the full shift on two symbols.

From the discussion of the horseshoe map in §2.1.4, Λ thus possesses a countably infinite set of periodic orbits, an uncountably infinite set of aperiodic orbits, a dense orbit, and it has sensitive dependence on initial conditions. That is, Λ is a chaotic set. This type of global

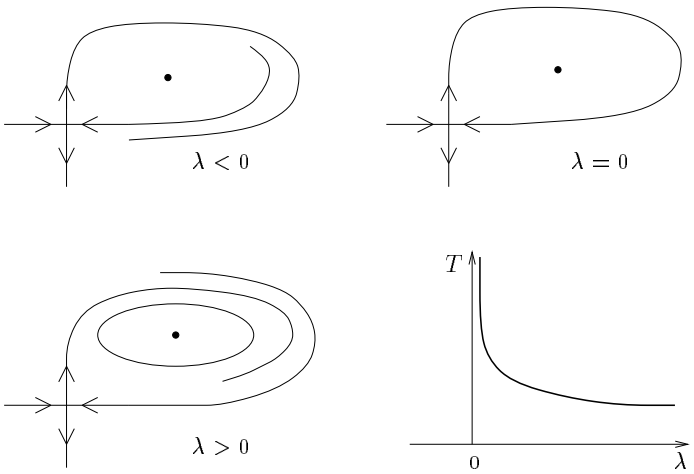

Figure 2.8: Phase portraits and bifurcation diagram for a planar homoclinic bifurcation giving birth to a stable periodic orbit as λ increases through 0. As $\lambda \to 0^+$ the periodic orbit approaches the homoclinic orbit which exists at $\lambda = 0$, and its period T diverges to infinity. No periodic orbit exists for $\lambda < 0$. The dots show fixed points which do not participate in the bifurcation.

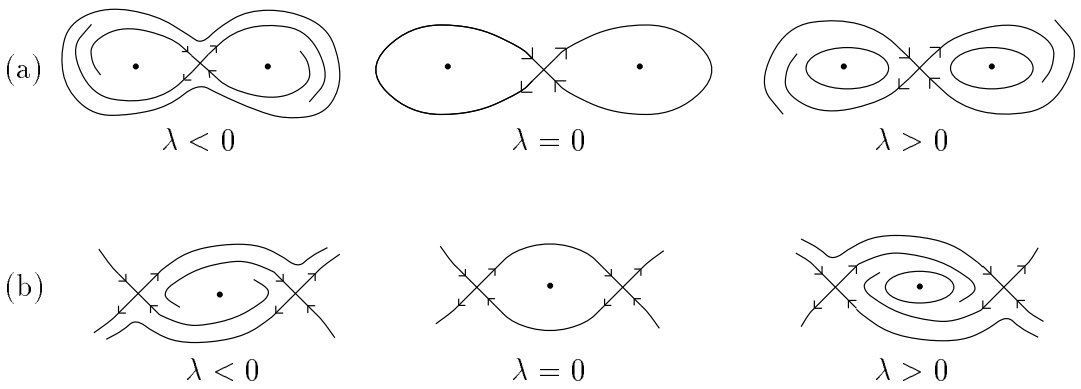

Figure 2.9: Example phase portraits for planar global bifurcations in the presence of Z_2 symmetry. The dots show fixed points which do not participate in the bifurcations. (a) As $\lambda \to 0^+$ the two symmetry-related periodic orbits approach the homoclinic orbits which exist at $\lambda = 0$ and "glue" together, giving a single periodic orbit for $\lambda < 0$. This is an example of a *gluing bifurcation*. (b) As λ is increased through zero, a periodic orbit is born from the heteroclinic orbits which form at $\lambda = 0$.

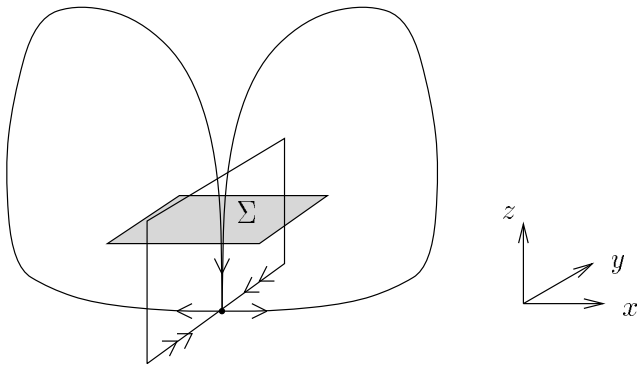

Figure 2.10: Two homoclinic orbits to the origin related by reflection symmetry.

bifurcation is called a *homoclinic explosion*, because the interesting behavior of the set Λ "explodes" into existence as λ crosses zero. There are no attractors in Λ near $\lambda = 0$, but sets may become attractors for large $|\lambda|$. In this way, a homoclinic explosion is responsible for the chaos found in the Lorenz equations.

For the above hypotheses except with $|\mu_3/\mu_1| > 1$, a *gluing bifurcation* occurs giving a transition to chaotic behavior with strange attractors arising via a cascade involving bifurcations of stable homoclinic orbits [66, 64].

2.6.3 Orbit Homoclinic to a Saddle-Focus: Shil'nikov Bifurcation

Consider $\dot{\mathbf{x}} = f(\mathbf{x}; \lambda)$ where $\mathbf{x} = (x, y, z) \in \mathbb{R}^3, \lambda \in \mathbb{R}$. Suppose that at $\lambda = \lambda_0$, the origin is a fixed point with eigenvalues $-\mu_s \pm i\omega$ and μ_u (that is, the origin is a saddle-focus fixed point) where $\mu_u > \mu_s > 0$. Furthermore, suppose that at $\lambda = \lambda_0$ the origin has a homoclinic orbit. Then [67, 41]

> At $\lambda = \lambda_0$, there are surfaces of section near the origin such that a countable infinity of distinct invariant Cantor sets Λ_k exist, on each of which the Poincaré

map P is homeomorphic to a full shift on two symbols.

The implications of this follow from the discussion of the horseshoe map. In particular, chaotic dynamics occur.

Interesting behavior also occurs for parameter values *near* those for which such a homoclinic orbit exists. Specifically, suppose that the dependence of the unstable manifold of the origin is assumed to depend on λ as shown in Figure 2.11. Then, letting $\delta \equiv \mu_s/\mu_u$, from the analysis of [68] (also see [41])

- For $\delta > 1$ there is a single, stable periodic orbit for $\lambda > \lambda_0$. As $\lambda \to \lambda_0$ the period of this orbit tends to infinity. The bifurcation diagram for this situation is shown in Figure 2.12(a).

- For $\delta < 1$ there are an infinite number of unstable periodic orbits at $\lambda = \lambda_0$. These orbits appear and disappear in saddle-node bifurcations as $\lambda \to \lambda_0$ from either side. If $\delta > 1/2$ one stable and one unstable periodic orbit is born in each saddle-node bifurcation, whereas if $\delta < 1/2$ both periodic orbits are unstable. There are also period-doubling bifurcations for parameters near those for which each saddle-node bifurcation occurs; the stable orbits which exist for $\delta > 1/2$ lose stability in these bifurcations. The corresponding bifurcation diagram is shown in Figure 2.12(b).

This spectrum of bifurcations which is associated with the homoclinic orbit to a saddle-focus fixed point is often called a *Shil'nikov bifurcation* in honor of pioneering work done on the problem by L. P. Shil'nikov [69]. A generalization in which parameters are chosen to be near those for which the fixed point also undergoes a Hopf bifurcation is considered in [70], and will be useful in the analysis done in Chapter 3.

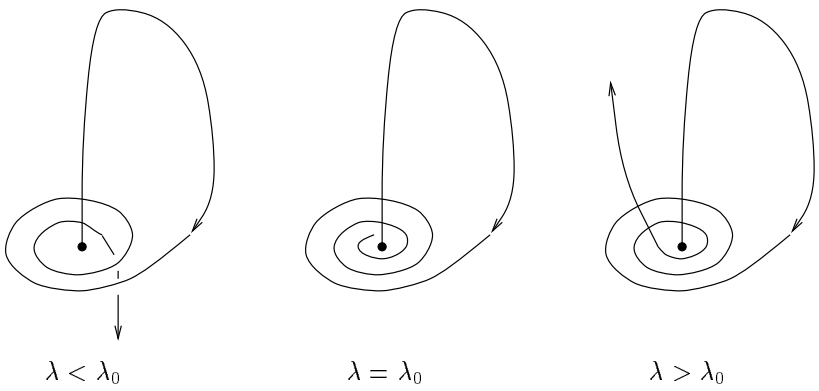

Figure 2.11: The dependence of the unstable manifold of the origin on λ. At $\lambda = \lambda_0$, a homoclinic orbit exists.

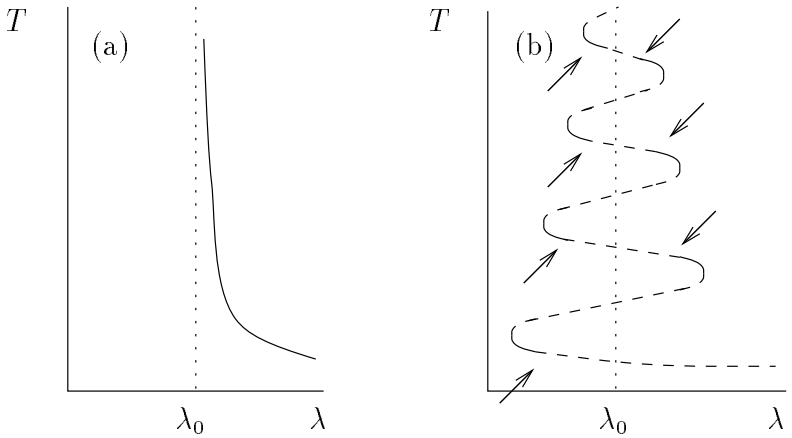

Figure 2.12: Bifurcation diagrams associated with a homoclinic orbit to a saddle-focus at $\lambda = \lambda_0$, where T is the period of the periodic orbit. (a) For $\delta > 1$ one stable periodic orbit is present. (b) For $\delta < 1$, the solution branch undergoes an infinite number of saddle-node bifurcations as it is followed to higher period, with the bifurcation values converging to λ_0 from both sides. The arrows show the locations of period-doubling bifurcations. Dashed lines correspond to unstable periodic orbits, while solid lines correspond to stable (unstable) periodic orbits for $\delta > 1/2$ ($< 1/2$).

2.7 Bifurcations with Symmetry

The presence of symmetry often forces eigenvalues to have multiplicity greater than one: this increases the dimensionality of the center manifold, and can thus lead to very rich dynamics. However, the multiplicity of the eigenvalues prevents the direct application of the bifurcation theory results discussed above, so new techniques are required. Useful references on bifurcations in the presence of symmetry include [35, 34].

Recall that a dynamical system $\dot{\mathbf{x}} = f(\mathbf{x}; \lambda)$ is equivariant with respect to the group G if $f(\gamma\mathbf{x}; \lambda) = \gamma f(\mathbf{x}; \lambda)$ for all $\gamma \in G$. A representation[7] of G is *irreducible* on $\mathbb{R}^n$ if the only proper subspace of $\mathbb{R}^n$ left invariant by G is the origin. It is *absolutely irreducible* on $\mathbb{R}^n$ if all linear maps A on $\mathbb{R}^n$ that commute with all $\gamma \in G$ are multiples of the identity matrix.

Suppose that the origin $\mathbf{x} = 0$ is a fixed point solution. For all $\gamma \in G$, $\gamma \cdot 0 = 0$. Thus, the origin is invariant under the full symmetry G. Bifurcating solutions from the origin may break some, but not necessarily all, of this symmetry. This is made precise by characterizing the symmetry of a solution $\mathbf{x_0}$ by the *isotropy subgroup* $\Sigma_{\mathbf{x_0}} \subset G$ defined as

$$\Sigma_{\mathbf{x_0}} = \{\gamma \in G : \gamma\mathbf{x_0} = \mathbf{x_0}\}.$$

The isotropy subgroup of $\mathbf{x_0}$ is thus the set of all group elements which leave the solution $\mathbf{x_0}$ unchanged. For example for the pitchfork bifurcation, $\Sigma_{x_{f0}} = Z_2$, the group generated by the reflection symmetry, and $\Sigma_{x_{f+}} = \Sigma_{x_{f-}} = \{\mathrm{Id}\}$, where Id is the identity. Since x_{f0} has more symmetry than x_{f+} and x_{f-}, the supercritical pitchfork bifurcation leads to a reduction in symmetry of the stable solution; this is called *spontaneous symmetry-breaking.*

[7] We do not make a notational distinction between elements of G and their representations.

Note that the equivariance of f guarantees that $\gamma\mathbf{x_0}$ will also be a solution for all $\gamma \in G$; this set of solutions is called the *group orbit*. Thus, for the pitchfork bifurcation, the existence of x_{f+} implies the existence of x_{f-}. The isotropy subgroups of $\mathbf{x_0}$ and $\gamma\mathbf{x_0}$ are related by the conjugacy $\Sigma_{\gamma\mathbf{x_0}} = \gamma\Sigma_{\mathbf{x_0}}\gamma^{-1}$, because if $\sigma\mathbf{x_0} = \mathbf{x_0}$, then $(\gamma\sigma\gamma^{-1})(\gamma\mathbf{x_0}) = \gamma\mathbf{x_0}$. Associated with the isotropy subgroup is a *fixed point subspace* given by

$$\mathrm{Fix}(\Sigma_{\mathbf{x_0}}) = \{\mathbf{x} \in \mathbb{R}^n : \sigma\mathbf{x} = \mathbf{x} \ \text{ for all } \ \sigma \in \Sigma_{\mathbf{x_0}}\}.$$

In words, the fixed point subspace is the set of points which are fixed by all elements of $\Sigma_{\mathbf{x_0}}$. Fixed point subspaces are invariant under the dynamics because $\sigma f(\mathbf{x};\lambda) = f(\sigma\mathbf{x};\lambda) = f(\mathbf{x};\lambda)$ for all $\sigma \in \Sigma$ and $\mathbf{x} \in \mathrm{Fix}(\Sigma)$.

With these definitions, it is now possible to state two useful results concerning bifurcations in the presence of symmetry [35]:

> **The Equivariant Branching Lemma**: Let G be a Lie group acting absolutely irreducibly on $\mathbb{R}^n$ and let $\dot{\mathbf{x}} = f(\mathbf{x};\lambda)$ be a G-equivariant bifurcation problem such that as λ passes through 0, real eigenvalues (of multiplicity n) of $\mathrm{D}f(0;0)$ pass through zero with nonzero speed. Let Σ be an isotropy subgroup satisfying
>
> $$\dim \mathrm{Fix}(\Sigma) = 1.$$
>
> Then there exists a unique solution branch $f = 0$ bifurcating from the origin such that the isotropy subgroup of each solution is Σ.
>
> **The Equivariant Hopf Bifurcation Theorem**: Let G be a Lie group acting G-simply on $\mathbb{R}^n$, where n is even.[8] Let $\dot{\mathbf{x}} = f(\mathbf{x};\lambda)$ be a G-equivariant bifurcation problem such that as λ passes through 0, complex conjugate eigenvalues (each of multiplicity $n/2$) pass through the imaginary axis with nonzero speed. Let $\Sigma \subset G \times S^1$ be an isotropy subgroup satisfying
>
> $$\dim \mathrm{Fix}(\Sigma) = 2.$$
>
> Then there exists a unique branch of periodic solutions bifurcating from the origin such that the isotropy subgroup of each solution is Σ.

[8] The representation of G acts *G-simply* on $\mathbb{R}^n$ if it satisfies one of the following two conditions: i) it is irreducible, but not absolutely irreducible, or ii) it is isomorphic to the direct sum of two copies of an absolutely irreducible representation. Generically for a bifurcation involving imaginary eigenvalues, G acts G-simply on the center eigenspace.

Note that the S^1 symmetry in the equivariant Hopf bifurcation theorem is associated with putting the vector field into normal form (see §2.3), and its action on a periodic solution may be interpreted as a time shift. These results are extremely useful because they *guarantee* that certain solutions will bifurcate from the origin. However, other solutions not guaranteed by these theorems may also bifurcate from the origin. The use of the equivariant Hopf bifurcation theorem is illustrated by the following two examples: the Hopf bifurcation with O(2) and with D_4 symmetry.

2.7.1 The Hopf Bifurcation with O(2) Symmetry

Here the center eigenspace is four-dimensional, with coordinates that may be taken as the complex variables z_1 and z_2. We assume the standard action so that $O(2) = \langle T_\phi, \kappa \rangle$, that is O(2) is generated by T_ϕ and κ, where

$$T_\phi : (z_1, z_2) \to (e^{-i\phi} z_1, e^{i\phi} z_2), \quad \phi \in [0, 2\pi) \qquad \kappa : (z_1, z_2) \to (z_2, z_1).$$

The normal form symmetry is S^1, with action

$$N_\sigma : (z_1, z_2) \to (e^{i\sigma} z_1, e^{i\sigma} z_2), \qquad \sigma \in [0, 2\pi).$$

The Hopf bifurcation with O(2) symmetry is often encountered in translation-symmetric systems with periodic boundary conditions, and may also arise in systems with geometric circular symmetry [34]. Our discussion follows that given in [35].

We first derive the isotropy subgroups for the group $O(2) \times S^1$. Consider the point $(z_1, z_2) = (ae^{i\psi_1}, be^{i\psi_2}) \equiv \mathbf{z_0}$, where a and b are real and positive. Then

$$N_{-(\psi_1+\psi_2)/2} T_{(\psi_1-\psi_2)/2} \mathbf{z_0} = (a, b),$$

which implies that $(z_1, z_2) = (a, b)$ lies on the same group orbit as $\mathbf{z_0}$. Since isotropy subgroups for solutions on the same orbit are related by conjugacy, without loss of generality we can consider $(z_1, z_2) = (a, b)$. Furthermore, the action of κ allows us to order a and b so that without loss of generality $a \geq b \geq 0$. There are four cases to consider:

- $a = b = 0$: Trivially, the isotropy subgroup is the full group $\mathrm{O}(2) \times S^1$.

- $a > b > 0$: The isotropy subgroup cannot include the element κ because $|z_1|$ and $|z_2|$ must be preserved. Now,

$$N_\sigma T_\phi(a, b) \to (e^{i(\sigma-\phi)}a, e^{i(\sigma+\phi)}b),$$

  which fixes (a, b) if and only if $\sigma \pm \phi = 0 \mod 2\pi$. Thus, the isotropy subgroup is isomorphic to Z_2, and we call it $Z_2^c \equiv \langle N_\pi T_\pi \rangle$.

- $a > 0$, $b = 0$: Here

$$N_\sigma T_\phi(a, 0) \to (e^{i(\sigma-\phi)}a, 0),$$

  which fixes $(a, 0)$ if and only if $\sigma - \phi = 0 \mod 2\pi$. Thus, the isotropy subgroup is $\tilde{\mathrm{SO}}(2) \equiv \{N_\phi T_\phi : \phi \in [0, 2\pi)\}$. Note that Z_2^c is included in $\tilde{\mathrm{SO}}(2)$.

- $a = b > 0$: From the same argument as given in the second case, the point (a, a) is fixed by the subgroup Z_2^c. It is also fixed by the subgroup $Z_2 \equiv \langle \kappa \rangle$. Putting these two subgroups together, the full isotropy subgroup is $Z_2 \times Z_2^c$.

The types of solutions, their isotropy subgroups, and the fixed point subspaces for this problem are summarized in Table 2.1. Thus, by the equivariant Hopf bifurcation theorem, there are branches of two types small-amplitude periodic solutions near $\lambda = 0$. From the

Name	Isotropy Subgroup	Fixed Point Subspace	Dimension of Fixed Point Subspace
trivial state	$O(2) \times S^1$	$z_1 = z_2 = 0$	0
SW	$Z_2(\kappa) \times Z_2^c$	$z_1 = z_2$	2
TW	$\tilde{SO}(2)$	$z_2 = 0$	2
nonsymmetric	Z_2^c	$\mathbb{C}^2$	4

Table 2.1: Symmetries of solutions for the Hopf bifurcation with O(2) symmetry.

interpretation of these solutions for translation-symmetric systems with periodic boundary conditions, we call these solutions traveling waves (TW) and standing waves (SW) [34].

In order to study the stability properties of these solutions, we consider the normal form equations for the Hopf bifurcation with O(2) symmetry truncated at cubic order:

$$\dot{z}_1 = (\lambda + i\omega)z_1 + A(|z_1|^2 + |z_2|^2)z_1 + B|z_1|^2 z_1, \tag{2.9}$$

$$\dot{z}_2 = (\lambda + i\omega)z_2 + A(|z_1|^2 + |z_2|^2)z_2 + B|z_2|^2 z_2, \tag{2.10}$$

where z_1, z_2, A, B are complex, and λ and ω are real. We assume the nondegeneracy conditions $A_R + B_R \neq 0$, $2A_R + B_R \neq 0$, and $B_R \neq 0$. These equations are most conveniently studied by letting

$$z_1 = r_1 e^{i\theta_1}, \qquad z_2 = r_2 e^{i\theta_2},$$

which gives

$$\dot{r}_1 = \lambda r_1 + A_R(r_1^2 + r_2^2)r_1 + B_R r_1^3, \tag{2.11}$$

$$\dot{r}_2 = \lambda r_2 + A_R(r_1^2 + r_2^2)r_2 + B_R r_2^3, \tag{2.12}$$

$$\dot{\theta}_1 = \omega + A_I(r_1^2 + r_2^2) + B_I r_1^2, \tag{2.13}$$

$$\dot{\theta}_2 = \omega + A_I(r_1^2 + r_2^2) + B_I r_2^2, \tag{2.14}$$

Name	Solution	Eigenvalues
trivial	$r_1 = r_2 = 0$	$\lambda,\ \lambda$
TW	$r_1 = \left(\frac{-\lambda}{A_R+B_R}\right)^{1/2},\ r_2 = 0$	$-2\lambda,\ \frac{\lambda B_R}{A_R+B_R}$
SW	$r_1 = r_2 = \left(\frac{-\lambda}{2A_R+B_R}\right)^{1/2}$	$-2\lambda,\ \frac{-2\lambda B_R}{2A_R+B_R}$

Table 2.2: Fixed point solutions to equations (2.11,2.12). The TW and SW solutions correspond to periodic orbits in the full equations (2.9,2.10); these are the solutions guaranteed to bifurcate from the trivial state by the equivariant Hopf bifurcation theorem. The eigenvalues -2λ for TW and SW solutions are for radial stability. Note that the listed TW solution has a κ-related counterpart for which $r_1 = 0$, $r_2 \neq 0$.

where $A = A_R + iA_I$, etc. Equations (2.11,2.12) have decoupled, and have the fixed point solutions given in Table 2.2. From equations (2.13,2.14), it is seen that the TW and SW solutions are periodic orbits in the full equations (2.9,2.10); indeed, these are the solutions which are guaranteed to bifurcate from the trivial state by the equivariant Hopf bifurcation theorem. Note that the -2λ eigenvalue for the TW and SW solutions corresponds to radial stability.[9] Figure 2.13 shows the (A_R, B_R) plane together with bifurcation diagrams for each of the six distinct regions.

2.7.2 The Hopf Bifurcation with D_4 Symmetry

We now consider the Hopf bifurcation with D_4 symmetry, or the symmetry of the square [71]. Here the center eigenspace is also four-dimensional, with coordinates that may be taken as the complex variables z_+ and z_-. The group $D_4 = \langle \kappa_1, \kappa_2 \rangle$, where

$$\kappa_1 : (z_+, z_-) \to (z_+, -z_-), \qquad \kappa_2 : (z_+, z_-) \to (z_-, z_+).$$

[9] This eigenvalue comes from perturbations which preserve the character of the solution, e.g., the stability of a TW solution with $r_1 \neq 0$ to perturbations for which the r_1 component is nonzero but the r_2 component is zero.

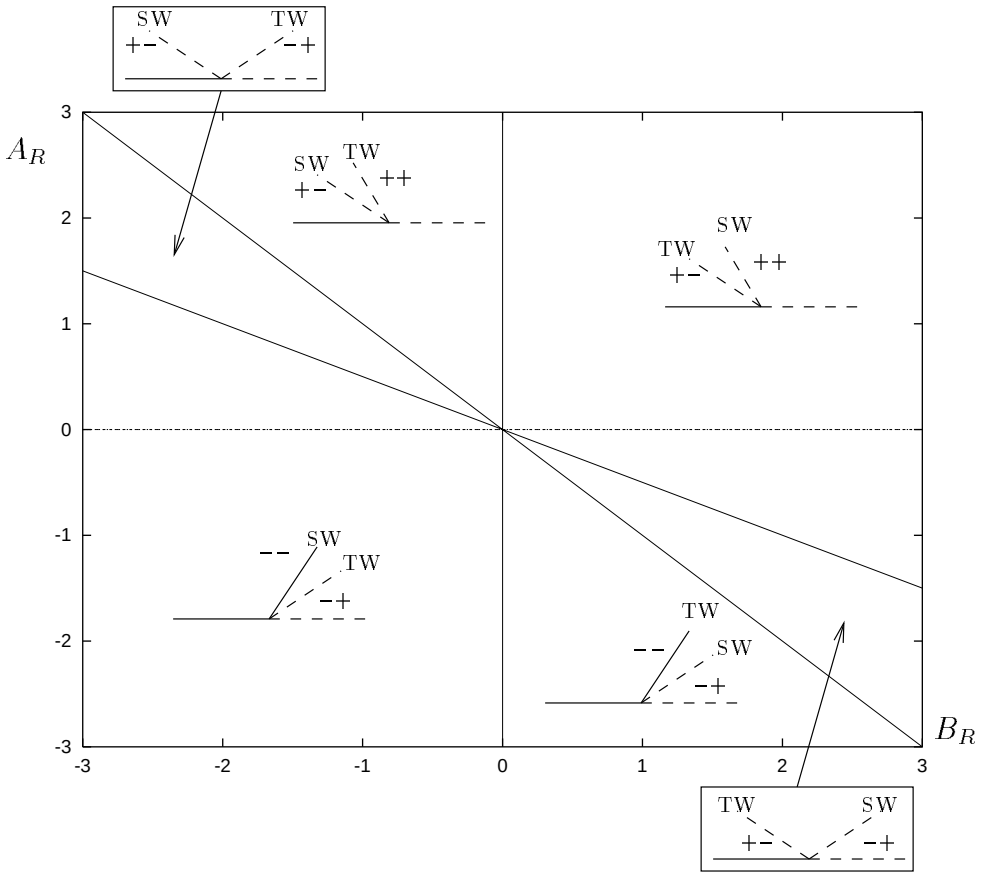

Figure 2.13: Possible bifurcation diagrams for the Hopf bifurcation with O(2) symmetry. Solid (dashed) lines are for stable (unstable) solutions. Here stability refers to *orbital stability*: the presence of continuous symmetry forces the TW and SW solutions to have neutral stability to perturbations along the group orbit generated by T_ϕ. The + and − signs denote the signs of the real parts of the eigenvalues determined by (2.11,2.12), with the first denoting radial stability or instability.

Name	Isotropy Subgroup	Fixed Point Subspace	Dimension of Fixed Point Subspace
trivial state	$\mathrm{D}_4 \times S^1$	$z_+ = z_- = 0$	0
u solution	$Z_2(\kappa_2) \times Z_2^c$	$z_+ = z_-$	2
v solution	$Z_2(N_{\pi/2}\kappa_2\kappa_1) \times Z_2^c$	$z_- = iz_+$	2
w solution	$Z_2(\kappa_1) \times Z_2^c$	$z_- = 0$	2
nonsymmetric	Z_2^c	$\mathbb{C}^2$	4

Table 2.3: Symmetries of solutions for the Hopf bifurcation with D_4 symmetry. The names of the solutions have been chosen to conform with the names from [71]. Notationally, $Z_2(\kappa_2)$ is the group $\langle\kappa_2\rangle$, which is isomorphic to Z_2, etc. $Z_2^c = \langle N_\pi(\kappa_2\kappa_1)^2\rangle$, and acts trivially on all points in $\mathbb{C}^2$.

The normal form symmetry is S^1, with action

$$N_\sigma : (z_+, z_-) \to e^{i\sigma}(z_+, z_-), \qquad \sigma \in [0, 2\pi).$$

The isotropy subgroups and fixed point subspaces for this problem are shown in Table 2.3. Thus, by the equivariant Hopf bifurcation theorem, there is a branch of small-amplitude periodic solutions of type u, v, and w near $\lambda = 0$. Let $\mathbf{z} = (z_+, z_-)$, and let $\mathbf{z_j}(t)$ be the type j solution with period T_j, where $j \in \{u, v, w\}$. Then, writing the action of the normal form symmetry in terms of a time shift, the periodic solutions are invariant under the nontrivial symmetries

$$\begin{aligned}
\mathbf{z_u}(t) &\to \kappa_2 \mathbf{z_u}(t), \\
\mathbf{z_v}(t) &\to \kappa_2\kappa_1 \mathbf{z_v}(t - T_v/4), \\
\mathbf{z_w}(t) &\to \kappa_1 \mathbf{z_w}(t).
\end{aligned}$$

Observe that $N_{\pi/2}$ corresponds to a time shift of one quarter period; $N_{2\pi}$ would correspond to a time shift of one full period. The trivial Z_2^c symmetry implies that $\mathbf{z_j}$ is invariant under

$$\mathbf{z_j}(t) \to (\kappa_2\kappa_1)^2\mathbf{z_j}(t - T_u/2), \qquad j \in \{u, v, w\}.$$

As stated above, the equivariant Hopf bifurcation theorem does not necessarily find all periodic solutions; as shown in [71], it is possible for nonsymmetric periodic orbits to also bifurcate from the origin.[10] The Hopf bifurcation with D_4 symmetry is described in more detail in Chapter 3, and the effects of breaking the interchange symmetry κ_2 and the normal form symmetry are described in Chapters 3 and 4, respectively.

2.8 Forced Symmetry-Breaking: A Preview

The pitchfork bifurcation is the generic steady bifurcation in systems with reflection symmetry. However, in real physical systems such a reflection symmetry is inevitably broken by imperfections. Thus, it is of interest to study how the dynamics associated with the pitchfork bifurcation are affected by the breaking of the reflection symmetry. In other words, it is of interest to study how *forced symmetry-breaking*, or the introduction of small perturbations that reduce the symmetry of a system, affects the dynamics.

In [72], it is shown that the *universal unfolding* of the supercritical pitchfork bifurcation is given by

$$\dot{x} = \lambda x - x^3 - \alpha - \beta x^2, \tag{2.15}$$

where α and β are unfolding parameters. This equation captures *all* possible effects of weak breaking of the reflection symmetry. Equation (2.15) is often referred to as the normal

[10] Also, quasiperiodic orbits may bifurcate from the origin (see [71] and Chapter 3).

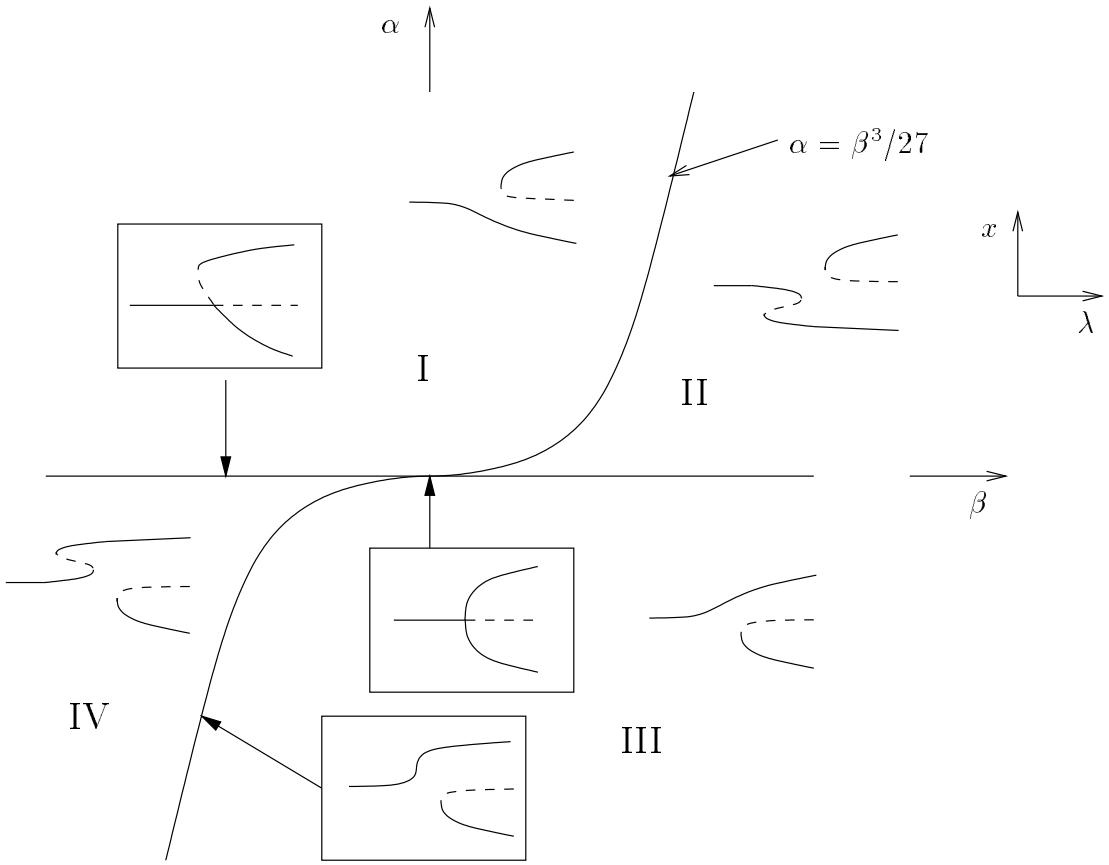

Figure 2.14: Bifurcation diagrams associated with the universal unfolding of the supercritical pitchfork bifurcation.

form for the *imperfect pitchfork bifurcation*; the associated bifurcation diagrams in the (α, β) unfolding space are shown in Figure 2.14. For $|\lambda|$ sufficiently large, the dynamics are always similar to that for the perfect pitchfork bifurcation ($\alpha = \beta = 0$). However, for small $|\lambda|$ the behavior changes. In regions II and IV, the branches disconnect so that as λ is quasistatically increased the trivial state loses stability in a saddle-node bifurcation, leading to a finite jump in the amplitude of the solution which is stable. This jump leads to hysteresis because the system response will be different for increasing or decreasing λ.

The other asymmetric solution can be stable, but since its branch is disconnected it can only be obtained by choosing suitable initial conditions. In regions I and III, the system evolves without hysteresis from negative λ to positive λ along the same branch as λ is quasistatically increased. The other asymmetric solution lies on a disconnected branch. For $\alpha = 0, \beta \neq 0$, the trivial state loses stability in a transcritical bifurcation. The curve $\alpha = \beta^3/27$ corresponds to the degeneracy in which the two saddle-node bifurcations on the branch have come together; this is known as a hysteresis bifurcation.

The remainder of this dissertation considers the effects of forced symmetry-breaking on the Hopf bifurcation with D_4 symmetry with applications to fluid dynamical systems. A universal unfolding is *not* derived for this bifurcation, so it cannot be argued that *all* possible types of dynamics which could arise due to weak symmetry-breaking are found. However, the behavior which *is* found is incredibly rich!

Chapter 3

Bursts in a Model of Large Aspect-Ratio Binary Fluid Convection

3.1 The Model

A binary fluid is a mixture of two miscible fluids such as water and ethanol or ^{3}He and ^{4}He. Convection in binary fluids can reveal phenomena which do not occur for convection in pure fluids (see, for example, pp. 998–1011 of [21]). Much of the richness of binary fluid convection comes from the fact that there are two contributions to the density gradient. One comes from thermal expansion, characterized by the coefficient of thermal expansion

$$\alpha \equiv -\frac{1}{\rho}\,\frac{\partial \rho}{\partial T},$$

where the partial derivative with respect to temperature T is taken at constant pressure p and concentration c. Typically $\alpha > 0$, so that heating from below causes a destabilizing density gradient. The other comes from a concentration gradient which is induced according to the Soret effect by the imposed temperature gradient.[1] This is characterized by the coefficient of solutal expansion

$$\beta \equiv -\frac{1}{\rho}\,\frac{\partial \rho}{\partial c},$$

where the partial derivative is taken at constant pressure and temperature. The net effect of the Soret effect on the stability of the system is described by the separation ratio

$$S \equiv -\frac{\beta}{\alpha}\, c\,(1-c)\, S_T,$$

where S_T is called the Soret coefficient. S is a property of a particular fluid mixture, and represents the ratio of the vertical density gradient induced by the Soret effect to that produced by thermal expansion. When $S < 0$, a destabilizing temperature gradient produces a stabilizing concentration gradient. Thus, the threshold for steady convection is elevated. However, as described in Figure 3.1, because the time scales for heat and mass diffusion typically differ substantially, the concentration gradient can temporally lag behind the thermal gradient leading to oscillations which set in at a lower Rayleigh number than that for the steady instability. Thus for $S < 0$, convection arises via a Hopf bifurcation.[2] For $S > 0$, convection arises via a steady bifurcation; since a destabilizing temperature gradient gives a destabilizing concentration gradient, the threshold for steady convection is

[1] We normally think of the concentration flux as being proportional to the concentration gradient, but the Soret effect implies that it also depends on the temperature gradient. A simple discussion of the Soret effect for a gas in terms of intermolecular forces is given in [73]. By analogy, the heat flux depends not only on the temperature gradient (as expected from the Fourier heat conduction law), but also on the concentration gradient; this is known as the Dufour effect, but it is negligible in liquids [21].

[2] There is a small region given by $S_{CT} < S < 0$ for which the stabilizing effect of the concentration gradient is not sufficiently strong to give rise to oscillatory behavior, so that onset is to steady convection.

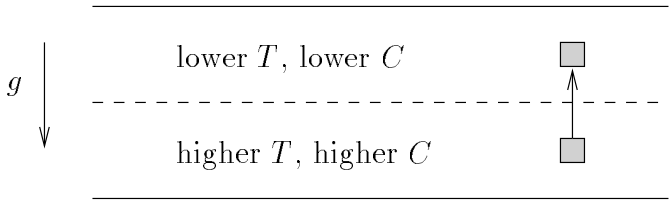

Figure 3.1: For $S < 0$, the Soret effect causes a destabilizing temperature gradient to produce a stabilizing concentration gradient, leading to the situation shown schematically here. Suppose that a small fluid element is displaced upwards as shown. The diffusion of heat is much faster than the diffusion of concentration so T equilibrates faster than C, resulting in the element being overdense relative to the ambient fluid. The element descends faster than it moved upwards because of the combination of its higher C and lower T, overshooting its original depth. This leads to exponentially growing oscillations which saturate due to nonlinear effects. Note that there is a small region $S_{CT} < S < 0$ for which the stabilizing effect of the concentration gradient is not sufficiently strong to overcome viscous drag, so oscillations do not occur.

lowered. The critical Rayleigh number R_c is shown schematically as a function of separation ratio in Figure 3.2. The cusp at $S = S_{CT}$ is a codimension two point corresponding to a double zero bifurcation [74].

In the Boussinesq approximation, binary fluid convection is described by the nondimensionalized equations [75]

$$\partial_t \mathbf{u} + (\mathbf{u}\cdot\nabla)\mathbf{u} = -\nabla p + PR[\theta(1+S) - S\eta]\hat{\mathbf{z}} + P\nabla^2\mathbf{u}, \tag{3.1}$$

$$\partial_t \theta + (\mathbf{u}\cdot\nabla)\theta = \mathbf{u}\cdot\hat{\mathbf{z}} + \nabla^2\theta, \tag{3.2}$$

$$\partial_t \eta + (\mathbf{u}\cdot\nabla)\eta = \tau\nabla^2\eta + \nabla^2\theta, \tag{3.3}$$

together with the incompressibility condition

$$\nabla\cdot\mathbf{u} = 0. \tag{3.4}$$

Here gravity acts in the $-\hat{\mathbf{z}}$ direction, $\mathbf{u}$ is the velocity field, p, θ and c denote the respective

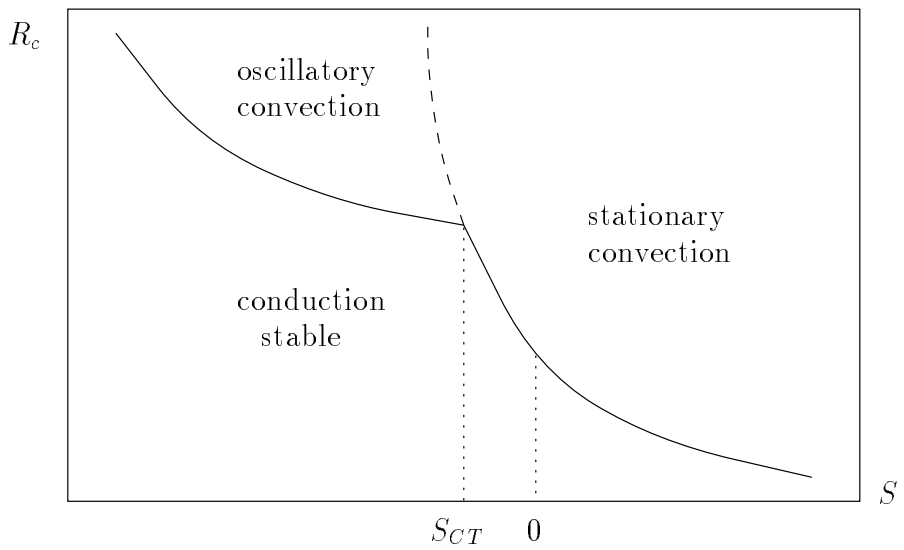

Figure 3.2: Critical Rayleigh number R_c versus separation ratio S (schematic). Note that $S_{CT} \lesssim 0$. For $S > S_{CT}$, the initial instability is via a steady bifurcation giving stationary convection. For $S < S_{CT}$, the initial instability is via a Hopf bifurcation giving oscillatory convection. The dashed line shows the marginal curve for steady convection for $S < S_{CT}$; however, oscillatory convection will set in for smaller R.

departures of the pressure, temperature and concentration fields from their conduction profiles, and $\eta \equiv \theta - c$. The system is specified by four dimensionless parameters: the separation ratio S defined above, the Prandtl number P and Rayleigh number R defined in (1.6), and the Lewis number $\tau \equiv \kappa_S/\kappa$, where κ_S is the mass diffusivity and κ is the thermal diffusivity. The boundary conditions appropriate to experiments are no-slip everywhere, with the temperature fixed at the top and bottom and no sideways heat flux. The final set of boundary conditions is provided by the requirement that there is no mass flux through any of the boundaries. Mathematically, the boundary conditions are $\mathbf{u} = \mathbf{n} \cdot \nabla\eta = 0$ on all boundaries where $\mathbf{n}$ is the unit normal to the boundary, $\theta = 0$ at the top and bottom, and $\partial_x\theta = 0$ at the sidewalls.

Of particular interest for this chapter is binary fluid convection in a container of large but finite aspect-ratio where the separation ratio of the mixture is sufficiently negative so that convection arises via a Hopf bifurcation. This is the case for the ^{3}He/^{4}He mixture used by Sullivan and Ahlers [76] in their experiment carried out in a rectangular container

$$D \equiv \left\{ x, y, z : -\frac{1}{2}\Gamma \leq x \leq \frac{1}{2}\Gamma, -\frac{1}{2}\Gamma_y \leq y \leq \frac{1}{2}\Gamma_y, -\frac{1}{2} \leq z \leq \frac{1}{2} \right\},$$

with aspect-ratio $\Gamma = 34$, and $\Gamma_y = 6.9$. The Prandtl and Lewis numbers were $P = 0.6, \tau = 0.03$. In this experiment, it was observed that immediately above threshold (the reduced Rayleigh number $\epsilon \equiv (R - R_c)/R_c = 3 \times 10^{-4}$) convective heat transport may take place in a sequence of irregular bursts of large dynamic range despite constant heat input. Here, dynamic range refers to the scaled range of amplitudes during each burst; such bursts are shown in Figure 3.3.

In this system the presence of sidewalls destroys translation symmetry in the x direction which would be present if the system were unbounded. However, with identical boundary conditions at the sidewalls the system retains a reflection symmetry about $x = 0$; the primary modes are thus either even or odd with respect to this reflection [2]. To describe the dynamical behavior near threshold we therefore suppose that the perturbation Ψ from the conduction state takes the form

$$\Psi(x, y, z, t) = \epsilon^{\frac{1}{2}} \mathrm{Re}\, \{ z_+(t) f_+(x, y, z) + z_-(t) f_-(x, y, z) \} + \mathcal{O}(\epsilon), \tag{3.5}$$

where $\epsilon \ll 1$, $f_\pm(-x, y, z) = \pm f_\pm(x, y, z)$. Here Ψ is a scalar quantity such as the temperature perturbation θ. Following [6], we now derive amplitude equations describing the evolution of the complex amplitudes z_+ and z_- using symmetry arguments. The requirement that a reflected state (obtained by letting $x \to -x$ in (3.5)) also be a state of the

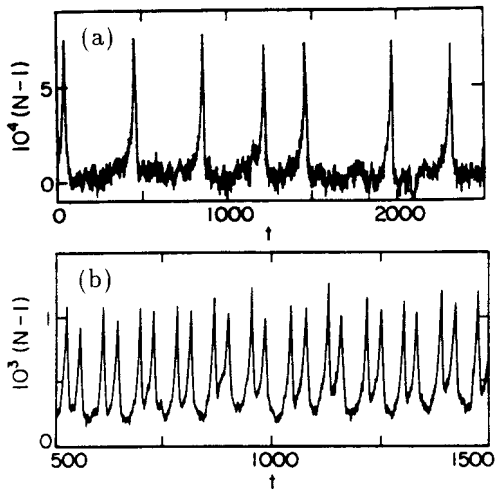

Figure 3.3: Bursts in binary fluid convection experiments with separation ratio $S = -0.021$ (see [76]). The Nusselt number N is the ratio of the actual heat transfer to what it would be if there was conduction but no convection. (a) $\epsilon = 3 \times 10^{-4}$, (b) $\epsilon = 3.6 \times 10^{-3}$. The dynamic range of the bursts, measured by the range of $(\mathrm{N}-1)/\epsilon$, decreases with increasing ϵ, while the burst frequency increases. Courtesy G. Ahlers.

system gives the requirement that the amplitude equations be equivariant with respect to the group action

$$\kappa_1 : (z_+, z_-) \to (z_+, -z_-). \tag{3.6}$$

Moreover, as argued by [6], the equations for the formally infinite system cannot distinguish between the two modes, so that in this limit the amplitude equations must also be equivariant with respect to the group action

$$\kappa_2 : (z_+, z_-) \to (z_-, z_+), \tag{3.7}$$

which we call an interchange symmetry. These two operations generate together the symmetry group D_4. For a container with large but finite length, this symmetry will be weakly broken; in particular, the even and odd modes typically become unstable at slightly different

Rayleigh numbers and with slightly different frequencies. The resulting equations are thus close to those for a 1:1 resonance, but with a special structure dictated by the proximity to D_4 symmetry. Finally, we may put the equations for z_+ and z_- into normal form; the normal form equations have the additional "phase shift" symmetry (see §2.3)

$$\hat{\sigma} : (z_+, z_-) \to e^{i\sigma}(z_+, z_-), \qquad \sigma \in [0, 2\pi). \tag{3.8}$$

Truncating the resulting equations at third order we obtain the amplitude equations[3]

$$\dot{z}_+ = [\lambda + \Delta\lambda + i(\omega + \Delta\omega)]z_+ + A(|z_+|^2 + |z_-|^2)z_+ + B|z_+|^2 z_+ + C\bar{z}_+ z_-^2, \tag{3.9}$$

$$\dot{z}_- = [\lambda - \Delta\lambda + i(\omega - \Delta\omega)]z_- + A(|z_+|^2 + |z_-|^2)z_- + B|z_-|^2 z_- + C\bar{z}_- z_+^2, \tag{3.10}$$

where the dot refers to differentiation with respect to time t, z_+, z_-, A, B, C are complex, and $\lambda, \Delta\lambda, \omega, \Delta\omega$ are real. These equations describe a Hopf bifurcation with broken D_4 symmetry. Here $\Delta\omega$ measures the difference in frequency between the two modes at onset, and $\Delta\lambda$ measures the difference in their linear growth rates. Under appropriate nondegeneracy conditions (which we assume here) we may neglect all interchange symmetry-breaking contributions to the nonlinear terms. We will see that when $\Delta\lambda$ and $\Delta\omega$ are nonzero, equations (3.9,3.10) can have bursting solutions. Thus, the bursting mechanism may be viewed as an interaction between spontaneous symmetry-breaking (in which case the trivial conduction state loses stability to a convecting state with less symmetry) and forced symmetry-breaking (in which the presence of sidewalls makes $\Delta\lambda$ and $\Delta\omega$ nonzero, thereby giving a Hopf bifurcation with broken D_4 symmetry).

[3]The equations are written using notation that allows us to make contact with earlier work of [71], who studied the Hopf bifurcation with *exact* D_4 symmetry, corresponding to $\Delta\lambda = \Delta\omega = 0$.

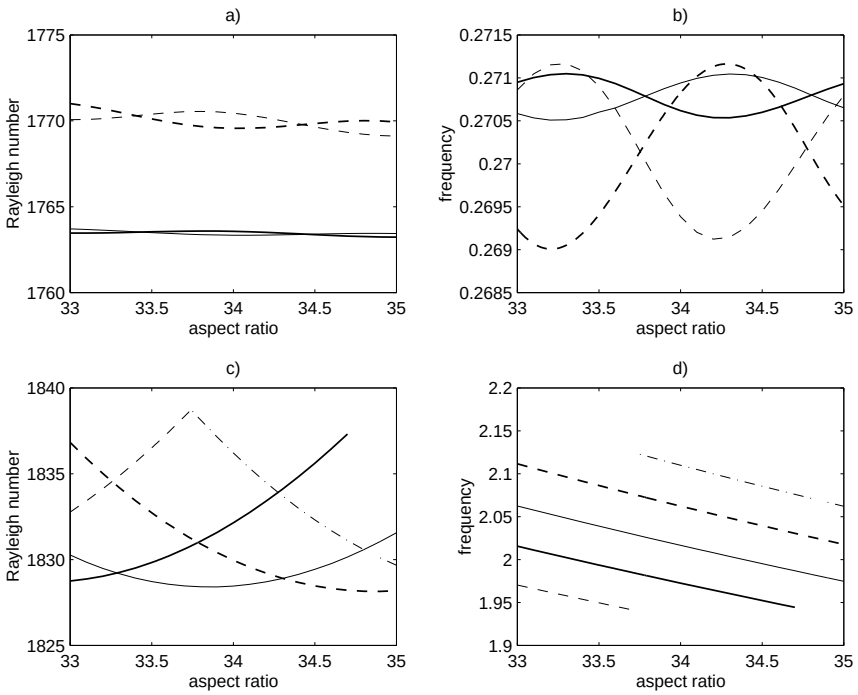

Figure 3.4: Onset of convection in ^{3}He/^{4}He mixtures ($P = 0.6$, $\tau = 0.03$) in large aspect-ratio containers. (a) Neutral stability curves and (b) corresponding frequencies for the first two even (thick lines) and the first two odd (thin lines) modes as a function of the aspect-ratio Γ for $S = -0.001$. (c,d) The same but for $S = -0.021$. Courtesy O. Batiste (see [77])

After being postulated in [6], the applicability of equations (3.9,3.10) to large aspect-ratio binary fluid convection was discussed in more detail in [77], in which the linear problem describing the stability properties of the conduction state $\mathbf{u} = \theta = \eta = 0$ to two-dimensional convection was solved numerically. Figure 3.4 shows results for parameter values used by Sullivan and Ahlers in their ^{3}He/^{4}He experiment, namely $P = 0.6$, $\tau = 0.03$, $\Gamma = 34.0$. The figure shows the neutral stability curves and corresponding frequencies for the first *four* modes in the range $33.0 \leq \Gamma \leq 35.0$ for $S = -0.001$ and $S = -0.021$. Observe that when $|S|$ is sufficiently small the first two families of neutral curves are separated by a gap

that is much larger than the amplitude of the "braids" within each family (Figure 3.4(a)). This is typical of what happens in Rayleigh-Bénard convection with non-Neumann boundary conditions [78] and makes it easy to justify projecting the fluid equations onto the first two modes that become unstable. However, the situation is not so simple. This is because this behavior does not persist for all Γ or all values of $|S|$. For larger values of these parameters the results take instead the form shown in Figures 3.4(c,d) which show the linear stability results for $S = -0.021$ and the same range of values of Γ as Figures 3.4(a,b). The modes from the different families now cross and the first unstable mode belongs to successively higher and higher families when extrapolated to small $|S|$ (see [77]). Figures 3.4(c,d) also show the crossing of two even modes involving a *nonresonant* double Hopf bifurcation. As discussed in detail in [77] the transition between the types of behavior shown in (a,b) and (c,d) of Figure 3.4 is mediated by a *resonant* 1:1 mode crossing at a somewhat smaller value of $|S|$. The experimental value of the separation ratio for the experiment by Sullivan and Ahlers, $S = -0.021$, corresponds to the "crossing" case, and the projection of the equations onto one odd and one even mode can only be rigorously justified in the neighborhood of appropriate mode crossing points.

We denote the growth rates and frequencies of the modes $z_\pm$ by $\lambda_\pm$ and $\omega_\pm$. For large aspect-ratios, the mode frequencies must go like $\omega_\pm \sim \omega_\infty + c_{1\pm}\Gamma^{-1} + c_{2\pm}\Gamma^{-2} + \cdots$. The fact that the frequency curves in Figure 3.4(d) are essentially parallel "straight lines" implies that $c_{1+} \approx c_{1-}$. Therefore, $\Delta\omega \equiv (\omega_+ - \omega_-)/2 = \mathcal{O}(\Gamma^{-2})$ for large Γ (see [77]). Moreover, as argued in [6], the parabolic minimum of the neutral stability curve leads to the expectation that $\Delta\lambda = \mathcal{O}(\Gamma^{-2})$. Thus, in the range $\lambda = \mathcal{O}(\Gamma^{-2})$, λ, $\Delta\lambda$, and $\Delta\omega$ are all of the

same order as $\Gamma \to \infty$, as required for the applicability of equations (3.9,3.10).[4] Of course, close enough to the mode crossing point $\Delta\lambda \ll \Delta\omega$, and in this region averaging methods can be used to eliminate the $(\bar{z}_+ z_-^2, \bar{z}_- z_+^2)$ terms from the mode interaction equations [6]. However, for typical values of $\Delta\lambda$ it appears likely that the system is correctly described by equations (3.9,3.10).

The first odd and even temperature eigenfunctions for $S = -0.021$ are shown in Figure 3.5 in the form of a space-time diagram, with time increasing upward. The eigenfunctions consist of waves propagating outwards from the center of the container; the amplitude has a local minimum at the center and increases outwards, peaking near the sidewalls. This type of eigenfunction was anticipated by [79] and is characteristic of eigenfunctions in systems with *positive* group velocity (although, strictly speaking, in a finite system one cannot define a group velocity since the allowed wave number is quantized by the sidewalls as well as being nonuniform). However, for the present purposes the most important observation is that for aspect-ratios as large as this, the odd and even eigenfunctions are essentially indistinguishable, as hypothesized by [6].

The remainder of this chapter is organized as follows. In §3.2 we discuss the symmetry properties of the equations describing the Hopf bifurcation with broken D_4 symmetry. In §3.3 we summarize the properties of the perfect D_4-symmetric system and identify parameter regimes in which heteroclinic cycles to infinity may form; excursions along these cycles are identified with bursting behavior. In §3.4 we describe the formation of such cycles when the D_4 symmetry is broken and illustrate the associated dynamics for several

[4]The frequency ω can be eliminated from equations (3.9,3.10) by letting $(z_+, z_-) \to e^{i\omega t}(z_+, z_-)$, a consequence of the normal form symmetry. Thus, there is no restriction on how ω must scale with the aspect-ratio Γ.

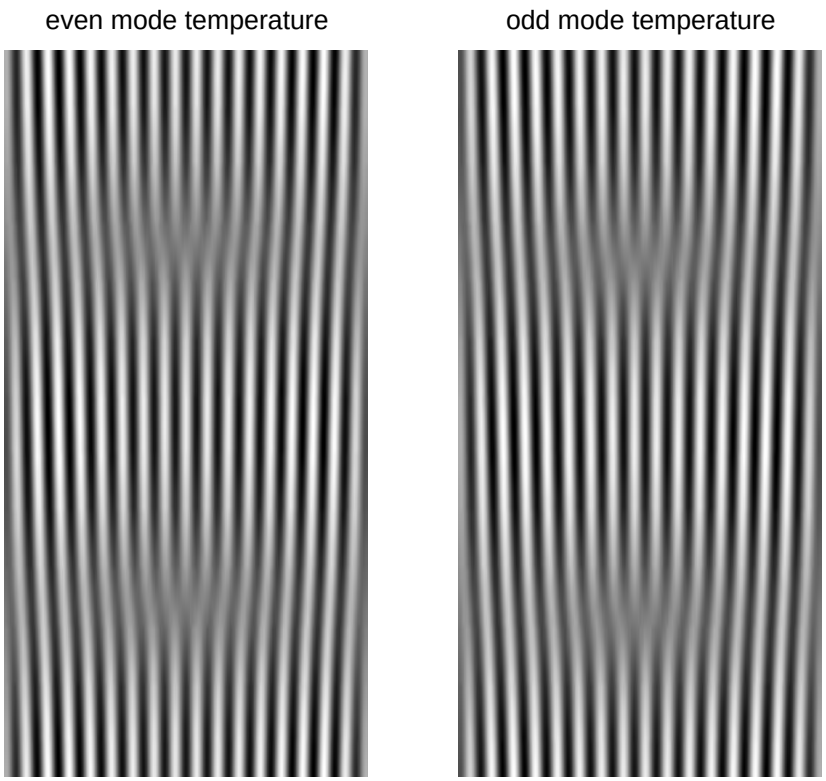

Figure 3.5: The first even and odd temperature eigenfunctions when $P = 0.6$, $\tau = 0.03$, $\Gamma = 34.0$ and $S = -0.021$ in the form of a space-time plot with time increasing upward. Courtesy O. Batiste (see [77]).

particular cases. In addition we identify a number of global bifurcations involving finite amplitude states. The analysis in this section is of necessity largely numerical and forms the bulk of the chapter. Throughout, the results will be interpreted for large aspect-ratio binary fluid convection. In §3.5 we discuss robustness of the results as the magnitude of the symmetry-breaking terms increases and investigate the effects of higher order terms. Concluding remarks are given in §3.6. Certain aspects of the analysis are relegated to Appendices A-D. Many of the results of this chapter have been published in [80, 81, 82].

3.2 Basic Equations and their Symmetries

When $\Delta\lambda = \Delta\omega = 0$, equations (3.9,3.10) have the symmetry $\mathrm{D}_4 \times S^1$, generated by the three operations

$$\kappa_1 : (z_+, z_-) \to (z_+, -z_-), \qquad \kappa_2 : (z_+, z_-) \to (z_-, z_+),$$

$$N_\sigma : (z_+, z_-) \to \mathrm{e}^{i\sigma}(z_+, z_-), \qquad \sigma \in [0, 2\pi).$$

The operations κ_1, κ_2 generate the group D_4; the remaining operation represents the action of the normal form symmetry S^1. When either $\Delta\lambda$ or $\Delta\omega$ are nonzero the symmetry is reduced to $Z_2 \times S^1$. [5] Consequently the only primary bifurcations are those to modes of odd or even parity [2].

In terms of the Swift variables [71] defined by

$$z_+ = r^{1/2}\cos(\theta/2)\mathrm{e}^{i(\phi+\psi)/2}, \qquad z_- = r^{1/2}\sin(\theta/2)\mathrm{e}^{i(-\phi+\psi)/2},$$

and a new time τ defined by $d\tau/dt = r$, equations (3.9,3.10) take the more convenient form

$$\frac{dr}{d\tau} = 2(\lambda + \Delta\lambda\cos\theta) + r[2A_R + B_R(1+\cos^2\theta) + C_R\sin^2\theta\cos 2\phi], \tag{3.11}$$

$$\frac{d\theta}{d\tau} = \sin\theta[\cos\theta(-B_R + C_R\cos 2\phi) - C_I\sin 2\phi] - \frac{2}{r}\Delta\lambda\sin\theta, \tag{3.12}$$

$$\frac{d\phi}{d\tau} = \cos\theta(B_I - C_I\cos 2\phi) - C_R\sin 2\phi + \frac{2}{r}\Delta\omega, \tag{3.13}$$

$$\frac{d\psi}{d\tau} = 2A_I + B_I + C_I\cos 2\phi + C_R\sin 2\phi\cos\theta + \frac{2\omega}{r}, \tag{3.14}$$

[5] Since $(\kappa_1)^2 = \mathrm{Id}$, $(N_\pi)^2 = \mathrm{Id}$, and $N_\pi \cdot \kappa_1 \cdot N_\pi = \kappa_1$, where Id is the identity element, we have that $\mathrm{D}_2 = \langle \kappa_1, N_\pi \rangle$. Thus, $Z_2 \times S^1 \cong \mathrm{D}_2 \times S^1$, where $\sigma \in [0, 2\pi)$ for the S^1 symmetry for the $Z_2 \times S^1$ symmetry, and $\sigma \in [0, \pi)$ for the $\mathrm{D}_2 \times S^1$ symmetry. Therefore, breaking the interchange symmetry may be thought of as reducing the D_4 symmetry to Z_2 or D_2.

where $A = A_R + iA_I$, etc. It will also sometimes be useful to consider the (u, v, w) coordinates defined by

$$u + iv = r \sin\theta \, \mathrm{e}^{i\phi} = 2z_+ \bar{z}_-,$$

$$w = r\cos\theta = |z_+|^2 - |z_-|^2,$$

$$\mathrm{e}^{i\psi} = \frac{z_+ z_-}{|z_+ z_-|}.$$

In these coordinates, equations (3.9,3.10) become

$$\frac{du}{dt} = 2\lambda u - 2\Delta\omega \, v + (2A_R + B_R + C_R)ru - (B_I + C_I)vw, \tag{3.15}$$

$$\frac{dv}{dt} = 2\lambda v + 2\Delta\omega \, u + (2A_R + B_R - C_R)rv + (B_I - C_I)uw, \tag{3.16}$$

$$\frac{dw}{dt} = 2\Delta\lambda \, r + 2\lambda w + 2(A_R + B_R)rw + 2C_I uv, \tag{3.17}$$

$$\frac{d\psi}{dt} = 2\omega + r\left(2A_I + B_I + C_I\frac{u^2 - v^2}{u^2 + v^2} + 2C_R\frac{uvw}{r(u^2 + v^2)}\right). \tag{3.18}$$

As a consequence of the S^1 symmetry of equations (3.9,3.10) the variable ψ decouples in both cases. In the following we refer to the equivalent sets of equations (3.11-3.13) and (3.15-3.17) as the *three-dimensional* system. Since ψ (modulo 4π) is periodic in time both for fixed points and periodic solutions of the three-dimensional system, such solutions in fact correspond respectively to periodic solutions and quasiperiodic solutions (tori) in the original four-dimensional system (3.9,3.10). The invariance of the system (3.11-3.14) with respect to reflections in the plane $\theta = \pi$ and the translations $\theta \to \theta + 2\pi$, $\phi \to \phi + \pi$ enables us to restrict the variables (θ, ϕ, ψ) to the intervals $0 \le \theta < \pi$, $0 \le \phi < \pi$, $0 \le \psi < 4\pi$. These symmetries imply that if (r, θ, ϕ) is a solution of equations (3.11-3.13) so are $(r, 2\pi - \theta, \phi)$ and $(r, \theta + 2m\pi, \phi + n\pi)$, where m and n are integers. However, since the restriction $0 \le \phi < \pi$ identifies symmetry-related solutions with distinct physical manifestations (for example,

the winking states described in §3.4 with bursts localized on the left or right side of the container would be identified), we continue using the range $-2\pi \leq \phi < 2\pi$. In the (u, v, w) variables,

$$\kappa_1 : (u, v, w) \to (-u, -v, w), \qquad \kappa_2 : (u, v, w) \to (u, -v, -w).$$

Thus, since equations (3.15-3.17) still have the reflection symmetry κ_1, if (u_0, v_0, w_0) is a solution then so is $(-u_0, -v_0, w_0)$. Consequently, a solution that is not invariant under κ_1 will have a κ_1-related counterpart. In the following we use $r = |z_+|^2 + |z_-|^2 = \sqrt{u^2 + v^2 + w^2}$ as a useful measure of the amplitude of the perturbation from the trivial state.

Equations (3.9,3.10) also have additional symmetries called parameter symmetries. For a parametrized family of ODEs given by $\dot{X} = f(X, \Lambda)$, Swift [71] defines a *parameter symmetry* as a symmetry of the extended system $\dot{X} = f(X, \Lambda), \dot{\Lambda} = 0$ such that

$$f(\gamma_x X, \gamma_\Lambda \Lambda) = \gamma_x f(X, \Lambda),$$

where γ_x is a group action on the phase space variables and γ_Λ is a group action on the parameters. This is to be distinguished from a *true symmetry* in which the group acts only on the phase space variables. The parameter symmetries are most easily given in the (u, v, w, ψ) variables; it is readily verified that the following group actions are parameter symmetries of equations (3.15-3.18):

$$P_2 : \quad (u, v, w, \psi) \to (-v, -u, -w, \psi)$$

$$(A, B, C, \lambda, \omega, \Delta\lambda, \Delta\omega) \to (A, B, -C, \lambda, \omega, -\Delta\lambda, -\Delta\omega),$$

$$P_3 : \quad (u, v, w, \psi) \to (u, v, w, \psi)$$

$$(A, B, C, \lambda, \omega, \Delta\lambda, \Delta\omega; t) \to (-A, -B, -C, -\lambda, -\omega, -\Delta\lambda, -\Delta\omega; -t),$$

$$P_4: \quad (u,v,w,\psi) \to (-u,-v,-w,-\psi)$$

$$(A,B,C,\lambda,\omega,\Delta\lambda,\Delta\omega) \to (\bar{A},\bar{B},\bar{C},\lambda,-\omega,-\Delta\lambda,\Delta\omega).$$

If $\Delta\lambda = \Delta\omega = 0$ and we restrict attention to the reduced phase space (u,v,w) an additional parameter symmetry is present:

$$P_1: \quad (u,v,w) \to (v,w,u)$$

$$(A,B,C,\lambda) \to (A+B-C, -\frac{1}{2}B+\frac{3}{2}C, -\frac{1}{2}B-\frac{1}{2}C, \lambda).$$

This symmetry is relevant to the *perfect* system, $\Delta\lambda = \Delta\omega = 0$, only.

3.3 The Perfect System ($\Delta\lambda = \Delta\omega = 0$): The Hopf Bifurcation with D_4 Symmetry

When the D_4 symmetry is exact ($\Delta\lambda = \Delta\omega = 0$), equations (3.12,3.13) for $\theta(\tau)$ and $\phi(\tau)$ decouple from the others. We may think of this two-dimensional system as describing dynamics on the surface of a *sphere* of variable radius $r(\tau)$ and refer to it, following Swift [71], as the associated spherical system. The radius $r(\tau)$ corresponding to a given solution of this system can be found by integrating the r-equation evaluated on this solution.

The fixed points (θ_0, ϕ_0) of the associated spherical system are summarized in Table 3.1 and correspond to periodic solutions to equations (3.9,3.10). This table summarizes the terminology we shall use to refer to the various solutions and defines the u, v and w fixed points in both the (θ,ϕ) and (u,v,w) variables. Recall that the isotropy subgroup is the set of group elements of $D_4 \times S^1$ which act as the identity on the solution (see §2.7). The isotropy subgroups reported in Tables 2.3 and 3.1 are obviously related, but differ because

Name	Isotropy Subgroup	(θ_0, ϕ_0)	(u_0, v_0, w_0)
u solution	$Z_2(\kappa_2) \times Z_2^c$	$\cos\theta_0 = 0$ $\cos 2\phi_0 = 1$	$v_0 = w_0 = 0$
v solution	$Z_2(\kappa_2\kappa_1) \times Z_2^c$	$\cos\theta_0 = 0$ $\cos 2\phi_0 = -1$	$u_0 = w_0 = 0$
w solution	$Z_2(\kappa_1) \times Z_2^c$	$\sin\theta_0 = 0$	$u_0 = v_0 = 0$
ns solution	Z_2^c	$\sin^2\theta_0 = \frac{\lvert C\rvert^2(\lvert B\rvert^2 - \lvert C\rvert^2)}{\lvert B\rvert^2\lvert C\rvert^2 - [\mathrm{Re}(B\bar{C})]^2}$ $\cos 2\phi_0 = \frac{\mathrm{Re}(B\bar{C})}{\lvert C\rvert^2}$	

Table 3.1: Fixed point solutions in the associated spherical system for the perfect system ($\Delta\lambda = \Delta\omega = 0$). These correspond to periodic orbits in the full four-dimensional system. The ns solutions only exist in the open regions of parameter space defined by $|B|^2 > |C|^2, |C|^2 > |\mathrm{Re}(B\bar{C})|$, and their form in the (u, v, w) variables is omitted. The isotropy subgroup is given in terms of its action on the (u, v, w) space. Notationally, $Z_2(\kappa_2)$ is the group $\langle\kappa_2\rangle$, which is isomorphic to Z_2, etc. $Z_2^c \equiv \langle(\kappa_2\kappa_1)^2\rangle$, and acts trivially on all points.

of the different variables: in the (u, v, w) variables the phase ψ has decoupled, so elements of the normal form symmetry do not appear in the isotropy subgroup in these variables. Note that the equivariant Hopf bifurcation from §2.7 only guaranteed the existence of u, v, and w solutions; it could not capture the possibility of periodic ns solutions. The amplitude of the solutions is given by

$$r = -\frac{2\lambda}{F(\theta_0, \phi_0)} > 0,$$

where

$$F(\theta, \phi) = 2A_R + B_R(1 + \cos^2\theta) + C_R \sin^2\theta \cos 2\phi.$$

Thus, if $F(\theta_0, \phi_0) < 0$ the fixed point branch bifurcates supercritically, while if $F(\theta_0, \phi_0) > 0$ the branch bifurcates subcritically. In the binary fluid context the u, v and w solutions represent mixed parity traveling wave states localized near one of the container walls, mixed parity chevron (or counterpropagating) states, and pure even ($\theta = 0$) or odd ($\theta = \pi$) parity chevron states, respectively [6]. Such states are shown in Figure 3.6 using the approximate eigenfunctions

$$f_{\pm}(x) = \left\{e^{-\gamma x + ix} \pm e^{\gamma x - ix}\right\} \cos\frac{\pi x}{L}, \tag{3.19}$$

where $\gamma = 0.15 + 0.025i$, $L = 80$ and $-\frac{L}{2} \leq x \leq \frac{L}{2}$. The ns solutions represent periodic waves which lack all non-trivial symmetry properties.

Swift also proved that in open regions of parameter space there exists a periodic orbit $(\theta^*(\tau), \phi^*(\tau))$ in the associated spherical system corresponding to a quasiperiodic solution (hereafter qp) to equations (3.9,3.10). The qp branch bifurcates supercritically from the trivial state if $\bar{F} < 0$ and subcritically if $\bar{F} > 0$, where

$$\bar{F} = \frac{1}{T_\tau}\int_0^{T_\tau} F(\theta^*(\tau'), \phi^*(\tau'))d\tau',$$

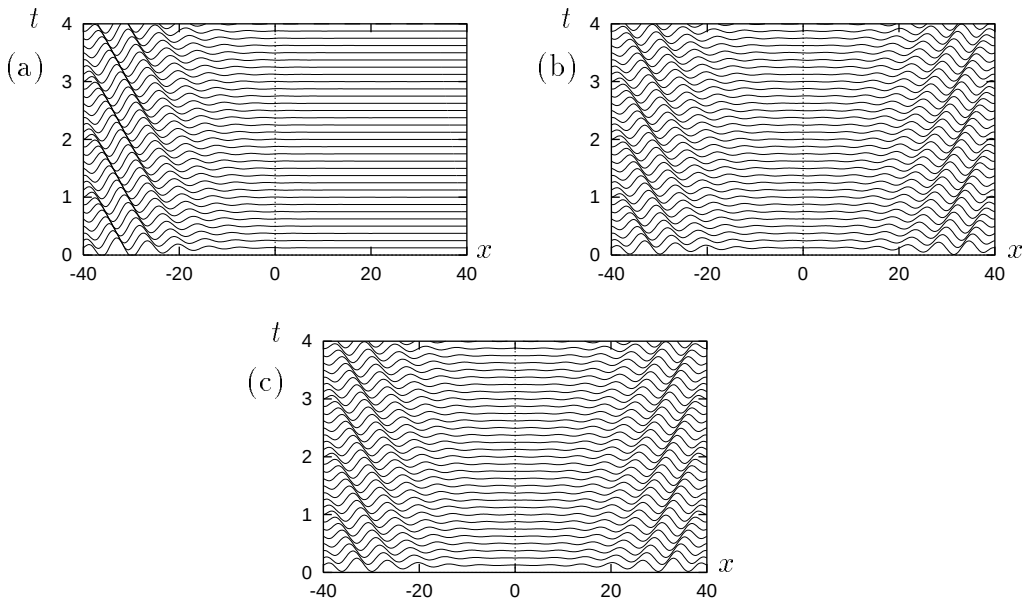

Figure 3.6: Space-time plots showing the perturbation Ψ from the trivial state for fixed point solutions of the associated spherical system with (a) $\theta_0 = \pi/2, \phi_0 = 0$ (u solution, mixed parity, identified with a traveling wave), (b) $\theta_0 = \phi_0 = \pi/2$ (v solution, mixed parity, identified with a mixed parity standing wave), (c) $\theta_0 = 0$ (w_e solution, even in x, identified with a standing wave). Time increases upwards, and the time axis is rescaled so that the perturbation has a period of 1. The identifications follow [6]. States consisting of oppositely traveling waves in the two halves of the container (here the v and w states) are often called chevron states.

and T_τ is the period of the orbit (cf. [83]), and can take the form of either a *libration* (where after one period the variable ϕ returns to its original value) or a *rotation* (where after one period the variable ϕ increases by a nonzero multiple of π) [84].

Table 3.2 summarizes the linear stability properties of the fixed point solutions of the three-dimensional system (3.11-3.13); note that in these equations the time τ is used. The branches are radially stable (unstable) if they bifurcate supercritically (subcritically) from the trivial state. The dependence of the angular eigenvalues of the solutions on parameters can be simplified using the parameter symmetries and rescaling time to restrict

solution	eigenvalues
u	$s_1^u \equiv 2A_R + B_R + C_R$ $\{s_2^u, s_3^u\}$: $s_2^u + s_3^u = B_R - 3C_R$ $s_2^u s_3^u = 2(C_R^2 + C_I^2 - B_R C_R - B_I C_I)$
v	$s_1^v \equiv 2A_R + B_R - C_R$ $\{s_2^v, s_3^v\}$: $s_2^v + s_3^v = B_R + 3C_R$ $s_2^v s_3^v = 2(C_R^2 + C_I^2 + B_R C_R + B_I C_I)$
w	$s_1^w \equiv 2(A_R + B_R)$ $\{s_2^w, s_3^w\}$: $s_2^w + s_3^w = -2B_R$ $s_2^w s_3^w = \|B\|^2 - \|C\|^2$
ns	$s_1^{ns} \equiv 2A_R + \frac{B_R\left[\|C\|^2(\|B\|^2+\|C\|^2) - 2(\mathrm{Re}(B\bar{C}))^2\right] + C_R(\|B\|^2 - \|C\|^2)\mathrm{Re}(B\bar{C})}{\|B\|^2\|C\|^2 - (\mathrm{Re}(B\bar{C}))^2}$

Table 3.2: Eigenvalues for fixed point solutions of the three-dimensional system (3.11-3.13) for the perfect problem. The radial eigenvalue s_1 is the amplitude eigenvalue and corresponds to perturbations with no component in the θ or ϕ direction, while the angular eigenvalues s_2 and s_3 correspond to perturbations in the associated spherical system. The radial eigenvalue for a fixed point with $(\theta, \phi) = (\theta_0, \phi_0)$ is $F(\theta_0, \phi_0)$, so if the radial eigenvalue is positive (negative) the branch bifurcates subcritically (supercritically). The ns fixed points are always saddles in the associated spherical system; thus $s_2^{ns} s_3^{ns} < 0$ [71]. The expressions for the determinants in the lower table on p. 361 of [71] are all too small by a factor of 2.

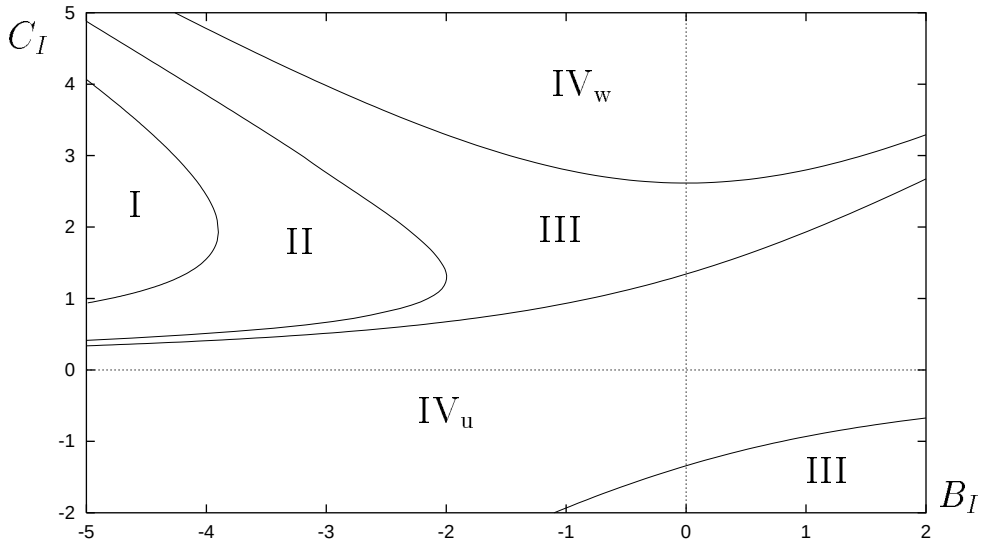

Figure 3.7: Distinct regions of parameter space with $B_R = -2.8$ and $C_R = -1$. The boundaries between regions I and II (given by $s_2^v s_3^v = 0$), III and IV_w (given by $s_2^w s_3^w = 0$), and III and IV_u (given by $s_2^u s_3^u = 0$) correspond to the condition for a pitchfork bifurcation of the v, w, and u fixed points, respectively; this bifurcation leads to the creation or destruction of ns solutions which exist only in regions II and III. The boundary between regions II and III corresponds to the condition that a heteroclinic orbit connecting two ns solutions forms, creating or destroying the qp solutions; the location of this boundary must be found numerically. Similar regions of parameter space exist for other values of B_R in the range $-3 < B_R < -1$ with $C_R = -1$.

attention to the parameter range

$$-3 < B_R < -1, \quad C_R = -1.$$

We may also restrict attention to the case $B_I < 0$. Appendix A describes how to deduce the properties of solutions for parameters which do not lie within this range. Note that the parameter symmetry can change a libration to a rotation and vice versa. For fixed B_R and C_R, the (B_I, C_I) plane may be divided into distinct regions (see Figure 3.7); the stability properties of the solutions in these regions are summarized in Table 3.3, and typical phase portraits for each region are shown in Figure 12 of [71]. As $B_R \to C_R$ the qp solution may approach a heteroclinic orbit connecting a pair of symmetry-related v

region	solution	properties
I	u	source
	v	saddle
	w	source
	ns	absent
	qp	sink
II	u	source
	v	sink
	w	source
	ns	saddle
	qp	sink
III	u	source
	v	sink
	w	source
	ns	saddle
	qp	absent
$\mathrm{IV_w}$	u	source
	v	sink
	w	saddle
	ns	absent
	qp	absent
$\mathrm{IV_u}$	u	saddle
	v	sink
	w	source
	ns	absent
	qp	absent

Table 3.3: Existence and angular stability properties of all solutions for $-3 < B_R < -1$ and $C_R = -1$. For given parameters the region is determined by the values of B_I and C_I (see Figure 3.7). In this parameter range the qp solutions are attractors if they exist and hence are sinks within the associated spherical system.

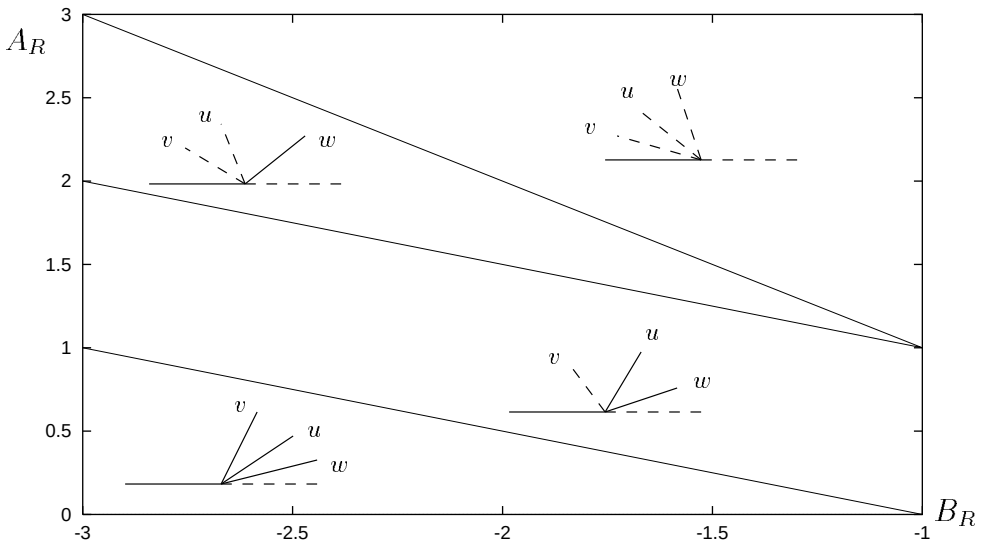

Figure 3.8: Possible bifurcation diagrams for $-3 < B_R < -1$, $C_R = -1$. Here, a solid (dashed) line indicates *radial* stability (instability) only. Only u, v, and w solutions are shown; the possibilities including *qp* and *ns* solutions are discussed in Appendix C.

fixed points (see Appendix B), and as $B_R \to 3C_R$ the *qp* solution approaches a u solution, with a Hopf bifurcation occurring at $B_R = 3C_R$. The dependence of the radial stability on parameters for the u, v, and w solutions may be easily deduced from the radial eigenvalues in Table 3.2; the resulting possibilities are shown in Figure 3.8. The radial stability of the *ns* and *qp* solutions is not discussed in [71] but may be understood through a combination of analytical and numerical arguments, a summary of which appears in Appendix C. A useful observation is that A_R may be thought of as controlling the radial stability of the solutions: as A_R increases with all other parameters held fixed it becomes more likely for any of the solutions to bifurcate subcritically.

3.4 Bursts in the Imperfect System ($\Delta\lambda \neq 0$, $\Delta\omega \neq 0$)

3.4.1 Burst Mechanism

As shown numerically in [6], breaking the D_4 symmetry leads to the possibility of bursting behavior for certain parameter values. Here we will elucidate the mechanism by which these bursts occur.

For the equations with broken D_4 symmetry ($\Delta\lambda \neq 0$ and/or $\Delta\omega \neq 0$) only the fixed points with even and odd parity remain as primary branches; these are the analogs of the w fixed points for the three-dimensional perfect system and are given by [6]

(i) w_e solution (even)

$$u = v = 0, \qquad r = w = \frac{-\lambda - \Delta\lambda}{A_R + B_R}; \qquad \theta = 0, \tag{3.20}$$

(ii) w_o solution (odd)

$$u = v = 0, \qquad r = -w = \frac{-\lambda + \Delta\lambda}{A_R + B_R}; \qquad \theta = \pi. \tag{3.21}$$

These solutions only exist for $r > 0$. The analogs of the remaining primary branches may bifurcate in secondary bifurcations from these or they may form disconnected branches; they are most easily found numerically.

To make the large amplitude behavior associated with bursts more manageable we let $\rho = 1/r$ in equations (3.11-3.13), giving

$$\frac{d\rho}{d\tau} = -\rho[2A_R + B_R(1 + \cos^2\theta) + C_R \sin^2\theta \cos 2\phi] - 2(\lambda + \Delta\lambda \cos\theta)\rho^2, \tag{3.22}$$

$$\frac{d\theta}{d\tau} = \sin\theta[\cos\theta(-B_R + C_R \cos 2\phi) - C_I \sin 2\phi] - 2\Delta\lambda \sin\theta\rho, \tag{3.23}$$

$$\frac{d\phi}{d\tau} = \cos\theta(B_I - C_I \cos 2\phi) - C_R \sin 2\phi + 2\Delta\omega\rho. \tag{3.24}$$

These equations have an important *invariant* subspace $\Sigma \equiv \{(\rho, \theta, \phi)|\rho = 0\}$ corresponding to *infinite* amplitude states. The invariance of this subspace lies at the heart of the bursting mechanism described below. In this subspace equations (3.23,3.24) reduce to equations (3.12,3.13) with $\Delta\lambda = \Delta\omega = 0$, i.e., to the perfect system. Thus the fixed points, limit cycles and heteroclinic orbits in the associated spherical system that governs the dynamics of the perfect system continue to exert significant effect on all large amplitude states of the imperfect system, and it is in this sense that the perfect system organizes the dynamics of the imperfect one. In the following we label the infinite amplitude fixed points by analogy to the (finite amplitude) fixed points for the perfect problem; for example, u_∞ fixed points have $\rho = 0, \cos\theta = 0, \cos 2\phi = 1,$ etc.

Because of the above relation between the two systems, the angular eigenvalues (Floquet multipliers) of any infinite amplitude fixed points (limit cycles) in the imperfect system are identical to those of the corresponding solution of the associated spherical system for the perfect problem already computed, i.e., $s_2^{u_\infty} = s_2^u$, $s_3^{u_\infty} = s_3^u$, etc. Equations (3.11) and (3.22) show that that the radial eigenvalue of an infinite amplitude fixed point in terms of the ρ variable is the negative of the radial eigenvalue of the corresponding finite amplitude fixed point in terms of the r variable. Thus, if a finite amplitude fixed point in the perfect system is radially unstable the corresponding infinite amplitude fixed point in the imperfect system is radially stable, and vice versa; a similar statement holds for the qp solutions. In particular, if a solution branch is subcritical in the perfect system there is a corresponding infinite amplitude solution of the imperfect system which is radially stable for $\lambda > 0$. In our scenario, a burst occurs for $\lambda > 0$ when a trajectory follows the stable

manifold of a fixed point (or a limit cycle) B $\in \Sigma$ that is *unstable* within Σ. The instability within Σ then kicks the trajectory towards another fixed point (or limit cycle) A $\in \Sigma$. If this point has an unstable ρ eigenvalue the trajectory escapes from Σ towards finite amplitudes, forming a burst. If $\Delta\lambda$ and/or $\Delta\omega \neq 0$ a value of λ may be found for which the unstable manifold of A lies within the stable manifold of B forming a heteroclinic cycle B $\rightarrow$ A $\rightarrow$ B. The bursts then repeat. We now classify all cycles of this type.

3.4.2 Codimension One Heteroclinic Cycles Involving Infinite Amplitude Solutions

Bursting behavior occurs for parameter values near those for which a heteroclinic cycle exists between infinite amplitude solutions. To specify a heteroclinic cycle we identify symmetry-related solutions (technically, we identify solutions with conjugate isotropy subgroups, i.e., solutions on the same group orbit, see §2.7 and [85]). Such a cycle between two infinite amplitude ($\rho = 0$) solutions A and B will exist if the following conditions hold:

(i) A is supercritical and B is subcritical for the perfect problem.

(ii) There is a trajectory B $\rightarrow$ A in the Σ subspace; this is possible if, within this subspace, or equivalently, for the perfect problem within the associated spherical system,

(a) B = source and A = sink,

(b) B = source and A = saddle,

(c) B = saddle and A = sink, or

(d) B = saddle and A = saddle.

Table 3.3 lists possible candidates for A and B when $-3 < B_R < -1, C_R = -1$. The

connecting trajectories are structurally stable to changes in λ because the dynamics in the $\rho = 0$ subspace are independent of λ.

(iii) There is a trajectory A $\rightarrow$ B out of the Σ subspace which exists for some value of the bifurcation parameter λ. The existence of such a trajectory must be demonstrated numerically.

Since the existence of the resulting heteroclinic cycle depends only on the parameter λ, it is a codimension one phenomenon. To enumerate all situations for which a heteroclinic cycle of this type may exist, we restrict attention to the parameter range $-3 < B_R < -1, C_R = -1$. For this parameter range, periodic orbits and heteroclinic orbits in the associated spherical system are considered to be sinks (see Tables 3.3 and B.1) and we deduce that the only possible ways to satisfy conditions (i) and (ii) are those shown in Figure 3.9.[6] By using parameter symmetries we can find possible heteroclinic cycles between other types of infinite amplitude solutions. In particular since these symmetries can change the *qp* solution from a libration present in the above parameter range to a rotation in other regimes the parameter symmetries can be used to generate necessary conditions for heteroclinic cycles involving rotations. However, since the trajectory from A $\rightarrow$ B out of the Σ subspace described in condition (iii) is not necessarily preserved under the action of a parameter symmetry its presence must be demonstrated numerically for each set of parameters. Note that no cycles involving the heteroclinic orbit separating librations and rotations in the associated spherical system are possible. For heteroclinic cycles involving

[6]Conditions (i) and (ii) may be satisfied for perfect D_4 symmetry ($\Delta\lambda = \Delta\omega = 0$), but there are no *attractors* associated with these cycles unless the symmetry is broken ($\Delta\lambda \neq 0$ and/or $\Delta\omega \neq 0$). The attractors for $\lambda > 0$ for the cases shown in Figure 3.9 in which the D_4 symmetry is exact are (a) v_∞, (b) v_∞, (c) *qp*, and (d) both *qp* and v_∞. The presence of such attractors prevents repeated bursting behavior.

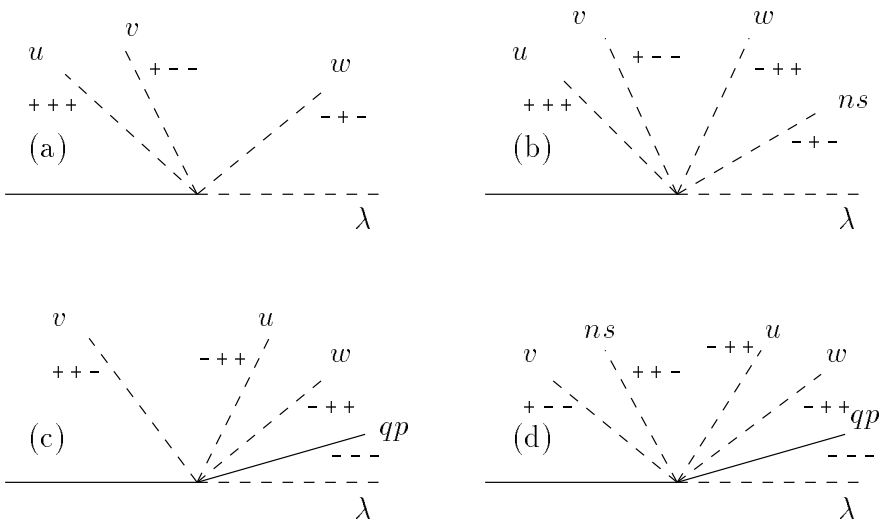

Figure 3.9: All bifurcation diagrams for the perfect system with the connections B $\rightarrow$ A of the type required for the existence of heteroclinic cycles involving infinite amplitude solutions when $-3 < B_R < -1, C_R = -1$ and B_I and C_I are chosen to be in (a) region IV_w (A $= w$, B $= u$), (b) region III (A $= ns$, B $= u$), (c) region I (A $= qp$, B $= v$), (d) region II (A $= qp$, B $= ns$). Solid (dashed) lines indicate stable (unstable) solution branches. The signs of the eigenvalues are indicated by + and $-$, with the first indicating radial stability. Parameter symmetries allow one to find possible heteroclinic connections involving other types of infinite amplitude solutions. For the heteroclinic cycle to exist there must also be a trajectory from A $\rightarrow$ B out of the Σ subspace. The branch names are defined in §3.3.

infinite amplitude solutions the trajectory reaches and returns from infinity in finite time t (see Appendix D); such heteroclinic cycles thus describe bursts of *infinite* dynamic range but *finite* duration.

We now briefly describe some results of the analysis of such heteroclinic cycles; these are illustrated in the examples which follow. The heteroclinic cycles may be analyzed within the three-dimensional system (3.11-3.13). First, suppose that A and B are infinite amplitude ($\rho = 0$) fixed points in this system. If A (B) has complex (real) eigenvalues in Σ, a Shil'nikov-like analysis is possible (see §2.6.3). The analysis shows that a periodic solution branch may undergo an infinite number of saddle-node bifurcations $\{\lambda_n\}$ as the

branch is followed to higher period, with $\lambda_{2j} \to \lambda_c+$ and $\lambda_{2j+1} \to \lambda_c-$ as $j \to \infty$. Here λ_c is the parameter value at which the heteroclinic cycle forms. If A is an infinite amplitude limit cycle (i.e., A $= qp_\infty$) and B is an infinite amplitude fixed point, an analysis along the lines of [70] becomes possible provided parameters (such as C_R) are chosen so that A has just undergone a Hopf bifurcation. In the present problem, the unstable (stable) manifold of A (B) is a tubular (planar) two-dimensional surface out of Σ; we denote these manifolds by W^U(A) (W^S(B)) (see Figure 3.10). Suppose that for a particular λ (say λ_{c1}), W^U(A) becomes tangent to W^S(B). In the presence of a (structurally stable) trajectory B $\to$ A within Σ (see (ii) above) this tangency implies the formation of a heteroclinic cycle at λ_{c1}. For slightly larger λ the tube W^U(A) will intersect W^S(B) along two distinct lines corresponding to the presence of *two* distinct heteroclinic cycles at the same λ value. These cycles are structurally stable, but unlike the situation studied in [85] this does not depend on the presence of fixed-point subspaces of A and B. Finally, when λ is increased far enough the tube W^U(A) emerges on the other side of W^S(B), forming a last tangency at, say, $\lambda = \lambda_{c2} > \lambda_{c1}$. Analysis of this process implies, cf. [70], that periodic solutions may undergo an infinite number of saddle-node bifurcations at $\lambda = \{\lambda_n\}$ as the branch is followed to higher period, with the sequences $\{\lambda_{2j}\}$ and $\{\lambda_{2j+1}\}$ tending to the two *different* values λ_{c1} and λ_{c2} as $j \to \infty$ (see, in particular, Figure 5 of [70]). As the Hopf bifurcation of A is approached (by varying C_R) these two heteroclinic cycles "merge" (the tubular W^U(A) shrinks to a line) and beyond the Hopf bifurcation only a single heteroclinic cycle exists (at $\lambda = \lambda_c$) connecting the resulting infinite amplitude fixed points.

We call such infinite sequences of saddle-node bifurcations along a periodic solution

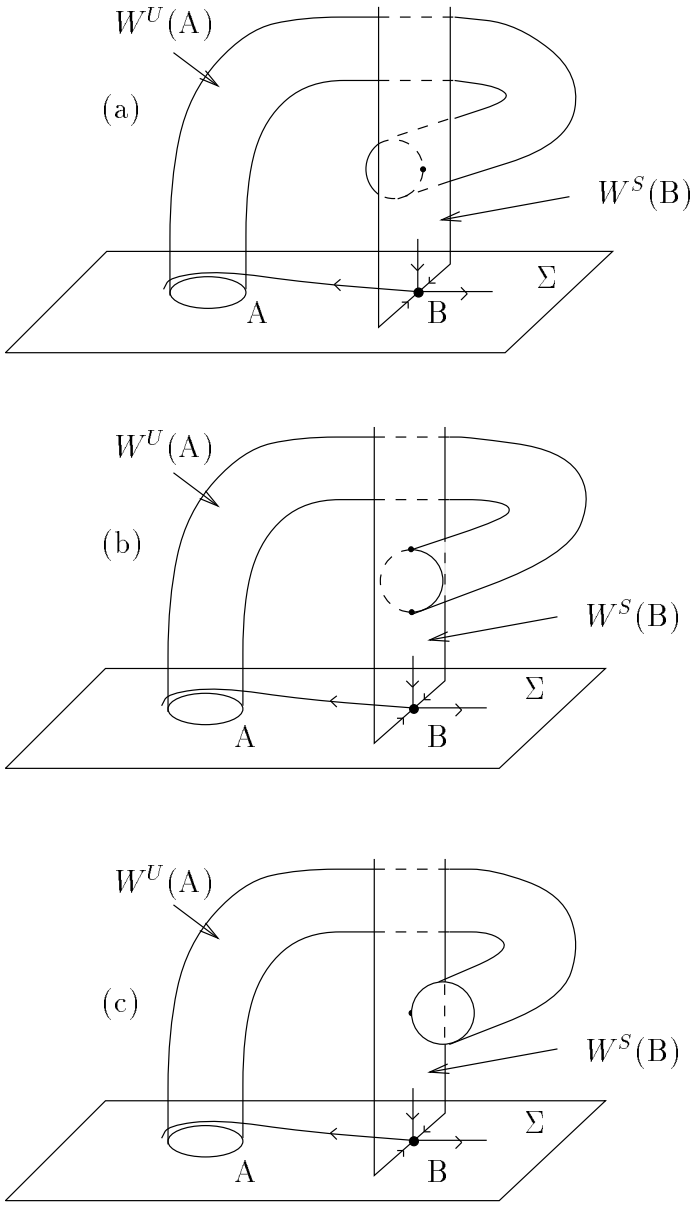

Figure 3.10: Invariant manifolds for the case that A is an infinite amplitude periodic orbit (A = qp_∞) and B is an infinite amplitude fixed point. The connection B $\to$ A within Σ is structurally stable. (a) At $\lambda = \lambda_{c1}$, a single structurally unstable heteroclinic cycle exists. (b) For $\lambda_{c1} < \lambda < \lambda_{c2}$ two distinct structurally stable heteroclinic cycles exist. (c) At $\lambda = \lambda_{c2}$, a single structurally unstable heteroclinic cycle exists.

branch "Shil'nikov-like behavior" and describe several examples in § 3.4.3. In addition, near each saddle-node bifurcation there is a period-doubling bifurcation [68], or if the periodic orbit is reflection-symmetric a symmetry-breaking pitchfork bifurcation [86]. The branch of periodic solutions that results may itself form a subsidiary heteroclinic cycle when followed to higher period, or it may reconnect to the same branch at another period-doubling or symmetry-breaking pitchfork bifurcation, forming a bifurcation "bubble" [87].

Finally, because symmetry-related solutions may have different physical manifestations it is also useful to consider the heteroclinic *network*, defined to be the set of all heteroclinic connections associated with a heteroclinic cycle in which symmetry-related solutions are *not* identified. This concept is important because on reaching an infinite amplitude state B that is a saddle in Σ a trajectory can exit in one of two directions which take it to different but symmetry-related states A and A$'$. Some consequences of the presence of such heteroclinic networks will be explored in the examples below.

3.4.3 Numerical Studies of the Imperfect System

For an unbounded system, that is, in the absence of endwalls, traveling waves are subcritical and standing waves are supercritical in the ranges $-0.0799 < S < -0.0138$ for typical ^{3}He/^{4}He mixtures and $-0.150 < S < -0.0042$ for typical ethanol/water mixtures [75]. In the large aspect-ratio binary fluid convection experiments (in which endwalls are present), bursts were observed for separation ratios $S = -0.021$ and $S = -0.044$ for ^{3}He/^{4}He mixtures [76] and, for example, $S = -0.032$ for ethanol/water mixtures [88]. We will assume that the aspect-ratio is so large for these experiments that the presence of the endwalls does not affect the direction of the solution branches. Therefore, identifying u so-

lutions with traveling waves, v solutions with mixed parity standing waves, and w solutions with standing waves (see Figure 3.6 and [6]), we focus on parameter values for the model (3.9,3.10) for which u solutions are subcritical and v and w solutions are supercritical when $\Delta\lambda = \Delta\omega = 0$. The coefficients B and C will be used to control whether the ns and/or qp solutions are also present. We use the *dstool* [89] simulation package to solve the differential equations with a fourth-order, variable-step Runge-Kutta integration scheme, and AUTO [90] to follow solution branches and detect bifurcations. For different purposes different variables are useful. For example, it is often easiest numerically to work in the (ρ, θ, ϕ) coordinates because this makes the large r behavior associated with bursts more manageable. The eigenvalues reported in this section are all calculated using equations (3.22-3.24). However, the variables (u, v, w) highlight the symmetry properties of the solutions and are therefore used in many of the phase space plots. Time series showing the bursting behavior will be plotted as $r = |z_+|^2 + |z_-|^2 = \sqrt{u^2 + v^2 + w^2} = 1/\rho$ versus time t. Bursts are associated with small ρ values, or equivalently, with large excursions from the neighborhood of $(u, v, w) = (0, 0, 0)$. In the phase space plots plus signs, squares, and diamonds indicate saddles, sources, and sinks, respectively.

The bifurcation diagrams typically show the average value of r,

$$\langle r \rangle \equiv \frac{1}{T} \int_0^T r dt = \frac{T_\tau}{\int_0^{T_\tau} \rho d\tau}, \tag{3.25}$$

as a function of the bifurcation parameter λ. Here T is the period of the solution in the original time t, and T_τ is the period of the solution to equations (3.22-3.24) found in terms of the rescaled time τ. Since the bursts are fast events in the time t (see Appendix D),

the average $\langle r \rangle$ for a sequence of large amplitude bursts may in fact be quite small.[7] The presence of such heteroclinic cycles can have a dramatic effect as discussed in the examples that follow. In particular, as branches associated with such cycles are followed, we find that $\langle r \rangle$ may locally increase or decrease, but $\langle r \rangle$ is larger at the saddle-node bifurcation at λ_{k+2} than at λ_k. In the resulting bifurcation diagrams the branch "spirals off to infinity." Sometimes, however, the oscillatory branch collides with a branch of finite amplitude fixed points; if this finite amplitude fixed point has complex eigenvalues the resulting heteroclinic cycle may also give rise to Shil'nikov-like behavior, while if it has real eigenvalues homoclinic explosions may be encountered (see §2.6.2). When such a global bifurcation is approached the periodic orbit on the branch spends more and more time near the fixed point(s) and $\langle r \rangle$ approaches the value of r for the fixed point(s). In the bifurcation diagrams solid (broken) lines indicate stable (unstable) solutions; circles, diamonds, squares, and triangles indicate Hopf, saddle-node, period-doubling, and symmetry-breaking pitchfork bifurcations, respectively. Many period-doubled branches are omitted. Often, saddle-node and period-doubling (or symmetry-breaking pitchfork) bifurcations occur at nearly the same value of λ due to rapid variation of one or more Floquet multipliers of the periodic solutions as the solution branch is followed. If the remaining nontrivial Floquet multiplier has modulus less than one between such a pair of bifurcations, there will be a small range of λ values in which the solutions are stable. Moreover, branches which arise from period-doubling (or symmetry-breaking pitchfork) bifurcations often undergo period-doubling bifurcations themselves near the λ values at which they come into existence; if the other nontrivial Floquet multiplier has

[7] However, for the actual heteroclinic cycles involving infinite amplitude solutions, equation (3.25) shows that $\langle r \rangle = \infty$.

modulus less than one between the subsequent period-doubling bifurcations, there will be a small range of λ values in which period-two solutions are stable. In the following we use RS (NRS) to indicate that a periodic or chaotic solution to the three-dimensional system is symmetric (not symmetric) with respect to the reflection symmetry κ_1.[8] For a RS periodic orbit, the action of κ_1 is equivalent to time translation by half a period. The symmetries of chaotic solutions may be thought of as symmetries *on the average*.

We now examine a number of examples chosen to illustrate different types of dynamical behavior. The eigenvalues and Floquet multipliers of the infinite amplitude solutions involved in heteroclinic cycles in the examples that follow are summarized in Table 3.4.

Example 1(a)

When

$$A = 1 - 1.5i,\ B = -2.8 + 5i,\ C = 1 + i; \quad \Delta\lambda = \Delta\omega = 0,$$

the u solutions are subcritical, the v, w, and qp solutions are supercritical, and the ns solutions are absent. Application of the parameter symmetry P_2 brings these parameters into the range $-3 < B_R < -1, C_R = -1$ and region I of parameter space; this corresponds to case (c) of Figure 3.9, suggesting the possibility of a heteroclinic cycle involving infinite amplitude solutions. In the original parameters this translates to the possibility of a heteroclinic cycle involving the u_∞ (saddle within Σ) and qp_∞ (sink within Σ) solutions. The (partial) bifurcation diagram for $\Delta\lambda = 0.03$, $\Delta\omega = 0.02$ is compared with the bifurcation diagram for $\Delta\lambda = \Delta\omega = 0$ in Figure 3.11. As $|\lambda|$ becomes large, the behavior of the im-

[8] This refers to the symmetry of the entire orbit, not the instantaneous symmetry of a point on the orbit.

Example	B	A
1(a)	u_∞ $s_1^{u_\infty} = -0.200$ $s_2^{u_\infty} = -5.868$ $s_3^{u_\infty} = 0.0682$	qp_∞ $\mathrm{FM}_1 = 57.46$ $\mathrm{FM}_2 = 1.000$ $\mathrm{FM}_3 = 0.604$
1(b)	u_∞ $s_1^{u_\infty} = -0.150$ $s_2^{u_\infty} = -5.801$ $s_3^{u_\infty} = 0.151$	qp_∞ $\mathrm{FM}_1 = 45.19$ $\mathrm{FM}_2 = 1.000$ $\mathrm{FM}_3 = 0.894$
2	u_∞ $s_1^{u_\infty} = -0.100$ $s_2^{u_\infty} = -5.734$ $s_3^{u_\infty} = 0.234$	v_∞ $s_1^{v_\infty} = 1.700$ $s_2^{v_\infty} = -0.05 + 2.929i$ $s_3^{v_\infty} = -0.05 - 2.929i$
3	ns_∞ $s_1^{ns_\infty} = -0.164$ $s_2^{ns_\infty} = -5.723$ $s_3^{ns_\infty} = 0.0319$	qp_∞ $\mathrm{FM}_1 = 77.97$ $\mathrm{FM}_2 = 1.000$ $\mathrm{FM}_3 = 0.581$
4	ns_∞ $s_1^{ns_\infty} = -0.0322$ $s_2^{ns_\infty} = -5.384$ $s_3^{ns_\infty} = 0.0870$	v_∞ $s_1^{v_\infty} = 1.730$ $s_2^{v_\infty} = -0.005 + 2.598i$ $s_3^{v_\infty} = -0.005 - 2.598i$

Table 3.4: Eigenvalues and Floquet multipliers from equations (3.22-3.24) for the infinite amplitude solutions involved in heteroclinic cycles for the examples of §3.4.3. The eigenvalues and Floquet multipliers with subscripts 1 (2,3) correspond to perturbations out of (within) the Σ subspace. All are independent of λ and hence are identical for all heteroclinic cycles that exist.

perfect system approaches the behavior of the perfect system. In particular, the w_e and w_o branches given by equations (3.20,3.21) approach the w branch for the perfect problem. In addition to the two primary bifurcations responsible for the $w_{e,o}$ branches the bifurcation diagram reveals the presence of a *disconnected* branch of fixed points. This branch, labeled u/v, must be computed numerically; as $\lambda \to -\infty$ $(+\infty)$ the fixed points on this branch approach the u (v) fixed points for the perfect system (hence the name). Finally, the Hopf bifurcation at $\lambda = 0.180681$ gives rise to a stable periodic orbit which approaches the stable

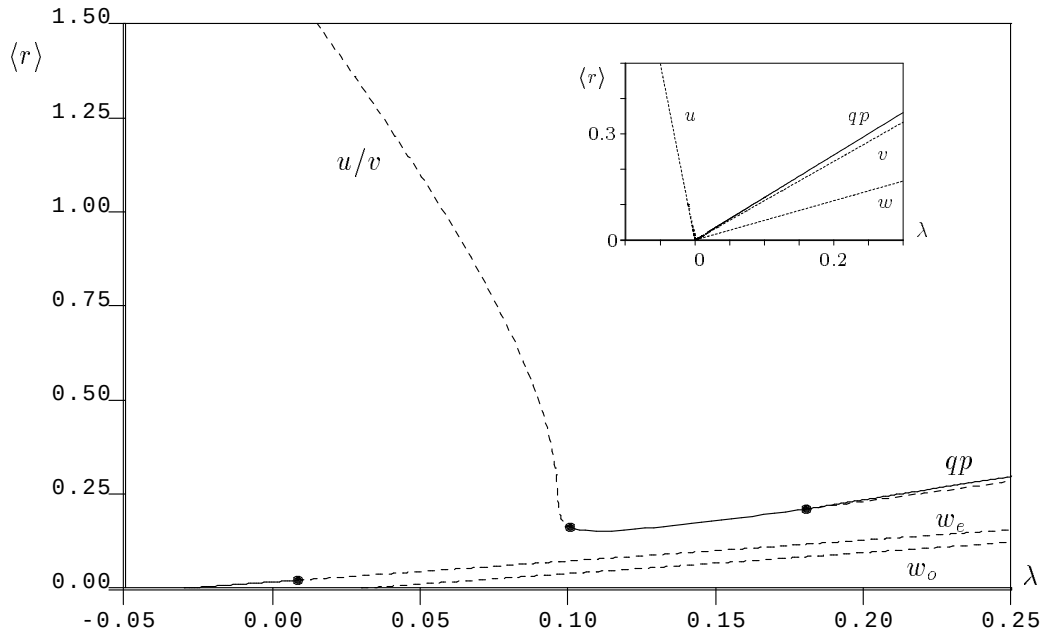

Figure 3.11: Partial bifurcation diagram for $A = 1 - 1.5i$, $B = -2.8 + 5i$, $C = 1 + i$ and $\Delta\lambda = 0.03$, $\Delta\omega = 0.02$. The Hopf bifurcations on the w_e branch at $\lambda = 0.00857143$ and on the u/v branch at $\lambda = 0.100750$ are indicated but the resulting branches are omitted (see Figure 3.12). In contrast to the perfect system (inset) with a stable qp primary branch, the stable primary branch in the imperfect system is the w_e branch.

qp solution for the perfect problem as $\lambda \to \infty$.

Figure 3.12 shows the results of a detailed bifurcation study for these parameters; however, not all period-doubled branches are shown. The w_e^1 branch arises from the Hopf bifurcation on the w_e branch at $\lambda = 0.00857143$; each trajectory on this branch visits the vicinity of different (but symmetry-related) u_∞ fixed points. These solutions are rotations (see Figure 3.13). Their physical manifestation for large-aspect ratio binary fluid convection is a *blinking* state in which successive bursts occur at opposite sides of the container, as shown in Figure 3.14(a), the name coming from states identified in binary fluid and double diffusive convection experiments in rectangular containers [91, 92, 93]. It is likely that the irregular bursts reported in [76] are due to such either a "noisy" periodic blinking

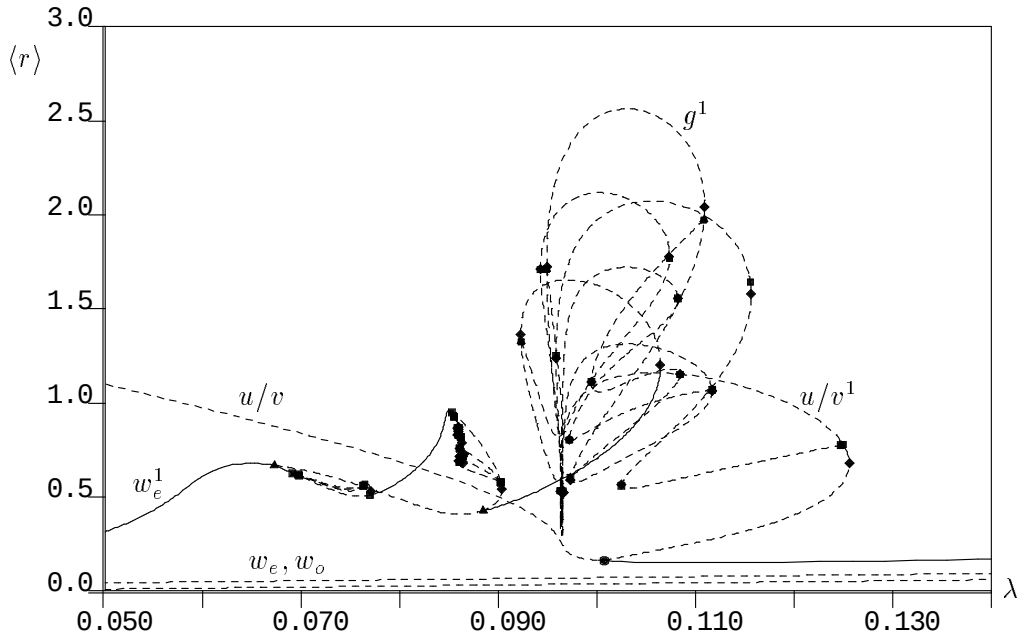

Figure 3.12: Detailed bifurcation diagram for the parameters $A = 1 - 1.5i$, $B = -2.8 + 5i$, $C = 1 + i$, and $\Delta\lambda = 0.03, \Delta\omega = 0.02$. Not all period-doubled branches are shown. The branch names are discussed in the text.

burst state, or a chaotic blinking burst state (see below). The u/v^1 branch is born in a Hopf bifurcation of the u/v branch at $\lambda = 0.100750$; each trajectory along this branch visits repeatedly the vicinity of *same* infinite amplitude fixed point. These solutions are librations (see Figure 3.15). Their physical manifestation for large-aspect ratio binary fluid convection is a *winking* state in which successive bursts occur at the same side of the container, as shown in Figure 3.14(b). Winking states have apparently not yet been observed in experiments. The g^1 branch will be described later. Notice that the w_e^1 solutions are stable for large ranges of λ values (for example, for $0.0885 < \lambda < 0.1065$) and u/v^1 solutions are stable for much smaller ranges (for example, for $0.1250 < \lambda < 0.1256$). In fact, for this range the stable u/v^1 solutions coexist with stable u/v solutions which are more likely to be observed if λ is ramped upwards from below 0.1250; thus, the (chevronlike) states associated with the

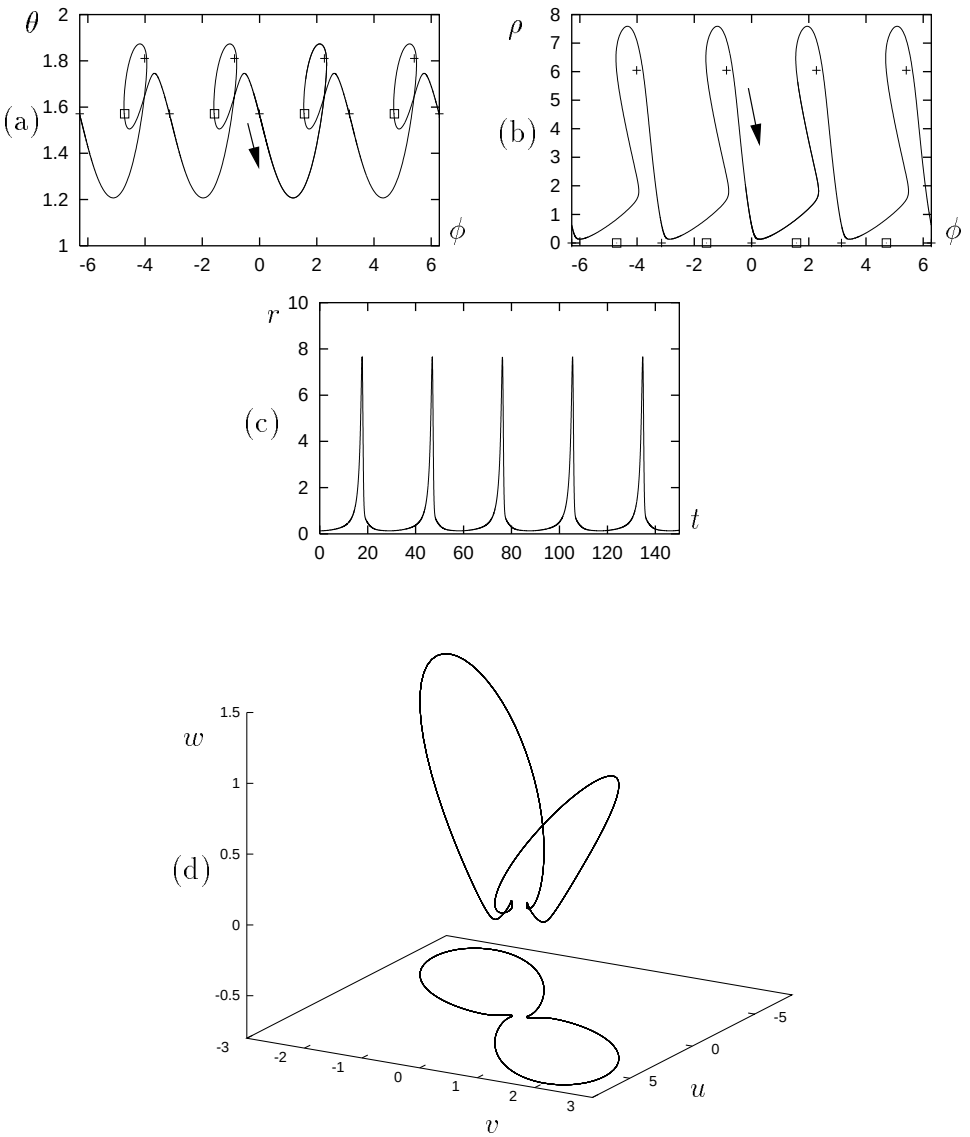

Figure 3.13: Stable periodic rotation with parameters as specified in the text and $\lambda = 0.1$. (a,b) The trajectory in the (ρ, θ, ϕ) variables. (c) Time series showing periodic bursts. (d) Trajectory in the (u, v, w) variables, with a projection onto the (u, v) plane.

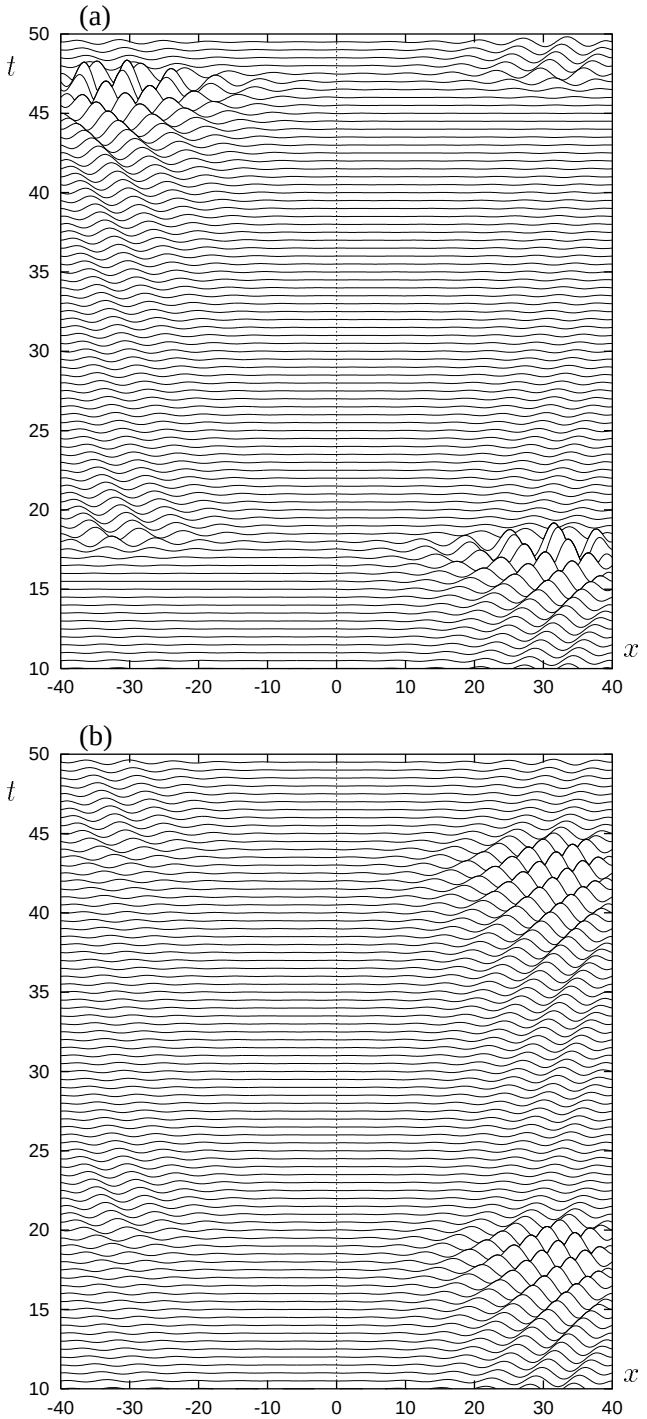

Figure 3.14: The perturbation Ψ from the trivial state represented in a space-time plot showing (a) the periodic blinking state (in which successive bursts occur at opposite sides of the container) from the trajectory in Figure 3.13, and (b) the periodic winking state (in which successive bursts occur at the same side of the container) for the trajectory in Figure 3.15.

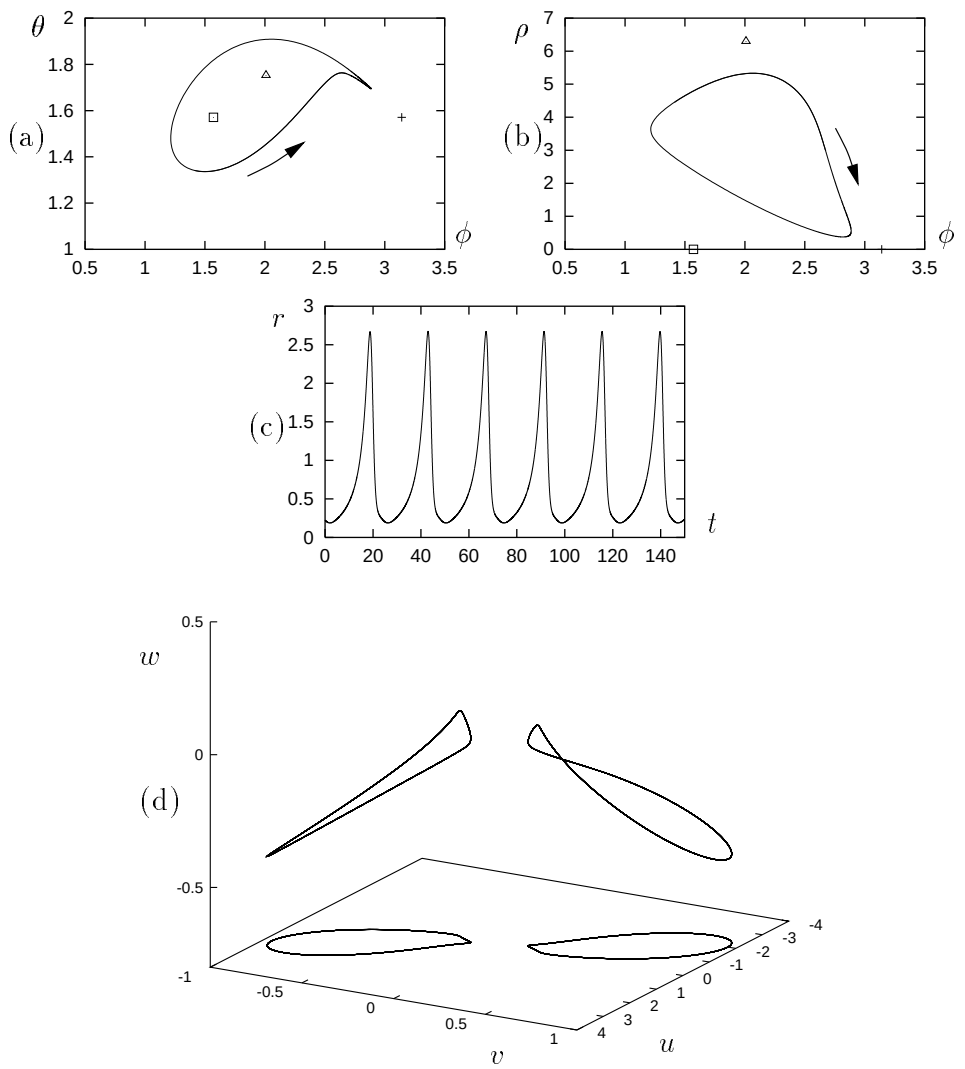

Figure 3.15: Stable periodic libration with parameters as specified in the text and $\lambda = 0.1253$. (a,b) The trajectory in the (ρ, θ, ϕ) variables. (c) Time series showing periodic bursts. (d) Trajectories for two κ_1-related librations in the (u, v, w) variables, with projections onto the (u, v) plane.

u/v solutions are more likely to be observed than winking states for binary fluid convection. We now describe the major characteristics of this bifurcation diagram.

(a) Heteroclinic cycle involving infinite amplitude solutions

As argued above, this example offers the possibility of a heteroclinic cycle involving the u_∞ and qp_∞ solutions. Examples of such cycles are shown in Figure 3.16. Here the effect of these cycles is "local"; the branches which might be expected to be affected by the heteroclinic cycles (e.g., the w_e^1 and u/v^1 branches) in fact terminate in global bifurcations involving finite amplitude u/v fixed points, i.e., instead of undergoing an infinite number of saddle-node bifurcations as they are followed to higher period, these branches only undergo a *finite* number before colliding with the finite amplitude u/v fixed points.

(b) Global bifurcations involving finite amplitude fixed points

The u/v fixed points do not lie in the reflection-invariant subspace $\mathrm{Fix}(\langle\kappa_1\rangle) \equiv \{(u,v,w)|\ u = v = 0\}$; thus there are two u/v solutions related by κ_1. Consequently, RS *heteroclinic* orbits connecting the two κ_1-related u/v fixed points or two κ_1-related *homoclinic* orbits to the κ_1-related u/v fixed points are both possible. The existence of these orbits is suggested by following many solution branches (e.g., the w_e^1 and u/v^1 branches) to very high period. As such a homoclinic or heteroclinic orbit is approached, the periodic orbit spends more and more time near the u/v fixed point(s) so that $\langle r\rangle$ approaches the value of r for these fixed point(s) (see Figure 3.17).

Figure 3.18 shows a *heteroclinic* orbit for $\lambda = 0.0964187$ connecting two u/v fixed points related by κ_1; another such orbit exists for $\lambda = 0.09654768$. At these global bifurca-

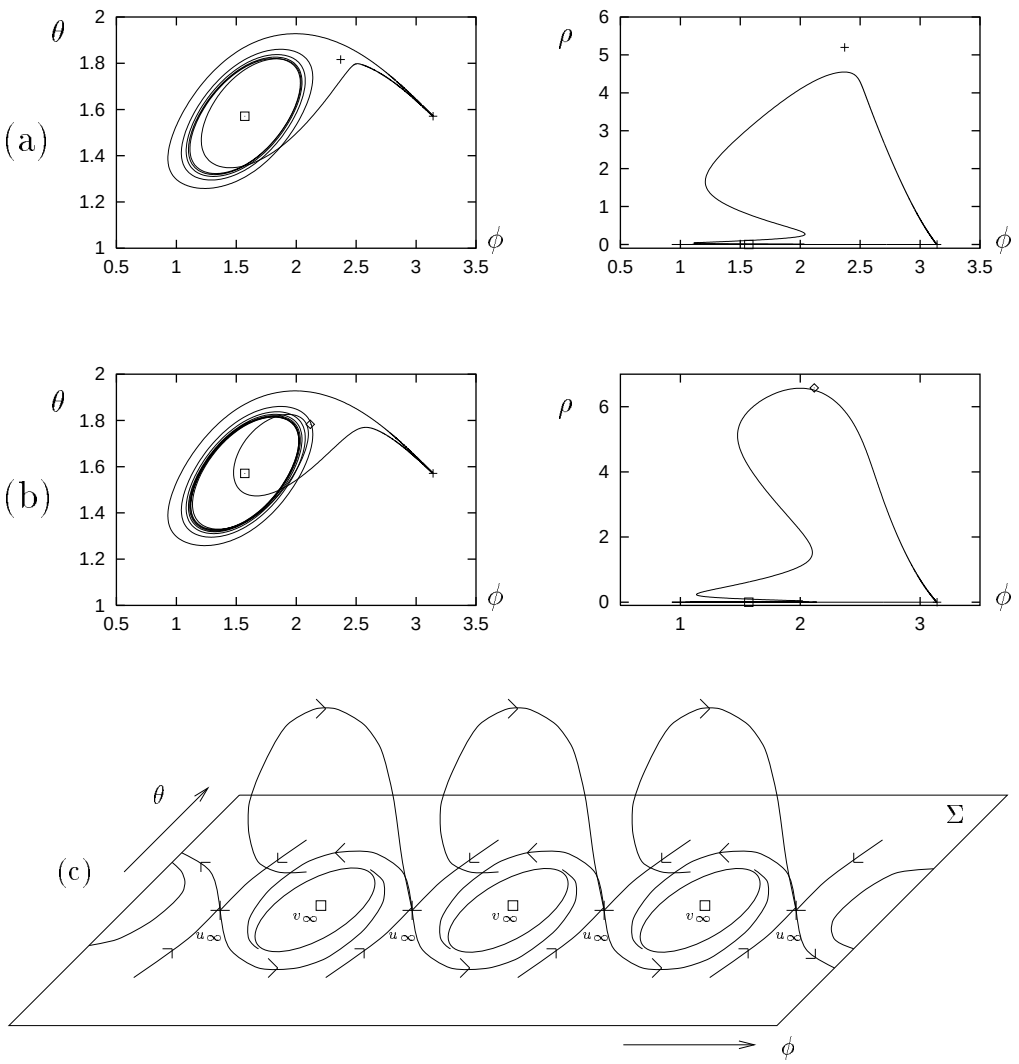

Figure 3.16: (a) A numerically calculated heteroclinic cycle involving the infinite amplitude fixed point u_∞ and the infinite amplitude limit cycle qp_∞ at $\lambda = 0.0974$. (b) Another heteroclinic cycle at $\lambda = 0.110$. (c) Sketch of the resulting complete heteroclinic network showing all connections.

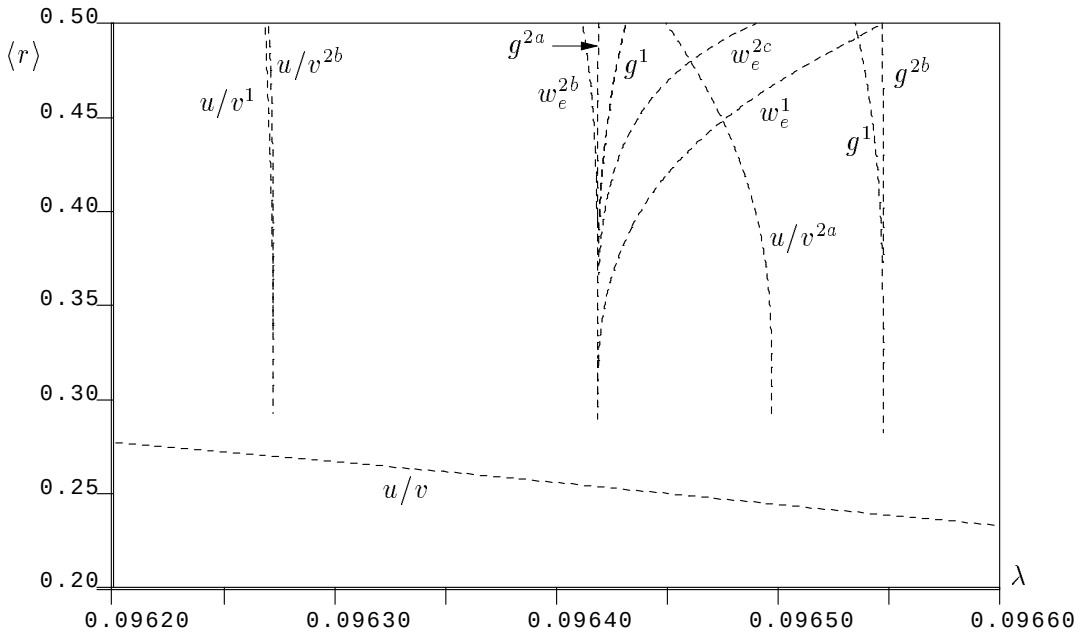

Figure 3.17: Bifurcation diagram showing global bifurcations involving the finite amplitude u/v fixed points. The u/v^{2a} and u/v^{2b} branches arise from period-doubling bifurcations from the u/v^1 branch, while the $w_e^{2b}, w_e^{2c}, g^{2a}$, and g^{2b} branches arise from symmetry-breaking pitchfork bifurcations from the w_e^1 and g^1 branches.

tions the u/v fixed points have purely real eigenvalues $s_1 > s_2 > 0 > s_3$ (see Figure 3.19); since $|\frac{s_2}{s_3}| < 1$ we expect that the global bifurcations will lead to homoclinic explosions as for the Lorenz equations (but with time reversed from the case which is typically studied); see §2.6.2. We have located a solution branch which is born in one of these global bifurcations and terminates in the other. An example of a stable solution on this branch (which we call a g^1 solution; such a solution is RS) and a bifurcation diagram is shown in Figure 3.20. Finally, Figure 3.21 shows two κ_1-related *homoclinic* orbits which exist for $\lambda = 0.0962724$; similar orbits exist also for $\lambda = 0.0964974$. Because there is only one homoclinic orbit for each fixed point, these global bifurcations do not produce homoclinic explosions [63].

(c) Complicated behavior for $0.065 < \lambda < 0.092$

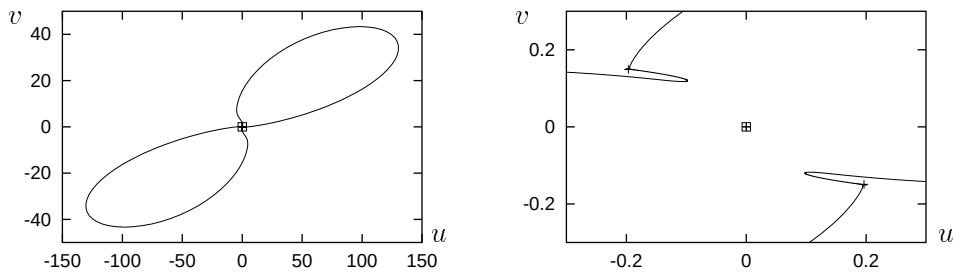

Figure 3.18: The RS heteroclinic orbit connecting two κ_1-related u/v fixed points at $\lambda = 0.0964187$ with $r_{\max} \approx 166$. The frame at right shows a blow-up of the frame at left. Another RS heteroclinic orbit exists at $\lambda = 0.09654768$ with $r_{\max} \approx 7378$. Here $r_{\max}$ denotes the maximum value of r along the orbit.

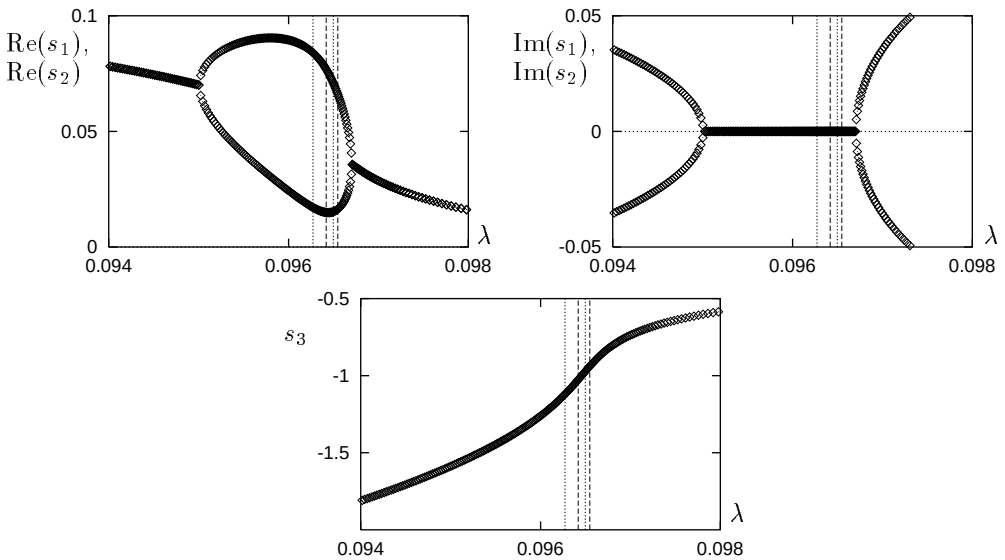

Figure 3.19: Eigenvalues s_1, s_2, and s_3 of the u/v fixed points; the former are real for $0.0950 < \lambda < 0.0967$. The vertical dashed (dotted) lines show the λ values for heteroclinic (homoclinic) bifurcations involving the finite amplitude u/v fixed points.

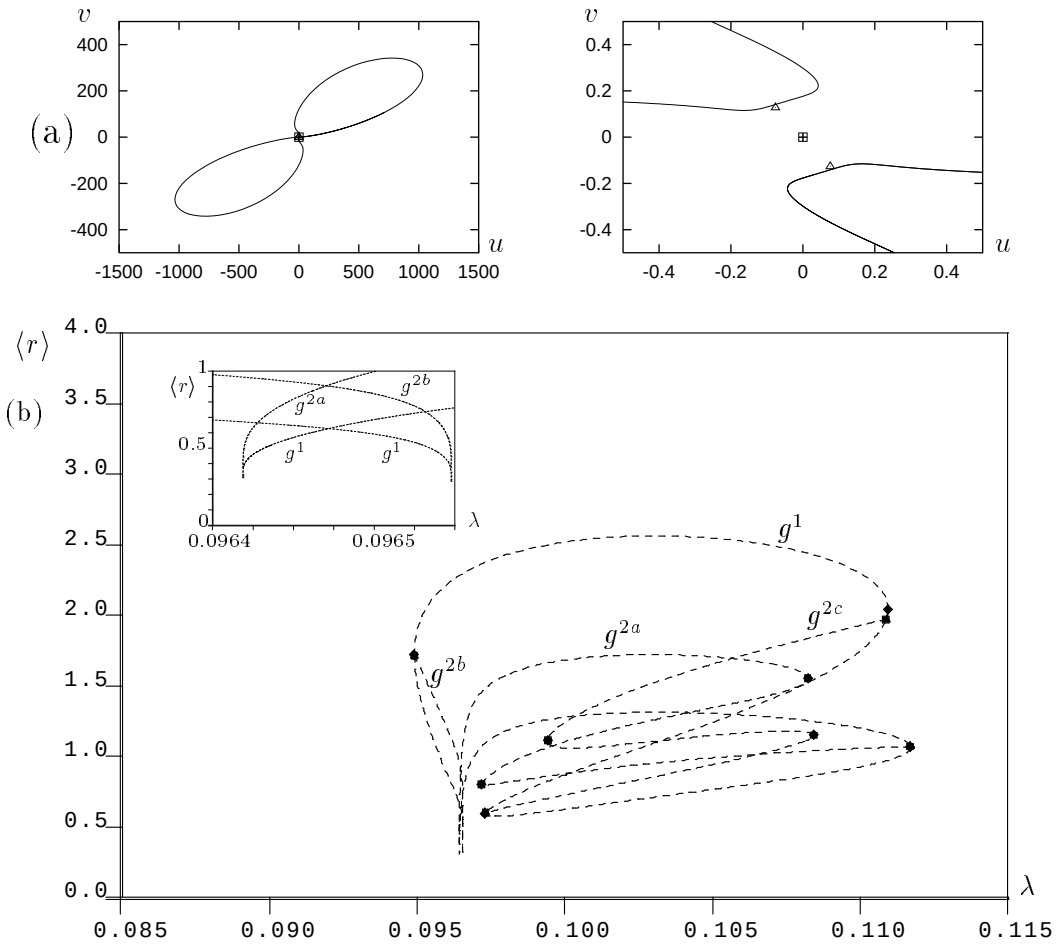

Figure 3.20: (a) Stable g^1 solution for $\lambda = 0.1109354$ with $\langle r \rangle \approx 2.045$. The frame at right shows a blow-up of the frame at left. (b) Bifurcation diagram showing the g^1 branch and the branches which bifurcate off the g^1 branch in symmetry-breaking pitchfork bifurcations. All subsequent period-doubled branches are omitted. Inset shows detail of (b).

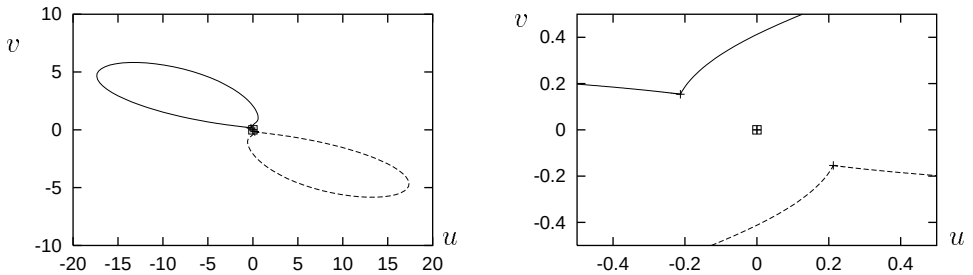

Figure 3.21: The two κ_1-related homoclinic orbits to the κ_1-related u/v fixed points at $\lambda = 0.0962724$ with $r_{\max} \approx 18.2$. The frame at right shows a blow-up of the frame at left. Such homoclinic orbits also exist at $\lambda = 0.0964974$ with $r_{\max} \approx 991$.

The range $0.065 < \lambda < 0.092$ contains much complicated behavior including period-doubling cascades to strange attractors, periodic windows, and symmetry-increasing bifurcations of strange attractors [94]. For example, Figure 3.22 shows bursts from an attractor describing chaotic rotations with $\lambda = 0.072$. This solution describes a chaotic blinking state because the trajectory makes successive visits to different but symmetry-related infinite amplitude u solutions. The complicated behavior in this parameter range is conveniently described using (approximately one-dimensional) Poincaré maps which take into account the reflection symmetry. We let

$$\Sigma_+ = \{(u, v, w) : u = v, u > 0\},$$

$$\Sigma_- = \{(u, v, w) : u = v, u < 0\},$$

and define the Poincaré maps $P : \Sigma_+ \to \Sigma_+$, $\tilde{P} : \Sigma_+ \to \Sigma_-$. All periodic orbits which pierce Σ_+ are fixed points of P. Because of the κ_1 symmetry the map from Σ_- to Σ_+ is identical to $\tilde{P}$ so that $P = \tilde{P} \cdot \tilde{P}$. For a RS periodic orbit the action of $\tilde{P}$ is the same as the action of κ_1; thus RS periodic orbits are fixed points of $\kappa_1 \cdot \tilde{P}$ in addition to being fixed points of P. On the other hand, NRS orbits are fixed points of P but not of $\kappa_1 \cdot \tilde{P}$. There may be RS and NRS periodic orbits embedded in a RS strange attractor; however, only NRS periodic orbits may be embedded in a NRS strange attractor, so for such attractors we expect that the map $\kappa_1 \cdot \tilde{P}$ will not have any fixed points.

Figure 3.23(a) shows a partial bifurcation diagram for $0.065 < \lambda < 0.080$. The RS w_e^1 branch is born at a Hopf bifurcation on the w_e branch when $\lambda = 0.00857143$, and is stable until a symmetry-breaking pitchfork bifurcation at $\lambda = 0.0672409$. This bifurcation gives rise to two κ_1-related stable NRS periodic solutions which we call w_e^2

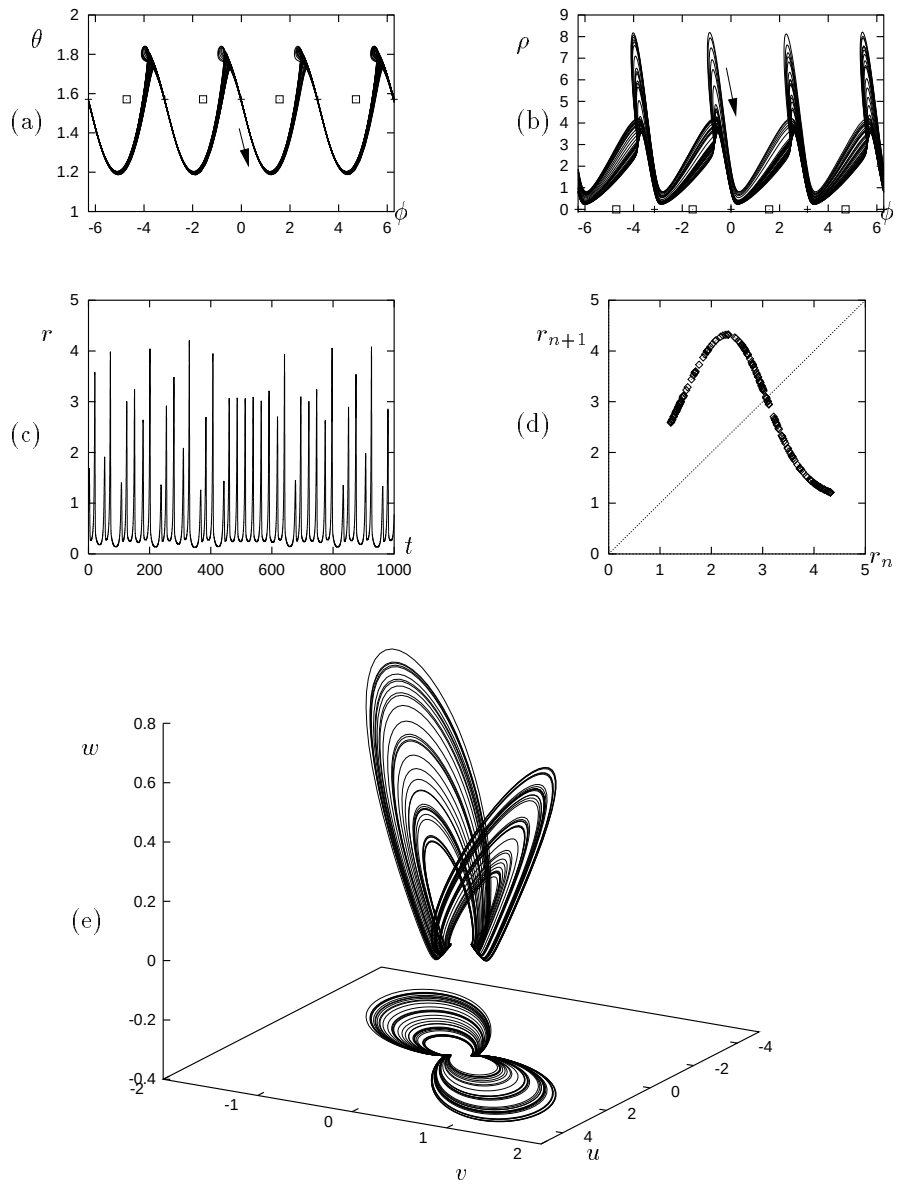

Figure 3.22: Chaotic rotation with parameters as defined in the text and with $\lambda = 0.072$. (a,b) The trajectory in the (ρ, θ, ϕ) variables. (c) Time series showing chaotic bursts. (d) Peak-to-peak plot for the bursts. (e) Trajectory in the (u, v, w) variables, with a projection onto the (u, v) plane.

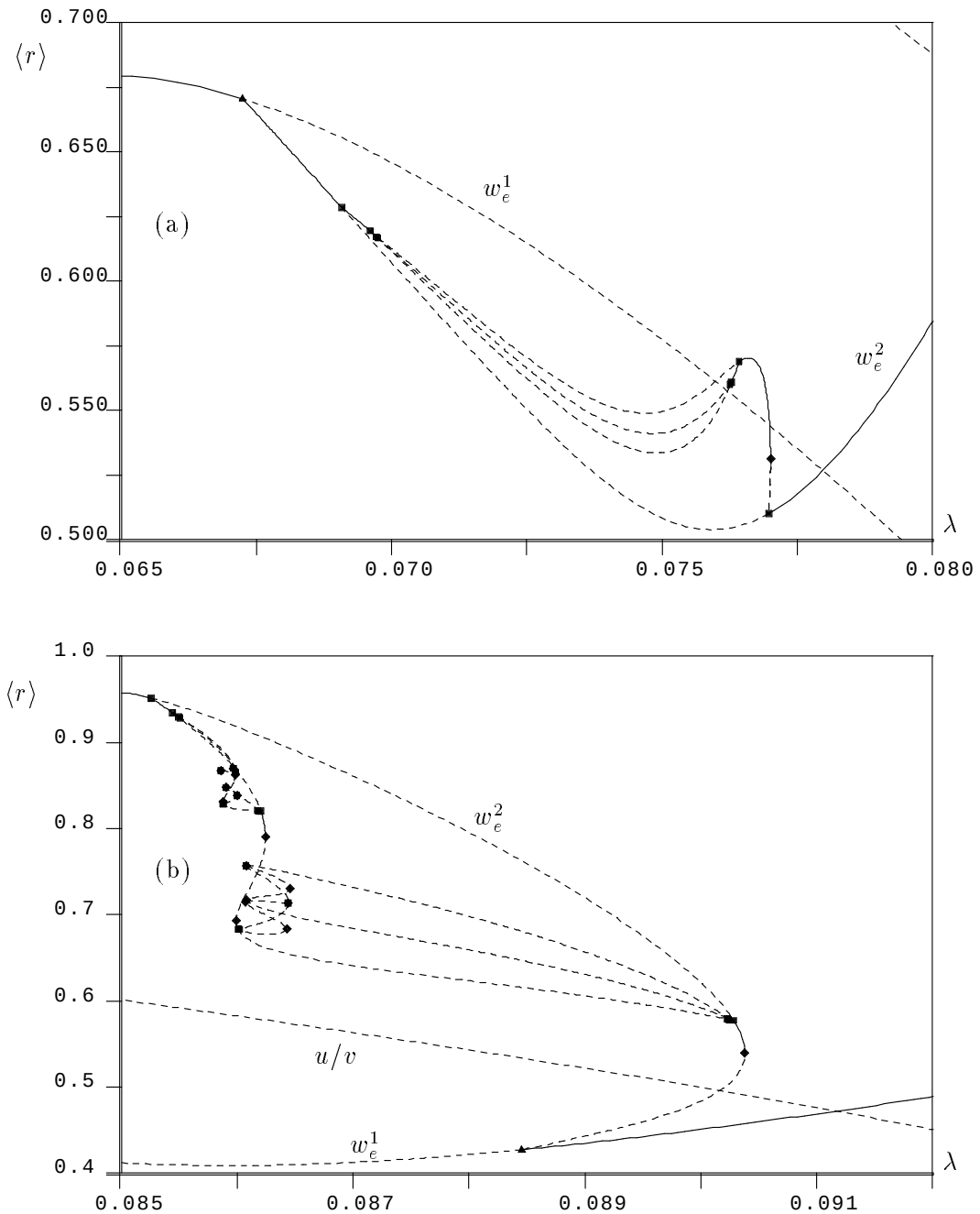

Figure 3.23: Detail of the bifurcation diagram for (a) $0.065 < \lambda < 0.080$ and (b) $0.085 < \lambda < 0.092$. Not all period-doubled branches are shown.

solutions; for these solutions successive bursts differ in amplitude (see Figure 3.24(a)). The w_e^2 solutions undergo identical period-doubling cascades which accumulate at $\lambda \approx 0.06975$ and lead to two κ_1-related NRS strange attractors. As λ is increased to 0.0701 a period 6 window (defined according to the number of successive bursts with distinct amplitudes) is formed with a periodic NRS orbit as shown in Figure 3.24(b). As λ is increased further the period 6 orbit itself undergoes a period-doubling cascade so that by $\lambda = 0.07013$ there are again two κ_1-related NRS strange attractors. At $\lambda \approx 0.070319$ these strange attractors merge in a symmetry-increasing bifurcation as illustrated in Figure 3.25 and 3.26. As λ is increased to 0.0707 a period 5 window is formed with a periodic RS orbit. This periodic orbit undergoes a symmetry-breaking pitchfork bifurcation and the resulting NRS periodic orbits then undergo period-doubling cascades leading to two κ_1-related NRS strange attractors. These attractors merge at $\lambda \approx 0.070779$ giving a RS strange attractor. Similar behavior is found as λ is increased further, with other periodic windows (such as a period 7 window near $\lambda = 0.07454$) which are destroyed in ways similar to those described above. There is a reverse period-doubling cascade which accumulates at $\lambda \approx 0.0762$. At $\lambda = 0.0769685$ the w_e^2 solutions regain stability.

The w_e^2 solutions remain stable as λ is increased to 0.0852558 at which point they undergo a period-doubling bifurcation. Figure 3.23(b) shows the bifurcation diagram for $0.085 < \lambda < 0.092$. In this range there are again period-doubling cascades, periodic windows (including a period 3 window at $\lambda = 0.088$), and symmetry-increasing bifurcations in which NRS strange attractors merge to form a RS strange attractor. A unique feature for this portion of the bifurcation diagram is the presence of many saddle-node and period-doubling

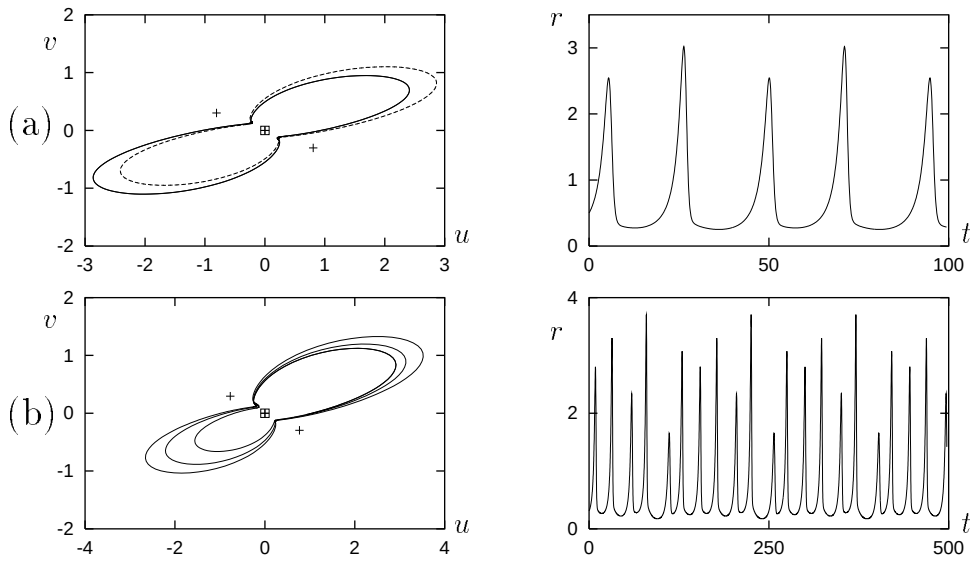

Figure 3.24: (a) Two stable κ_1-related NRS w_e^2 solutions at $\lambda = 0.0675$ with $\langle r \rangle \approx 0.665$. At right is the time series for one of these solutions. (b) Stable NRS period 6 orbit and burst sequence at $\lambda = 0.0701$. The κ_1-related orbit is omitted.

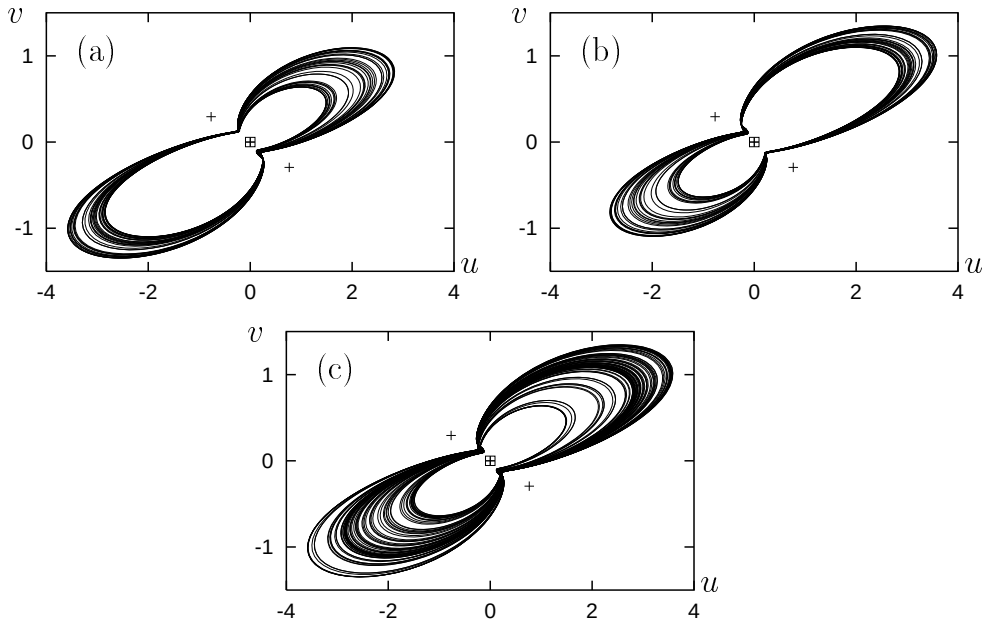

Figure 3.25: (a,b) Two κ_1-related NRS strange attractors at $\lambda = 0.070318$. At $\lambda \approx 0.070319$ these attractors merge in a symmetry-increasing bifurcation. (c) The resulting RS strange attractor at $\lambda = 0.070320$.

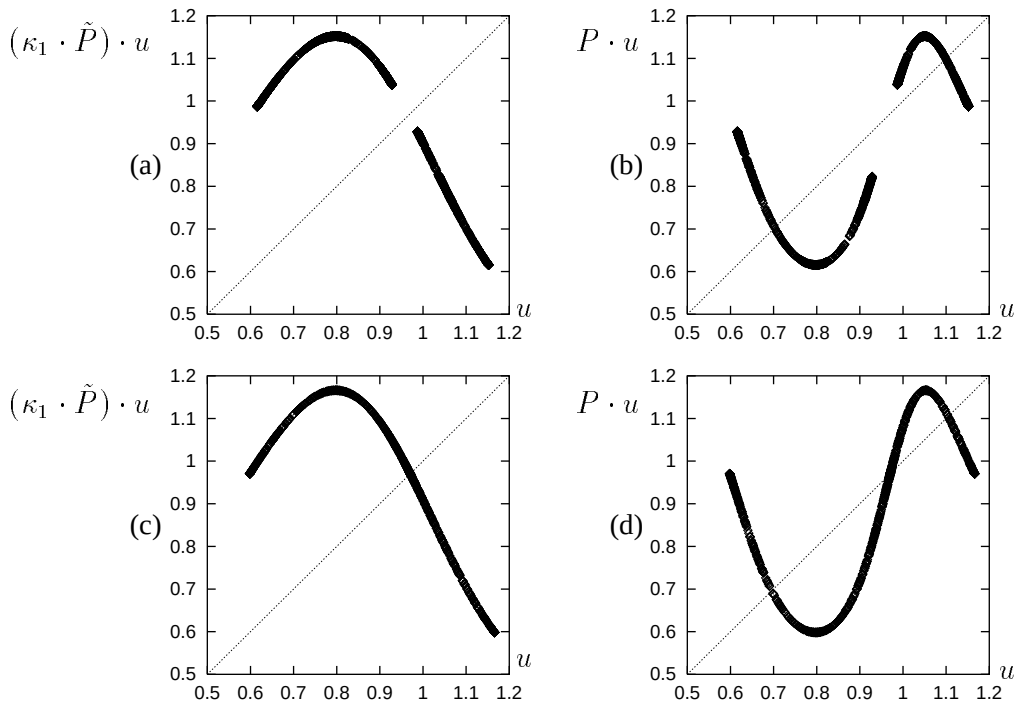

Figure 3.26: The maps (a) $\kappa_1 \cdot \tilde{P}$ and (b) P for the two κ_1-related NRS strange attractors when $\lambda = 0.07013$. The gap near $(\kappa_1 \cdot \tilde{P}) \cdot u = u$ in (a) indicates that there are no RS periodic solutions embedded in these attractors. The two fixed points in (b) correspond to κ_1-related NRS periodic solutions. When λ is increased to 0.070319 a symmetry-increasing bifurcation occurs, and the $\kappa_1 \cdot \tilde{P}$ map (c) has a fixed point indicating a RS periodic solution embedded in the strange attractor. The P map (d) has three fixed points, one corresponding to this RS periodic solution and the other two corresponding to κ_1-related NRS periodic solutions.

bifurcations for $0.0858 < \lambda < 0.0865$; the origin of this behavior has not been determined. At $\lambda = 0.0884534$ the w_e^2 branch reconnects with the w_e^1 branch in a symmetry-restoring pitchfork bifurcation.

Complicated behavior such as that described here also occurs for appropriate λ values for the remaining examples, but will not be emphasized.

Example 1(b)

We now decrease the value of C_R choosing

$$A = 1 - 1.5i, B = -2.8 + 5i, C = 0.95 + i.$$

When $\Delta\lambda = \Delta\omega = 0$ the u solutions are still subcritical, the v, w, and qp solutions supercritical and the ns solutions absent. As before we take $\Delta\lambda = 0.03, \Delta\omega = 0.02$. Holding the other parameters fixed, the v_∞ solutions undergo a subcritical Hopf bifurcation which destroys the qp_∞ solutions as C_R decreases through $-\frac{B_R}{3} = \frac{14}{15} \approx 0.93333$; for the above parameter values the qp_∞ solution therefore still exists but the system is closer to a Hopf bifurcation. As in Example 1(a) application of the parameter symmetry P_2 and rescaling of time brings these parameters into the range $-3 < B_R < -1, C_R = -1$ and region I of parameter space, i.e., to case (c) of Figure 3.9. The resulting bifurcation diagram is shown in Figure 3.27, with branch names defined as in Example 1(a). The main point to be emphasized here is that although the u/v^1 branch terminates in a global bifurcation involving the finite amplitude u/v fixed points as in Example 1(a), the w_e^1 branch does not; instead, it undergoes Shil'nikov-like behavior due to a heteroclinic cycle involving the u_∞ and qp_∞ solutions. In this case the saddle-node bifurcations on the w_e^1 solution branch accumulate, in the notation of §3.4.2, to $\lambda_{c1} \approx 0.089$ and $\lambda_{c2} \approx 0.095$. Figure 3.28 shows the period $\frac{1}{2}T_\tau$ between successive bursts on the w_e^1 branch as a function of λ together with projections of the solution at two successive saddle-node bifurcations. As the period increases the number of turns near qp_∞ increases and the solutions become better and better approximations to heteroclinic cycles consisting of a trajectory connecting a u_∞ fixed point to a qp_∞ solution within Σ, followed by return trajectory lying outside Σ to another u_∞ fixed

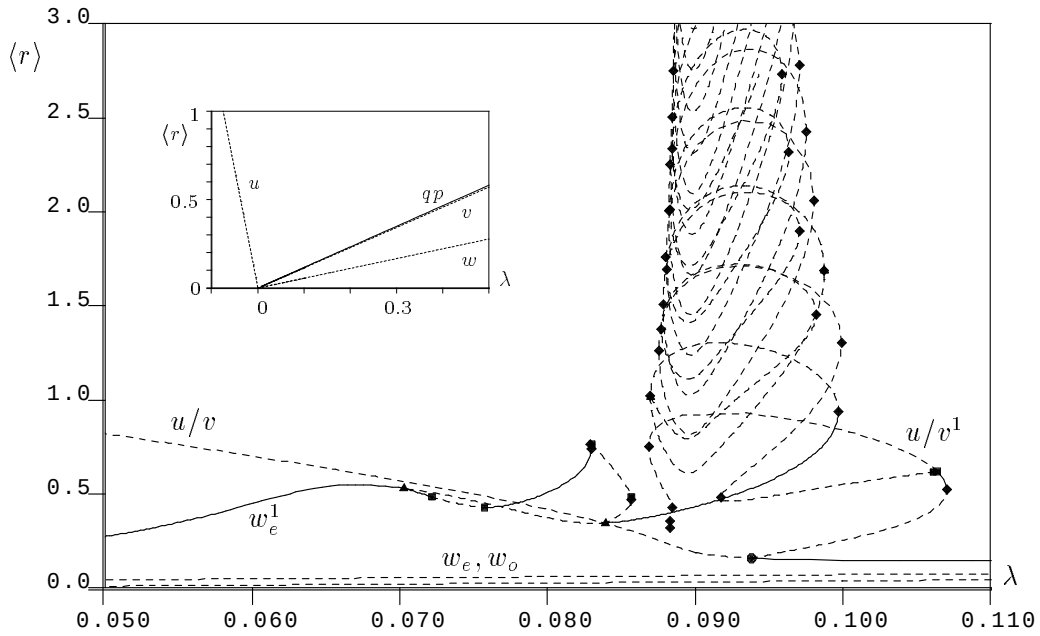

Figure 3.27: Bifurcation diagram for the parameters $A = 1-1.5i$, $B = -2.8+5i$, $C = 0.95+i$, $\Delta\lambda = 0.03$, $\Delta\omega = 0.02$ for comparison with Figure 3.12. Not all period-doubled branches are shown. The inset shows the corresponding bifurcation diagram for the perfect system.

point shifted in ϕ by π from the first one. Branches which arise from symmetry-breaking pitchfork and period-doubling bifurcations from the w_e^1 and u/v^1 branches, respectively, also show Shil'nikov-like behavior.

Example 2

When C_R is decreased even further the qp_∞ solution is destroyed in a Hopf bifurcation on the v_∞ solution. Thus, when

$$A = 1 - 1.5i, B = -2.8 + 5i, C = 0.9 + i; \quad \Delta\lambda = \Delta\omega = 0,$$

the u solutions are subcritical, the v and w solutions are supercritical, but the ns and qp solutions are now both absent. Application of the parameter symmetry $P_3 \cdot P_1$ and a rescaling of time brings these parameters into the range $-3 < B_R < -1, C_R = -1$ and

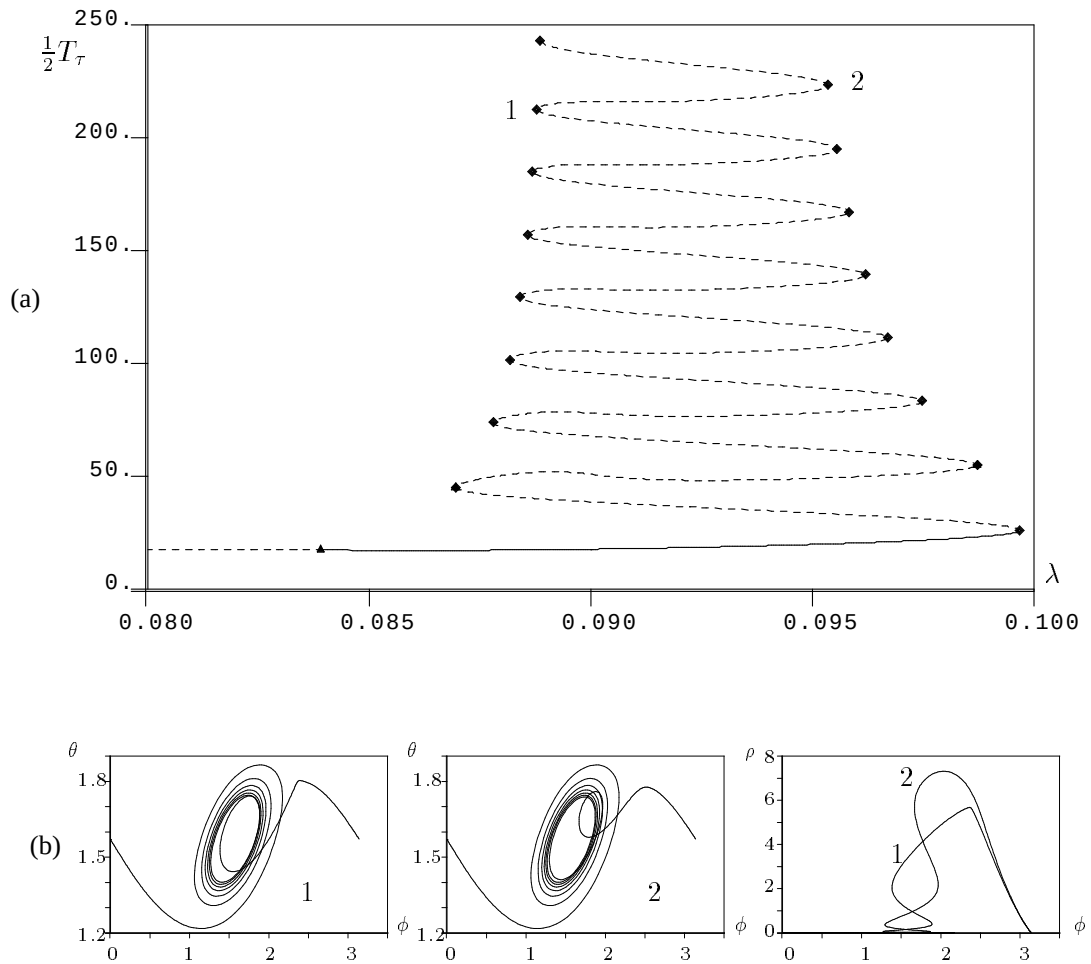

Figure 3.28: (a) The period $\frac{1}{2}T_\tau$ between successive bursts on the w_e^1 branch as a function of λ. (b) Trajectories for the points labeled 1 and 2 in (a). These approximate the two distinct heteroclinic cycles between the infinite amplitude fixed points u_∞ and the infinite amplitude periodic solutions qp_∞, cf. Figure 3.16, with $\lambda \equiv \lambda_{c1} \approx 0.089$ and $\lambda \equiv \lambda_{c2} \approx 0.095$.

region IV_w of parameter space, i.e., to case (a) of Figure 3.9. In the original parameters, this translates to the possibility of a heteroclinic cycle involving the u_∞ and v_∞ solutions. The bifurcation diagram for $\Delta\lambda = 0.03, \Delta\omega = 0.02$ is shown in Figure 3.29 and includes (a) a heteroclinic cycle involving the infinite amplitude u_∞ and v_∞ solutions near $\lambda = 0.08461$ (see Figure 3.30), and (b) global bifurcations involving finite amplitude fixed points. Because of the periodicity in ϕ the heteroclinic network consists of two basic units, as illustrated in Figures 3.31. This is because on arriving at u_∞ a trajectory can go, within Σ, to either of two v_∞ fixed points that are related by periodicity in ϕ. In fact, since the trajectory out of Σ is the same for both units as sketched in Figure 3.31(c,d), the periods along the u/v^1 and w_e^1 branches become infinite at the *same* λ value. Subsidiary heteroclinicities, sketched in Figure 3.32, are also present but form at different λ values.

It is also possible to find global bifurcations which involve one or both of the u/v fixed points. For example, for $\lambda = 0.08208$ there are two κ_1-related homoclinic orbits to κ_1-related u/v fixed points, while for $\lambda = 0.0795$ there is a RS heteroclinic orbit connecting the two u/v fixed points. Figure 3.33 shows the eigenvalues $s_1, s_2, \bar{s_2}$ for the u/v fixed points for the λ range of interest; both of these global bifurcations occur with $|\frac{\mathrm{Re}(s_2)}{s_1}| < 1$, so Shil'nikov-like behavior occurs (but with time reversed from the case which is typically studied because $\mathrm{Re}(s_2) > 0$). We have located a solution branch (which we call the s^1 branch) which terminates at both ends in the global bifurcation at $\lambda \approx 0.0795$ (see Figure 3.34).

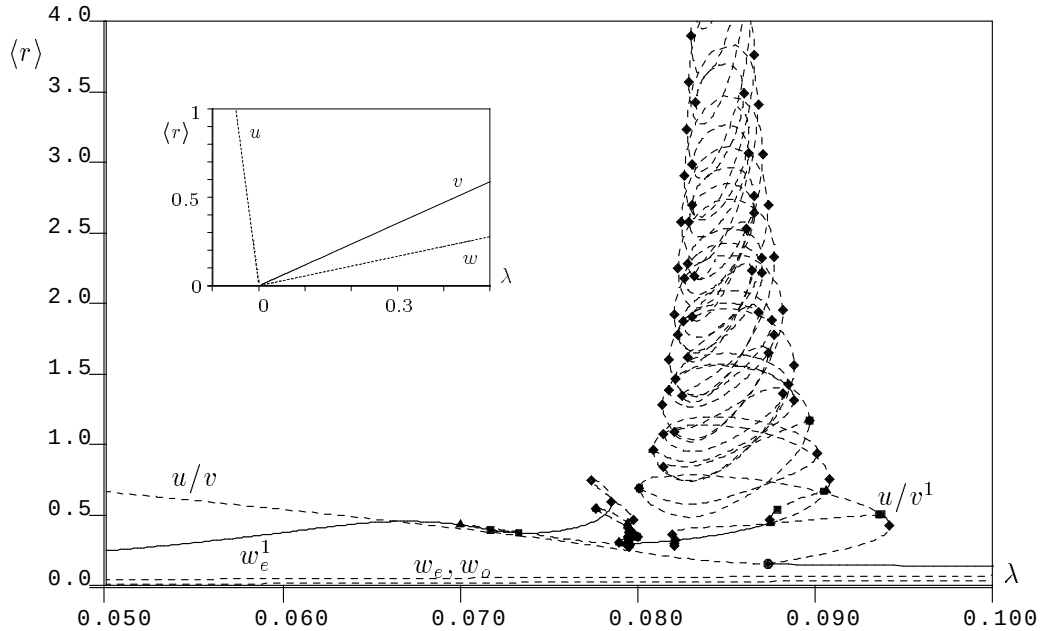

Figure 3.29: Bifurcation diagram for the parameters $A = 1-1.5i$, $B = -2.8+5i$, $C = 0.9+i$, $\Delta\lambda = 0.03$, $\Delta\omega = 0.02$ for comparison with Figure 3.27. Not all period-doubled branches are shown. The inset shows the corresponding bifurcation diagram for the perfect system.

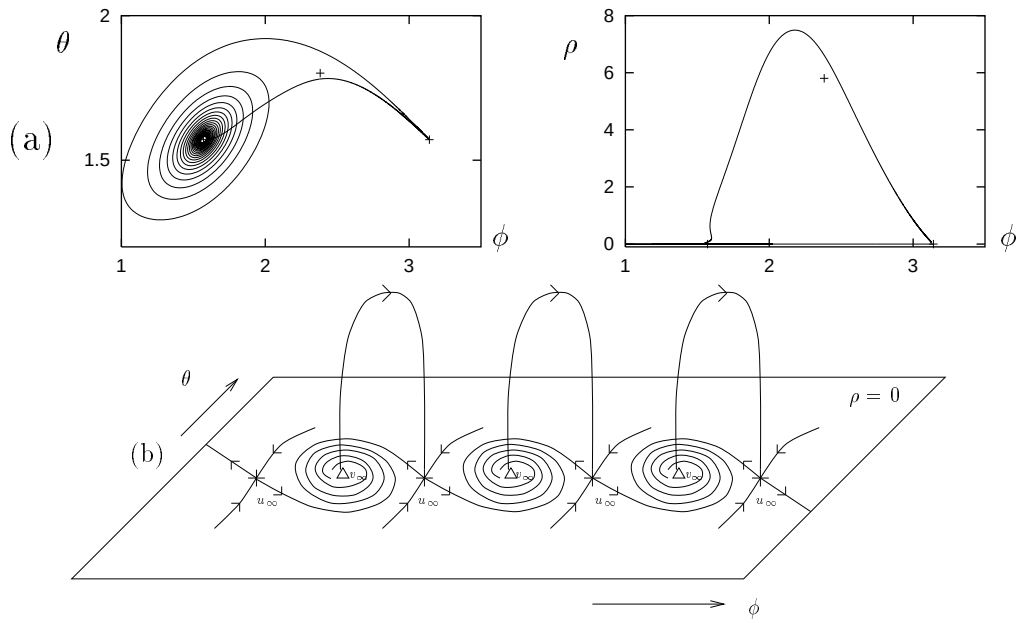

Figure 3.30: (a) A numerically calculated heteroclinic cycle involving the infinite amplitude fixed points u_∞ and v_∞ at $\lambda = 0.08461$. (b) Sketch of the complete heteroclinic network showing all connections.

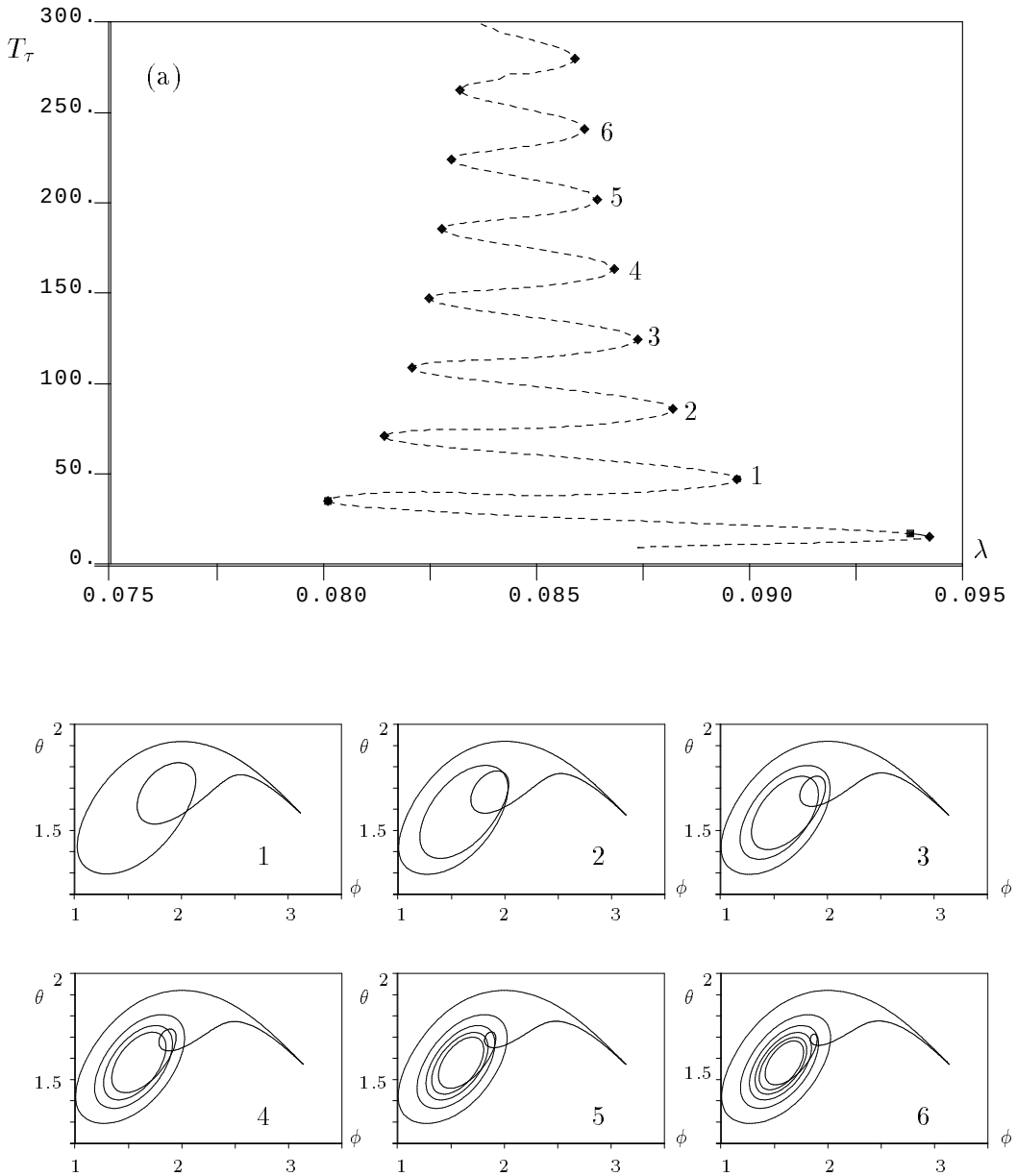

Figure 3.31: (a) The u/v^1 and (b) the w_e^1 solution branches as a function of λ. The time between successive bursts in terms of the τ time is T_τ ($\frac{1}{2}T_\tau$) for the u/v^1 (w_e^1) branch. The accompanying phase space projections show the approach to the two basic units of the heteroclinic network, sketched in (c,d) as solid lines. The cycle forms at $\lambda_c = 0.08461$.

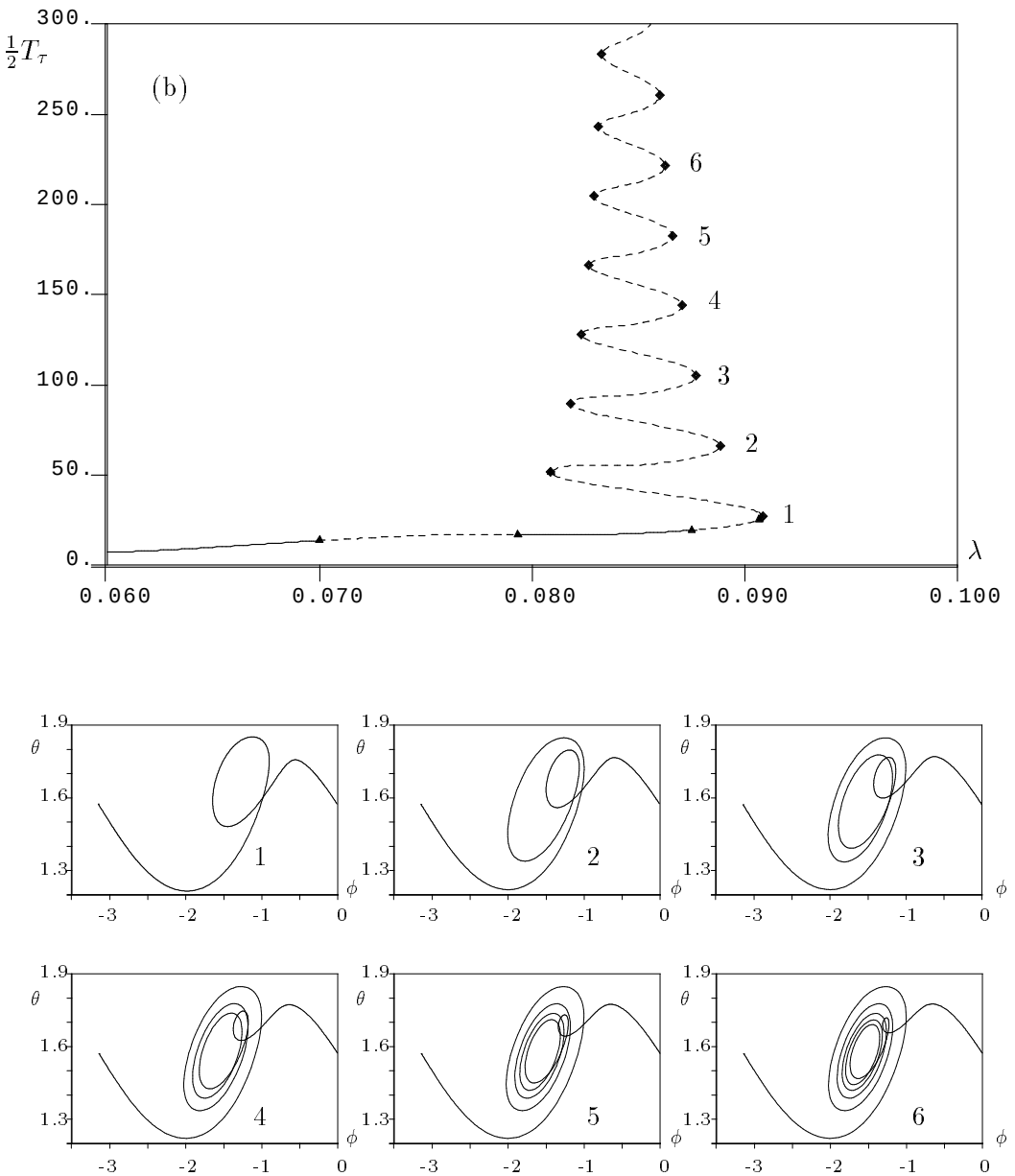

Figure 3.31: *Continued.*

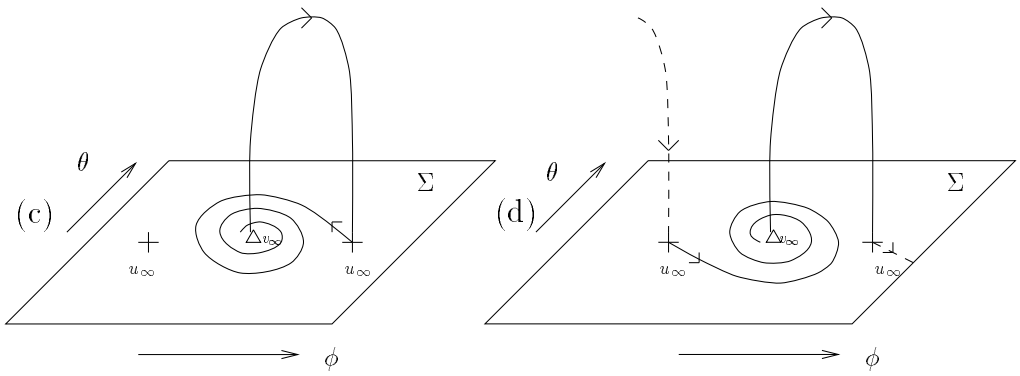

Figure 3.31: *Continued.*

Example 3

When

$$A = 1 - 1.5i, B = -2.8 + 5i, C = 1 + 0.92i; \quad \Delta\lambda = \Delta\omega = 0$$

the u and ns solutions are subcritical and the v, w and qp solutions are supercritical. Application of the parameter symmetry P_2 and a rescaling of time brings these parameters into the range $-3 < B_R < -1, C_R = -1$ and region II of parameter space, i.e., case (d) of Figure 3.9. The bifurcation diagram for $\Delta\lambda = 0.03, \Delta\omega = 0.02$ is shown in Figure 3.35(a). In this example the w_e^1 branch undergoes Shil'nikov-like behavior with the saddle-node bifurcations clearly accumulating at two different λ values $\lambda_{c1} \approx 0.1047$ and $\lambda_{c2} \approx 0.1181$; see Figure 3.35(b). Also, the branches which arise from symmetry-breaking pitchfork bifurcations from the w_e^1 branch do not form subsidiary heteroclinicities (see Figure 3.35(c)). In addition, the u/v^1 branch now terminates in a global bifurcation involving the u/v solutions; numerically, this occurs at the point at which the u/v solutions undergo a saddle-node

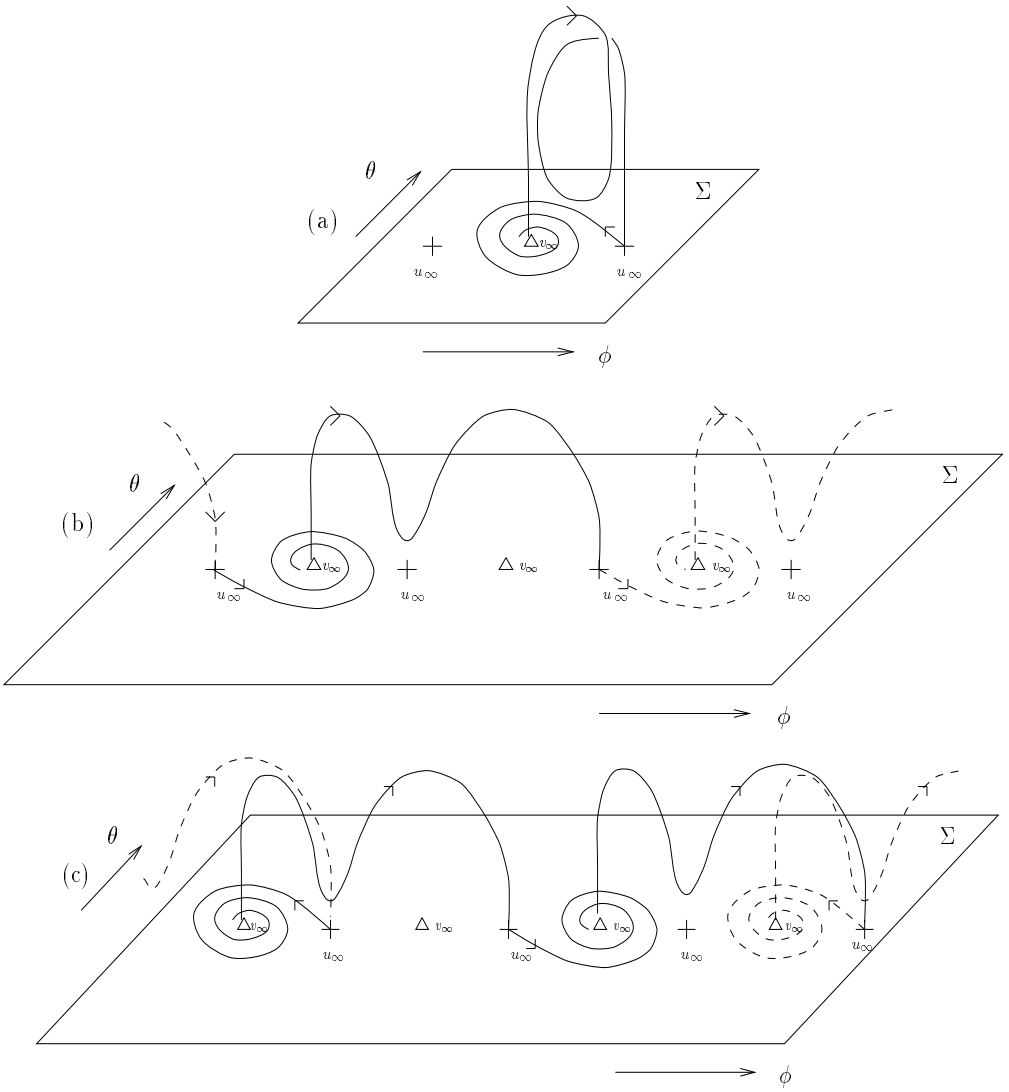

Figure 3.32: Sketches of several subsidiary heteroclinic cycles arising from a period-doubling bifurcation on (a) the u/v^1 branch and (b) the w_e^1 branch, respectively. Figure (c) shows a further possibility not detected numerically. Solid lines indicate the basic units for each cycle.

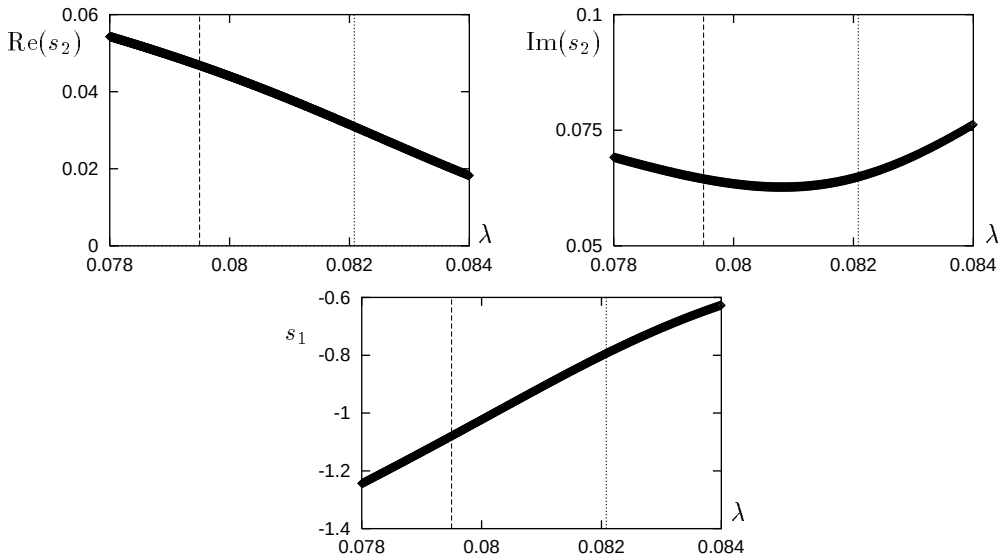

Figure 3.33: The eigenvalues $s_1, s_2, \bar{s_2}$ of the u/v fixed points as a function of λ. The vertical dashed (dotted) lines show the λ values at which the heteroclinic (homoclinic) bifurcations involving the finite amplitude u/v fixed points occur.

bifurcation.

Example 4

When

$$A = 1 - 1.5i, B = -2.8 + 4.5i, C = 0.93 + 0.94i; \quad \Delta\lambda = \Delta\omega = 0$$

the u and ns solutions are subcritical, the v and w solutions supercritical, and qp solutions absent. Application of the parameter symmetry $P_3 \cdot P_1$ and a rescaling of time brings these parameters into the range $-3 < B_R < -1, C_R = -1$ and region III of parameter space and hence case (b) of Figure 3.9. The bifurcation diagram for $\Delta\lambda = 0.03, \Delta\omega = 0.02$ is shown in Figure 3.36. The w_e^1 branch again exhibits Shil'nikov-like behavior, as do the branches born in symmetry-breaking pitchfork bifurcations on the w_e^1 branch (only one such branch is shown in Figure 3.36). For the λ values studied, the u/v branch does not undergo a Hopf

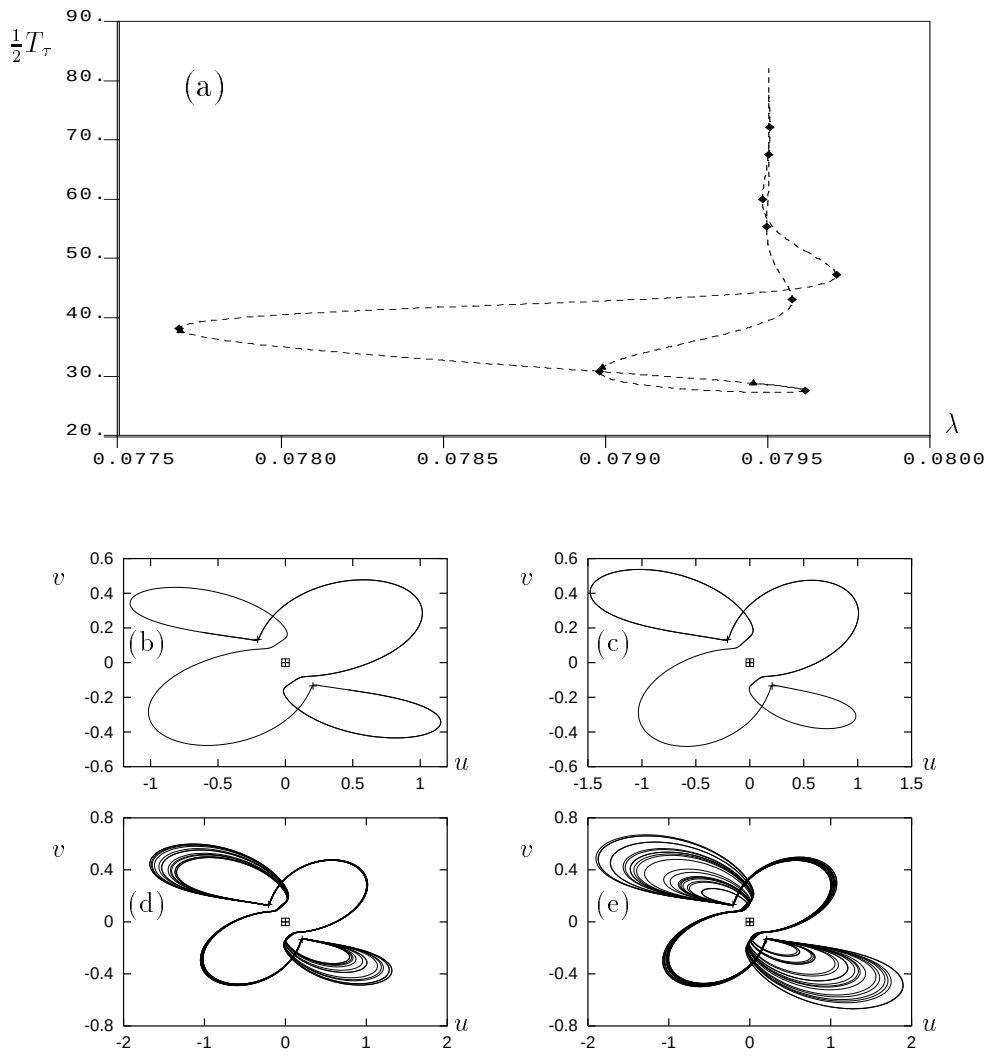

Figure 3.34: (a) Bifurcation diagram for the s^1 solution branch. This branch terminates at both ends in the global bifurcation at $\lambda \approx 0.0795$. Branches which bifurcate from the s^1 branch in symmetry-breaking pitchfork bifurcations are not shown. (b) Stable RS s^1 solution at $\lambda = 0.0795$ with $\frac{1}{2}T_\tau \approx 28.7$. (c) Stable NRS periodic orbit at $\lambda = 0.0794$, arising from a symmetry-breaking pitchfork bifurcation on the s^1 branch at $\lambda = 0.07945762$. (d) One of the NRS strange attractors at $\lambda = 0.07935$. (e) A RS strange attractor at $\lambda = 0.0793$ produced from two κ_1-related NRS attractors in a symmetry-increasing bifurcation at $\lambda = 0.0793499$.

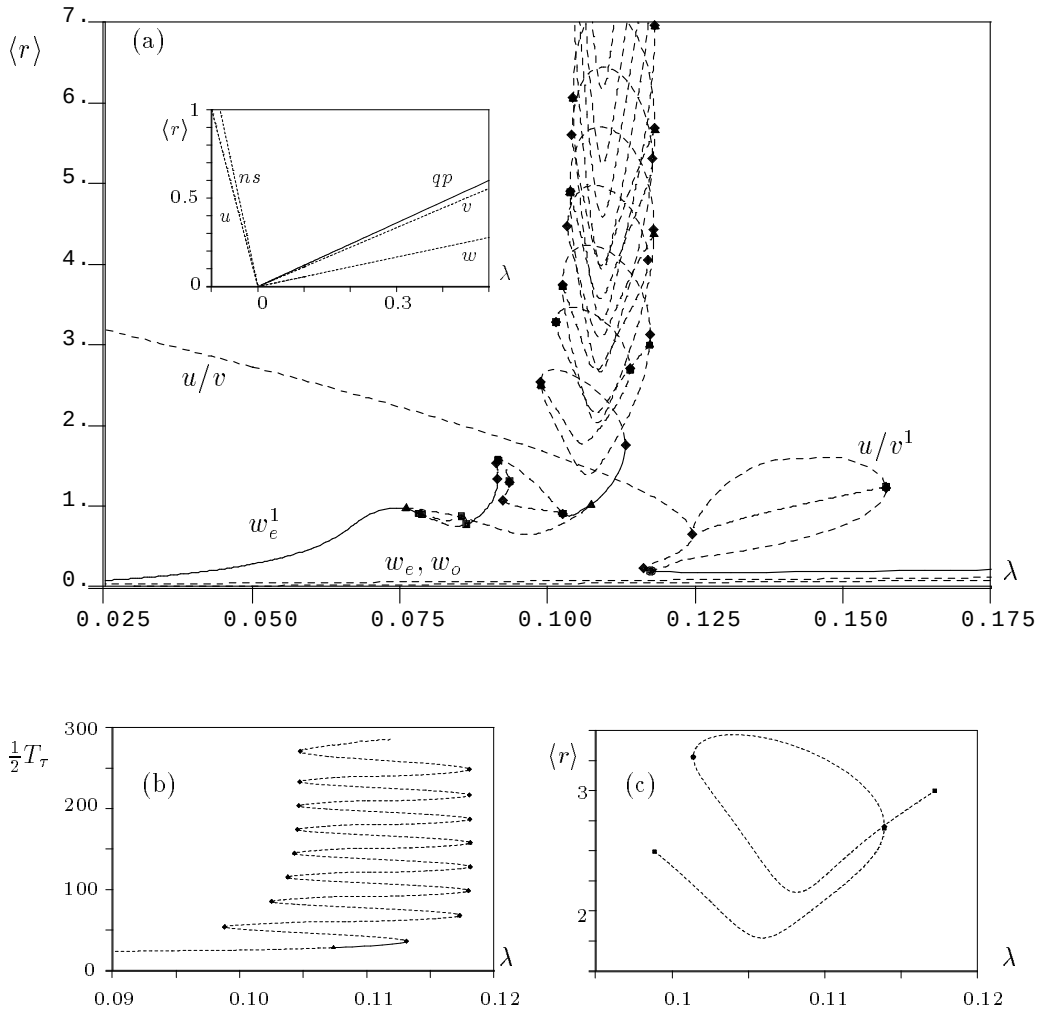

Figure 3.35: (a) Bifurcation diagram for the parameters $A = 1 - 1.5i$, $B = -2.8 + 5i$, $C = 0.92 + i$, $\Delta\lambda = 0.03$, $\Delta\omega = 0.02$. Not all period-doubled branches are shown. The inset shows the corresponding bifurcation diagram for the perfect system. (b) Shil'nikov-like behavior on the w_e^1 branch with saddle-node bifurcations accumulating at $\lambda_{c1} \approx 0.1047$ and $\lambda_{c2} \approx 0.1181$. (c) The branch arising from a symmetry-breaking bifurcation on the w_e^1 branch at $\lambda = 0.09878$, $\langle r \rangle = 2.545$, terminating at $\lambda = 0.1173$, $\langle r \rangle = 3.001$.

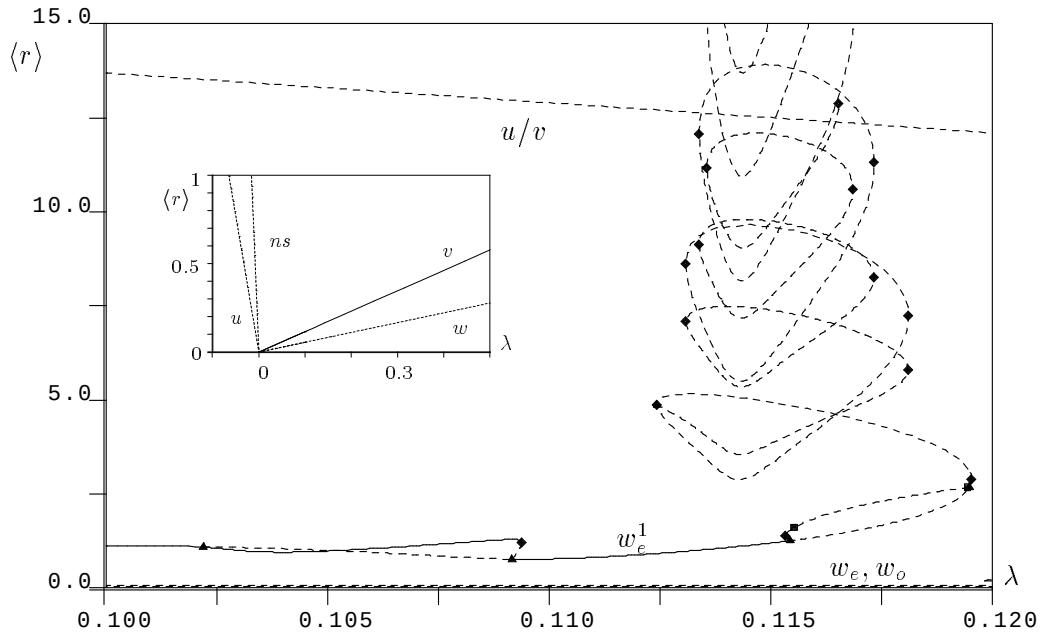

Figure 3.36: Bifurcation diagram for the parameters $A = 1 - 1.5i$, $B = -2.8 + 4.5i$, $C = 0.93 + 0.94i$, $\Delta\lambda = 0.03$, $\Delta\omega = 0.02$. Not all period-doubled branches are shown. The inset shows the corresponding bifurcation diagram for the perfect system.

bifurcation and no u/v^1 branch is present.

In the next section we discuss the effects of changing the magnitude of the forced symmetry-breaking and, given the large amplitude of the bursts, of including higher order terms in these equations.

3.5 Robustness of Results

3.5.1 Symmetry-Breaking Parameters

We focus on equations (3.9,3.10) with parameters as in Example 1(a) but different values of $\Delta\omega$. The Hopf bifurcation on the w_e branch that gives rise to the w_e^1 solution occurs when

$$2\lambda + (2A_R + B_R)r_{w_e} = 0$$

$\Delta\omega$	$r_{\max}$	T_b
0.02	7.649	29.27
0.1	0.763	7.85
0.5	0.296	2.69

Table 3.5: Maximum burst amplitude ($r_{\max}$) and time between bursts (T_b) for stable periodic solutions when $A = 1 - 1.5i$, $B = -2.8 + 5i$, $C = 1 + i$, $\lambda = 0.1$, $\Delta\lambda = 0.03$, and different values of $\Delta\omega$.

provided

$$\begin{vmatrix} 2\lambda + (2A_R + B_R + C_R)r_{w_e} & -2\Delta\omega - (B_I + C_I)r_{w_e} \\ 2\Delta\omega + (B_I - C_I)r_{w_e} & 2\lambda + (2A_R + B_R - C_R)r_{w_e} \end{vmatrix} > 0.$$

Here r_{w_e} is given by (3.20). Thus $\Delta\omega$ does not affect the location of this bifurcation which continues to occur at $\lambda = 0.00857143$, although it does affect the resulting Hopf frequency. Bifurcation diagrams for $\Delta\omega = 0.1$ and $\Delta\omega = 0.5$ are shown in Figure 3.37. We see that the w_e^1 branch still terminates at a global bifurcation involving the finite amplitude u/v solutions; however, this occurs at higher λ values than for $\Delta\omega = 0.02$. Moreover, the u/v^1 solutions no longer exist. As $\Delta\omega$ increases the phase ϕ slips more and more rapidly, cf. equation (3.13), and averaging then eliminates the parameter C from equations (3.11,3.12), giving

$$r = -\frac{2\lambda}{2A_R + B_R}, \qquad \theta = \cos^{-1}\left(-\frac{2\Delta\lambda}{rB_R}\right).$$

Since r is now constant in time the bursts fade away with increasing $\Delta\omega$ and are replaced by smaller amplitude, higher frequency states (see Table 3.5 and Figure 3.38). However, even for extreme values of $\Delta\omega$ it is apparently still possible to choose λ values so that bursts of large dynamic range occur (see Figure 3.39).

We next consider the parameters of Example 1(a) but with $\Delta\omega = -0.02$. The

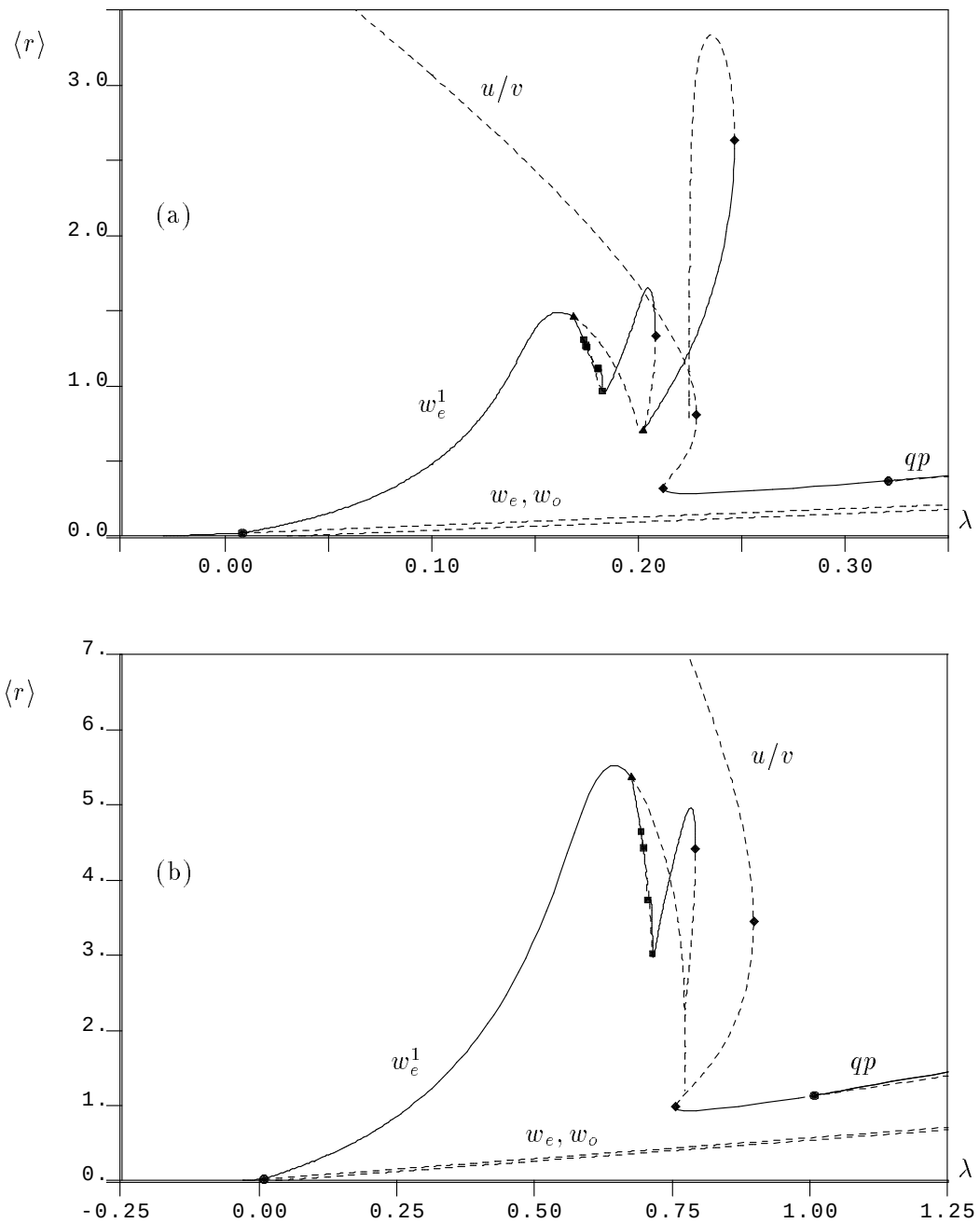

Figure 3.37: Bifurcation diagrams for the parameters $A = 1 - 1.5i$, $B = -2.8 + 5i$, $C = 1 + i$, $\Delta\lambda = 0.03$ and (a) $\Delta\omega = 0.1$ (b) $\Delta\omega = 0.5$.

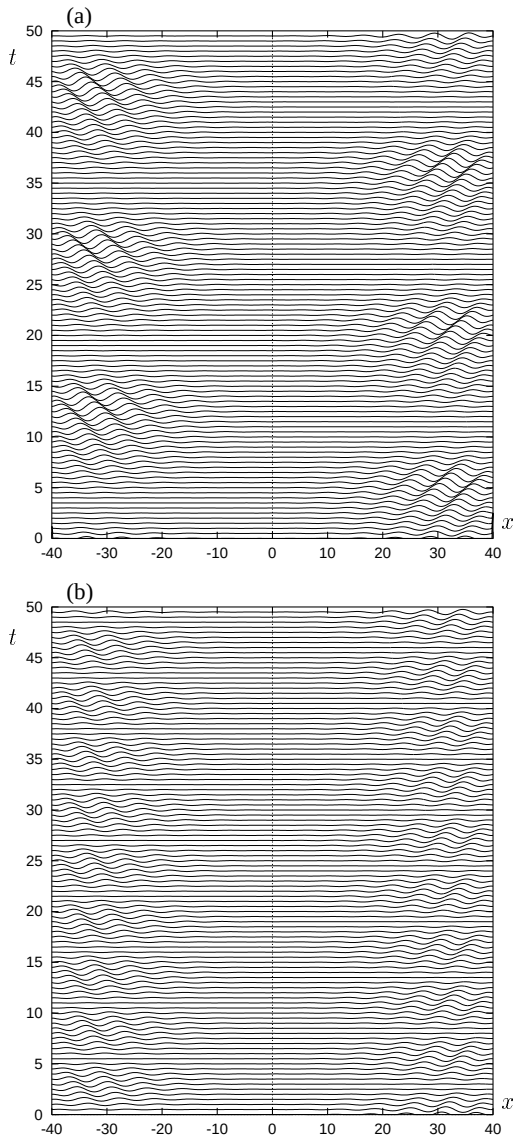

Figure 3.38: The perturbation Ψ from the trivial state showing stable periodic solution for the parameters of Example 1(a) except with (a) $\Delta\omega = 0.1$ and (b) $\Delta\omega = 0.5$. From these and Figure 3.14 we see that the bursts fade away with increasing $\Delta\omega$ and are replaced by smaller amplitude, higher frequency states. The amplitude scales are the same here as for Figure 3.14.

resulting bifurcation diagram is shown in Figure 3.40. Both w_e^1 and u/v^1 branches undergo Shil'nikov-like behavior, with the saddle-node bifurcations accumulating to $\lambda_{c1} \approx 0.02554$ and $\lambda_{c2} \approx 0.03642$. New types of solutions found for these parameter values include stable chaotic states which visit the vicinity of the same infinite amplitude fixed point (see Figure 3.41 (a)) and stable chaotic states which are characterized by successive visits to the vicinity of the Σ subspace sometimes near the *same* and sometimes near a *different* but symmetry-related infinite amplitude fixed point (see Figure 3.41 (b)), much as already described by [95].[9] Figure 3.41(c) demonstrates that for $\lambda_{c1} < \lambda < \lambda_{c2}$ two distinct heteroclinic cycles exist for the *same* λ value, as expected from §3.4.2.

When $\Delta\omega$ is held fixed bursts persist for a range of $\Delta\lambda$ values as well. However, we have not attempted a detailed classification of the properties of equations (3.9,3.10) for arbitrary values of $\Delta\lambda$ and $\Delta\omega$. A quick exploration has revealed the possibility of bursts of extremely large dynamic range (see Figure 3.42), which emphasizes that the dynamic range for this burst mechanism is *infinite*.

3.5.2 Higher Order Terms

Thus far we have studied equations (3.9,3.10) which have been truncated at third order in the amplitudes z_+ and z_-. The presence of bursts of large amplitude requires, however, that we reexamine the truncation that led us to these equations. Recall that in the derivation that leads to these equations the *physical* amplitudes are $\epsilon^{1/2} z_\pm$, where $\epsilon \equiv (R - R_c)/R_c$ measures the distance above threshold. It follows that the physical amplitudes remain small provided $\epsilon^{1/2}|z_\pm|_{\max} \ll 1$. Under these conditions all fifth order

[9] The term $-0.75 r_1^3$ in equation (4b) of [95] should be $-0.75 r_1^3 \rho$.

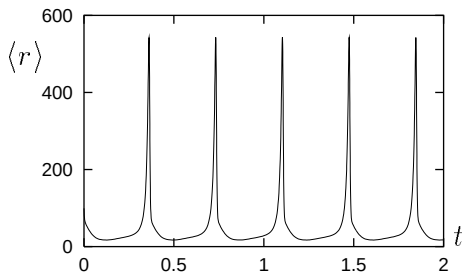

Figure 3.39: Bursts with large dynamic range at $\lambda = 15$ and $A = 1 - 1.5i$, $B = -2.8 + 5i$, $C = 1 + i$, $\Delta\lambda = 0.03$ and $\Delta\omega = 10$.

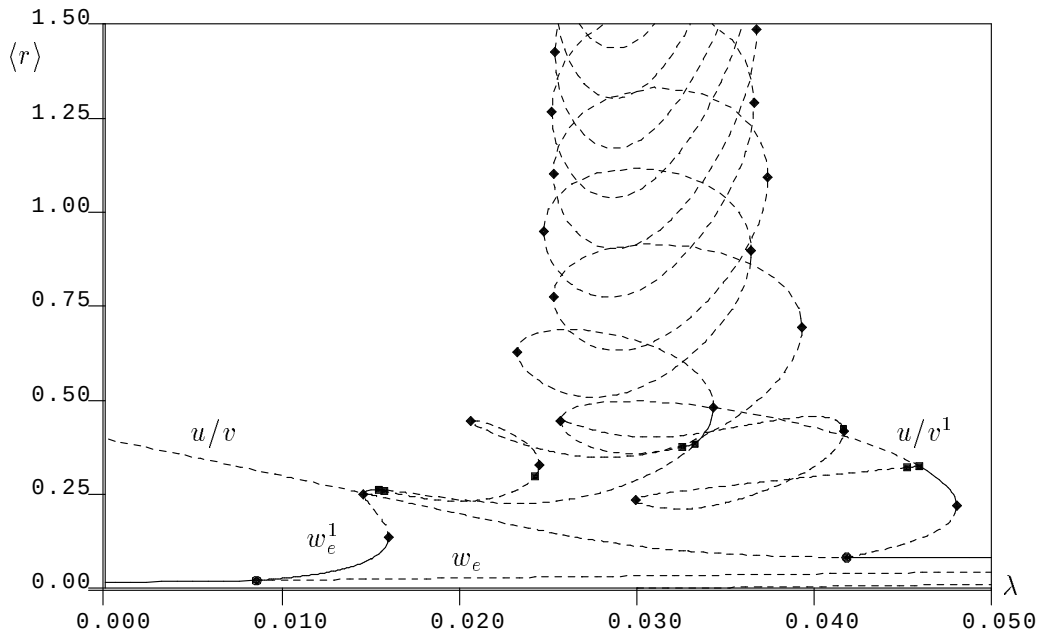

Figure 3.40: Bifurcation diagram for the parameters $A = 1-1.5i$, $B = -2.8+5i$, $C = 1+i$, $\Delta\lambda = 0.03$, $\Delta\omega = -0.02$. The bifurcation diagram for the perfect system is shown in the inset of Figure 3.11.

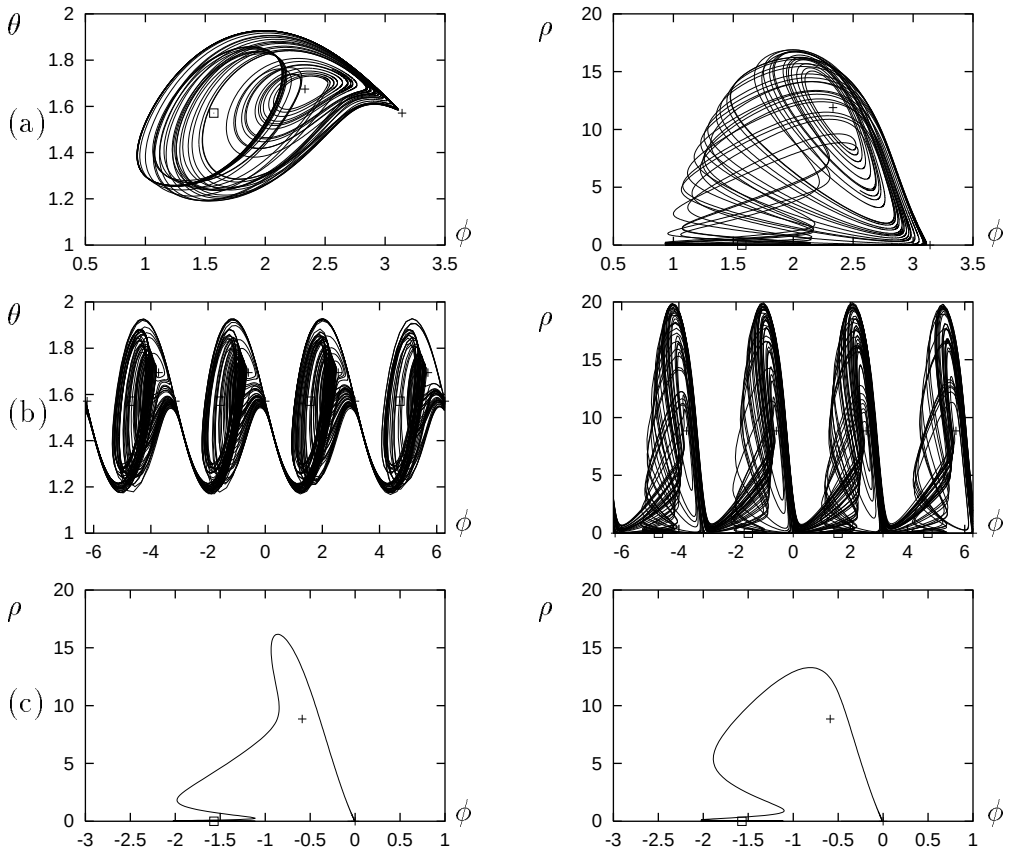

Figure 3.41: (a) Stable chaotic state with repeated visits to the vicinity of the same infinite amplitude states for $A = 1 - 1.5i$, $B = -2.8 + 5i$, $C = 1 + i$, $\Delta\lambda = 0.03$, $\Delta\omega = -0.02$ and $\lambda = 0.04$, corresponding to a chaotic winking state. (b) Stable chaotic state at $\lambda = 0.03$ which makes repeated visits to either the same infinite amplitude state or symmetry-related ones. The resulting state is neither purely blinking or purely winking. (c) Two distinct heteroclinic cycles exist for $\lambda = 0.03$ which lies between λ_{c1} and λ_{c2}.

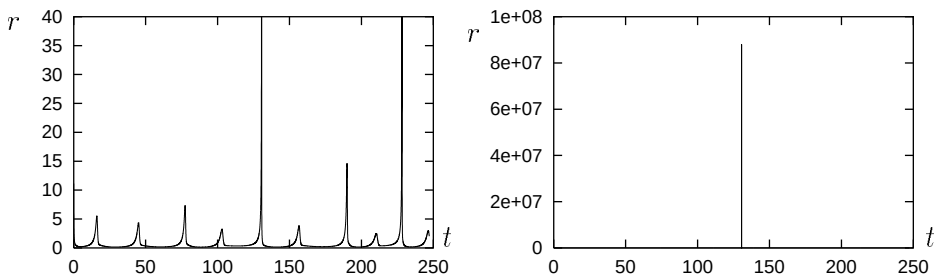

Figure 3.42: Bursts with extremely large dynamic range for the parameters of Example 1(a) except with $\Delta\lambda = 0.06$, $\Delta\omega = -0.01$, $\lambda = 0.1$.

terms in equations (3.9,3.10) enter the derivation with $\mathcal{O}(\epsilon)$ coefficients and remain small relative to the cubic terms retained. However, the presence of even small fifth order terms has an effect: if such terms are stabilizing the solutions responsible for the bursting behavior cannot reach arbitrarily large amplitude and instead have large but *finite* amplitudes. As an example we consider the system

$$\begin{aligned}
\dot{z}_+ &= [\lambda + \Delta\lambda + i(\omega + \Delta\omega)]z_+ + A(|z_+|^2 + |z_-|^2)z_+ + B|z_+|^2 z_+ + C\bar{z}_+ z_-^2 + D|z_+|^4 z_+, \\
\dot{z}_- &= [\lambda - \Delta\lambda + i(\omega - \Delta\omega)]z_- + A(|z_+|^2 + |z_-|^2)z_- + B|z_-|^2 z_- + C\bar{z}_- z_+^2 + D|z_-|^4 z_-,
\end{aligned}$$

and analyze the consequences of the new terms, choosing the $\mathcal{O}(\epsilon)$ coefficient $D \equiv D_R + iD_I$ such that the subcritical branch undergoes a saddle-node bifurcation. In this case solutions on this branch exist even for $\lambda > 0$. Equations (3.22-3.24) become

$$\begin{aligned}
\frac{d\rho}{d\tau} &= -\rho[2A_R + B_R(1 + \cos^2\theta) + C_R \sin^2\theta \cos 2\phi] - 2(\lambda + \Delta\lambda \cos\theta)\rho^2 \\
&\quad -\frac{5}{4}D_R - \frac{3}{4}D_R \cos 2\theta \\
\frac{d\theta}{d\tau} &= \sin\theta[\cos\theta(-B_R + C_R \cos 2\phi) - C_I \sin 2\phi] - 2\Delta\lambda \sin\theta\rho - \frac{D_R}{\rho}\cos\theta \sin\theta \\
\frac{d\phi}{d\tau} &= \cos\theta(B_I - C_I \cos 2\phi) - C_R \sin 2\phi + 2\Delta\omega\rho + \frac{D_I \cos\theta}{\rho}.
\end{aligned}$$

We consider the parameter values from Example 2 with $(D_R, D_I) = \epsilon(-1, 1)$. For $\epsilon > 0$, the u_∞ fixed points have moved out of the $\rho = 0$ plane which is no longer invariant; we call these u_{finite} fixed points. Fixed points analogous to the v_∞ fixed points do not exist for these parameters. Bursts now occur when the trajectory makes visits near the large but finite amplitude u_{finite} fixed points (see Figure 3.43). To explore the effect of the fifth order terms on the bifurcation diagrams, we focus our discussion on the u/v^1 branch; similar results hold for other branches. Figure 3.44 compares the bifurcation diagrams for

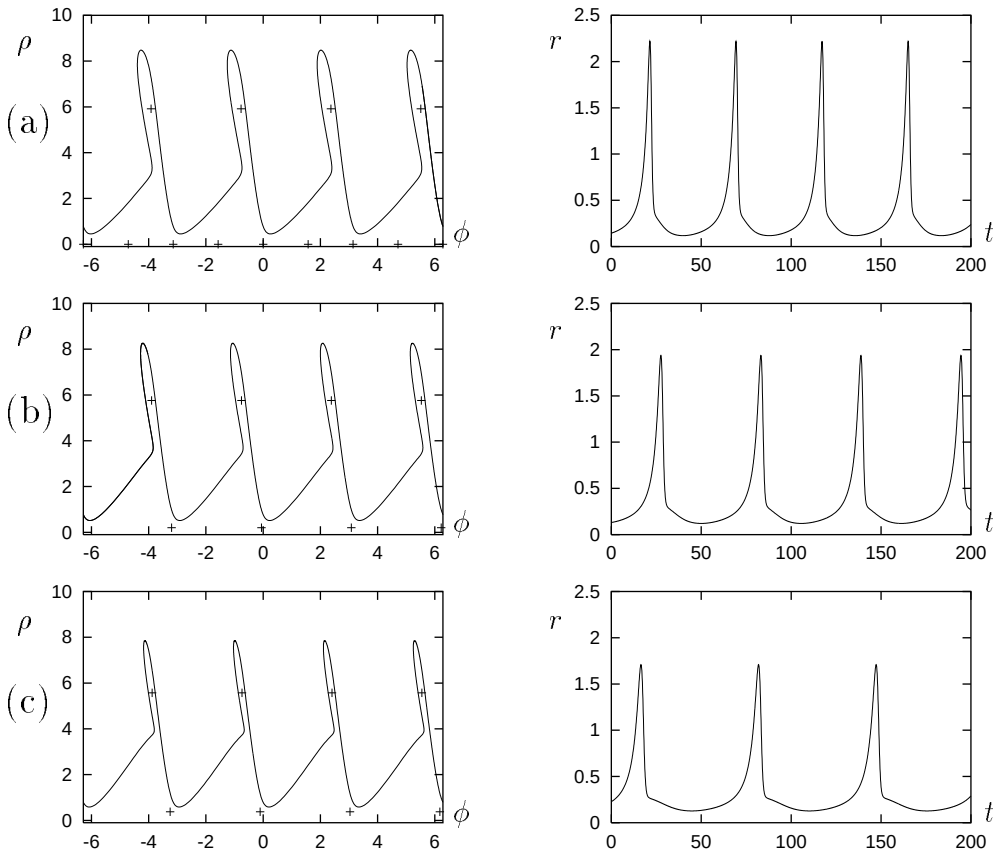

Figure 3.43: Robustness of the bursts for the parameters of Example 2 and $\lambda = 0.085$ to the addition of a small fifth order term. (a) shows the stable w_e^1 solution for $\epsilon = 0$. The bursts persist for (b) $\epsilon = 0.05$ and (c) $\epsilon = 0.1$. The u_∞ fixed point for (a) has moved out of the $\rho = 0$ plane for (b) and (c), giving u_{finite} fixed points.

$\epsilon = 0.01$, $\epsilon = 0.00001$ and $\epsilon = 0$, and demonstrates that as ϵ decreases the system behavior approaches that for $\epsilon = 0$, i.e., the limit $\epsilon \to 0$ captures the mechanism responsible for the generation of bursts near threshold of the primary instability. Moreover, in this example, the "complexity" of the dynamical behavior increases with decreasing ϵ, in contrast with typical situations in the study of the transition to complex behavior where the "complexity" of a system increases with the distance above threshold.

Finally, it should also be noted that when ρ is small any D_4-breaking terms omitted

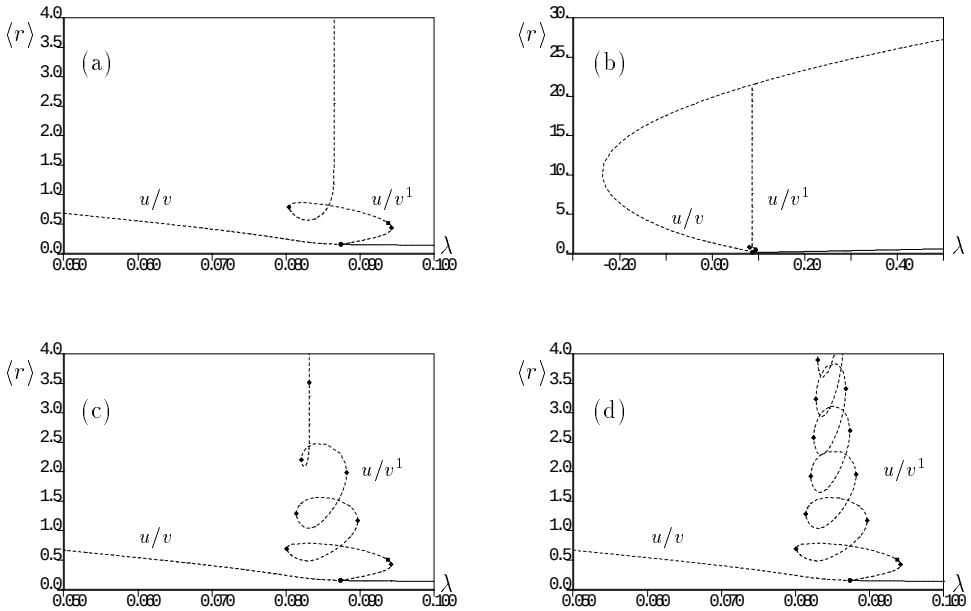

Figure 3.44: Bifurcation diagrams for the u/v^1 branch for (a,b) $\epsilon = 0.01$, (c) $\epsilon = 0.00001$, and (d) $\epsilon = 0$. For $\epsilon > 0$ the u/v^1 solution collides with a new u_{finite} fixed point; this global bifurcation manifests itself as a vertical branch in the bifurcation diagrams. At the same time $\langle r \rangle$ approaches the value of r for the new fixed point.

from the cubic terms in equations (3.9,3.10) may also become significant and change the detailed dynamics near $\rho = 0$. The effect of this has not been studied.

3.6 Concluding Remarks

3.6.1 Summary

In this chapter, we have described a simple geometrical mechanism responsible for the presence of bursts, both periodic and nonperiodic, very close to threshold of an oscillatory instability in systems with broken D_4 symmetry. The mechanism relies on the presence of structurally stable connections in an invariant subspace Σ corresponding to infinite amplitude states together with a connection out of Σ back to Σ, and is of codimension

one. The D_4 symmetry must be broken in order for repeated bursts to occur; in this sense, forced symmetry-breaking is responsible for the bursting behavior. We emphasize that the mechanism requires that at least of the solution branches bifurcates subcritically and one supercritically for the perfect problem ($\Delta\lambda = \Delta\omega = 0$). Also, we have shown that the mechanism is robust with respect to the addition of small higher order terms in the amplitude equations. We have not considered the possibility that the burst amplitude can become large enough for secondary instabilities not captured by the ansatz (3.5) to be triggered; such instabilities could occur on very different scales and result in *turbulent* bursts. The mechanism described in this dissertation provides an explanation for bursts in binary fluid convection in containers with large aspect-ratio, such as the bursts of convective heat transport which occur immediately above threshold for a ^{3}He/^{4}He mixture in a large aspect-ratio container as reported in [76] and described in §3.1. Similar results are expected for the mathematically identical counterrotating Taylor-Couette system where counterpropagating spiral vortices play the same role as traveling waves in convection [96, 97]. Chapter 4 will show that related bursts may arise due to resonant temporal forcing of a system undergoing a Hopf bifurcation with exact D_4 symmetry. Other burst mechanisms which have been proposed for hydrodynamical systems are reviewed and compared to this new mechanism in Chapter 5.

The bursts described in this chapter are the result of competition between two nearly degenerate modes of opposite parity and "frozen" spatial structure. Consequently, the burst mechanism applies in systems in which bursts occur very close to threshold. A large aspect-ratio Γ is required for the presence of the approximate D_4 symmetry. If the size

of the D_4 symmetry-breaking terms $\Delta\lambda$, $\Delta\omega$ is increased too much the bursts fade away and are replaced by smaller amplitude, higher frequency states. Thus, we expect that bursts will not be present if the aspect-ratio Γ is too small or the reduced Rayleigh number ϵ too large.

3.6.2 An Alternative Model

An alternative approach to modeling large aspect-ratio binary fluid convection is given in [1, 2, 5], and is based on a description using left-moving and right-moving traveling waves. In this approach one supposes that the large aspect-ratio system can be viewed as a perturbation of the unbounded system with periodic boundary conditions. If the system is also symmetric under reflections in any vertical plane, the primary instability is a Hopf bifurcation with O(2) symmetry (cf. §2.7.1). Specifically, if we write the perturbation to the conduction state in the form

$$\Psi \sim \mathrm{Re}\{z_1 e^{ikx} + z_2 e^{-ikx}\},$$

where z_1 and z_2 are amplitudes of left-moving and right-moving traveling waves, then z_1 and z_2 evolve according to equations (2.9,2.10). However, in the real system the presence of endwalls breaks the horizontal translation symmetry of the unbounded system; if this symmetry-breaking is assumed to be weak, only the small linear translation symmetry-breaking terms $(\dot{z}_1, \dot{z}_2) \sim (z_2, z_1)$ modify equations (2.9,2.10). As an example, consider the case in which in the absence of symmetry-breaking the TW bifurcate subcritically and SW supercritically (see Figure 3.45(a)). When the translation symmetry is broken, the SW remain as primary solutions (although they are split into two branches of odd

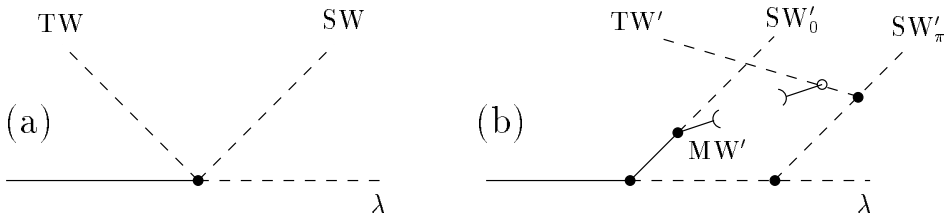

Figure 3.45: Possible schematic bifurcation diagrams for the O(2)-equivariant Hopf bifurcation (a) in the absence of symmetry-breaking, (b) with broken translation symmetry. The filled (open) circles indicate local (global) bifurcations. The MW′ branch represents modulated waves, and the break in this curve indicates the onset of complicated behavior which might include stable chaos.

and even parity) and continue to bifurcate supercritically (see Figure 3.45(b)). The TW, however, can no longer bifurcate from the trivial state and hence *must* bifurcate off one of the SW branches in a secondary bifurcation. As a consequence the small amplitude SW are "unmasked" and stable small amplitude states are now present [75]. In this regime, a number of global bifurcations and associated (stable) chaos is found [5]. In the absence of forced symmetry-breaking the values of λ for which the nontrivial TW and SW states are present do not overlap; consequently no recurrent dynamics are possible. The important consequence of breaking the translation symmetry is precisely the generation of a small interval in λ in which both types of solutions coexist, thereby allowing connections between them.

This model, considered in detail in [1, 2, 5], can be compared with the approach of this dissertation by rewriting equations (3.9,3.10) in the "traveling wave coordinates" [6, 77]

$$z_1 = \frac{1}{2}(z_+ + z_-), \qquad z_2 = \frac{1}{2}(z_+ - z_-).$$

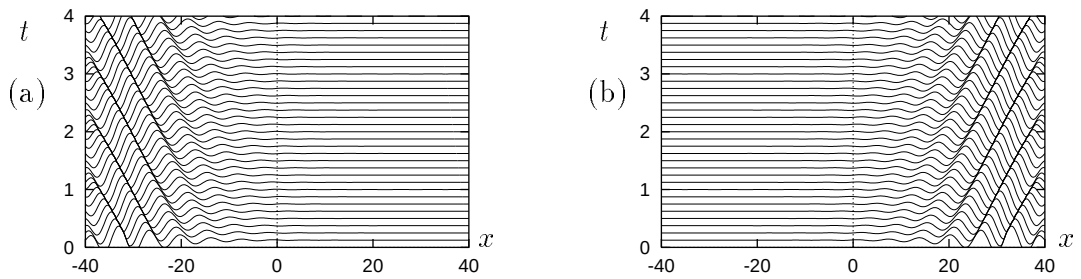

Figure 3.46: Space-time plots showing the perturbation from the conduction state Ψ for (a) $z_1 \sim e^{i\omega t}, z_2 = 0$, and (b) $z_1 = 0, z_2 \sim e^{i\omega t}$. Time increases upwards, and the time axis is rescaled so that the Ψ has a period of 1. Thus, z_1 and z_2 are the amplitudes of a left-moving and right-moving traveling wave, respectively.

Then the perturbation (3.5) to the conduction state takes the form

$$\Psi \sim \mathrm{Re}\{z_1(t)f_1 + z_2(t)f_2\},$$

where $f_1 = f_+ + f_-$ and $f_2 = f_+ - f_-$. The interpretation of the traveling wave coordinates, using the approximate eigenfunctions $f_\pm$ from equation (3.19), is shown in Figure 3.46. In these coordinates equations (3.9,3.10) become

$$\dot{z}_1 = (\lambda + i\omega)z_1 + (\Delta\lambda + i\Delta\omega)z_2 + a(|z_1|^2 + |z_2|^2)z_1 + b|z_1|^2 z_1 + c\bar{z}_1 z_2^2, \quad (3.26)$$

$$\dot{z}_2 = (\lambda + i\omega)z_2 + (\Delta\lambda + i\Delta\omega)z_1 + a(|z_1|^2 + |z_2|^2)z_2 + b|z_2|^2 z_2 + c\bar{z}_2 z_1^2, \quad (3.27)$$

where $a = 2(A+B+C)$, $b = 3C - B$, and $c = B + C$. These equations contain the expected small linear translation symmetry-breaking terms (z_2, z_1), but differ from the equations considered in [1, 2, 5] because they also contain the nonlinear terms $(\bar{z}_1 z_2^2, \bar{z}_2 z_1^2)$. As argued in this dissertation, these are generically expected to be $\mathcal{O}(1)$ even for large aspect-ratios, and hence do not represent a perturbation of the O(2)-symmetric system.

To illustrate the potential importance of these nonlinear terms, we now show that in their absence bursts *cannot* occur. For $c = 0$, equations (3.26,3.27) describe the O(2)-

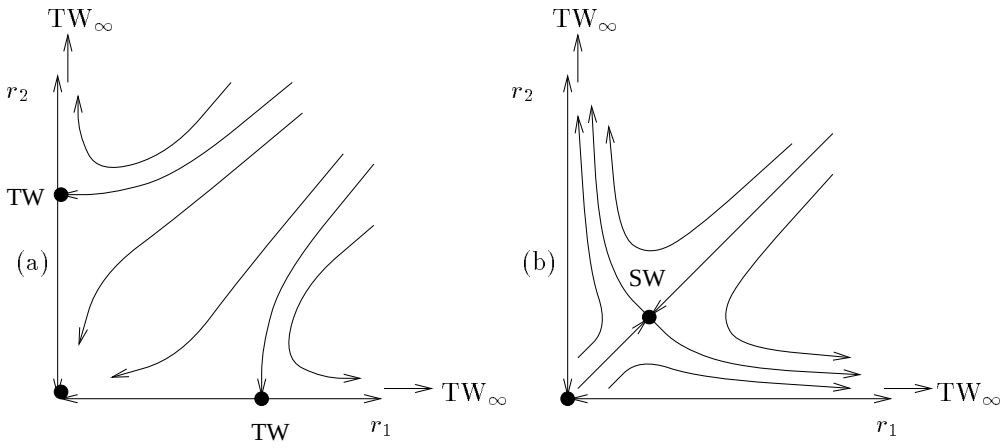

Figure 3.47: Phase portraits for equations (3.26,3.27) with $c = 0$ for the case that TW solutions are subcritical and SW solutions are supercritical. Here $z_1 = r_1 e^{i\theta_1}, z_2 = r_2 e^{i\theta_2}$, and the r_1 and r_2 equations decouple (see §2.7.1). Both for (a) $\lambda < 0$ and (b) $\lambda > 0$ certain initial conditions give trajectories which asymptote to TW$_\infty$. The lack of a return mechanism from infinite amplitudes prevents heteroclinic cycles involving infinite amplitude solutions from existing.

equivariant Hopf bifurcation with weakly broken translation symmetry as considered in [1, 2, 5]. In these equations the dynamics "at infinity" are again governed by the problem with perfect symmetry ($\Delta\lambda = \Delta\omega = 0$), and solutions at infinity are radially stable (unstable) if the corresponding solution branch bifurcates subcritically (supercritically) for the perfect problem. Thus, for example, for the case in Figure 3.45(a), the TW$_\infty$ state is radially stable. However, in this case the other eigenvalue of the TW solutions is also negative, and the TW$_\infty$ solutions are therefore attractors (see Figure 3.47). Therefore, trajectories tend directly to the TW$_\infty$ solutions (cf. [98]), and there is no return mechanism to finite amplitude. Similar situations occur for other parameter regimes, so heteroclinic cycles involving infinite amplitude solutions cannot exist in the Hopf bifurcation with O(2) symmetry which is weakly broken. Given this significant difference, it would be very interesting to explore

the connection between the dynamics in the Hopf bifurcation with broken O(2) symmetry considered in [1, 2, 5] and the Hopf bifurcation with broken D_4 symmetry considered in this chapter in more detail by varying the coefficient C.

3.6.3 Comparison with the Experiments

Recall that in this chapter the coefficients in equations (3.9,3.10) have been chosen to reflect the appropriate sub- and supercriticality of the TW and SW branches in large aspect-ratio binary fluid convection experiments, with numerical values otherwise arbitrary. Thus, the relevance of the results of this chapter to binary fluid experiments remains qualitative. However, the model produces bursts very similar to those which are observed experimentally in [76] (for example, compare Figure 3.13(c) with Figure 3.3), suggesting that the model merits further study. In particular, it would be of interest to calculate the actual numerical values of the coefficients A, B, and C in order to *quantitatively* compare the predictions of equations (3.9,3.10) using these values with the experimental results and results from direct numerical simulations of the fully nonlinear problem (cf. [99]). The calculation of these coefficients is straightforward in principle (see [100, 101] for related calculations) but highly nontrivial in practice because even the linear problem must be solved numerically [77].

Chapter 4

Wrinkled Tori and Bursts due to Resonant Temporal Forcing of the Hopf Bifurcation with D_4 Symmetry

Recall that the normal form equations for the Hopf bifurcation with square symmetry are equivariant with respect to the group $D_4 \times S^1$, where D_4 is generated by the operations

$$\kappa_1 : (z_+, z_-) \to (z_+, -z_-), \qquad \kappa_2 : (z_+, z_-) \to (z_-, z_+),$$

and S^1 is the normal form symmetry

$$N_\sigma : (z_+, z_-) \to e^{i\sigma}(z_+, z_-) \qquad \sigma \in [0, 2\pi).$$

Chapter 3 showed in detail that periodic or chaotic bursts of very large dynamic range can occur when the interchange symmetry κ_2 is weakly broken. In this chapter, we demonstrate that bursts can also arise when the normal form symmetry is broken by resonant temporal forcing, although the necessary symmetry-breaking is much larger.

4.1 Normal Forms For Nonautonomous Equations

As mentioned in §2.3, the normal form symmetry for a Hopf bifurcation may be interpreted as a continuous time-translation symmetry. In the presence of external temporally periodic forcing this symmetry is broken because the system is only unchanged under the *discrete* time-translations $t \to t + \frac{2\pi}{\omega_e} j$, where j is an integer and ω_e is the angular frequency of the forcing.

We first give a general characterization of the terms which appear in the normal form equations in the presence of temporally periodic forcing. Consider the nonautonomous system

$$\frac{d\mathbf{U}}{dt} = L\mathbf{U} + f_1(\mathbf{U}) + \delta F(\mathbf{U}, t),$$

where L is a matrix, f_1 is a nonlinear function of the dependent variables $\mathbf{U}$, δ is the strength of the forcing, and

$$F(\mathbf{U}, t + \frac{2\pi}{\omega_e}) = F(\mathbf{U}, t).$$

Then, the corresponding normal form describing the evolution on the center manifold is [102]

$$\frac{d\mathbf{z}}{dt} = A\mathbf{z} + N(\mathbf{z}, t, \delta),$$

where A is the projection of L onto the center manifold coordinates, and

$$\frac{d}{dt}\left[\exp(A^\dagger t)N(\exp(-A^\dagger t)\mathbf{z},t,\delta)\right]=0. \tag{4.1}$$

The variables $\mathbf{z}$ and t are treated as independent variables in this expression. The relation of this result to the result in the *absence* of forcing is as follows. In the absence of forcing, the discussion in §2.3 implies that the normal form is

$$\frac{d\mathbf{z}}{dt}=A\mathbf{z}+N(\mathbf{z}),$$

where

$$\exp(-A^\dagger t)N(\mathbf{z})=N(\exp(-A^\dagger t)\mathbf{z}).$$

Therefore

$$\frac{d}{dt}\left[\exp(A^\dagger t)N(\exp(-A^\dagger t)\mathbf{z})\right]=\frac{d}{dt}N(\mathbf{z})=0.$$

We conclude that all terms which appear in the normal form in the *absence* of forcing still appear in the normal form when forcing is present. However, *additional* terms due to the forcing may also be present.

As an example, consider the standard Hopf bifurcation. In the absence of external forcing, the normal form is

$$\frac{dz}{dt}=i\omega_0 z+g_1(|z|^2)z,$$

where $z\in\mathbb{C}$ and $\omega_0\in\mathbb{R}$ is the Hopf frequency. Consider now the effect of external periodic forcing with angular frequency ω_e. Suppressing the forcing amplitude δ for notational simplicity, let

$$N(z,t)=\sum_{l=-\infty}^{\infty}\sum_{r,s\geq 0}N_{lrs}z^r\bar{z}^s e^{i\omega_e lt},$$

where $N_{lrs} \in \mathbb{C}$. Using $\exp(A^\dagger t) = e^{-i\omega_0 t}$ equation (4.1) implies that

$$\begin{aligned} 0 &= \frac{d}{dt}\left(\sum_{l=-\infty}^{\infty}\sum_{r,s\geq 0} N_{lrs} z^r \bar{z}^s e^{i[\omega_e l+(r-s-1)\omega_0]t}\right) \\ &= \sum_{l=-\infty}^{\infty}\sum_{r,s\geq 0} i\left[\omega_e l + (r-s-1)\omega_0\right] N_{lrs} z^r \bar{z}^s e^{i[\omega_e l+(r-s-1)\omega_0]t} \end{aligned}$$

for all $t, z, \bar{z}$. Thus, $N_{lrs} = 0$ for all l, r, s such that

$$\omega_e l + (r-s-1)\omega_0 \neq 0.$$

For $l = 0$, N_{lrs} can be nonzero for $r = s+1$; these correspond to the terms which are also present in the absence of forcing. Now, assume the resonance condition

$$\frac{\omega_0}{\omega_e} = \frac{m}{n}, \tag{4.2}$$

where m and n are relatively prime integers. The additional term which is of lowest order in $|z|$ for which N_{lrs} can be nonzero is given by $l = m, r = 0, s = n-1$. Thus, to leading order, the normal form for the periodically forced Hopf bifurcation is

$$\frac{dz}{dt} = i\omega_0 z + g(|z|^2)z + f\bar{z}^{n-1}e^{im\omega_e t}.$$

This is unfolded to give

$$\frac{dz}{dt} = (\lambda + i\omega_0)z + g(|z|^2)z + f\bar{z}^{n-1}e^{im\omega_e t},$$

where $\lambda \in \mathbb{R}$ represents the distance from the Hopf bifurcation in the absence of forcing. The coefficient f is related to the strength of the forcing and may without loss of generality be taken to be real. This equation can be rewritten in autonomous form by letting

$$z = ye^{i\frac{m}{n}\omega_e t},$$

giving

$$\frac{dy}{dt} = (\lambda + i\omega)y + g(|y|^2)y + f\bar{y}^{n-1}. \tag{4.3}$$

Here the quantity

$$\omega \equiv \omega_0 - \frac{m}{n}\omega_e$$

is called the detuning; taking $\omega \neq 0$ allows the consideration of cases in which the resonance (4.2) is not exact.

Equation (4.3) is equivariant with respect to the group $Z_n = \langle T_n \rangle$, where

$$T_n : y \to e^{i2\pi/n} y$$

is interpreted as the discrete time-translation $t \to t + \frac{2\pi}{\omega_e} \approx t + \frac{2\pi}{n\omega_0}$. Therefore, the resonant temporal forcing has reduced to normal form symmetry from S^1 to Z_n. For the strong resonances $n = 1, 2, 3, 4$, equation (4.3) truncated at cubic order is

$$\frac{dy}{dt} = (\lambda + i\omega)y + (a + ib)|y|^2 y + f\bar{y}^{n-1}. \tag{4.4}$$

This equation has been studied in detail: partial studies for the case $n = 2$ include [103, 104], and a classification of the possible dynamics for $n = 1, 2, 3$ including local and global bifurcations was given in [105]. Also, see the related problems considered in [62, 106, 56]. A discussion of the dynamics for $n = 2$ is given in Appendix E.

4.2 Equations for the Hopf Bifurcation with D_4 Symmetry with Resonant Temporal Forcing

We now consider the effect of temporally periodic forcing with angular frequency ω_e on the Hopf bifurcation with D_4 symmetry and with Hopf frequency ω_0. Making use of

the interchange symmetry κ_2, the normal form is

$$\begin{aligned}\frac{dz_+}{dt} &= i\omega_0 z_+ + N(z_+, z_-, t),\\ \frac{dz_-}{dt} &= i\omega_0 z_- + N(z_-, z_+, t),\end{aligned}$$

where from equation (4.1)

$$\frac{d}{dt}\left[e^{-i\omega_0 t}N(e^{i\omega_0 t}z_+, e^{i\omega_0 t}z_-, t)\right] = 0.$$

Letting

$$N(z_+, z_-, t) = \sum_{l=-\infty}^{\infty}\sum_{\alpha,\beta,\gamma,\mu\geq 0} N_{l\alpha\beta\gamma\mu} z_+^\alpha \bar{z}_+^\beta z_-^\gamma \bar{z}_-^\mu e^{il\omega_e t},$$

we conclude that $N_{l\alpha\beta\gamma\mu} = 0$ for all l, α, β, γ, and μ such that

$$\omega_e l + (\alpha - \beta + \gamma - \mu - 1)\omega_0 \neq 0.$$

Note that the terms in the normal form must also be consistent with the other symmetries of the system. For $l = 0$, we obtain the terms in the normal form which are present in the absence of forcing (cf. [71]).

We now restrict attention to $\frac{\omega_0}{\omega_e} = \frac{1}{2}$. The possible additional terms which are of lowest order in the amplitudes z_+ and z_- for which $N_{l\alpha\beta\gamma\mu}$ can be nonzero are then

$$(l, \alpha, \beta, \gamma, \mu) = (1, 0, 1, 0, 0): \qquad \dot{z}_+ \sim \bar{z}_+ e^{i\omega_e t}, \quad \dot{z}_- \sim \bar{z}_- e^{i\omega_e t},$$

$$(l, \alpha, \beta, \gamma, \mu) = (1, 0, 0, 0, 1): \qquad \dot{z}_+ \sim \bar{z}_- e^{i\omega_e t}, \quad \dot{z}_- \sim \bar{z}_+ e^{i\omega_e t}.$$

It is readily shown that the first case is consistent with the reflection symmetry κ_1 while the second case is not. Thus, keeping only the lowest order term which arises due to the forcing and truncating the other terms at cubic order, the normal form equations are

$$\frac{dz_+}{dt} = i\omega_0 z_+ + f\bar{z}_+ e^{i\omega_e t} + A(|z_+|^2 + |z_-|^2)z_+ + B|z_+|^2 z_+ + C\bar{z}_+ z_-^2,$$

$$\frac{dz_-}{dt} = i\omega_0 z_- + f\bar{z}_- e^{i\omega_e t} + A(|z_+|^2 + |z_-|^2)z_- + B|z_-|^2 z_- + C\bar{z}_- z_+^2.$$

Here the coefficients A, B, C are complex and f can without loss of generality be taken to be real. As in Chapter 3, $A = A_R + iA_I$, etc. Finally, letting $z_\pm = e^{i\omega_e t/2}\tilde{z}_\pm$, dropping the tildes, and unfolding the equations by introducing the parameter λ to represent the distance from the Hopf bifurcation in the absence of forcing, we obtain the autonomous normal form equations

$$\frac{dz_+}{dt} = (\lambda + i\omega)z_+ + f\bar{z}_+ + A(|z_+|^2 + |z_-|^2)z_+ + B|z_+|^2 z_+ + C\bar{z}_+ z_-^2, \qquad (4.5)$$

$$\frac{dz_-}{dt} = (\lambda + i\omega)z_- + f\bar{z}_- + A(|z_+|^2 + |z_-|^2)z_- + B|z_-|^2 z_- + C\bar{z}_- z_+^2. \qquad (4.6)$$

Here $\omega \equiv \omega_0 - \frac{\omega_e}{2}$ is the detuning, and f is related to the strength of the forcing.[1] These equations are equivariant with respect to the group $D_4 = \langle \kappa_1, \kappa_2 \rangle$, although they are not the most general such equations because the S^1 normal form symmetry of equations (3.9,3.10) with $\Delta\lambda = \Delta\omega = 0$ is broken only at leading order.[2] Equations (4.5,4.6) are expected to be relevant to a variety of physical systems, including electroconvection [107], spring-supported fluid-conveying tubes with pulsatile flow (cf. [108, 109]), and the parametric excitation of surface water waves by the vertical oscillation of a square container holding a fluid [110, 111, 112, 113, 114]. The most detailed study of these equations for arbitrary coefficients is given in [107]. However, this analysis only considers fixed points and their local bifurcations. Equations (4.5,4.6) also contain four invariant subspaces ($z_- = 0$; $z_+ = 0$; $z_+ = z_-$; $z_+ = -z_-$) on which the dynamics are governed by equation (4.4) with $n = 2$ (see

[1] Equations (4.5,4.6) also apply to the case that $\omega_e \approx \omega_0$ because the reflection symmetry κ_1 prevents the terms $\dot{z}_\pm \sim$ *constant* from appearing; in this case the detuning is $\omega \equiv \omega_0 - \omega_e$.

[2] By analogy with the effect of resonant temporal forcing on the standard Hopf bifurcation, it might be expected that the S^1 symmetry will be reduced to Z_2 symmetry by the forcing, where Z_2 is generated by the action $(z_+, z_-) \to e^{i\pi}(z_+, z_-) = (-z_+, -z_-)$. However, $(\kappa_2\kappa_1)^2 : (z_+, z_-) \to (-z_+, -z_-)$, so this symmetry is already captured by the D_4 symmetry.

Appendix E). In particular, much of the behavior on these subspaces is governed by double zero bifurcations both with and without Z_2 symmetry (cf. [40]).

It is useful to make the change of variables

$$z_+ = \rho^{-1/2}\cos(\theta/2)e^{i(\phi+\psi)/2}, \qquad z_- = \rho^{-1/2}\sin(\theta/2)e^{i(-\phi+\psi)/2},$$

with the new time τ defined by $d\tau/dt = 1/\rho$. In these variables, equations (4.5,4.6) take the form

$$\begin{aligned}
\frac{d\rho}{d\tau} &= -\rho[2A_R + B_R(1+\cos^2\theta) + C_R\sin^2\theta\cos 2\phi] \\
&\quad -2[\lambda + f(\cos\phi\cos\psi - \cos\theta\sin\phi\sin\psi)]\rho^2, \qquad (4.7)\\
\frac{d\theta}{d\tau} &= \sin\theta[\cos\theta(-B_R + C_R\cos 2\phi) - C_I\sin 2\phi] + 2f\rho\sin\phi\sin\psi\sin\theta, \qquad (4.8)\\
\frac{d\phi}{d\tau} &= \cos\theta(B_I - C_I\cos 2\phi) - C_R\sin 2\phi - 2f\rho\cos\psi\sin\phi, \qquad (4.9)\\
\frac{d\psi}{d\tau} &= 2A_I + B_I + C_I\cos 2\phi + C_R\sin 2\phi\cos\theta + 2\omega\rho - 2f\rho\cos\phi\sin\psi. \qquad (4.10)
\end{aligned}$$

If $f = 0$ the variable ψ decouples, but for $f \neq 0$ the system is fully four-dimensional. We let $r = 1/\rho = |z_+|^2 + |z_-|^2$ denote the amplitude of a solution. Like equations (3.22-3.24), these equations have an invariant subspace at $\rho = 0$ (corresponding to infinite amplitude states) on which the dynamics are equivalent to those for the system with $f = 0$. The infinite amplitude solutions and the dynamics on this invariant subspace were described in detail in Chapter 3, and this suggests the possibility of bursting behavior for appropriate parameters.

4.3 An Example

The parameter values

$$A = 1 - 1.5i, \qquad B = -2.8 + 5i, \qquad C = 1 + i, \qquad \omega = 1.$$

illustrate well the type of behavior that may be expected. For $f = 0$, the resulting bifurcation diagram for these parameters with λ as the bifurcation parameter is shown in the inset in Figure 3.11. The periodic, unstable u solutions bifurcate subcritically from the trivial state $z_+ = z_- = 0$, while the periodic, unstable v and w solutions and quasiperiodic, attracting qp solutions bifurcate supercritically. From the discussion of Chapter 3 (particularly §3.4.3 Example 1(a)), it is known that for these parameters and appropriate initial conditions the trajectory can go from finite amplitude toward a u_∞ solution, get kicked toward a qp_∞ solution, then return to finite amplitude, thereby forming a burst. In the absence of symmetry-breaking the trajectory is then attracted by the finite amplitude qp solution (if $\lambda > 0$) or the trivial state (if $\lambda < 0$), and repeated bursts cannot occur. Symmetry-breaking can produce open regions of parameter space in which neither the finite amplitude qp nor the trivial state is an attractor, and in these intervals *repeated* periodic or chaotic bursts might be observed. In the following, we fix $\lambda = 0.1$; in the absence of forcing, the finite amplitude solutions which exist are thus the unstable trivial state, the unstable, periodic w and v solutions, and the attracting, quasiperiodic qp solutions. Infinite amplitude $u_\infty, v_\infty, w_\infty$, and qp_∞ solutions also exist.

4.3.1 The Effect of Forcing on the w and v Solutions and the Supergluing Bifurcation

In the absence of forcing ($f = 0$), there are two distinct w periodic solutions, one of which lies in the invariant subspace $z_- = 0$ and the other in the invariant subspace $z_+ = 0$. In the presence of forcing these subspaces remain invariant and analogs of the w solutions continue to exist. Figure 4.1 shows a bifurcation diagram and sketches of representative phase portraits for the dynamics restricted to these subspaces; stability is indicated only for perturbations within the subspaces. For $0 \leq f < \sqrt{\lambda^2 + \omega^2} = 1.00499$, only the (unstable) trivial state and the (stable) analog of the w solution exist. At $f = 1.00499$ the trivial state undergoes a pitchfork bifurcation which gives birth to two new unstable fixed points labeled FP_w. The FP_w fixed points undergo a Hopf bifurcation at $f = 1.09835$ giving two symmetry-related unstable periodic orbits labeled P. These periodic orbits deform as f is increased to produce via the gluing bifurcation SG a pair of orbits homoclinic to the trivial state at $f = 1.12225$ (cf. Figure 2.9); for $f \gtrsim 1.12225$ the P periodic orbits no longer exist but a new unstable periodic orbit w' does. For reference, at the bifurcation SG the eigenvalues of the origin with eigenvectors within the two-dimensional subspace for these parameters are 0.609 and -0.409. The periodic orbits w and w' are annihilated in a saddle-node bifurcation at $f = 1.12968$, and for larger f only the (stable) FP_w solutions and (unstable) trivial state exist.

At the bifurcation SG, the connections to the trivial state occur in *both* subspaces $z_+ = 0$ and $z_- = 0$ simultaneously.[3] We call SG a *supergluing* bifurcation because the

[3]For the parameters at which this bifurcation occurs, there are no such connections in the invariant subspaces $z_+ = \pm z_-$.

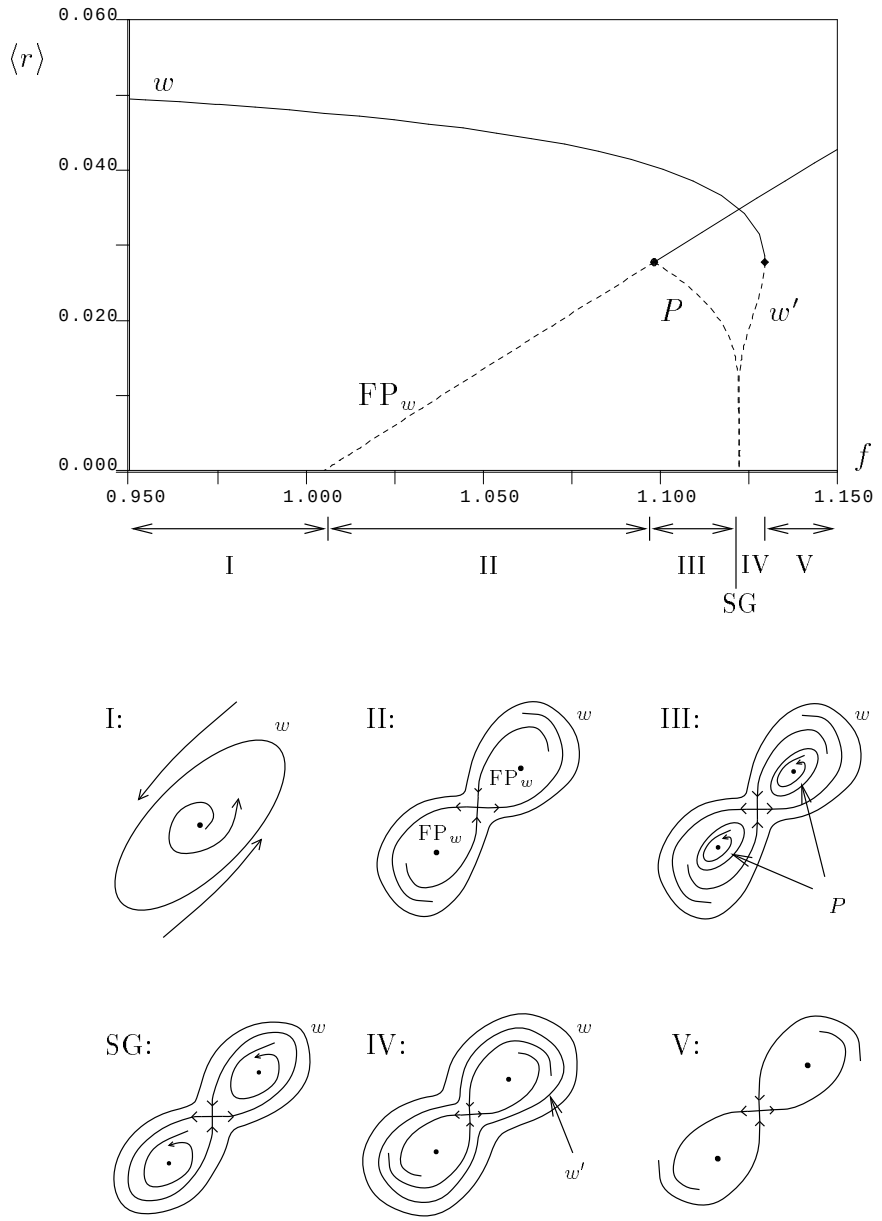

Figure 4.1: Bifurcation diagram and sketches of phase portraits for the dynamics in the two-dimensional invariant subspaces $z_+ = 0$ and $z_- = 0$. In the bifurcation diagram, solid (broken) lines indicate stable (unstable) branches, where stability refers only to perturbations within the invariant subspace. See the text for more detail. Here $\langle r \rangle$ is the average value of r for the solution with respect to the time t. As SG is approached, the periodic orbits spend more and more time near the origin so $\langle r \rangle \to 0$.

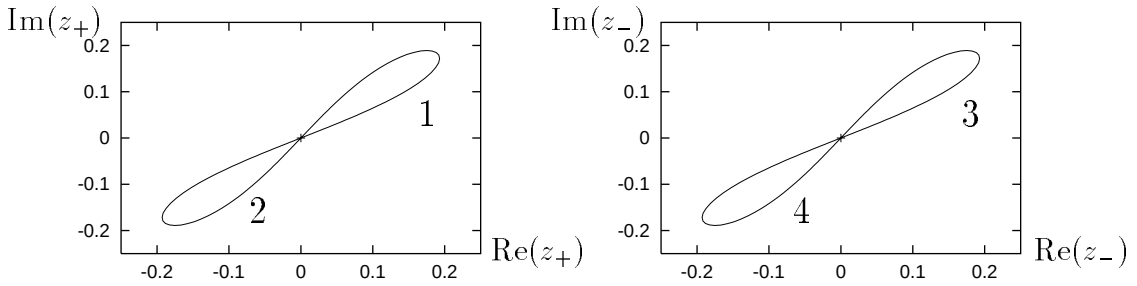

Figure 4.2: At the supergluing bifurcation at $f = 1.12225$ there are four symmetry-related orbits forming homoclinic connections to the trivial state. Orbits 1 and 2 lie in the invariant subspace $z_- = 0$ while orbits 3 and 4 lie in the invariant subspace $z_+ = 0$.

dynamics associated with this bifurcation are richer than would be expected from two independent gluing bifurcations. The dynamics associated with a supergluing bifurcation have already been described for the Takens-Bogdanov bifurcation with D_4 symmetry in the limit that the equations are nearly O(2)-symmetric [115], and there is a strong resemblance between the behavior found there and the behavior described in this section. Indeed, the supergluing bifurcation found in this example occurs at $(\lambda, \omega, f) = (0.1, 1, 1.12225)$ which is close to the codimension two point $\lambda = 0, \omega = f$ for which equations (4.5,4.6) have a Takens-Bogdanov bifurcation with D_4 symmetry; however, the values of A, B, and C are not near the O(2)-symmetric limit. Note that [116] has made progress on the symbolic dynamics of trajectories near a related bifurcation that occurs in the Takens-Bogdanov bifurcation with D_3 symmetry.

Figure 4.2 shows the four distinct orbits involved in this supergluing bifurcation. The numbers labeling these orbits are used to label the solution branches for the full four-dimensional problem (cf. [116]). For example, the solutions along the branch for the w solution which lies in the $z_- = 0$ subspace approach the connection with the trivial state in

which the trajectory traces out orbit 1 then orbit 2, then 1 again, etc. We thus label this branch 12.[4] Similarly, the P solution branch is labeled as 1.

Figure 4.3 shows bifurcation diagrams for the full four-dimensional system. These include the results shown in the bifurcation diagram in Figure 4.1, except now stability is indicated for *all* possible perturbations instead of just those in the appropriate invariant subspace. The analog of the w solution (labeled 12 in Figure 4.3) is now always unstable, and a new branch (labeled 1323) whose solutions do not lie in one of the invariant subspaces $z_\pm = 0$ bifurcates from this branch at $f = 0.97592$. Successive bifurcations from this branch include the 123 branch and branches whose solutions are followed to the subsidiary global bifurcations at $f = 1.110772$ and $f = 1.127792$. The period-doubling bifurcation from the 123 branch may be the beginning of a period-doubling cascade (see [115]), but the chaos for these parameters would apparently not be attracting.

We now consider the analogs of the periodic v solutions. For $f = 0$ the v solutions lie in the invariant subspaces $z_+ = iz_-$ and $z_+ = -iz_-$; however, these subspaces are no longer invariant in the presence of forcing. This is because the isotropy subgroup of the v solutions involves an element of the normal form symmetry (see Table 3.1), and this symmetry is broken by the temporal forcing. Although they no longer lie in an invariant subspace, the analogs of the v solutions in the presence of forcing are still invariant under the action $\mathbf{z_v}(t) \to \kappa_2\kappa_1\mathbf{z_v}(t - T_v/4)$ in the notation of §2.7.2. The resulting periodic solution branch is followed to the supergluing bifurcation SG, and is labeled 1324. Before this, however, there is a bifurcation off this branch at $f = 0.95059$ to a new periodic solution

[4] There is also a symmetry-related connection that the w solution which lies in the $z_+ = 0$ subspace will approach as the branch is followed; this branch would be labeled 34. For simplicity, such symmetry-related branches will not be indicated in the following.

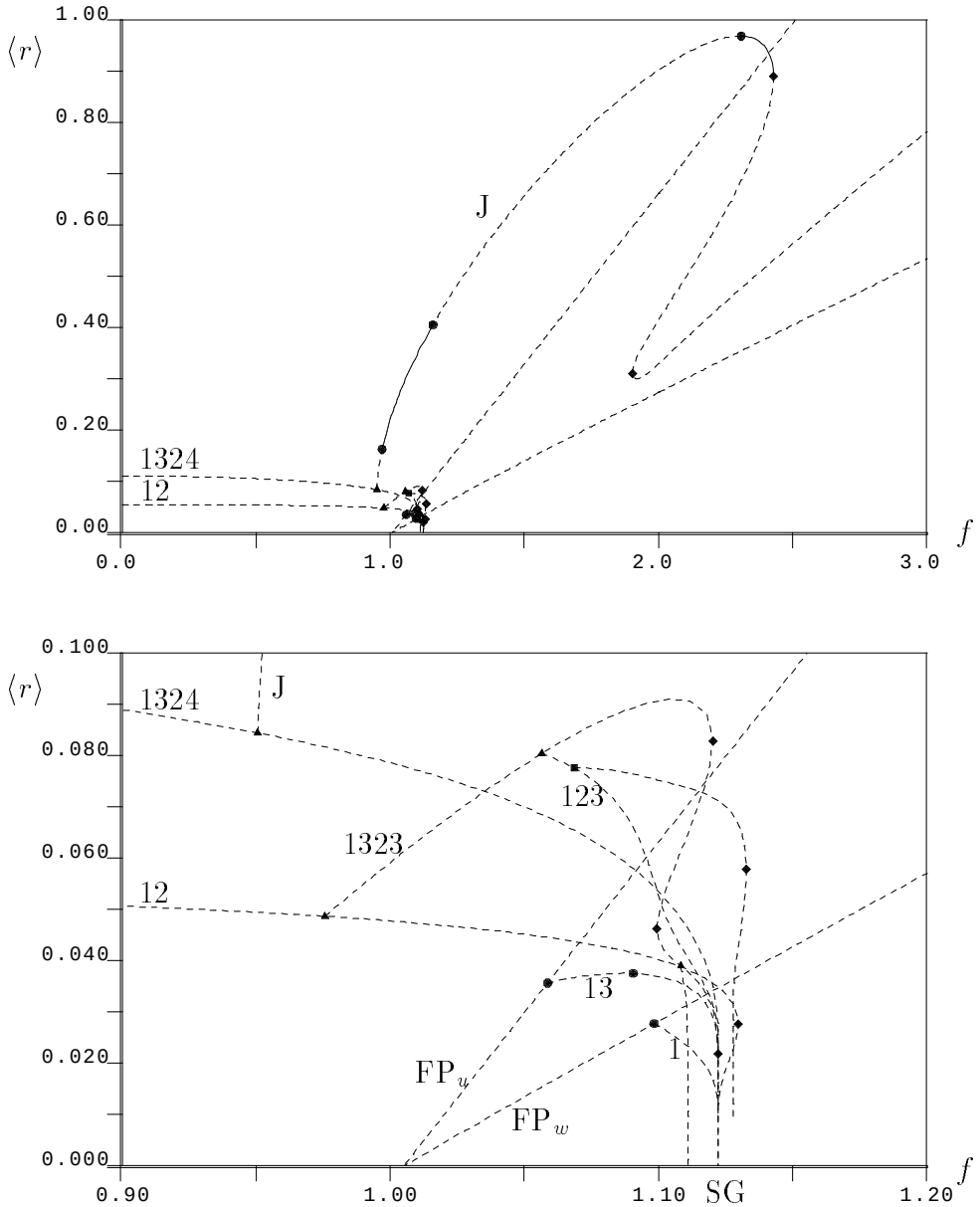

Figure 4.3: Bifurcation diagrams showing the effect of forcing on the v (labeled 1324) and w (labeled 12) periodic solutions. Other related solutions are also shown. The lower diagram is a blow-up of the upper diagram, and circles, diamonds, squares, and triangles indicate Hopf, saddle-node, period-doubling, and symmetry-breaking pitchfork bifurcations, respectively. The supergluing bifurcation occurs at point SG. See text for more detail.

branch labeled J whose solution is *stable* for $0.97019 < f < 1.15898$ and $2.30718 < f < 2.42837$; we will encounter the J solution several times in §4.3.2.

Finally, at $f = \sqrt{\lambda^2 + \omega^2} = 1.00499$ another type of fixed point solution in addition to the FP_w fixed points bifurcates from the trivial state [107]; these lie in the invariant subspaces $z_+ = \pm z_-$ and are labeled FP_u. These fixed points undergo a Hopf bifurcation giving a periodic solution which remains in the invariant subspace and may be followed to the supergluing bifurcation SG; this branch is labeled 13. Note that the 13 periodic solutions undergo a torus bifurcation at $f = 1.09051$ which gives a *nonattracting* quasiperiodic solution. It is likely that this quasiperiodic solution will wrinkle and have periodic windows similar to the attracting quasiperiodic solutions considered in §4.3.2.

4.3.2 Attractors: Wrinkled Tori and Bursts

Figure 4.4 shows the attracting quasiperiodic solution which exists in the absence of forcing ($f = 0$) and for $f = 0.5$. As f increases further, this quasiperiodic solution deforms as it is "dragged" toward the u_∞ solutions (see Figure 4.5); notice that the time series for $f = 0.98$ and $f = 0.995$ show burst-like behavior when the trajectory comes near the u_∞ solutions. The dynamic range of these bursts is large but finite because the trajectories do not come *arbitrarily* close to infinite amplitude solutions. As f is increased over this range, there are also windows for which periodic solutions exist; examples of such solutions are shown in Figure 4.6.

A useful way to represent this change in the attractor is to consider Poincaré maps constructed by intersecting the flow with a hyperplane defined by $\psi = constant$.[5]

[5] ψ is an angular variable which takes values in $[0, 4\pi)$. For these solutions it tends to increase in time,

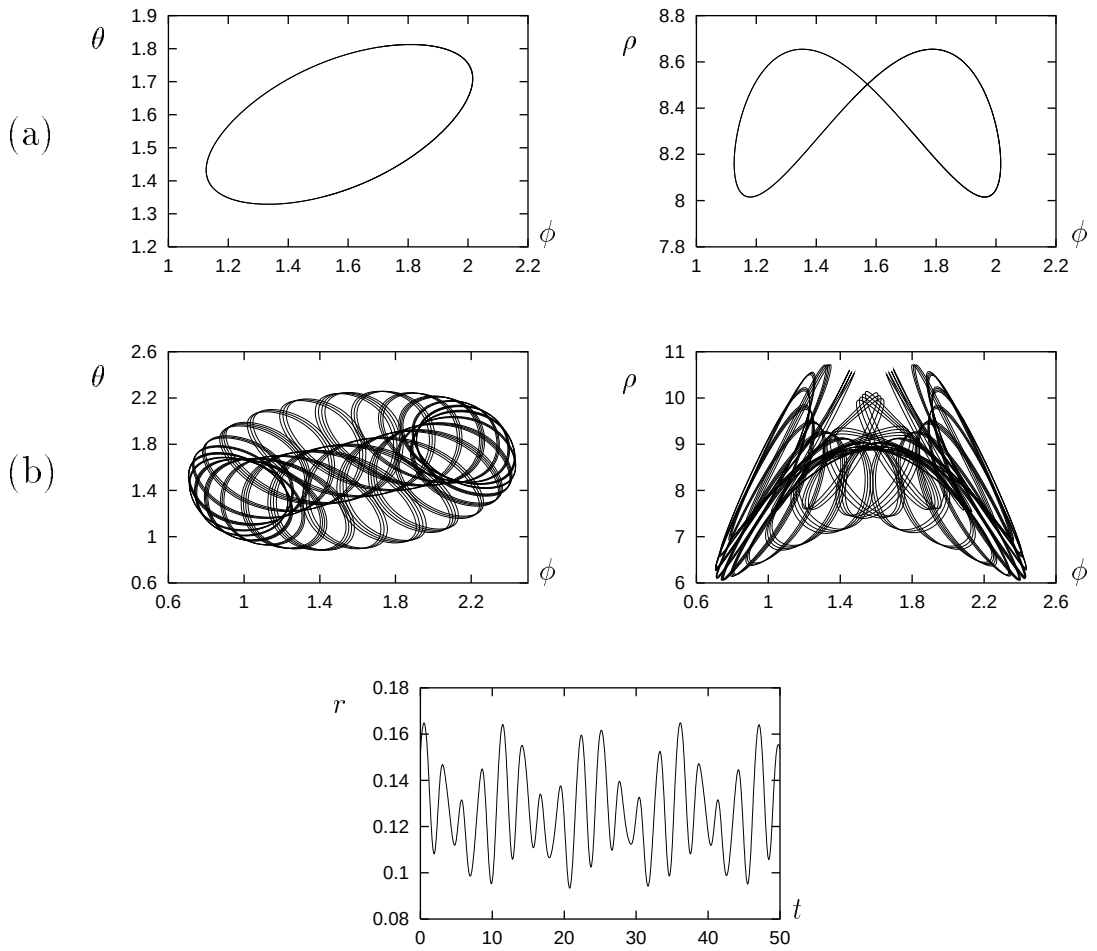

Figure 4.4: Quasiperiodic solutions for (a) $f = 0$ and (b) $f = 0.5$. The solution shown in (a) appears periodic, but there is another frequency associated with the decoupled variable ψ.

If such a map traces out a circle, the corresponding solution to the full equations lies on a torus and is quasiperiodic; on the other hand, if such a map traces out a discrete set of points then the corresponding solution to the full equations is periodic. Poincaré maps for different values of f are shown in Figure 4.7. It is seen that as f is increased, the circle develops wrinkles and is eventually destroyed, giving chaotic behavior. There are also windows for which periodic solutions exist. Such a transition from a quasiperiodic solution

though not necessarily monotonically.

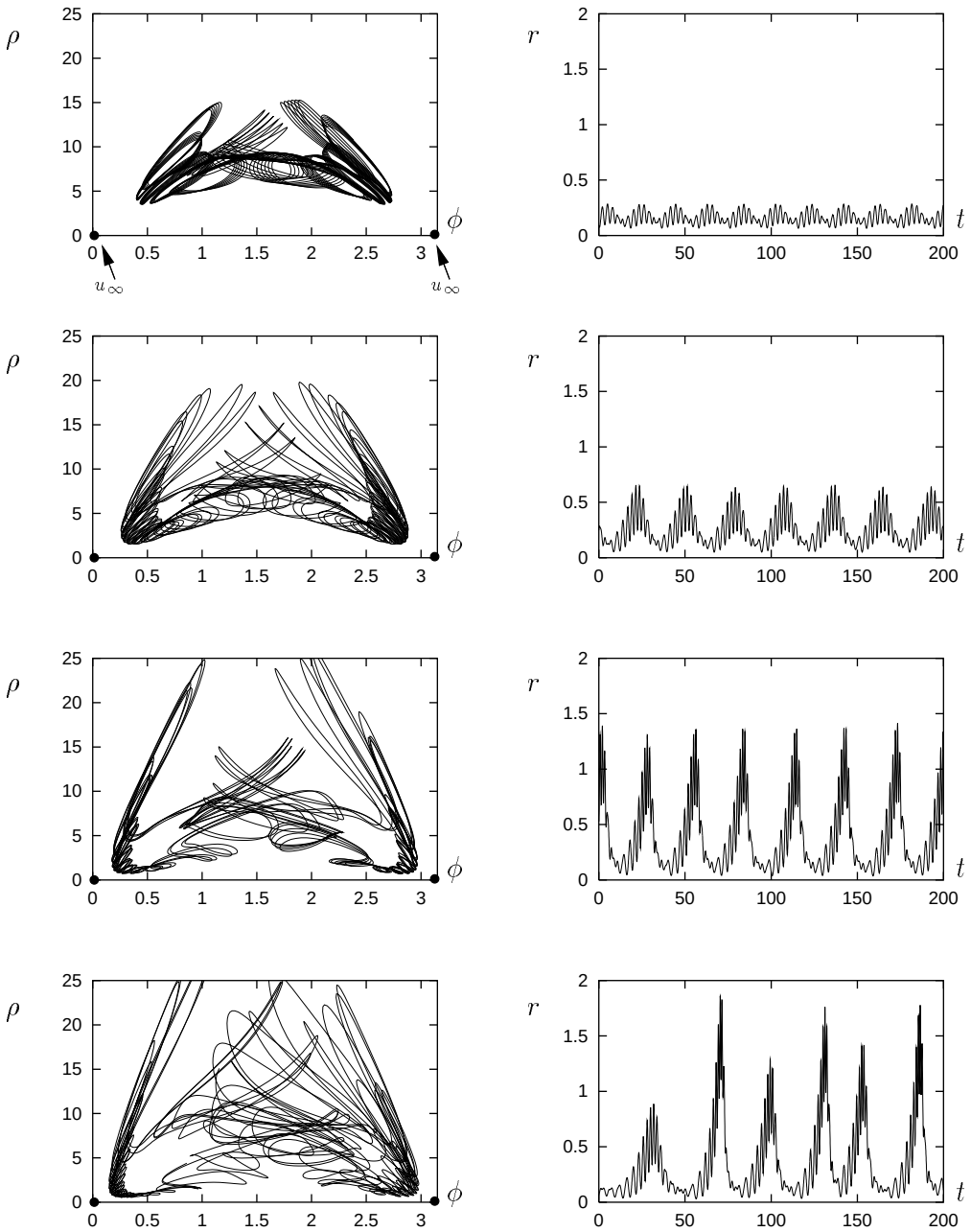

Figure 4.5: Trajectory and time series for attractors for (a) $f = 0.8$, (b) $f = 0.91$, (c) $f = 0.98$, and (d) $f = 0.995$. As f increases, the attractors are being "dragged" toward the u_∞ solutions which are denoted by the dots.

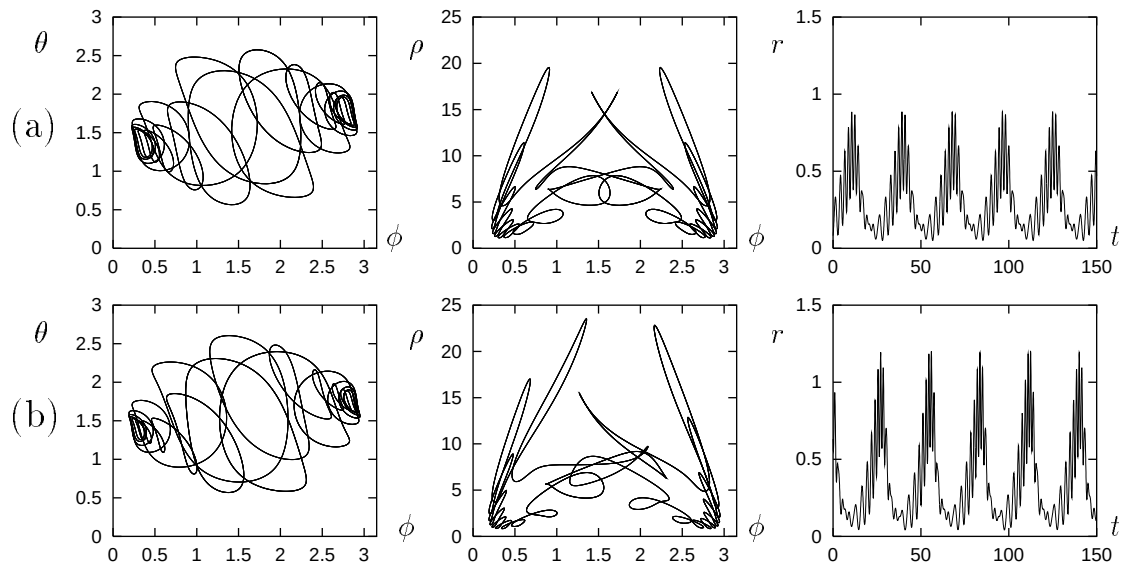

Figure 4.6: Stable periodic solutions for (a) $f = 0.94$ and (b) $f = 0.968$. Notice that different periodic solutions may have different symmetry properties.

to chaos with periodic windows has been observed experimentally [117, 118, 119, 120], in numerical studies of ordinary differential equations [121, 122], and in related numerical studies of two-dimensional maps [123, 61, 124]. The discussion of [61] is particularly useful for understanding the transition. Here the delayed logistic map, which contains an invariant circle for a range of parameters, is embedded in a two-parameter family of maps. This allows the formation of periodic solutions on the invariant circle to be associated with the traversal in parameter space through Arnol'd tongues (see §2.5). These periodic solutions may be labeled by their rotation number as follows. Define Θ to be the angular coordinate on the invariant circle. The rotation number for a periodic orbit is then

$$\rho \equiv \frac{1}{2\pi} \lim_{m\to\infty} \frac{1}{m} \sum_{n=0}^{m-1} (\Theta_{n+1} - \Theta_n),$$

where Θ_n is the Θ value for the n^{th} iteration of the Poincaré map. The rotation number thus measures the "average fraction" around the invariant circle that the solution moves

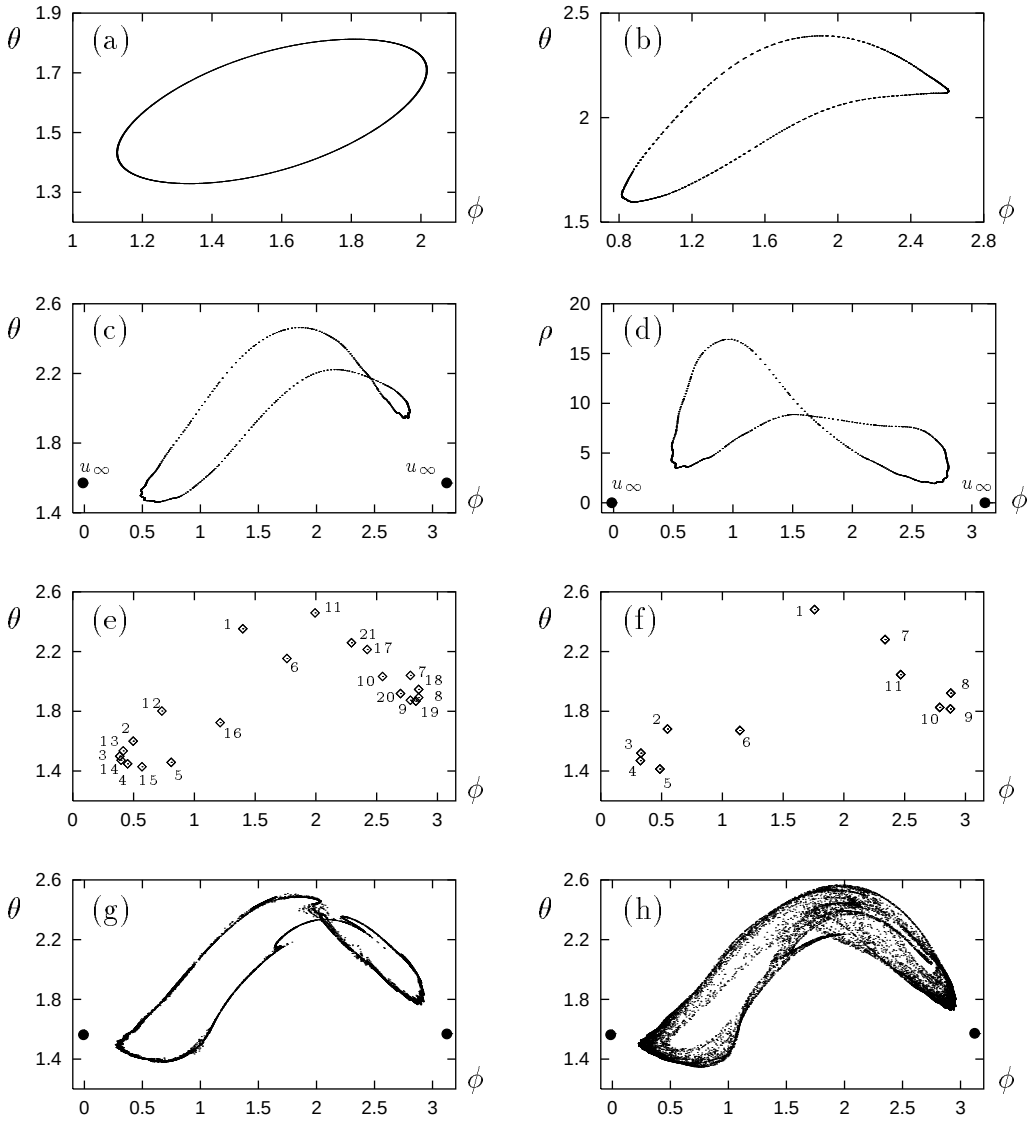

Figure 4.7: Poincaré maps constructed by intersecting the flow with the hyperplane $\psi = 10$ (from smaller to larger values) for (a) $f = 0$, (b) $f = 0.8$, (c,d) $f = 0.91$, (e) $f = 0.94$, (f) $f = 0.968$, (g) $f = 0.98$, (h) $f = 0.995$. (c,d) shows the wrinkling associated with the torus coming close to the u_∞ solutions. The numbers in (e) and (f) label the successive locations for which the flow pierces the hyperplane; the rotation numbers for these periodic orbits are thus (e) 2/21 and (f) 1/11. In (g) and (h) the torus has been destroyed, and the system behavior is chaotic. Note that the apparent self-intersections of the attractors are an artifact of the projection which has been chosen for display and are not real.

under each iteration of the Poincaré map. It is conjectured in [61] that by varying a single system parameter there is an infinite number of intervals for which only periodic orbits with a unique rotation number exist, and these are interspersed among an infinite number of intervals for which periodic orbits with different rotation numbers coexist. The details of the periodic windows are thus expected to be very complicated. It is also demonstrated in [61] that far from the tip of the Arnol'd tongue, the invariant circle becomes wrinkled due to tangencies of invariant manifolds of the periodic orbits which arise at the saddle-node bifurcations at the edge of a tongue; there is then chaotic behavior inside the tongue. Overall, the behavior of the system is governed by the approach as parameters are varied of the invariant circle to the stable manifold of an unstable fixed point of the system. This fits well with what is observed in the present problem: the wrinkling of the torus into chaos and the formation of periodic windows appear to be governed by the approach for increasing f of the attractor to the periodic u_∞ solutions. We have only given an indication of the associated complexity which is expected for the present problem.

This attractor does not reach the u_∞ solutions, however, because it is destroyed in a boundary crisis at $f \approx 0.9975$ in which the attractor collides with the stable manifold of an unstable periodic orbit (see §5.6.2). Figure 4.8 clearly shows the occurrence of this crisis and other important transitions in the attractor as f is varied. For $f \gtrsim 0.9975$ the attractor is the J solution shown for $f = 1$ in Figure 4.9. The J solution loses stability in a torus bifurcation at $f = 1.15898$ giving a quasiperiodic solution which wrinkles with increasing f as shown in Figure 4.10. At $f \approx 1.29$ the attractor is enlarged in an interior crisis (see Figure 4.8) to give bursting behavior in which the trajectory makes visits very

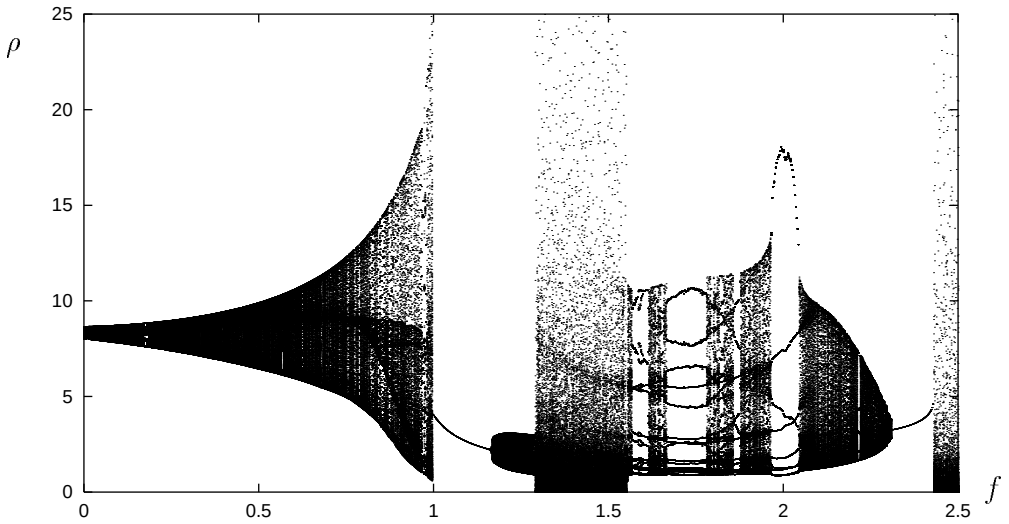

Figure 4.8: Bifurcation diagram showing the instantaneous value of ρ whenever the trajectory pierces the Poincaré section defined by $\psi = 10$ (from smaller to greater values) after the transients have died out. The attractor which is shown corresponds to adiabatically increasing the value of f from $f = 0$. Therefore, coexisting attractors (including symmetry-related attractors) are not shown. See the text for more detail.

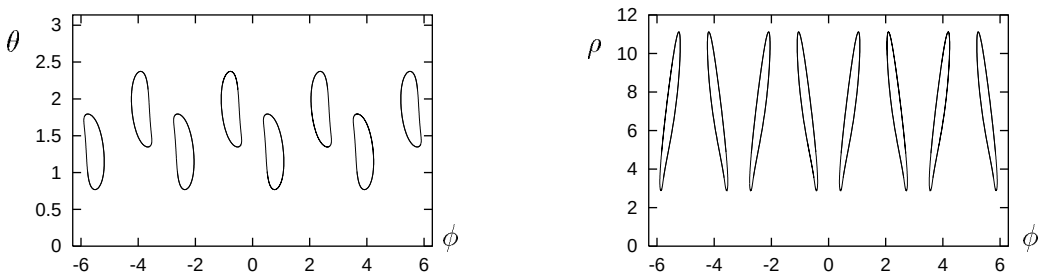

Figure 4.9: Symmetry-related stable, periodic J solutions for $f = 1$.

close to $\rho = 0$ (see Figure 4.11). Similar to the situation described in Chapter 3, a burst occurs when the trajectory makes a visit near a u_∞ solution and then is kicked toward a qp_∞ solution and returns to small amplitude. These bursts have unlimited dynamic range in contrast with most other bursts which have been studied (see Chapter 5).

The J solution is also stable for $2.30718 \lesssim f \lesssim 2.42837$; at $f \approx 2.30718$ it undergoes a torus bifurcation and the resulting attractor wrinkles into chaos with periodic windows as f is decreased (see Figure 4.12, also Figure 4.8). Here the onset of bursting as f decreases through $f \approx 1.55$ is due to an interior crisis. As shown in Figure 4.3, at $f \approx 2.42837$ the J solution is destroyed in a saddle-node bifurcation. Bursts occur for larger f (see Figure 4.13, also Figure 4.8), and thus the onset of bursting as f increases through 2.42837 is via Type I intermittency (see §5.6.1). In particular, for $f \gtrsim 2.42837$ the system makes occasional visits near a "ghost" J solution, but also makes large excursions away from such solutions. This is similar is spirit to Type I intermittency found for the Lorenz equations [125], but the change in dynamic range on either side of the saddle-node bifurcation is much larger (infinite!) for the present system. Finally, Figure 4.14 shows that bursts persist for larger values of f.

4.4 Concluding Remarks

4.4.1 Summary

The example considered in this chapter gives some idea of the richness of the effect of resonant temporal forcing on the Hopf bifurcation with D_4 symmetry. By considering the effect of the forcing on the w and v periodic solutions (which are known to exist in

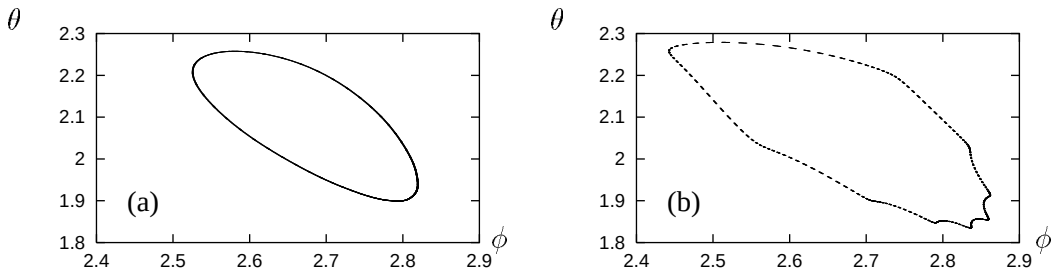

Figure 4.10: Poincaré maps constructed by intersecting the flow with the hyperplane $\psi = 10$ for (a) $f = 1.2$ showing the attracting quasiperiodic solution which lies on a torus, and (b) $f = 1.28$ showing the wrinkled torus.

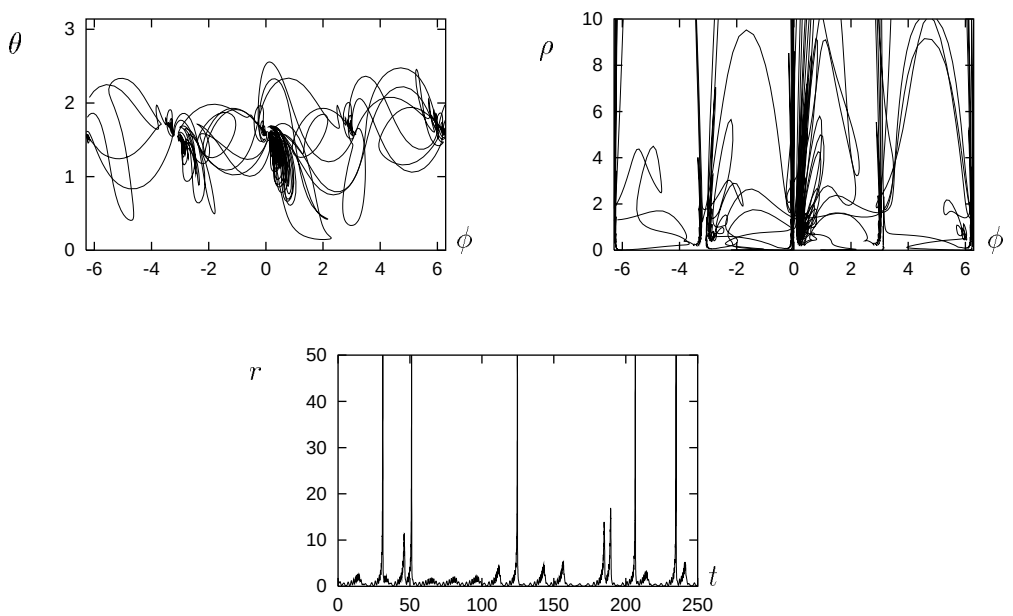

Figure 4.11: Attractor for $f = 1.5$ giving bursts when the trajectory makes visits near the u_∞ solutions at $(\rho, \theta, \phi) = (0, \pi/2, m\pi)$, where $m = -2, -1, 0, 1, 2$, and then is kicked toward a qp_∞ solution and returns to small amplitude. The time series shows the very large dynamic range for the bursts; indeed, bursts with arbitrarily large r are expected to occur.

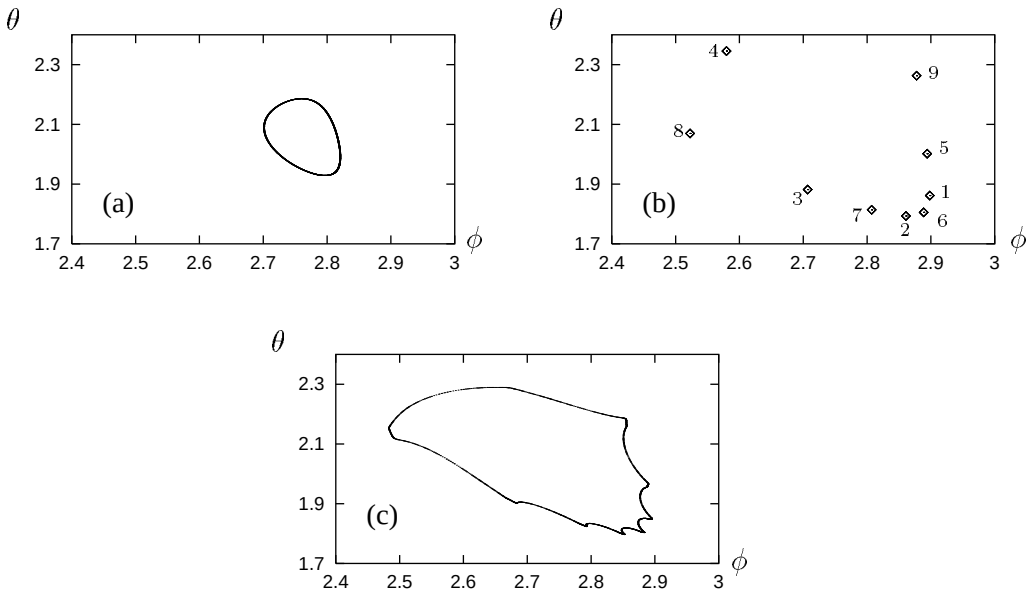

Figure 4.12: Poincaré maps constructed by intersecting the flow with the hyperplane $\psi = 10$ for (a) $f = 2.25$ showing the attracting quasiperiodic solution which lies on a torus, (b) $f = 2$ showing a stable periodic orbit, and (c) $f = 1.9$ showing how the torus has become wrinkled. The numbers in (b) label the successive locations for which the flow pierces the hyperplane; the periodic orbit thus has rotation number 2/9.

the absence of forcing) we have found a type of gluing bifurcation (called a "supergluing bifurcation") which organizes these and other periodic orbits which exist in the presence of forcing. This helps to connect the analysis of the Hopf bifurcation with D_4 symmetry in the *absence* of forcing [71] with the local bifurcation analysis of fixed points in the *presence* of forcing [107]. We have also shown that the attracting quasiperiodic solution which exists in the absence of forcing "wrinkles" into chaos as the forcing is increased, with the overall behavior being governed by the approach of the attractor to periodic u_∞ solutions. Windows in which stable periodic solutions exist are also found, and these are associated with the traversal in parameter space through Arnol'd tongues. This attractor does not reach the u_∞ solutions because it is destroyed in a boundary crisis. However,

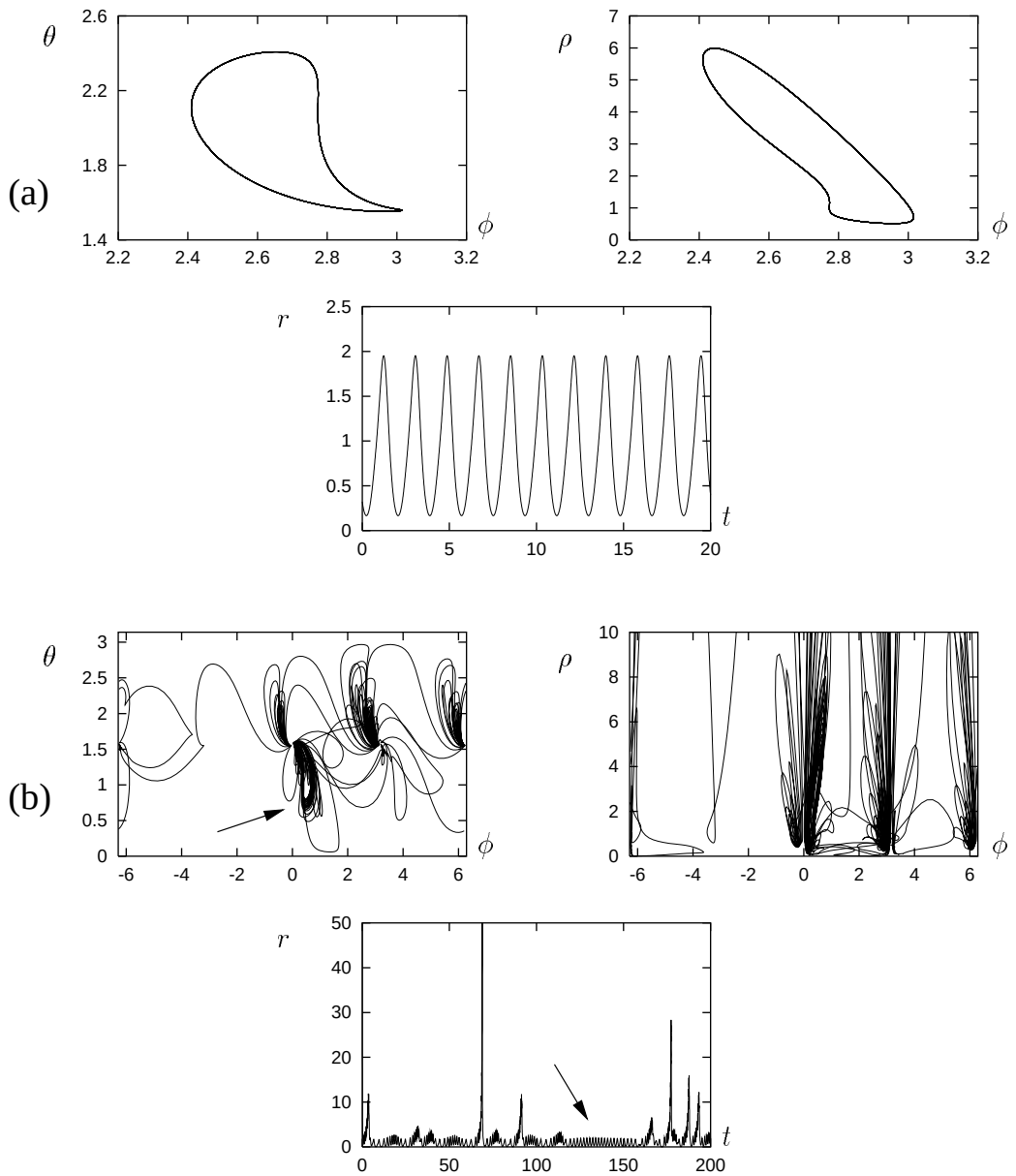

Figure 4.13: Attractors for (a) $f = 2.4283$ and (b) $f = 2.4284$. The attractor in (a) is a stable J solution; such solutions cease to exist due to the saddle-node bifurcation at $f = 2.42837$. The attractor in (b) gives bursts due to visits near u_∞ and qp_∞ solutions, and also makes occasional visits near the "ghost" of a J solution as indicated by the arrow. The onset of bursting as f increases through 2.42837 is via Type I intermittency.

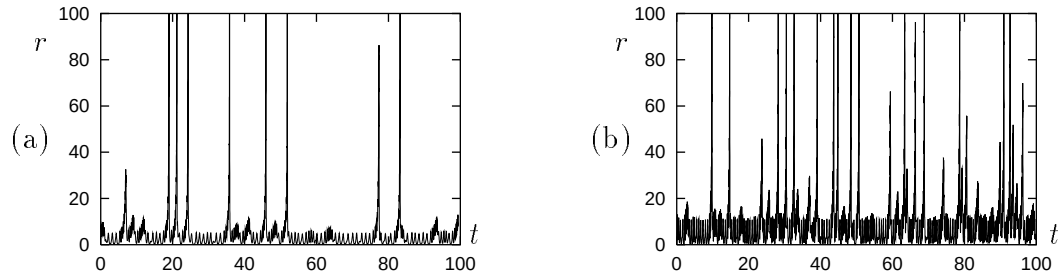

Figure 4.14: Time series showing that bursts persist for (a) $f = 5$ and (b) $f = 10$.

there *are* other ranges of f for which the attractor does come arbitrarily close to the u_∞ solutions; here the trajectory makes a visit near an infinite amplitude u_∞ solution and then is kicked toward a qp_∞ solution and returns to small amplitude, forming a burst. Similar to the situation described in Chapter 3, these bursts can have *infinite* dynamic range. It has been shown for this example that the onset of bursting of this type can be via an interior crisis or Type I intermittency.

By similar reasoning to that given in §3.5.2, it is expected that the bursting behavior will persist when higher terms in equations (4.5,4.6) are retained. Bursts will then be associated with the trajectory making visits near large but *finite* amplitude solutions. Thus, we are hopeful that bursts similar to those described in this chapter may be observed in real physical systems. Note, however, that our example has $\lambda > 0$, so the results are expected to be more directly applicable to electroconvection or spring-supported fluid-conveying tubes with pulsatile flow rather than the parametric excitation of surface waves by the vertical oscillation of a square container holding a fluid for which $\lambda < 0$ represents damping. The key conditions for the possibility of bursting behavior are that in the absence of forcing there is a subcritical solution branch (say, B) and a supercritical solution branch (say, A),

and that there is a trajectory between the infinite amplitude counterparts $B_\infty \to A_\infty$. A burst occurs when the trajectory goes from finite amplitude toward a B_∞ solution, gets kicked toward an A_∞ solution, and returns to finite amplitude. Breaking the symmetry (here, breaking the normal form symmetry due to resonant temporal forcing) may produce parameter regimes in which repeated bursts can occur.

4.4.2 Further Remarks on the Supergluing Bifurcation

Equations (4.5,4.6) restricted to the invariant subspaces $z_+ = 0$ or $z_- = 0$ take the form

$$\dot{y} = (\lambda + i\omega)y + f\bar{y} + (A + B)|y|^2 y, \qquad y \in \mathbb{C}. \tag{4.11}$$

Thus, if a gluing bifurcation occurs for equation (4.11), it occurs in *both* invariant subspaces $z_+ = 0$ and $z_- = 0$. Such a gluing bifurcation is of codimension one, and thus the supergluing bifurcation for equations (4.5,4.6) is also of codimension one. Equations (4.5,4.6) also have the invariant subspaces $z_+ = z_-$ and $z_+ = -z_-$ on which the dynamics are governed by the equation

$$\dot{z} = (\lambda + i\omega)z + f\bar{z} + (2A + B + C)|z|^2 z, \qquad z \in \mathbb{C}. \tag{4.12}$$

If a gluing bifurcation occurs for equation (4.12), it occurs in both invariant subspaces $z_+ = z_-$ and $z_+ = -z_-$, and corresponds to a supergluing bifurcation with four connections to the origin for equations (4.5,4.6). The supergluing bifurcation in which the connecting orbits exist in these subspaces is also of codimension one.

Letting

$$\tilde{y} = \sqrt{A_R + B_R}\, y, \qquad \tilde{z} = \sqrt{2A_R + B_R + C_R}\, z,$$

equations (4.11,4.12) become

$$\dot{\tilde{y}} = (\lambda + i\omega)\tilde{y} + f\bar{\tilde{y}} + \left(1 + i\frac{A_I + B_I}{A_R + B_R}\right)|\tilde{y}|^2\tilde{y}, \tag{4.13}$$

$$\dot{\tilde{z}} = (\lambda + i\omega)\tilde{z} + f\bar{\tilde{z}} + \left(1 + i\frac{2A_I + B_I + C_I}{2A_R + B_R + C_R}\right)|\tilde{z}|^2\tilde{z}, \tag{4.14}$$

where $A = A_R + iA_I$, etc. Equations (4.13,4.14) are *identical* when

$$(A_R + B_R)(2A_I + B_I + C_I) = (A_I + B_I)(2A_R + B_R + C_R).$$

Under this additional condition, a gluing bifurcation in one of the invariant subspaces $z_+ = 0, z_- = 0, z_+ = z_-, z_+ = -z_-$ implies a gluing bifurcation in the other three, giving a total of eight connections to the origin. Note that the connections in the subspaces $z_+ = 0$ and $z_- = 0$ are "scaled" relative to the connections in the subspaces $z_+ = z_-$ and $z_+ = -z_-$. This bifurcation is of codimension two. Finally, equations (4.11,4.12) are made identical by choosing $A = -C$, giving eight *identical* connections to the origin. This is a codimension three bifurcation because it requires $A_R = -C_R$ and $A_I = -A_I$, and one more parameter (such as f) needs to be varied in order to reach it.

It is natural to ask if related bifurcations can occur for resonant temporal forcing of the Hopf bifurcation with O(2) symmetry. If the Hopf frequency is ω_0 and the external forcing frequency is $\omega_e \approx n\omega_0$ for $n = 1, 2$, the normal form equations for this situation are [126, 127]

$$\dot{z_1} = (\lambda + i\omega)z_1 + f\bar{z}_2 + A(|z_1|^2 + |z_2|^2)z_1 + B|z_1|^2 z_1,$$

$$\dot{z_2} = (\lambda + i\omega)z_2 + f\bar{z}_1 + A(|z_1|^2 + |z_2|^2)z_2 + B|z_2|^2 z_2,$$

where f is related to the strength of the forcing and can without loss of generality be taken to be real, and $\omega \equiv w_0 - \frac{\omega_e}{n}$ is the detuning. These equations have a *circle* of invariant

subspaces $(z_1, z_2) = (e^{-i\sigma}z, e^{i\sigma}z)$, where $z \in \mathbb{C}$ and $\sigma \in [0, 2\pi)$, on which the dynamics are governed by the equation

$$\dot{z} = (\lambda + i\omega)z + f\bar{z} + (2A + B)z. \tag{4.15}$$

Thus, if a gluing bifurcation occurs for equation (4.15), it occurs in each of the invariant subspaces which makes up the circle of invariant subspaces, and there are an infinite number of distinct (but symmetry-related) homoclinic connections to the origin. This is in contrast with the supergluing bifurcation for resonant temporal forcing of the Hopf bifurcation with D_4 symmetry in which gluing bifurcations occur in a *finite* number of invariant subspaces. The dynamics associated with a supergluing bifurcation in the limit that the equations are nearly O(2)-symmetric are described in [115].

Chapter 5

Other Burst Mechanisms for Hydrodynamical Systems

This chapter discusses other mechanisms that lead to behavior that has been called "bursting," and compares and contrasts them with the new mechanism described in this dissertation. This helps to put the new mechanism into its proper context. As detailed further below, bursts come in many different forms, distinguished by their dynamic range (i.e., the range of amplitudes during each burst), duration, and recurrence properties. Particularly important for the purposes of this chapter is the question of whether the observed bursts occur close to the threshold of a primary instability or whether they are found far from threshold. In the former case a dynamical systems approach is likely to be successful: in this regime the spatial structure usually resembles the eigenfunctions of the linear problem and it is likely that only a small number of degrees of freedom participate in the burst. Such bursts take place fundamentally in the time domain with their spatial manifestation

of secondary importance, in contrast to *pulses* which are structures localized in both time *and* space; the latter are not considered here. Since the equations governing the evolution of primary instabilities are often highly symmetric [34], global bifurcations are likely to occur and these serve as potential candidates for bursting mechanisms. In contrast, bursts found far from threshold usually involve many degrees of freedom but even here some progress is sometimes possible. Much of the material in this chapter has been published in [129, 130].

5.1 Bursts in the Wall Region of a Turbulent Boundary Layer

The presence of coherent structures in a turbulent boundary layer is well established (see, e.g., [131] and the collection of articles in [132]). The space-time evolution of these structures is often characterized by intermittent bursting events involving low speed streamwise "streaks" of fluid. Specifically, let x_1, x_2, and x_3 be the streamwise, wall normal, and spanwise directions with associated velocity components $U + u_1, u_2$, and u_3, respectively; here $U(x_2)$ is the mean flow. In a "burst" the streak breaks up and low speed fluid moves upward away from the wall ($u_1 < 0, u_2 > 0$); this is followed by a "sweep" in which fast fluid moves downward towards the wall ($u_1 > 0, u_2 < 0$). After the burst/sweep cycle the streak reforms, often with a lateral spanwise shift.

A low-dimensional model of the burst/sweep cycle was developed by [133]; further details and later references may be found in [134, 135]. To construct such a model the authors used a Karhunen-Loève decomposition of the data to identify an energetically dominant empirical set of eigenfunctions, hereafter "modes". The original study [133] used

experimental data for pipe flow with $Re \sim 6750$, while later studies used data for channel flow from direct numerical simulation with $Re \sim 3000 - 4000$ and large eddy simulations with $Re \sim 13800$ [135]. The model was constructed by projecting the Navier-Stokes equation onto this basis and consists of a set of coupled ODEs for the amplitudes of these modes. The fixed points of these equations are to be associated with the presence of coherent structures. There are two types, related by half-wavelength spanwise translation.

Numerical integration of the model reveals that these fixed points are typically unstable and that they are connected by a heteroclinic cycle. In such a cycle the trajectory alternately visits the vicinities of the two unstable fixed points. In the model of [133] this heteroclinic cycle is found to be structurally stable, i.e., it persists over a *range* of parameter values. This is a consequence of the O(2) symmetry of the equations inherited from periodic boundary conditions in the spanwise direction. Moreover, for the parameter values of interest this cycle is *attracting*, i.e., it attracts all nearby trajectories. Since the transition from one fixed point to the other corresponds to a spanwise translation by half a wavelength, the recurrent excursions along such a heteroclinic cycle can be identified with the burst/sweep cycle described above. However, since this cycle is attracting, the time between successive bursts will increase as time progresses. This is not observed and [133] appeals to the presence of a random pressure term modeling the effect of the outer fluid layer to kick the trajectory from the heteroclinic cycle. In the language of [136] such a pressure term results in a *statistical* limit cycle, with the bursting events occurring randomly in time but with a well-defined mean rate. The resulting temporal distribution of the burst events is characterized by a strong exponential tail, matching experimental observations.

Attracting structurally stable heteroclinic cycles occur in a number of problems of this type, i.e., mode interaction problems with O(2) symmetry [137, 138, 85, 139, 140, 141].

5.2 Bursts in Shear Flows Undergoing Subcritical Transition to Turbulence

Experimental studies of plane Couette flow and Poiseuille (pipe) flow have shown that at high enough values of the Reynolds number Re the basic laminar flow becomes turbulent. However, these laminar flows are linearly stable at all Re (see, e.g. [10]). Consequently, the transition to turbulence in these systems must arise from finite (i.e., not infinitesimal) perturbations to the basic flow; such transitions are called subcritical since the turbulent state exists for values of Re for which the laminar state is stable. Much recent work (reviewed in [142]) has emphasized the importance of the fact that the linear operators L governing the evolution of perturbations of these flows are non-normal, i.e., $L^\dagger L \neq LL^\dagger$, where $L^\dagger$ is the adjoint of L. Linear systems with a non-normal L can exhibit transient growth even though the laminar state is linearly stable; if the growth is large enough, nonlinearities in the system may then trigger a transition to turbulence. Analysis of low-dimensional models supported by numerical simulations suggests that the minimum perturbation amplitude ϵ that results in turbulence scales as $\epsilon = \mathcal{O}(Re^\alpha)$ for some $\alpha < -1$ [142]. Thus, ϵ decreases rapidly with increasing Re, and the experimentally determined Re for transition should be that value at which ϵ is roughly equal to perturbations due to noise or imperfections in the system.

The turbulence excited by finite amplitude perturbations in shear flows often takes

the form of turbulent spots which can move, grow, split, and merge (see, e.g., [143]). Turbulent spots can also burst intermittently. For example, [144] observed intermittent turbulent bursts in plane Couette flow for $Re \approx 325$; these bursts were triggered by a spanwise wire through the center of the channel, and could be localized in space by introducing a bead into the central plane. We focus here on this burst-like behavior, also found in low-dimensional models of the subcritical transition to turbulence. The important issue in such models is the attractor to which the flow settles after an appropriate finite perturbation to the basic laminar flow. This will depend crucially on nonlinear terms in the equations, a point emphasized, for example, by [145, 146, 147, 148] and [149]. If this attractor is a fixed point, the system settles into a steady state in which bursts do not occur. On the other hand, if this attractor is a limit cycle it may be appropriate to interpret the resulting behavior as burst-like. This is the case in the model studied in [145] in which the amplitudes of streamwise streaks, streamwise rolls, and the streak instability can periodically undergo short-lived explosive growths at the expense of the mean shear. Waleffe [145, 146] refers to this as a self-sustaining process. Since the laminar state is linearly stable, such limit cycles cannot bifurcate off the laminar state. Instead, as pointed out in [146, 147], they may be born in a Hopf bifurcation (from a fixed point other than that corresponding to the laminar state) or a homoclinic bifurcation in which a trajectory homoclinic to a fixed point forms at some value of Re such that for smaller (larger) values of Re a limit cycle exists (does not exist), or vice versa. Near such a homoclinic bifurcation, bursts are expected because the trajectory spends a long time near the fixed point, bursting away and returning in a periodic or chaotic fashion, depending on the eigenvalues of the fixed point. Other generic

codimension one bifurcations leading to the appearance or disappearance of limit cycles are saddle-node bifurcations of limit cycles and saddle-nodes in which a pair of fixed points appears on the limit cycle [150]. Limit cycles could also come in from or go off to infinity. In other models chaotic attractors have been found (see, e.g., [151] and [152]) and these may also give rise to burst-like behavior.

The relation of the bursts described in this section (which occur for moderate values of Re, e.g., $Re \approx 325$) to those which occur in the turbulent boundary layer (which occur for high values of Re) is not completely clear. However, the similarities in the phenomenology has led [148] to propose that the self-sustaining process will continue to have importance in the near-wall region of high Re flows.

5.3 Heteroclinic Connections to Infinity

Another mechanism involving heteroclinic connections, distinct from that discussed in §5.1, has been investigated by [153, 154] as a possible model for spatio-temporal intermittency in turbulent flow. The authors suggest that such systems may be viewed as nearly Hamiltonian except during periods of localized intense dissipation. A related "punctuated Hamiltonian" approach to the evolution of two-dimensional turbulence has met with considerable success [155, 156]. For their description, [153, 154] divides the instantaneous states of the flow into two categories, a turbulent soup (TS) characterized by weak coherence, and a singular (S) state characterized by strong coherence, and suppose that the TS and S states are generalized saddles in an appropriate phase space. Furthermore, they suppose that in the Hamiltonian limit the unstable manifold of TS (S) intersects transversally the

stable manifold of S (TS). If the constant energy surfaces are noncompact (i.e., unbounded), the evolution of the Hamiltonian system may take the system into regions of phase space with very high ("infinite") velocities and small scales. These regions are identified with the S states and high dissipation. In such a scenario the strong dissipation events are therefore identified with excursions along heteroclinic connections to infinity. Perturbations to the system (such as the addition of dissipative processes) may prevent the trajectory from actually reaching infinity, but this underlying unperturbed structure implies that large excursions are still possible.

These ideas are applied to the two-dimensional nonlinear Schrödinger equation (NLSE) with perturbations in the form of special driving and dissipative terms which act at large and small scales, respectively. Here S consists of "filament" solutions to the unperturbed NLSE which become singular in finite time and represent coherent structures which may occur at any position in the flow field. When the solution is near S a large portion of the energy is in small scales; for the perturbed equations the dissipative term then becomes important so that the filament solution is approached but collapses before it is reached. This leads to a spatially and temporally random occurrence of localized burst-like events for the perturbed equation. The rate of attraction at S is determined by the faster than exponential rate at which the filament becomes singular, while the rate of repulsion at S is governed by the dissipative process and hence is unrelated to the rate of attraction.

This bursting mechanism shares characteristics with that described in [88] in which solutions of a single complex Ginzburg-Landau equation with periodic boundary conditions undergo faster than exponential bursting due to a destabilizing nonlinearity and collapse

due to strong nonlinear dispersion (see also [157]). A study of a generalization of Burger's equation modeling nonlocality effects suggests the presence of burst-like events through a similar scenario [158].

5.4 Bursts in the Kolmogorov Flow

The Kolmogorov flow $\mathbf{u} = (k \sin ky, 0)$ is an exact solution of the two-dimensional incompressible Navier-Stokes equation with unidirectional forcing $\mathbf{f}$ at wavenumber k: $\mathbf{f} = (\nu k^3 \sin ky, 0)$. With increasing Reynolds number $Re \equiv \nu^{-1}$ this flow becomes unstable, and direct numerical simulation with 2π-periodic boundary conditions shows that for moderately high Reynolds numbers and $k > 1$ the resulting flow is characterized by intermittent bursting [159, 160, 161, 162, 163, 164, 165, 166]. A burst occurs when the system evolves from a coherent vortex-like modulated traveling wave (MW) to a spatially disordered state following transfer of energy from large to small scales. The system then relaxes to the vicinity of another symmetry-related MW state, and the process continues with bursts occurring irregularly but with a well-defined mean period.

The details of what actually happens appear to depend on the value of k because k determines the symmetry of the nonlinear equation describing the evolution of the perturbation streamfunction ϕ about the Kolmogorov flow. Although there is no compelling reason for it, all simulations of this equation have been performed with 2π-periodic boundary conditions in both directions. With these boun-dary conditions this equation has a symmetry which is the semi-direct product of the dihedral group D_{2k} (generated by the actions $(x, y, \phi) \to (-x, -y, \phi)$ and $(x, y, \phi) \to (-x, y + \pi/k, -\phi)$) and the group SO(2)

(representing the symmetry under translations $x \to x+\text{const}$). In the simplest case, $k = 1$, this symmetry group is isomorphic to the direct product of the group O(2) of rotations and reflections of a circle and the group Z_2 representing reflections in the y-direction. Unfortunately, when $k = 1$ the Kolmogorov flow with 2π-periodic boundary conditions is not unstable for any value of Re [167, 168, 169], and one is forced to consider $k > 1$. Reference [166] analyzed carefully the $k = 2$ case, and showed that while a heteroclinic cycle between the MW states does form, it is not structurally stable; the bursts are therefore not produced by a mechanism of the type described in §5.1. It is possible, however, that the onset of bursting is associated with a symmetry-increasing bifurcation at $Re \equiv Re_s$ (see, e.g. [128]). This would explain why the system stays in a single MW state for Re just below Re_s but visits the vicinity of different but symmetry-related MW states for Re just above Re_s. However, despite much work a detailed understanding of the bursts in this system remains elusive.

An alternative approach is to consider periodic domains with different periodicities in the two directions. In particular, if we consider the domain $\{-\pi < x \leq \pi, -\pi/k < y \leq \pi/k\}$ with $k > 1$ the symmetry group remains $O(2)\times Z_2$ but sufficiently long perturbations now grow. The unstable modes are either even or odd under the reflection $(x, y) \to (-x, -y)$ with respect to a suitable origin. Mode interaction between these two steady modes can result in a sequence of transitions summarized in Figure 5.1; see [141]): the Kolmogorov flow loses stability to an even mode (Z), followed by a steady state bifurcation to a mixed parity state ($MM_{\pi/2}$). Since each of these states is defined to within a translation in x modulo 2π, we say that it forms a *circle* of states. The $MM_{\pi/2}$ state then loses stability

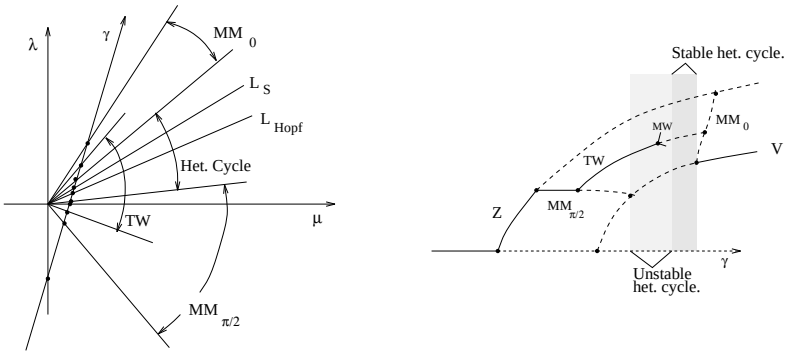

Figure 5.1: Sample bifurcation diagram for the interaction of an odd and even mode for the Kolmogorov flow obtained by traversing the parameter space along the line γ. A structurally stable heteroclinic cycle exists for a range of parameters. After [141]. Other cuts through parameter space give different bifurcation diagrams.

in a further steady state bifurcation to a traveling wave (TW) which in turn loses stability at a Hopf bifurcation to a MW. The MW two-torus terminates in a collision with the two circles of pure parity states, forming an attracting structurally stable heteroclinic cycle connecting them and their quarter-wavelength translates [141]. In this regime the behavior would resemble that found in the numerical simulations, with higher modes kicking the system away from this cycle. Indeed this sequence of transitions echoes the results obtained by [159, 160, 161, 162, 163] for $k = 8$. While it is likely that the $k = 1$ scenario is relevant to these calculations because of the tendency towards an inverse cascade in these two-dimensional systems, we emphasize that, as mentioned above, a careful analysis of the $k = 2$ case by [166] shows that while a heteroclinic cycle of the required type does indeed form, it is not structurally stable. The case $k = 4$ has also been studied [170] and a similar sequence of transitions found. Undoubtedly simulations on the domain $\{-\pi < x \leq \pi, -\pi/k < y \leq \pi/k\}$ would shed new light on the problem, cf. [171].

The group $O(2)\times Z_2$ also arises in convection in rotating straight channels [172] and in natural convection in a vertical slot [173]. In both of these cases the linear eigenfunctions are either even or odd with respect to a rotation by π and the systems exhibit similar transitions. Related behavior has recently been observed in three-dimensional magnetoconvection with periodic boundary conditions on a square lattice. Unlike the Kolmogorov flow the evolution equation describing a steady state secondary instability of a square pattern is isotropic in the horizontal. Numerical simulations [174] show intermittent breakdown of a square pattern followed by its restoration modulo translation.

5.5 Bursts in the Taylor-Couette System

The Taylor-Couette system consists of concentric cylinders enclosing a fluid-filled annulus [175]. The cylinders can be rotated independently. In the counterrotating regime the first state consists of spiral vortices of either odd or even parity with respect to midheight. Slightly above onset the flow resembles interpenetrating spiral (IPS) flow which may be intermittently interrupted by bursts of turbulence which fill the entire flow field [176, 177, 178]. With periodic boundary conditions in the axial direction numerical simulations show that the IPS flow is temporally chaotic and consists of coexisting modes with different axial and azimuthal wavenumbers [177, 178]. This flow is confined primarily to the vicinity of the inner cylinder where the axisymmetric base flow is subject to an inviscid Rayleigh instability. References [177, 178] conclude that the onset of turbulence is correlated with a secondary instability of one of the coexisting modes of the IPS flow, namely the basic spiral vortex flow with azimuthal wavenumber $m = 4$. Indeed, when this

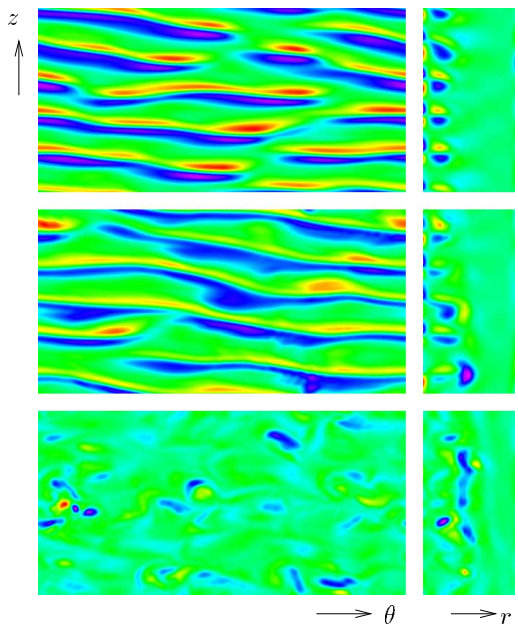

Figure 5.2: Azimuthal component of vorticity in the laminar interpenetrating spiral state (top), just before a burst (middle), and in the turbulent state (bottom), labeled using polar coordinates. After [178]. Courtesy K. Coughlin.

mode is taken as the initial flow for parameters chosen such that the full IPS flow undergoes bursts, a secondary Hopf bifurcation from this state with the same azimuthal wavenumber but four times the axial wavelength is identified. The secondary instability grows in amplitude and ultimately provides a finite amplitude perturbation to the inviscidly stable flow near the outer cylinder, triggering a turbulent burst throughout the whole apparatus. During a burst small scales are generated throughout the apparatus leading to a rapid collapse of the turbulence and restoration of the IPS flow; the bursting process then repeats roughly periodically in time (see Figure 5.2).

As discussed in Chapter 3, in a finite Taylor-Couette apparatus there is a natural mechanism for generating bursts close to onset. This mechanism operates in the regime

$\epsilon \sim \Gamma^{-2}$, where ϵ measures the fractional distance above threshold for the primary instability and Γ is the aspect-ratio of the annulus [6, 179]. For larger ϵ the influence of the boundaries no longer extends throughout the apparatus and is confined to boundary layers near the top and bottom. In this regime the dynamics in the bulk may be described by imposing periodic boundary conditions with period that is a multiple of the wavelength of the primary instability. The success of the simulation of the observed turbulent bursts using such periodic boundary conditions [177, 178] suggests that these bursts occur too far above threshold to be explained by the mechanism described in Chapter 3. This suggestion is supported by Figure 5.3 which compares the location of the regime where this mechanism may be expected to operate with ϵ_b, the experimental value of ϵ for the onset of bursts, as a function of Γ. The latter is obtained using the approximation $\epsilon_b \approx (R_b - R_{IPS})/R_{IPS}$, where R_{IPS} and R_b are the inner cylinder Reynolds numbers for the onset of IPS flow and bursts, and [176]

$$\begin{aligned} R_{IPS} &= (3837 \pm 374)\Gamma^{-1} + 680 \pm 14 \\ R_b &= (3680 \pm 374)\Gamma^{-1} + 701 \pm 14 \end{aligned}$$

This is a good approximation for strongly counterrotating cylinders because the IPS flow sets in for inner cylinder Reynolds number only about 1% above the primary onset to spiral vortices [176]. The figure suggests that the observed bursts may fall within the range of validity of the theory described in Chapter 3 for Γ only slightly smaller than those used in the experiments ($\Gamma = 17.9, 26$); for such bursts the presence of endwalls should become significant.

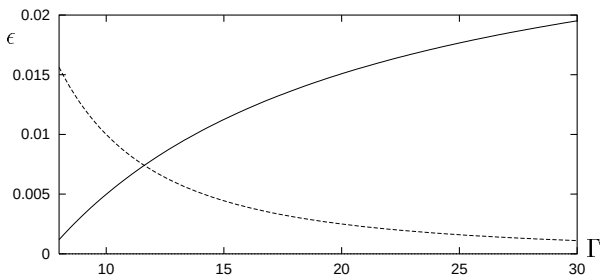

Figure 5.3: The solid line shows the inner cylinder reduced Reynolds number ϵ_b for the onset of bursts obtained from data in [176]. The dashed line shows the estimate $\epsilon = \Gamma^{-2}$ near and below which the asymptotic bursting mechanism described in Chapter 3 is expected to apply. The bursts found at $\Gamma = 17.9$ and $\Gamma = 26$ [176, 178] apparently fall outside the range of validity of the theory of Chapter 3.

5.6 Intermittency

The term intermittency refers to occasional, non-periodic switching between different types of behavior; such transitions may be viewed as bursts. In this section we describe different types of intermittency, dividing them into three classes.

5.6.1 Low-dimensional Intermittency

It is often the case that fluid dynamical systems may be modeled by low-dimensional Poincaré maps. Fixed points of such maps correspond to limit cycles of an appropriate dynamical system; when these lose stability intermittency may result. Without loss of generality we assume that for $\lambda < \lambda_p$ the system is in a "laminar" state corresponding to a stable fixed point of the map, and the onset of intermittency occurs at $\lambda = \lambda_p$. For $\lambda > \lambda_p$ the state of the system will resemble the stable laminar state which existed for $\lambda < \lambda_p$ for some time but will intermittently undergo "bursts" away from this state, followed by "reinjections" to the vicinity of the laminar state. The three types of intermittency identified

by [125] correspond to three different ways in which the laminar state ceases to exist or loses stability at $\lambda = \lambda_p$: Type I intermittency results when a stable and unstable limit cycle annihilate in a saddle-node bifurcation, Type II results when the limit cycle loses stability in a subcritical Hopf bifurcation, while in Type III the limit cycle loses stability in an inverse period-doubling bifurcation. Type I and Type III intermittency have been observed, for example, in Rayleigh-Bénard convection (see [180] and [181], respectively), while Type II intermittency has been observed in a hot wire experiment [182]. A different type of intermittency, called Type X, was observed in [183] in a variant of the Taylor-Couette system; this is similar to Type I intermittency but involves a hysteretic transition due to the nature of the reinjection. Another type of intermittency, called Type V, was introduced in [184] and [185]; this is similar in spirit to Type I intermittency but involves one-dimensional maps which are nondifferentiable or discontinuous. These different types of intermittency have distinct properties, such as the scaling behavior of the average time between bursts with $\lambda - \lambda_p$.

5.6.2 Crisis-induced Intermittency

A crisis is a sudden change in a strange attractor as a parameter is varied [186, 187, 188]. There are three types of crises, and without loss of generality we assume that the crisis occurs as λ is increased through λ_c. In a boundary crisis, at $\lambda = \lambda_c$ the strange attractor collides with a coexisting unstable periodic orbit which lies on the boundary of the basin of attraction of the strange attractor. This leads to the destruction of the strange attractor, but chaotic transients will still exist. Intermittency is not associated with this crisis. In an interior crisis the strange attractor collides with a coexisting unstable periodic orbit at

$\lambda = \lambda_c$, but here this leads to a widening rather than the destruction of the strange attractor. For λ slightly larger than λ_c the trajectory stays near the region of phase space occupied by the strange attractor before the crisis for long times, but intermittently bursts into a new region. In an attractor merging crisis two strange attractors with basins of attraction separated by a basin boundary are present when $\lambda < \lambda_c$. At λ_c the two strange attractors simultaneously touch the basin boundary and "merge" to form a larger strange attractor for $\lambda > \lambda_c$. Such a crisis is often associated with a symmetry-increasing bifurcation [94]. For $\lambda > \lambda_c$ there is a single strange attractor on which the trajectory intermittently switches between states resembling the distinct strange attractors which existed for $\lambda < \lambda_c$.

5.6.3 Intermittency Involving an Invariant Manifold

A manifold in phase space is invariant if every initial condition on the manifold generates an orbit that remains on the manifold. Invariant manifolds often exist due to symmetries, but this is not necessary. There are several mechanisms for intermittency involving strange attractors on an invariant manifold.

First, suppose that as a bifurcation parameter λ is increased through λ_p, the strange attractor on the invariant manifold loses stability transverse to the manifold; this is called a blowout bifurcation [189]. Suppose that the dynamics *within* the invariant subspace do not depend on λ. Such a system thus has a skew-product structure [190], and λ is called a normal parameter [191]. If the blowout bifurcation is "supercritical" [189] then for λ just above λ_p a trajectory will spend a long time near the invariant manifold, intermittently bursting away from it, only to return due to the presence of a reinjection mechanism. This scenario is known as on-off intermittency, where the "off" ("on") state corresponds to the

system being near (away from) the invariant manifold (see, e.g., [190, 192]). Recently it has been shown that in appropriate circumstances a blowout bifurcation can lead to a structurally stable (possibly attracting) heteroclinic cycle between chaotic invariant sets [193].

For systems which lack a skew-product structure and thus are governed by non-normal parameters, in-out intermittency is possible [191, 194]). Here the attraction and repulsion to the invariant subspace are controlled by *different* dynamics. This occurs when the attractor for dynamics restricted to the invariant subspace is smaller than the intersection of the attractor for the full dynamics with the invariant subspace, and may be viewed as a generalization of on-off intermittency in which the attraction to and repulsion from the invariant subspace are controlled by the *same* dynamics.

Another mechanism for bursting occurs when the strange attractor on the invariant manifold attracts typical orbits near the surface but is unstable in the sense that there are unstable periodic orbits embedded within the chaotic set which are transversely repelling. If the trajectory comes near such an unstable periodic orbit, there will be a burst away from the invariant surface. Such bursts may occur intermittently if noise is present or small changes (called "mismatch") are made to the dynamical system that destroy the invariant surface. The loss of transverse stability of one of these periodic orbits as a parameter is varied is known as a bubbling transition (see, e.g., [195, 196, 197]).

5.7 Bursts in Neural Systems

In neural systems, bursting refers to the switching of an observable such as a voltage or chemical concentration between an active state characterized by rapid (spike)

oscillations and a rest state. Models of such bursting typically involve singularly perturbed vector fields in which system variables are classified as being "fast" or "slow" depending on whether or not they change significantly over the duration of a single spike. The slow variables may then be thought of as slowly varying parameters for the equations describing the fast variables [198, 199, 200, 201, 150]. As the slow variables evolve, the state of the system in the fast variables may change from a stable periodic orbit (corresponding to the active state) to a stable fixed point (corresponding to the rest state) and vice versa; such transitions are often associated with a region of bistability for the periodic orbit and the fixed point, but need not be. Mechanisms by which such transitions can occur repeatedly have been classified [198, 199, 200, 201]. Behavior of the time interval between successive spikes near a transition from the active to the rest state is discussed in [150]; in this paper the presence of a subcritical Hopf-homoclinic bifurcation is also identified as a possible mechanism for the transition from an active to a rest state.

5.8 Discussion

In this chapter we have seen that there are many different mechanisms responsible for bursting in hydrodynamical systems. Table 5.1 summarizes the different mechanisms described in terms of properties that are most relevant to hydrodynamics. Thus no single mechanism can be expected to provide a universal explanation for all observations of bursting behavior. The bursts found experimentally in Taylor-Couette flow (cf. §5.5) and large aspect-ratio binary fluid convection (§3.1) occur very close to the threshold of a primary instability and thus have the greatest potential for a successful dynamical systems interpre-

tation of the type emphasized here. We have seen, however, that even for fully developed turbulent boundary layers at very large Reynolds numbers a dynamical systems approach can be profitable (cf. §5.1).

Although nearly all of the mechanisms we have described rely on the presence of global bifurcations, there are important differences among them. For example, the bursts in the wall region of a turbulent boundary layer described in §5.1 are due to a (structurally stable) heteroclinic cycle connecting fixed points with *finite* amplitude; such a cycle leads to bursts with a limited dynamic range. In contrast, in the new mechanism described in this dissertation the dynamic range is unlimited. Moreover, the role of the fixed points is different: in the former the bursts are associated with the *excursions* between the fixed points while in the latter the bursts are associated *with* the fixed points. Because of the asymptotic stability of the cycle the time between successive bursts in the model of §5.1 will increase without bound unless the stochastic pressure term is included; such a stochastic term is not required in the mechanism described in this dissertation. In particular, in this mechanism the duration of the bursts remains finite despite the fact that they are associated with a heteroclinic connection. This is because of the faster than exponential escape to "infinity" that is typical of this mechanism. This is so also for the mechanism described in §5.3; both of these mechanisms involve global connections to infinity and hence are capable of describing bursts of arbitrarily large dynamic range.

It is interesting that the burst mechanism described in this dissertation and the cases of intermittency involving an invariant manifold (§5.6.3) fit into a broader class of dynamical systems in which there is an invariant subspace Σ containing an invariant set

A which is unstable to perturbations out of Σ. For example, in on-off intermittency a strange attractor in Σ loses stability in the transverse direction when a parameter λ is varied; however, the dynamics in Σ do not depend on λ, giving a skew product structure. For in-out intermittency there may be several invariant sets in Σ, possibly nonchaotic, with different transverse stability properties, all of which vary with the parameter λ. The resulting bursts away from Σ and back for on-off and in-out intermittency do not require *per se* proximity to a heteroclinic connection (although such a bifurcation is inevitably in the background), and hence have finite duration and a finite dynamic range determined by the global reinjection mechanism. The mechanism described in this dissertation also describes bursts of finite duration, but this is because the escape to and return from infinity occurs in finite time. Also, it differs in that the bursts are associated with visits to Σ, not away from it, and they have arbitrarily large dynamic range. In addition, the set-up for the bursts described in this dissertation has the skew product structure of on-off intermittency, but chaotic bursts are produced despite the absence of a chaotic set in Σ. Note that as for the bursts described in this dissertation, [202, 203] obtain chaotic behavior associated with a heteroclinic cycle between nonchaotic sets A and B which lie in an invariant subspace, with A (B) stable (nonstable) within Σ and nonstable (attracting) in $\mathbb{R}^n \backslash \Sigma$. However, that heteroclinic cycle is traced out in infinite time, unlike the finite time excursions for the burst mechanism described in this dissertation.

section	mechanism	burst recurrence properties	dynamic range
5.1	structurally stable, attracting heteroclinic cycle	increasing period in absence of random pressure force	finite
5.2	periodic orbit near homoclinic bifurcation	periodic or chaotic	finite
5.3	heteroclinic connection to infinity	"random"	unlimited
5.4	symmetry-increasing bifurcation?	irregular but with well-defined mean period	finite
5.5	finite amplitude trigger to inviscidly stable flow from secondary instability	roughly periodic	finite
5.6.1	laminar state ceases to exist or loses stability	chaotic	finite
5.6.2	crisis of strange attractor	chaotic	finite
5.6.3	loss of stability out of invariant manifold	chaotic	finite
5.7	slow variables cause effective change in parameters causing change in state	periodic or chaotic	finite
Ch. 3,4	heteroclinic cycles involving infinite amplitude states	periodic or chaotic	unlimited

Table 5.1: The different mechanisms for bursting discussed in this dissertation. The term dynamic range refers to the range of amplitudes during each burst.

Chapter 6

Conclusion

In this dissertation, it has been shown that forced symmetry-breaking, or the introduction of small perturbations that reduce the symmetry of a system, can be responsible for complex dynamics in a system that would otherwise behave in a regular manner. In particular, it has been shown that for the Hopf bifurcation with D_4 symmetry, weakly breaking the interchange symmetry can lead to periodic or irregular bursts of very large dynamic range (cf. Chapter 3). Related bursts can also arise when the normal form symmetry is strongly broken by resonant temporal forcing (cf. Chapter 4). Bursts occur when the system makes visits near solutions "at infinity," and are associated with global bifurcations involving such solutions. We emphasize that in order for such bursts to occur, at least one solution branch must be subcritical and at least one must be supercritical in the absence of symmetry-breaking. Also, we have shown that the mechanism is robust with respect to the addition of small higher order terms in the amplitude equations. Other interesting behavior including wrinkled tori and global connections involving finite amplitude states (such as the

supergluing bifurcation in Chapter 4) has also been presented.

The normal form for the Hopf bifurcation has $D_4 \times S^1$ symmetry, where $D_4 = \langle \kappa_1, \kappa_2 \rangle$ and $\kappa_1 : (z_+, z_-) \to (z_+, -z_-)$ is called the reflection symmetry, $\kappa_2 : (z_+, z_-) \to (z_-, z_+)$ is called the interchange symmetry, and S^1 is the normal form symmetry $N_\sigma : (z_+, z_-) \to e^{i\sigma}(z_+, z_-)$ for $\sigma \in [0, 2\pi)$. For completeness, we show that weakly breaking the reflection symmetry κ_1 can *also* lead to bursts of very large dynamic range. Keeping only the term which breaks the reflection symmetry at linear order and truncating the other terms at cubic order, the normal form equations are

$$\frac{dz_+}{dt} = (\lambda + i\omega)z_+ + \alpha z_- + A(|z_+|^2 + |z_-|^2)z_+ + B|z_+|^2 z_+ + C\bar{z}_+ z_-^2, \qquad (6.1)$$

$$\frac{dz_-}{dt} = (\lambda + i\omega)z_- + \alpha z_+ + A(|z_+|^2 + |z_-|^2)z_- + B|z_-|^2 z_- + C\bar{z}_- z_+^2, \qquad (6.2)$$

where $\alpha \in \mathbb{C}$. It is useful to make the change of variables

$$z_+ = \rho^{-1/2} \cos(\theta/2) e^{i(\phi+\psi)/2}, \qquad z_- = \rho^{-1/2} \sin(\theta/2) e^{i(-\phi+\psi)/2},$$

with the new time τ defined by $d\tau/dt = 1/\rho$. In these variables, equations (6.1,6.2) take the form

$$\begin{aligned}
\frac{d\rho}{d\tau} &= -\rho[2A_R + B_R(1 + \cos^2\theta) + C_R \sin^2\theta \cos 2\phi] - 2[\lambda + \alpha_R \cos\phi \sin\theta]\rho^2, \\
\frac{d\theta}{d\tau} &= \sin\theta[\cos\theta(-B_R + C_R \cos 2\phi) - C_I \sin 2\phi] + 2(\alpha_R \cos\phi \cos\theta - \alpha_I \sin\phi)\rho, \\
\frac{d\phi}{d\tau} &= \cos\theta(B_I - C_I \cos 2\phi) - C_R \sin 2\phi - \frac{2\rho}{\sin\theta}(\alpha_I \cos\phi \cos\theta + \alpha_R \sin\phi), \\
\frac{d\psi}{d\tau} &= 2A_I + B_I + C_I \cos 2\phi + C_R \sin 2\phi \cos\theta + 2\omega\rho + \frac{2\rho}{\sin\theta}(\alpha_I \cos\phi + \alpha_R \cos\theta \sin\phi),
\end{aligned}$$

where $A = A_R + iA_I$, etc. As in Chapters 3 and 4, these equations have an invariant subspace at $\rho = 0$ (corresponding to infinite amplitude states) on which the dynamics are equivalent

to those for the system with $\alpha = 0$. Also, the solutions at infinity are radially stable (unstable) if the corresponding solution branch bifurcates subcritically (supercritically) for $\alpha = 0$. We choose parameters

$$A = 1 - 1.5i, \qquad B = -2.8 + 5i, \qquad C = 1 + i, \qquad \omega = 1,$$

so that for $\alpha = 0$ the u solution bifurcates subcritically while the v, w, and qp solutions bifurcate supercritically (see the inset of Figure 3.11), suggesting the possibility of bursts. The trajectory and time series showing chaotic bursting behavior for the attractor for $\lambda = -0.02, \alpha = 0.1 + 0.1i$ is shown in Figure 6.1(a). It is also possible to find periodic burst solutions, such as the one shown in Figure 6.1(b) for the same parameters except with $\lambda = 0.02$. A more detailed analysis of the effect of breaking the reflection symmetry κ_1 has not yet been undertaken.

It is also interesting to consider the effect of simultaneously breaking more than one of the symmetries of $\mathrm{D}_4 \times S^1$. For example, suppose that both the interchange symmetry κ_2 is broken (for example by the presence of sidewalls in a large aspect-ratio binary fluid convection system, cf. Chapter 3) and the normal form symmetry symmetry is broken (for example by resonant temporal forcing, cf. Chapter 4). This leads to the consideration of the equations

$$\begin{aligned}
\frac{dz_+}{dt} &= [\lambda + \Delta\lambda + i(\omega + \Delta\omega)]z_+ + f\bar{z}_+ + A(|z_+|^2 + |z_-|^2)z_+ + B|z_+|^2 z_+ + C\bar{z}_+ z_-^2, \\
\frac{dz_-}{dt} &= [\lambda - \Delta\lambda + i(\omega - \Delta\omega)]z_- + f\bar{z}_- + A(|z_+|^2 + |z_-|^2)z_- + B|z_-|^2 z_- + C\bar{z}_- z_+^2,
\end{aligned}$$

where $\Delta\lambda$, $\Delta\omega$, and f are real. Consider the parameters (cf. Example 1(a) of §3.4.3)

$$A = 1 - 1.5i, \qquad B = -2.8 + 5i, \qquad C = 1 + i,$$

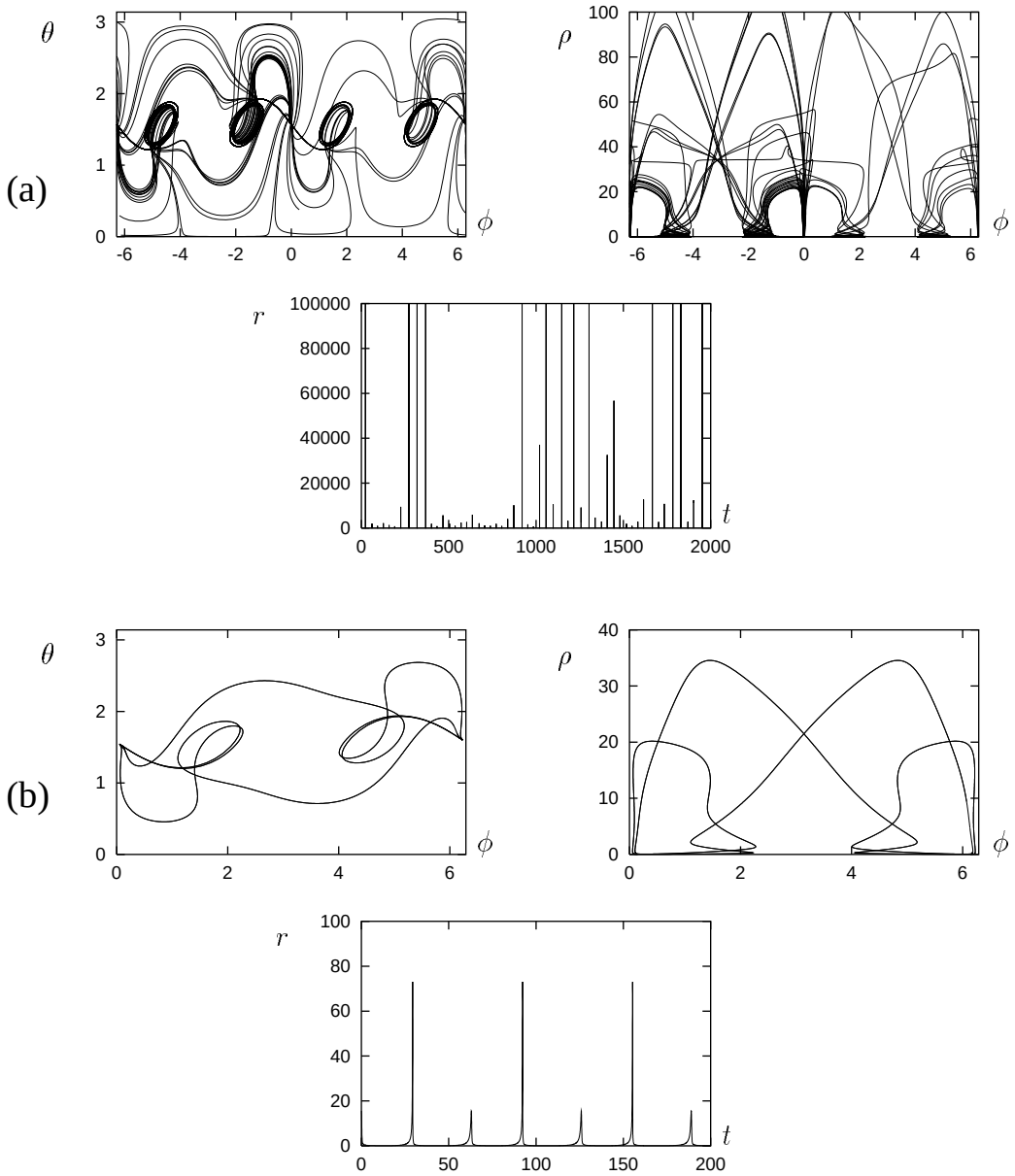

Figure 6.1: Attractor for the Hopf bifurcation with D_4 symmetry with broken reflection symmetry κ_1 with the parameters given in the text and (a) $\lambda = -0.02$, showing chaotic bursts, (b) $\lambda = 0.02$, showing periodic bursts. The bursts are associated with the trajectory going from finite amplitude toward a u_∞ solution at $(\rho, \theta, \phi) = (0, \pi/2, 2\pi m)$ for $m = -1, 0, 1$, getting kicked toward a qp_∞ solution, and then returning to finite amplitude.

$$\lambda = 0.1, \qquad \omega = 1, \qquad \Delta\lambda = 0.03, \qquad \Delta\omega = 0.02.$$

Figure 6.2 shows that resonant temporal forcing causes the *periodic* bursts which exist for $f = 0$ to become *irregular*. This may be understood by recognizing that bursts occur when the system evolves toward an infinite amplitude state along its stable manifold. In the presence of resonant temporal forcing, there will be a larger burst if the forcing kicks the system closer to the stable manifold, and a smaller burst if the forcing kicks it away. In fact, sufficiently large forcing can provide a large enough kick to destroy a pure rotation state (in which successive visits are to different but symmetry-related infinite amplitude solutions), causing the trajectory to sometimes make visits near the *same* infinite amplitude solution (see Figure 6.2(d)). Of course, this only scratches the surface on the types of behavior which are possible when more than one symmetry is simultaneously broken.

Our interpretation of the bursts which arise due to forced symmetry-breaking has primarily been for the model of large aspect-ratio binary fluid convection discussed in Chapter 3. However, there are a number of other systems of interest where an approximate D_4 symmetry arises in a natural way and the burst mechanism described in this dissertation may be relevant. These include overstable convection in small aspect ratio containers with nearly square cross-section [204, 205] and more generally any partial differential equation on a nearly square domain describing the evolution of an oscillatory instability, cf. [206]. Other systems in which this mechanism for bursting might be detected are electrohydrodynamic convection in liquid crystals [207, 107, 208], lasers [209], spring-supported fluid-conveying tubes [108], four coupled oscillators with nearly identical coupling [71, 210, 211], and dynamo theories of magnetic field generation in the Sun [212, 213]. Also of interest is the possibility

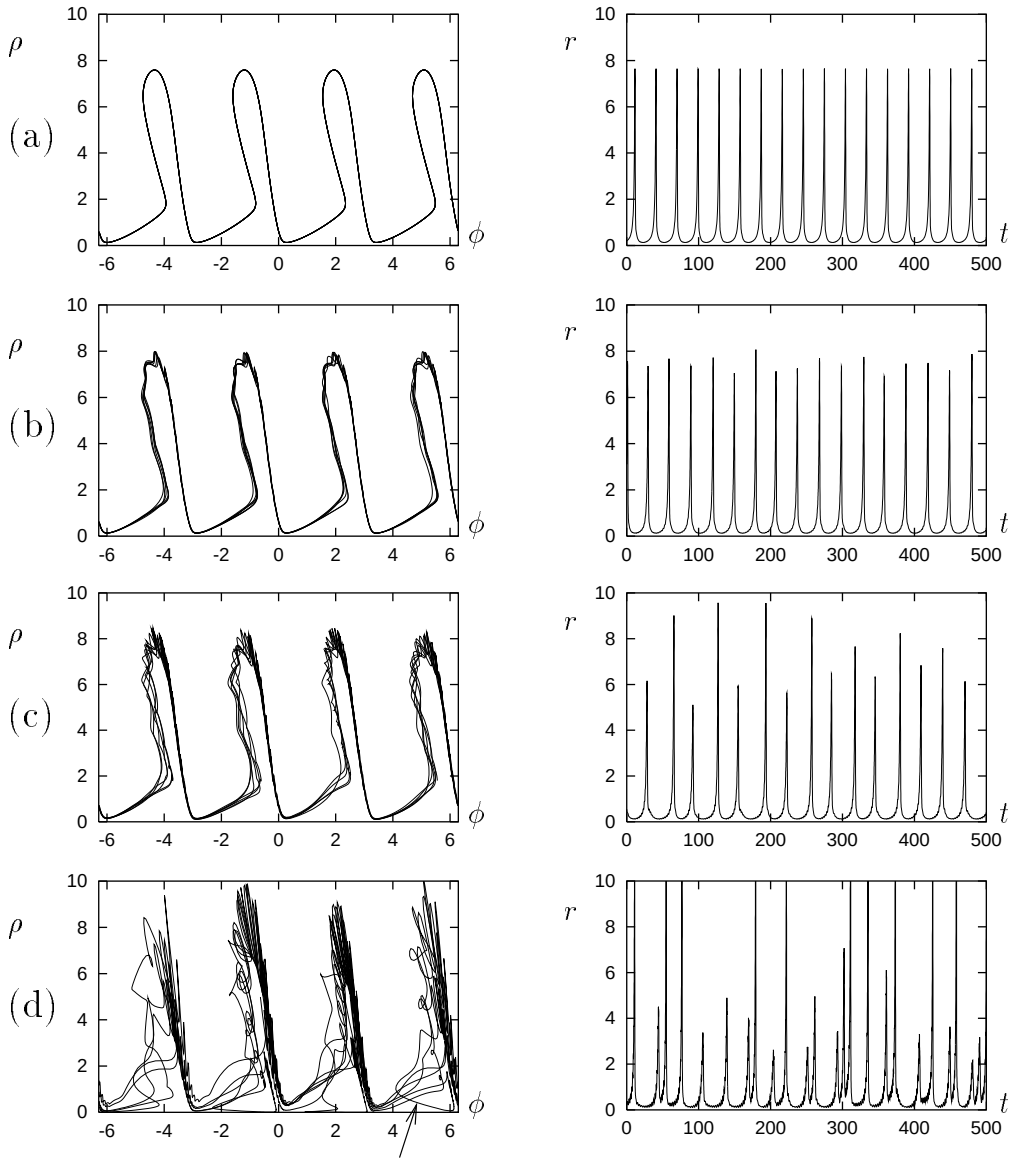

Figure 6.2: Trajectory and time series for attractors with parameters given in the text and (a) $f = 0$, (b) $f = 0.1$, (c) $f = 0.2$, (d) $f = 0.5$. Bursts are associated with visits near the infinite amplitude u_∞ solutions at $(\rho, \phi) = (0, \pi m)$ where $m = -2, -1, 0, 1, 2$. The forcing causes the periodic bursts shown in (a) to become irregular. The arrow in (d) shows an example of where the trajectory makes two successive visits near the same u_∞ solution, showing that large enough forcing can destroy a pure rotation state.

that large scale spatial modulation due to distant walls may produce bursting in a fully nonlinear state with D_4 symmetry undergoing a symmetry-breaking Hopf bifurcation. As an example we envisage a steady pattern of fully nonlinear two-dimensional rolls. With periodic boundary conditions with period four times the basic roll period, the roll pattern has D_4 symmetry since the pattern is preserved under spatial translations by 1/4 period and a reflection. If such a pattern undergoes a secondary Hopf bifurcation with a *spatial* Floquet multiplier $\exp i\pi/2$, the Hopf bifurcation breaks D_4 symmetry. If the invariance of the basic pattern under translations by 1/4 period is only approximate (this would be the case if the roll amplitude varied on a slow spatial scale), the D_4 symmetry itself would be weakly broken and the new mechanism described above could operate.

Special mention should also be made of parametrically excited surface waves in a nearly square container. In this system, gravity-capillary waves are excited on the surface of a viscous fluid by vertical vibration of the container, usually as a result of a subharmonic resonance. Simonelli and Gollub [111] studied the effect of changing the shape of the container from a square to a slightly rectangular container, focusing on the $(3,2)$, $(2,3)$ interaction in this system. These modes are degenerate in a square container and only pure and mixed modes were found in this case. In a slightly rectangular container the degeneracy between these modes is broken, however, and in this case a region of quasiperiodic and chaotic behavior was present near onset. When these oscillations first appear they take the form of relaxation oscillations in which the surface of the fluid remains flat for a long time before a "large wave grows, reaches a maximum, and decays, all in a time short compared with the period". The duration of the spikes is practically independent of the forcing

amplitude, while the interspike period appears to diverge as the forcing amplitude *decreases*. The spikes themselves possess the characteristic asymmetry seen in the bursts, for example, in Figures 3.13 and 3.15. This behavior occurs when the forcing frequency lies *below* the resonance frequency of the square container, i.e., precisely when D_4-symmetric problem has a *subcritical* fixed point branch. Irregular bursts are also found, depending on parameters, but these are distinct from the chaotic states found by Nagata [114] far from threshold and present even in a square container. Understanding the details of this behavior will require a very careful examination of the interplay between the effect of resonant temporal forcing which strongly breaks the normal form symmetry, and the change in the container from square to rectangular which breaks the interchange symmetry.

We also note that given the inevitability of noise in physical systems, it would be interesting to consider the effect of noise on this mechanism for bursting. As in the situation described above for a system with both the interchange and normal symmetries broken, there will be a larger burst if the noise kicks the system closer to the stable manifold of an infinite amplitude solution, and a smaller burst if the noise kicks it away. Thus, for example, a periodic burst state in the absence of noise will still burst in the presence of noise but the successive burst amplitudes and the time between successive bursts may differ substantially. Noise may also affect the physical manifestation of the bursts, for example destroying the pure blinking or pure winking states described in Chapter 3. The analysis of the effect of noise on these bursts would involve numerical computation and analytical work along the lines of [214, 215], but the results would differ in many respects because of the different characteristics of the heteroclinic cycles involved.

Finally, it is natural to ask if heteroclinic cycles involving infinite amplitude solutions can exist for systems with other symmetry properties. Clearly such cycles can exist in systems with broken quaternion symmetry undergoing a Hopf bifurcation since the normal form for a Hopf bifurcation with the symmetry of the quaternion group is identical to the normal form for a Hopf bifurcation with D_4 symmetry [216]. On the other hand, as discussed in §3.6, such cycles *cannot* exist for the Hopf bifurcation with O(2) symmetry. Similarly, it can be shown that they cannot exist for the system [217]

$$\begin{aligned} \dot{x} &= x(\lambda + ax^2 + by^2 + cz^2), \\ \dot{y} &= y(\lambda + ay^2 + bz^2 + cx^2), \\ \dot{z} &= z(\lambda + az^2 + bx^2 + cy^2), \end{aligned}$$

where all variables and parameters are real. Here there are three types of fixed point solutions $(x,0,0)$, $(x,x,0)$, and (x,x,x); while it is possible for one solution branch to bifurcate subcritically and another supercritically, the solutions don't have the appropriate "angular" stability properties for heteroclinic connections involving infinite amplitude solutions to form. The insight gained from the study of the Hopf bifurcation with broken D_4 symmetry will hopefully be useful in discovering systems for which bursts occur by a related mechanism; indeed, bursts associated with a heteroclinic cycle involving solutions "at infinity" have recently been found for a system with $Z_4 \ltimes T^2$ symmetry [218]. An exciting possibility is that more exotic types of infinite amplitude solutions, such as an infinite amplitude homoclinic or heteroclinic orbit, can be involved in the burst mechanism for some systems and parameter regimes; the associated bursts could have very different properties from those studied in this dissertation.

Appendix A

Parameter Symmetries for the Hopf Bifurcation with D_4 Symmetry

Suppose that the original parameters do not lie in the wedge in parameter space given by $3C_R < B_R < C_R$ for the Hopf bifurcation with exact D_4 symmetry (equations (3.9,3.10) with $\Delta\lambda = \Delta\omega = 0$); then it is possible to act with parameter symmetries to bring the parameters into this wedge with the phase space suitably relabeled. Time may then be rescaled so that $C_R = -1$. The existence and stability results in Chapter 3 for solutions with $-3 < B_R < -1$ and $C_R = -1$ may then be applied to the transformed system. By "undoing" the relabeling of phase space we can deduce the existence and stability properties for the original parameters. Note that care should be used in determining the stability properties because the parameter symmetry P_3 reverses time, thereby changing the signs of

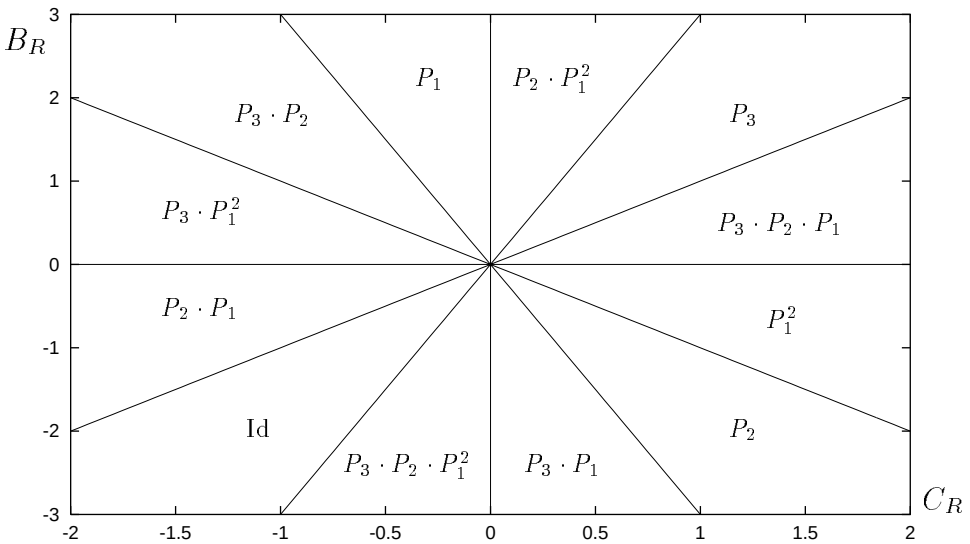

Figure A.1: The parameter symmetries required to transform different regions of the parameter space into the wedge $3C'_R < B'_R < C'_R$.

the eigenvalues; also, changing the sign of the radial eigenvalue changes subcritical branches into supercritical branches and vice versa. For given values of B_R and C_R, Figure A.1 shows the necessary action to bring the parameters into the wedge $3C'_R < B'_R < C'_R$. Note that if after this action $B'_I > 0$ a further action of P_4 will make $B'_I < 0$, if desired.

We illustrate the use of parameter symmetries with an example. Suppose $A = 1 - 1.5i$, $B = -2.8 + 5i$, and $C = 1 + i$ (the system behavior for these parameters is studied carefully in Example 1(a) of §3.4.3). Since $B_R = -2.8, C_R = 1$, from Figure A.1 the action P_2 brings the parameters into the desired wedge in parameter space. This gives $B'_I > 0$ so we then act with P_4. Overall

$$\begin{aligned} P_4 \cdot P_2 : \qquad (u, v, w) &\rightarrow (v, u, w) \equiv (u', v', w') \\ (A, B, C) &= (1 - 1.5i, -2.8 + 5i, 1 + i) \\ &\rightarrow (1 + 1.5i, -2.8 - 5i, -1 + i) \equiv (A', B', C'). \end{aligned}$$

Since $C_R' = -1$ it is not necessary to rescale time to apply the results from the main text. We find (see Figure 3.7) that the transformed parameters lie just within region I of parameter space. Letting u' solutions be fixed point solutions with $v' = w' = 0$, etc., we find that u', v', and w' solutions are respectively a source, saddle, and source in the associated spherical system (see Table 3.3); also the v' solutions are subcritical and u' and w' solutions are supercritical. A supercritical qp' solution also exists enclosing the u' solution in the associated spherical system. As an example of "undoing" the relabeling of phase space, consider the u' solutions. Since these solutions satisfy $v' = w' = 0$, in the original parameters they correspond to solutions with $u = w = 0$, i.e., v solutions. The stability properties of the v solutions in the original parameters are identical to the stability properties of the u' solutions in the transformed parameters. We thus conclude that for $A = 1 - 1.5i,\ B = -2.8 + 5i$, and $C = 1 + i$ the u solution is a subcritical saddle and that the v, w solutions are supercritical sources. There is also a supercritical qp libration around the v solution in the associated spherical system.

Appendix B

Heteroclinic Orbits in the Hopf Bifurcation with D_4 Symmetry

Following [71], we give the conditions for heteroclinic orbits to exist connecting symmetry-related u, v, or w solutions for a Hopf bifurcation with exact D_4 symmetry (equations (3.9,3.10) with $\Delta\lambda = \Delta\omega = 0$). The necessary conditions on B and C are most easily understood by considering a heteroclinic orbit which connects the w solution with $\theta = 0$ to the w solution with $\theta = \pi$. This orbit is present when $C_R = 0$. Then from (3.13)

$$\frac{d\phi}{d\tau} = \cos\theta(B_I - C_I \cos 2\phi),$$

and hence there is an invariant line $\phi = \frac{1}{2}\cos^{-1}(\frac{B_I}{C_I})$ provided $|B_I| < |C_I|$. For this to be a heteroclinic orbit connecting $\theta = 0$ to $\theta = \pi$ it is necessary that there not be any fixed points on this line. Equation (3.12) with $C_R = 0$ evaluated at this value of ϕ,

$$\frac{d\theta}{d\tau} = \sin\theta \left[-B_R \cos\theta \pm \sqrt{C_I^2 - B_I^2} \right],$$

fixed points	conditions for existence	condition for angular stability
u	$B_R + C_R = 0$ $\|C\|^2 - B_R C_R - B_I C_I < 0$ $\|-\frac{1}{2}B_I + \frac{3}{2}C_I\| < \|\frac{1}{2}B_I + \frac{1}{2}C_I\|$	$B_R - 3C_R < 0$
v	$B_R - C_R = 0$ $\|C\|^2 + B_R C_R + B_I C_I < 0$ $\|\frac{1}{2}B_I + \frac{3}{2}C_I\| < \|\frac{1}{2}B_I - \frac{1}{2}C_I\|$	$B_R + 3C_R < 0$
w	$C_R = 0$ $\|B_I\| < \|C_I\|$ $\|B\|^2 < \|C\|^2$	$B_R > 0$

Table B.1: Conditions for existence and stability of heteroclinic orbits in the associated spherical system connecting pairs of u, v and w fixed points, obtained by applying parameter symmetries to the results of [71].

shows that there are fixed points in θ when either $\sin\theta = 0$ (corresponding to w solutions) or

$$\cos\theta = \frac{\pm\sqrt{C_I^2 - B_I^2}}{B_R}.$$

Since $C_R = 0$ the heteroclinic orbit will therefore exist provided $|C|^2 > |B|^2$; this orbit is stable if $\mathrm{Tr}_w \equiv s_2^w + s_3^w < 0$. Conditions for the existence and stabilities of heteroclinic orbits connecting other symmetric fixed points may be found using the parameter symmetries (see Appendix A); we summarize these conditions in Table B.1. Of particular relevance for our discussion of the parameter range $-3 < B_R < -1, C_R = -1$ are the heteroclinic orbits connecting the v solutions which may exist for $B_R = C_R = -1$. The regions of (B_I, C_I) space for which these heteroclinic orbits exist are shown in Figure B.1. The heteroclinic orbits are attracting in the associated spherical system and will thus be considered to be

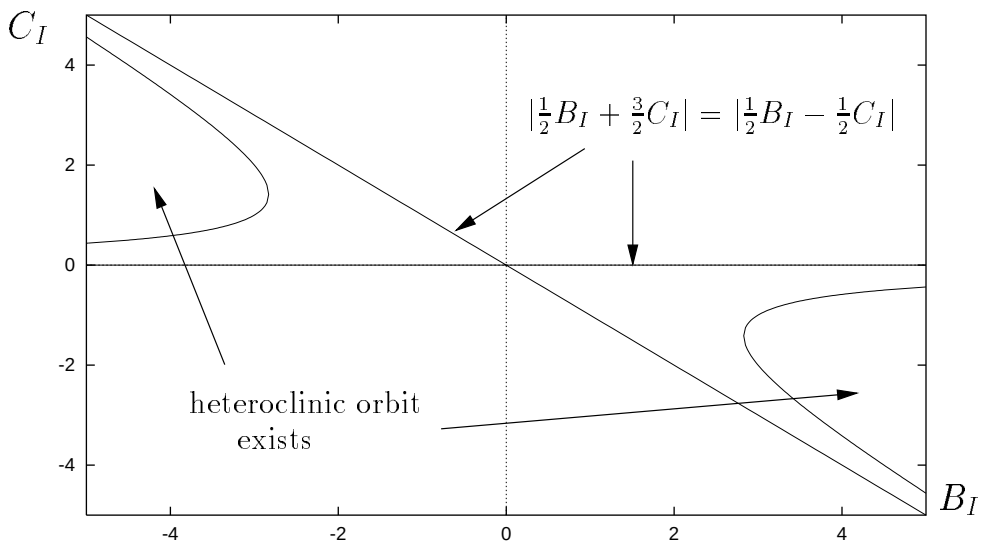

Figure B.1: Region in parameter space with a heteroclinic orbit connecting symmetry-related v solutions when $B_R = C_R = -1$ for the Hopf bifurcation with exact D_4 symmetry.

sinks since B_R+3C_R is negative in this parameter range. Their radial stability is determined by the radial stability of the v solutions.

Appendix C

Radial Stability of ns and qp Solutions for the Hopf Bifurcation with D_4 Symmetry

For the parameter range $-3 < B_R < -1, C_R = -1$ for the Hopf bifurcation with exact D_4 symmetry (equations (3.9,3.10) with $\Delta\lambda = \Delta\omega = 0$), we can place the following restrictions on the radial stabilities of the ns and qp solutions. Recall that these solutions are radially stable (unstable) if they bifurcate supercritically (subcritically) from the trivial state.

(i) Suppose that ns solutions exist. If the v solutions are supercritical, then the ns solutions must also be supercritical. If the w solutions are subcritical, then the ns solutions must also be subcritical.

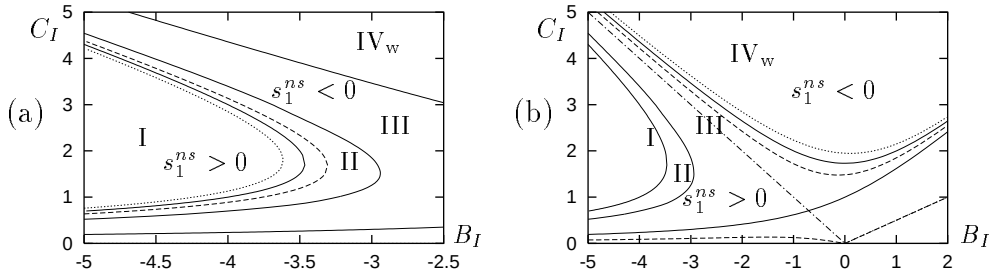

Figure C.1: When $B_R = -2$, $C_R = -1$ the radial eigenvalue s_1 of the v, u and w solutions vanishes for $A_R = 0.5$, 1.5 and 2.0, respectively. (a) The dotted (dashed) lines show where $s_1^{ns} = 0$ for $A_R = 0.4$ (0.6). For $A_R = 0.4$, $s_1^{ns} < 0$ in regions II and III (the only regions in which the ns solutions exist) and the ns solutions are always supercritical. For $A_R = 0.6$ the curve $s_1^{ns} = 0$ has moved beyond the boundary between regions I and II and the ns solutions may be supercritical or subcritical depending on the values of B_I and C_I. (b) The dot-dashed, dashed, and dotted lines show where s_1^{ns} switches signs for $A_R = 1.5$, 1.8, and 2.2, respectively. For $A_R = 1.5$, $s_1^{ns} < 0$ only outside regions I and II. For $A_R = 1.8$ the ns solutions may be supercritical or subcritical depending on the values of B_I and C_I. For $A_R = 2.2$ the curve $s_1^{ns} = 0$ has moved beyond the boundary between regions III and IV$_w$; since ns solutions only exist in regions II and III the ns solutions are now always subcritical. Similar behavior is found for other values of B_R in the range $-3 < B_R < -1$.

These results follow from the observations that when $s_1^v = 0$, the condition $s_2^v s_3^v = 0$ is identical to the condition $s_1^{ns} = 0$, and similarly, when $s_1^w = 0$, the condition $s_2^w s_3^w = 0$ is identical to the condition $s_1^{ns} = 0$. In words, this says that when A_R is chosen so that the radial stability of the v or w solution is degenerate, the condition for the pitchfork bifurcation which causes the creation or destruction of the ns solutions is identical to the condition that the radial stability of the ns solutions is degenerate. Using this result and a numerical study of how the curve $s_1^{ns} = 0$ varies in (B_I, C_I) space with A_R, we verify (i) (see Figure C.1).

(ii) Suppose qp solutions exist. If the u solutions are subcritical then the qp solutions are also subcritical.

We write

$$\bar{F} = 2A_R + \frac{1}{T_\tau}\int_0^{T_\tau} G(\theta^*(\tau'), \phi^*(\tau'))d\tau' \equiv 2A_R + \bar{G},$$

where

$$G(\theta, \phi) = B_R(1 + \cos^2\theta) + C_R \sin^2\theta \sin 2\phi,$$

and define $A_R^* = A_R^*(B_R, B_I, C_R, C_I)$ to be the value of A_R for which $\bar{F} = 0$ (so that if $A_R^* > A_R$ ($< A_R$) the qp branch is supercritical (subcritical)). Thus,

$$A_R^* = -\frac{\bar{G}}{2}.$$

The value of $\bar{G}$ for a periodic orbit can be calculated by numerical integration or extracted from the Floquet multipliers calculated by AUTO [90]. In Figure C.2 we plot the dependence of A_R^* on B_I for different values of C_I (here $B_R = -2, C_R = -1$ are fixed; the results also hold for other values of B_R in the range $-3 < B_R < -1$). We see that A_R^* is always less than the values of A_R for which the radial stabilities of the u solutions are degenerate; thus, if the u solutions are subcritical then the qp solutions are also subcritical.

(iii) Let $C_I = C_I'$ be fixed, and define B_I' to be the value of B_I for which (B_I', C_I') lies on the boundary between regions II and III. If the ns solutions are supercritical with $(B_I, C_I) = (B_I', C_I')$, then the qp solutions will be supercritical for all values of (B_I, C_I') for which they exist.

Without loss of generality we consider $B_I < 0$. Numerical calculations show that A_R^* is a monotonically decreasing function of B_I (see Figure C.2); for $C_I = C_I'$ it reaches its minimum value $A_{R,min}^*$ when $B_I = B_I'$ because for larger values of B_I the qp solutions

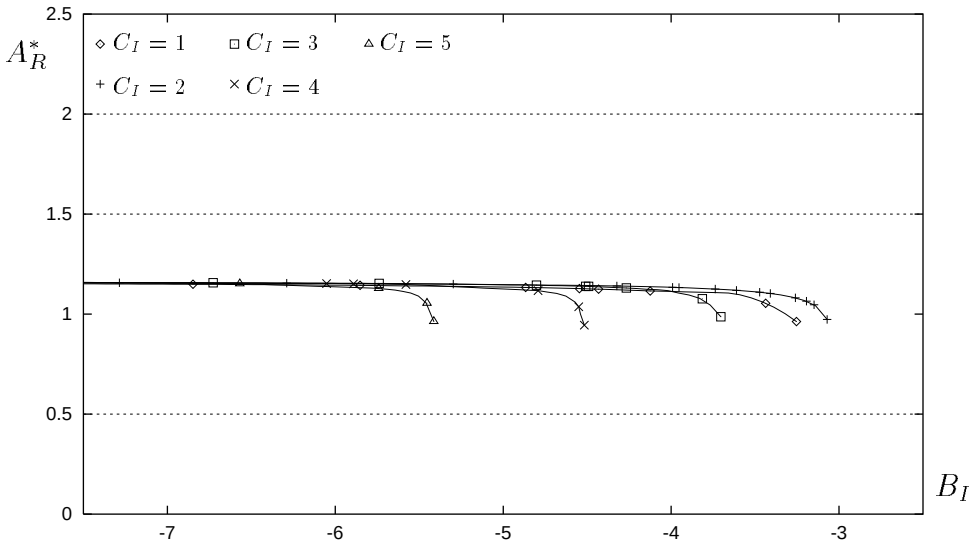

Figure C.2: The dependence of A_R^* on B_I for different fixed values of C_I with $B_R = -2$ and $C_R = -1$. These data points are extracted from the Floquet multipliers calculated by AUTO. For a particular value of C_I, the maximum value of B_I is reached when the *qp* solution collides with the *ns* solutions, corresponding to the boundary between regions II and III. The dotted lines at $A_R^* = 0.5, 1.5$, and 2.0 are for the respective A_R values at which the radial stabilities of the v, u, and w solutions are degenerate. Similar behavior is found for other values of B_R in the range $-3 < B_R < -1$.

do not exist. For $(B_I, C_I) = (B_I', C_I')$ the periodic orbit has become a heteroclinic orbit connecting *ns* solutions; therefore $\bar{F}$ is dominated by the *ns* solutions so that

$$\bar{G} = F(\theta_{ns}, \phi_{ns}) - 2A_R$$

and hence

$$A_{R,min}^* = A_R - \frac{1}{2}F(\theta_{ns}, \phi_{ns}).$$

But in this equation $F(\theta_{ns}, \phi_{ns}) < 0$ because the *ns* solutions are supercritical for $(B_I, C_I) = (B_I', C_I')$; thus $A_{R,min}^* > A_R$. But for all other values of B_I for which *qp* solutions exist $A_R^* > A_{R,min}^*$ so that $A_R^* > A_R$; therefore the *qp* solutions are supercritical.

This leads to the following restrictions on the possible radial stabilities of the solutions. First, we know numerically that if the *ns* solutions are supercritical anywhere

in region II with $C_I = C_I'$ they will also be supercritical at $(B_I, C_I) = (B_I', C_I')$ (see, e.g., Figure C.1(a)); thus, if the ns and qp solutions exist and the ns solutions are supercritical, then the qp solutions must also be supercritical. Second, if A_R, B_R, and C_R have been chosen so that the v solutions are supercritical, then from (i) the ns solutions with the same values of these parameters will be supercritical; in particular, they will be supercritical with $(B_I, C_I) = (B_I', C_I')$ so that the qp solutions must be supercritical.

(iv) Suppose that the u and v solutions are subcritical, and ns solutions exist and are supercritical. Then qp solutions cannot exist.

Consider the value $A_R = -\frac{1}{2}(B_R + C_R)$ for which the radial stability of the u solution is degenerate; then

$$s_1^{ns} = \frac{B_I + C_I}{B_R C_I - B_I C_R}(|C|^2 - \mathrm{Re}(B\bar{C})).$$

In order for ns solutions to exist it is necessary that $|C|^2 - \mathrm{Re}(B\bar{C}) > 0$. Thus, the curves defined by $B_I + C_I = 0$ or $B_R C_I - B_I C_R = 0$ divide the (B_I, C_I) plane into regions in which s_1^{ns} is positive or negative (see Figure C.1(b)). Numerically it is seen that $s_1^{ns} < 0$ only outside of the regions I and II; in other words, if ns solutions are supercritical then qp solutions cannot exist. Based on a numerical study of how the curve $s_1^{ns} = 0$ varies in (B_I, C_I) space with A_R (Figure C.1), we conclude that this also cannot happen for larger values of A_R for which the u solutions are subcritical.

All possibilities for the radial stability of the ns and qp solutions which do not violate the restrictions (i)-(iv) occur for open regions of parameter space with $-3 < C_R < -1$ and $C_R = -1$. These possibilities are shown in Figure C.3.

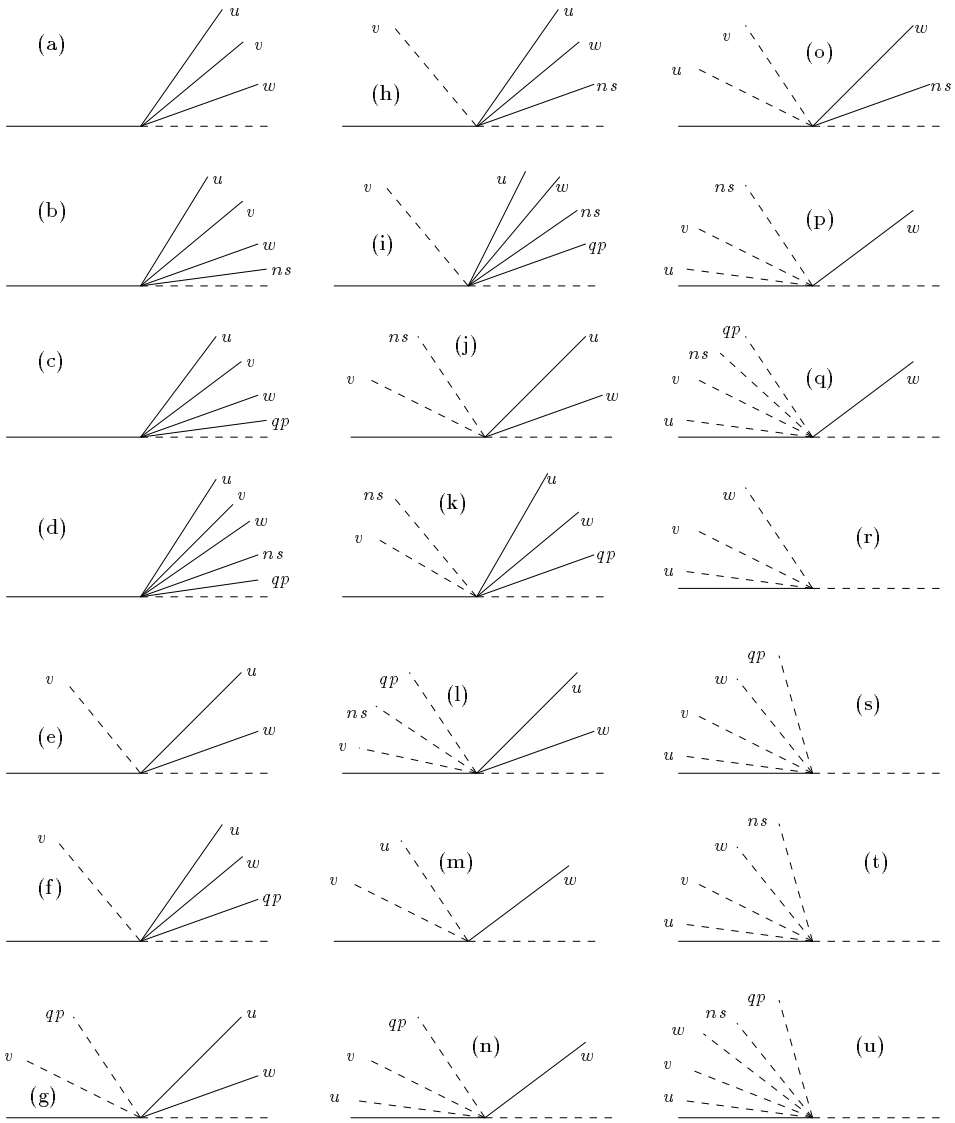

Figure C.3: Possible bifurcation diagrams for $-3 < B_R < -1$, $C_R = -1$, including ns and qp solutions in addition to u, v, and w solutions (cf. Figure 3.8). Here, a solid (dashed) line indicates *radial* stability (instability) only. Representative parameters for each diagram are $B_R = -2, C_R = -1$, and (A_R, B_I, C_I) = (a) (0.1,-1,3); (b) (0.1,-2,1.5); (c) (0.1,-4,2); (d) (0.1,-3.25,1.5); (e) (0.7,-1,3); (f) (0.7,-4,2); (g) (1.2,-4,2); (h) (0.7,-2,1); (i) (0.7,-3.1,1.5); (j) (1.2,-2.7,1); (k) (0.7,-3.3,1.5); (l) (1.2,-3.25,1.5); (m) (1.7,-1,3); (n) (1.7,-4,2); (o) (1.7,-0.5,1.6); (p) (1.7,-2,1); (q) (1.7,-3.25,1.5); (r) (2.5,-1,3); (s) (2.5,-4,1.5) (t) (2.5,-2,1); (u) (2.5,-3.25,1.5). Note that these parameters are not representative of all possibilities for angular stability.

Appendix D

Proof that Heteroclinic Cycles Involving Infinite Amplitude Solutions are Traced Out in Finite Time

Consider a heteroclinic cycle involving the two infinite amplitude fixed points A and B as shown in Figure D.1. Near B, local coordinates are chosen so that

$$\frac{dx_1}{d\tau} = s_3^{\mathrm{B}} x_1, \qquad \frac{d\rho}{d\tau} = s_1^{\mathrm{B}} \rho, \qquad \frac{dz_1}{d\tau} = s_2^{\mathrm{B}} z_1, \tag{D.1}$$

where $s_3^{\mathrm{B}} > 0, s_1^{\mathrm{B}} < 0$, and $s_2^{\mathrm{B}} < 0$. Near A, local coordinates are chosen so that

$$\frac{dx_2}{d\tau} = \alpha x_2 + \beta z_2, \qquad \frac{d\rho}{d\tau} = s_1^{\mathrm{A}} \rho, \qquad \frac{dz_2}{d\tau} = -\beta x_2 + \alpha z_2, \tag{D.2}$$

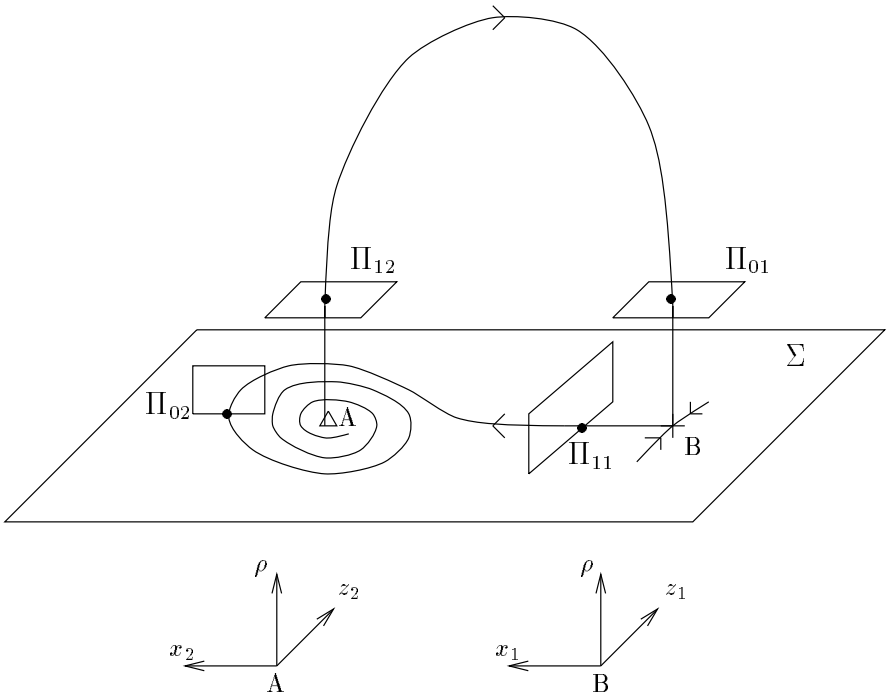

Figure D.1: Heteroclinic cycle involving the A and B infinite amplitude fixed points. The cross-sections $\Pi_{01}, \Pi_{11}, \Pi_{02}$, and Π_{12} are defined in the text.

where $\alpha < 0$, $s_1^{\mathrm{A}} > 0$, and $\beta > 0$. As shown in Figure D.1, we construct cross-sections near B defined by $\Pi_{01} \equiv \{\rho = \epsilon\}$ and $\Pi_{11} \equiv \{x_1 = \epsilon\}$, and cross-sections near A defined by $\Pi_{02} \equiv \{z_2 = 0\}$ and $\Pi_{12} \equiv \{\rho = \epsilon\}$. The parameter ϵ is small but finite and is chosen so that the mappings from $\Pi_{01} \to \Pi_{11}$ and from $\Pi_{02} \to \Pi_{12}$ may be suitably approximated by the linearization of the flow about the fixed points B and A, respectively. In terms of the time τ, the heteroclinic cycle is traced out in infinite time. However, in terms of the original time t the situation is more subtle because the transformation $\frac{dt}{d\tau} = \rho$ fails for $\rho = 0$; thus, we consider a limiting procedure in which a trajectory approaches the heteroclinic cycle between the infinite amplitude fixed points. This consists of four parts.

(i) $P_{01}^{L} : \Pi_{01} \to \Pi_{11}$

Suppose that at $\tau = 0$ a trajectory passes through Π_{01} with coordinates $(x_1, \rho, z_1) = (x_{01}, \epsilon, z_{01})$, with $x_{01} = z_{01} = 0$ denoting the point on the heteroclinic cycle. From equations (D.1),

$$x_1(\tau) = x_{01} e^{s_3^{\mathrm{B}} \tau}, \qquad \rho(\tau) = \epsilon e^{s_1^{\mathrm{B}} \tau}, \qquad z_1(\tau) = z_{01} e^{s_2^{\mathrm{B}} \tau}.$$

The time τ for the trajectory to go from Π_{01} to Π_{11} (determined by the time required for x_1 to go from x_{01} to ϵ) is $\tau = \frac{1}{s_3^{\mathrm{B}}} \log \frac{\epsilon}{x_{01}}$, a quantity which diverges as $x_{01} \to 0$ (i.e., as the heteroclinic cycle is approached). If, however, we work in the original time t defined by $\frac{dt}{d\tau} = \rho$, equations (D.1) become

$$\frac{dx_1}{dt} = \frac{s_3^{\mathrm{B}} x_1}{\rho}, \qquad \frac{d\rho}{dt} = s_1^{\mathrm{B}}, \qquad \frac{dz_1}{dt} = \frac{s_2^{\mathrm{B}} z_1}{\rho},$$

with solution

$$x_1(t) = x_{01} \left(\frac{s_1^{\mathrm{B}} t + \epsilon}{\epsilon} \right)^{s_3^{\mathrm{B}}/s_1^{\mathrm{B}}}, \qquad \rho(t) = s_1^{\mathrm{B}} t + \epsilon,$$

$$z_1(t) = z_{01} \left(\frac{s_1^{\mathrm{B}} t + \epsilon}{\epsilon} \right)^{s_2^{\mathrm{B}}/s_1^{\mathrm{B}}}.$$

The time t to go from Π_{01} to Π_{11} is thus

$$t = \frac{\epsilon}{s_1^{\mathrm{B}}} \left[\left(\frac{x_{01}}{\epsilon} \right)^{|s_1^{\mathrm{B}}/s_3^{\mathrm{B}}|} - 1 \right].$$

In the limit $x_{01} \to 0$ (i.e., as the heteroclinic cycle is approached) $t \to \frac{\epsilon}{|s_1^{\mathrm{B}}|}$, i.e., a *finite* time in the original time variable.

(ii) $P_{11}^{L} : \Pi_{11} \to \Pi_{02}$

Reset time so that at $\tau = 0$ the trajectory passes through Π_{11} with coordinates $(x_1, \rho, z_1) = (\epsilon, \rho_{11}, z_{11})$, where the trajectory would be on the heteroclinic cycle if $\rho_{11} =$

$z_{11} = 0$. Using the time τ, it takes a finite time T_τ to go from Π_{11} to Π_{02}. Using the time t, this takes a time

$$T = \int_0^T dt = \int_0^{T_\tau} \rho d\tau \leq \rho_{\max} \int_0^{T_\tau} d\tau = \rho_{\max} T_\tau,$$

where $\rho_{\max}$ is the maximum ρ value of the trajectory between Π_{11} and Π_{02}. Thus, since T_τ is finite, so is T. In fact, $\rho_{\max} \to 0$ in the limit $\rho_{11} \to 0, z_{11} \to 0$; thus, in the limit as the trajectory approaches the heteroclinic cycle, the time of flight from Π_{11} to Π_{02} is *zero* in the original time variable.

(iii) $P_{02}^L : \Pi_{02} \to \Pi_{12}$

We now reset time so that at $\tau = 0$ the trajectory passes through Π_{02} with coordinates $(x_2, \rho, z_2) = (x_{02}, \rho_{02}, 0)$ chosen such that the heteroclinic cycle forms when $\rho_{02} = 0$ and x_{02} takes an appropriate value. From equations (D.2), $\rho(\tau) = \rho_{02} e^{s_1^{\mathrm{A}} \tau}$. The time τ for the trajectory to go from Π_{02} to Π_{12} (determined by the time required for ρ to go from ρ_{02} to ϵ) is $\tau = \frac{1}{s_1^{\mathrm{A}}} \log \frac{\epsilon}{\rho_{02}}$ which diverges as $\rho_{02} \to 0$. If, however, we work in the original time t, then $\frac{d\rho}{dt} = s_1^{\mathrm{A}}$ with solution $\rho(t) = s_1^{\mathrm{A}} t + \rho_{02}$. The time t to go from Π_{02} to Π_{12} is thus $t = \frac{1}{s_1^{\mathrm{A}}}(\epsilon - \rho_{02})$. In the limit $\rho_{02} \to 0$ (i.e., as the heteroclinic cycle is approached) $t \to \frac{\epsilon}{s_1^{\mathrm{A}}}$, a *finite* time in the original time variable.

(iv) $P_{12}^L : \Pi_{12} \to \Pi_{01}$

Using the time τ, it takes a finite time T_τ to go from Π_{12} to Π_{01}. As for case (ii), using the time t this takes a time $T \leq \rho_{\max} T_\tau$ where $\rho_{\max}$ is the maximum ρ value of the trajectory between Π_{12} and Π_{01}. Since T_τ is finite, so is T.

Since each part of the heteroclinic cycle is traced out in finite or zero time the whole cycle is traced out in finite time. A similar argument holds for heteroclinic cycles involving an infinite amplitude limit cycle.

Appendix E

Perturbation of a Hopf Bifurcation by Resonant Temporal Forcing

Suppose that a system undergoing a Hopf bifurcation with Hopf frequency ω_0 is resonantly forced with frequency $\omega_e \approx 2\omega_0$. At leading order, the dynamics are governed by the equation

$$\dot{z} = (\lambda + i\omega)z + f\bar{z} + (a + ib)|z|^2 z, \tag{E.1}$$

where λ represents the distance from the Hopf bifurcation in the absence of forcing, f is related to the strength of the forcing and may without loss of generality be taken to be real and positive, and $\omega = \omega_0 - \frac{\omega_e}{2}$ is the detuning (see §4.1). This equation is equivariant under the action $z \to -z$, and thus has Z_2 symmetry. The most detailed studies of equation (E.1) are given in [105, 106]; here we discuss these results in detail and relate them to the analysis of a codimension three bifurcation considered in [219]. Finally, we point out that the dynamics of equation (E.1) with an additional fifth order term can be related to

the codimension four bifurcation considered in [220].

E.1 Local Bifurcations

We first consider fixed point solutions and the associated local bifurcations. The trivial fixed point solution $z = 0$ exists for all parameter values, and its eigenvalues are readily shown to be $\lambda \pm \sqrt{f^2 - \omega^2}$. The following cases hold for the stability of the trivial fixed point:

- $\lambda > 0, \lambda^2 + \omega^2 > f^2$: source,
- $\lambda < 0, \lambda^2 + \omega^2 > f^2$: sink,
- $\lambda^2 + \omega^2 < f^2$: saddle.

If the trivial state is a source or a sink, its eigenvalues are real (complex) if $f^2 > \omega^2$ ($f^2 < \omega^2$). The trivial state undergoes a steady bifurcation at

$$\lambda^2 + \omega^2 = f^2; \tag{E.2}$$

this is a pitchfork bifurcation because of the Z_2 symmetry. It also undergoes a Hopf bifurcation at $\lambda = 0$ provided $\omega^2 > f^2$.

Nontrivial fixed points $z_0 \equiv r_0 e^{i\phi_0}$ (with $r_0 \neq 0$) satisfy

$$(a^2 + b^2) r_0^4 + 2(\lambda a + \omega b) r_0^2 + \lambda^2 + \omega^2 - f^2 = 0, \tag{E.3}$$

$$\tan 2\phi_0 = -\frac{\omega + b r_0^2}{\lambda + a r_0^2}.$$

For each $r_0 > 0$ satisfying equation (E.3) there will be two fixed points related by the Z_2 symmetry. The number of such nontrivial fixed point solutions in different regions of parameter space is as follows:

- $\lambda a + \omega b > 0, \lambda^2 + \omega^2 > f^2$: no solutions
- $\lambda^2 + \omega^2 < f^2$: one pair of symmetry-related solutions
- $\lambda a + \omega b < 0, \lambda^2 + \omega^2 > f^2$, $(\lambda a + \omega b)^2 - (a^2 + b^2)(\lambda^2 + \omega^2 - f^2) < 0$: no solutions
- $\lambda a + \omega b < 0, \lambda^2 + \omega^2 > f^2$, $(\lambda a + \omega b)^2 - (a^2 + b^2)(\lambda^2 + \omega^2 - f^2) > 0$: two pairs of symmetry-related solutions

We now consider the stability of the nontrival fixed point solutions. Letting $z = z_0 + u$, we obtain

$$\dot{u} = [\lambda + i\omega + 2(a + ib)|z_0|^2]u + [f + (a + ib)z_0^2]\bar{u} + \text{h.o.t.}$$

These solutions satisfy

$$0 = \dot{z_0} = (\lambda + i\omega)z_0 + f\bar{z}_0 + (a + ib)|z_0|^2 z_0,$$

so that

$$f + (a + ib)z_0^2 = -\frac{(\lambda + i\omega)z_0}{\bar{z}_0}.$$

Thus

$$\begin{pmatrix} \dot{u} \\ \dot{\bar{u}} \end{pmatrix} = \begin{pmatrix} \lambda + i\omega + 2(a + ib)|z_0|^2 & -\frac{(\lambda+i\omega)z_0}{\bar{z}_0} \\ -\frac{(\lambda-i\omega)\bar{z}_0}{z_0} & \lambda - i\omega + 2(a - ib)|z_0|^2 \end{pmatrix} \begin{pmatrix} u \\ \bar{u} \end{pmatrix} + \text{h.o.t.}$$

The stability matrix for the nontrivial fixed point solutions has determinant

$$\text{Det} \equiv |\lambda + i\omega + 2(a + ib)|z_0|^2|^2 - |\lambda + i\omega|^2,$$

and trace

$$\mathrm{Tr} \equiv 2(\lambda + 2a|z_0|^2),$$

where $|z_0|^2 = r_0^2$ satisfies equation (E.3). The eigenvalues are given by

$$\lambda_\pm = \frac{1}{2}\left[\mathrm{Tr} \pm \sqrt{(\mathrm{Tr})^2 - 4\mathrm{Det}}\right].$$

The nontrivial fixed points have real (complex) eigenvalues for $\mathrm{Tr}^2 - 4\mathrm{Det} > 0$ (< 0).

There will be a steady bifurcation involving the nontrivial fixed point solutions when Det vanishes. One such possibility occurs for $|z_0|^2 = 0$ which requires $f^2 = \lambda^2 + \omega^2$ from equation (E.3). This corresponds to the pitchfork bifurcation from the trivial state discussed above. This bifurcation is forward (backward) with increasing λ if $\lambda_0/[a\lambda_0 + b\omega] < 0$ (> 0), where $\lambda_0 \equiv \pm\sqrt{f^2 - \omega^2}$ is the value of the bifurcation parameter at which the bifurcation from the trivial state occurs. This is seen by considering $\lambda = \lambda_0 + \delta$ and determining whether the small quantity δ must be positive or negative for a small solution r_0^2 to equation (E.3) to be positive, and thus, for a nontrivial fixed point solution to exist. Specifically, dropping the very small r_0^4 term in equation (E.3), solving for r_0^2, and expanding the solution to $O(\delta)$, we find that

$$r_0^2 \approx \frac{-\lambda_0\delta}{[a\lambda_0 + b\omega]}, \tag{E.4}$$

from which the stated result follows. There is also a steady bifurcation for the nontrivial fixed points for

$$|z_0|^2 = -\frac{\lambda a + \omega b}{a^2 + b^2},$$

$$f^2 = \frac{(\lambda b - \omega a)^2}{a^2 + b^2}.$$

This is equivalent to

$$(\lambda a + \omega b)^2 - (a^2 + b^2)(\lambda^2 + \omega^2 - f^2) = 0, \tag{E.5}$$

and corresponds to a saddle-node bifurcation provided $\lambda a + \omega b < 0$ and $\lambda^2 + \omega^2 > f^2$. Finally, a Hopf bifurcation for the nontrivial fixed points occurs when Tr vanishes provided that Det> 0. This implies that such a bifurcation occurs at

$$|z_0|^2 = -\frac{\lambda}{2a},$$

$$f^2 = \frac{(\lambda b - 2\omega a)^2 + (\lambda a)^2}{4a^2},$$

provided Det > 0.

E.2 Numerical Results

In order to motivate the codimension two bifurcations which occur for equation (E.1), Figure E.1 shows bifurcation sets for $f = 2.9, a = -5.9, b = 5.0$. The bifurcation sets give values of the parameters λ and ω at which particular bifurcations occur, and divide parameter space into regions which have distinct dynamics (see Figure E.2). Note that the behavior for these parameters is typical of other parameter values. The dots in Figure E.1 labeled by letters show the locations of codimension two bifurcations; these will be discussed in more detail in §E.3. Table E.1 gives approximate numerical values at which the codimension two bifurcations occur for these parameters.

The bifurcation sets corresponding to local bifurcations may be found analytically from the results in §E.1. In particular, the bifurcation set for the pitchfork bifurcation of the origin is the circle centered at $(\lambda, \omega) = (0, 0)$ with a radius of $f = 2.9$. The bifurcation

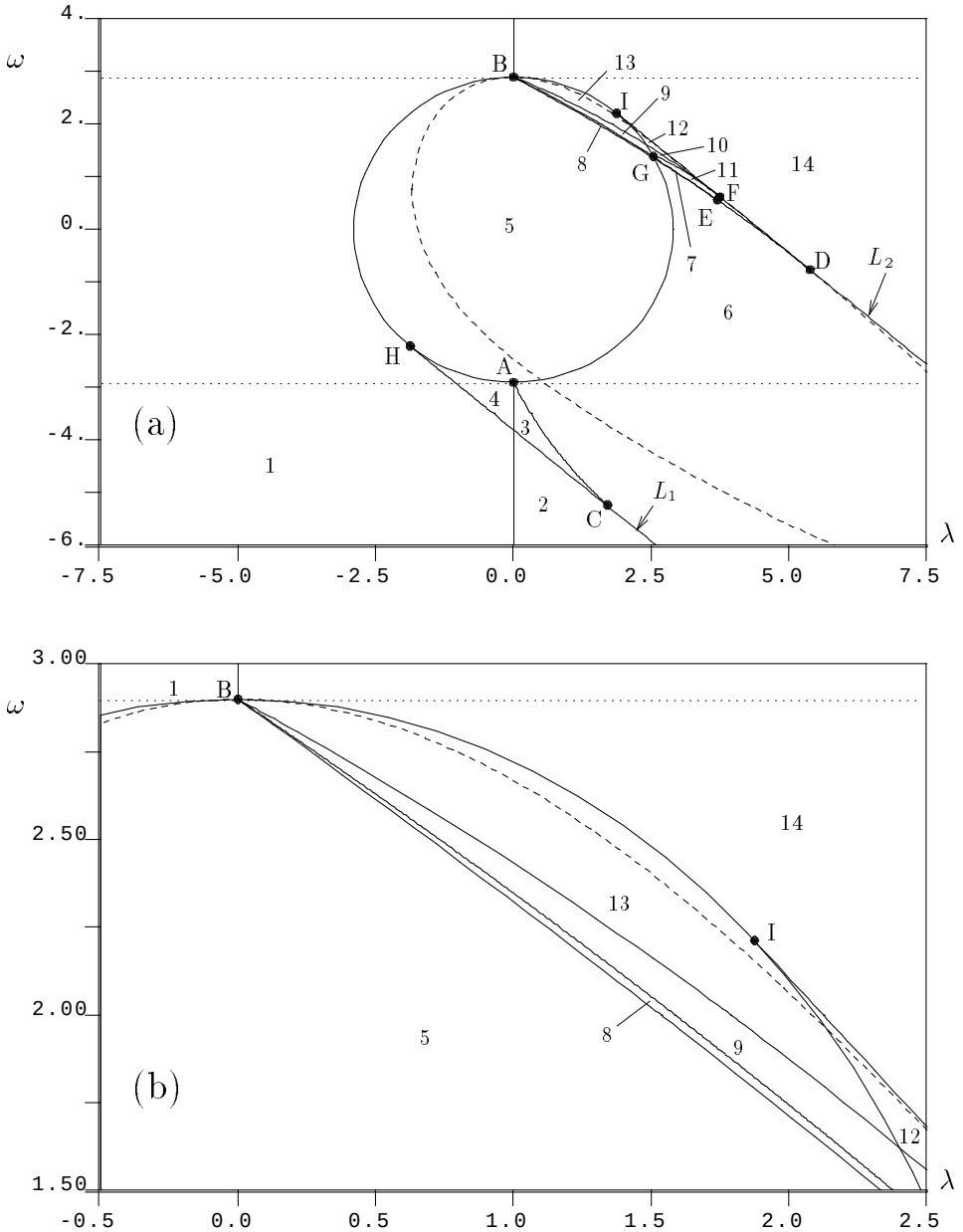

Figure E.1: Solid lines show bifurcation sets for $f = 2.9, a = -5.9, b = 5.0$. (b) and (c) are enlargements of (a). The numbers refer to regions of parameter space with distinct dynamics; sketches of the phase space for each region are shown in Figure E.2. The dots show the locations of codimension two bifurcations. The dotted (dashed) lines divide regions into subregions where the eigenvalues of the trivial state (nontrivial fixed points) are real or are complex; these lines correspond to $f^2 = \omega^2$ ($\mathrm{Tr}^2 = 4\mathrm{Det}$).

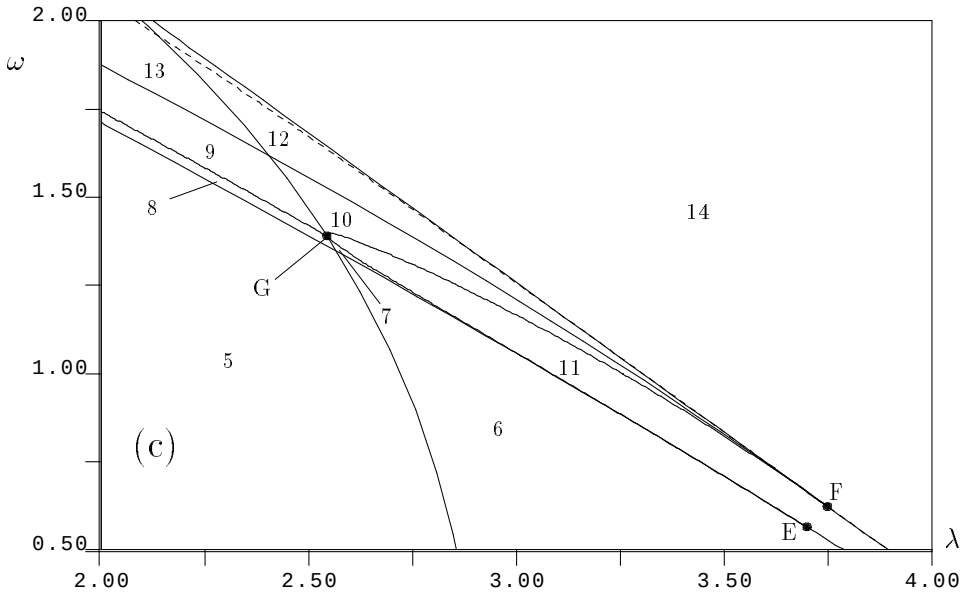

Figure E.1: *Continued.*

sets for the Hopf bifurcation of the origin are the vertical lines emerging from points A and B. The bifurcation sets for the saddle-node bifurcation of the nontrivial fixed points are the straight lines emerging from points H and I. Finally, the bifurcation set for the Hopf bifurcation of the nontrivial fixed points is the line from point B to point F. The other bifurcation sets were calculated numerically using AUTO [90] and are described in §E.3.

E.3 Codimension Two Bifurcations

The codimension two bifurcations for equation (E.1) serve as organizing centers for the dynamics. We now discuss these bifurcations and their associated bifurcation sets.

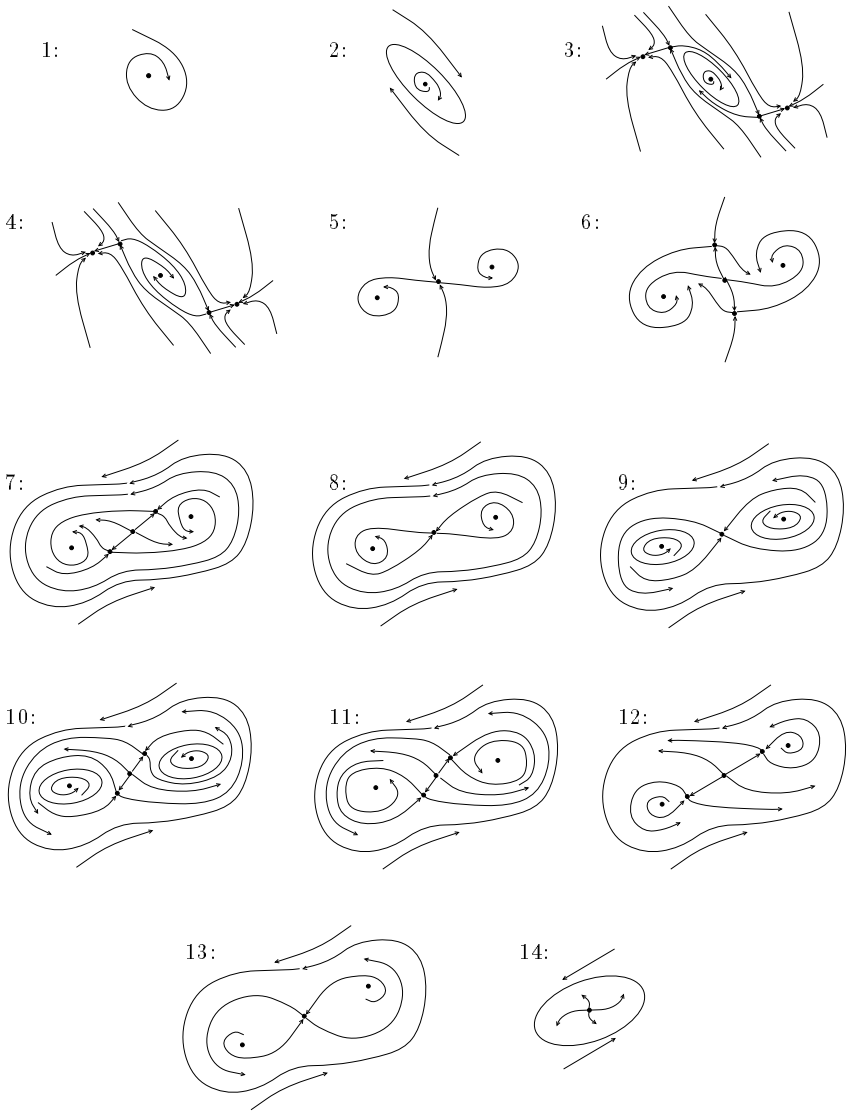

Figure E.2: Sketches of representative phase portraits for each region shown in Figure E.1. Some regions may be divided into subregions where the eigenvalues of some fixed points are real or are complex (see the dotted and dashed lines in Figure E.1). For simplicity, we only show one such possibility for each region corresponding to the placement of the number in Figure E.1(a).

Codimension two bifurcation point	(λ, ω)
A	(0,-2.90)
B	(0,2.90)
C	(1.71,-5.23)
D	(5.38,-0.76)
E	(3.70,0.57)
F	(3.75,0.62)
G	(2.54,1.39)
H	(-1.87,-2.21)
I	(1.87,2.21)

Table E.1: Approximate numerical values at which codimension two bifurcations occur in Figure E.1.

E.3.1 Double Zero Bifurcations

First consider point F. Here the Hopf and saddle-node bifurcations of a nontrivial fixed point coincide, giving double zero eigenvalues. Because the nontrivial fixed points lack the Z_2 symmetry, it is appropriate to unfold this bifurcation without any symmetry restrictions. Following §7.3 of [40] a universal unfolding of this after rescaling is given by

$$\begin{aligned} \dot{x} &= y, \\ \dot{y} &= \mu_1 + \mu_2 y + x^2 + \alpha x y, \end{aligned}$$

where $\alpha = \pm 1$. It is only necessary to consider the case $\alpha = 1$ because if $\alpha = -1$ the action $(y, \mu_2, t) \to (-y, -\mu_2, -t)$ changes the sign of α (note that this transformation reverses time so that, for example, the stability of a periodic orbit will change). The dynamics near point F in terms of the unfolding parameters μ_1 and μ_2 are summarized in Figure 7.3.3 of [40]. We conclude that the bifurcation set given by the line from F to G gives the condition for the existence of two symmetry-related homoclinic bifurcations (see Figure E.3(a)). The

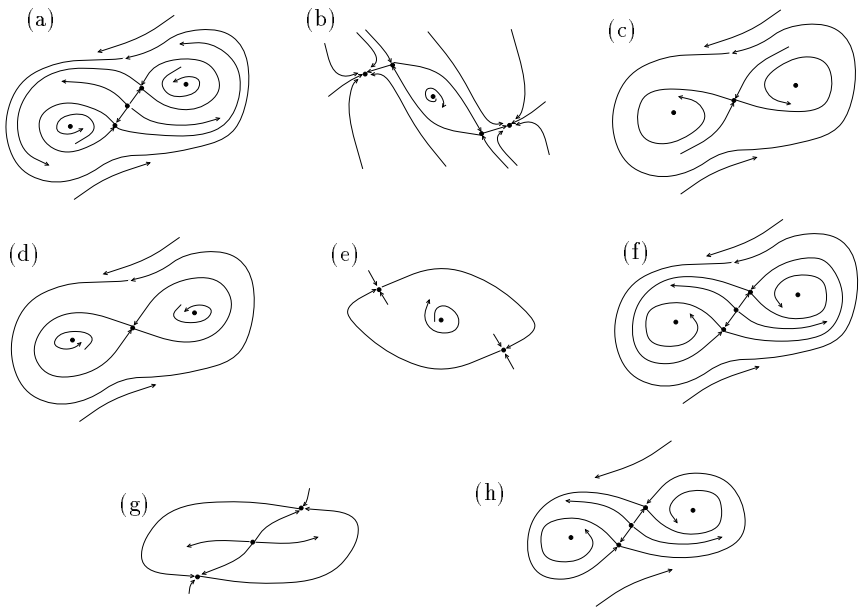

Figure E.3: Sketches of representative phase portraits on the bifurcation sets which do not correspond to local bifurcations. The bifurcation sets are given by the lines (a) from F to G, (b) from A to C, (c) from B to E; here the periodic orbit is undergoing a saddle-node bifurcation, (d) from B to G, (e) L_1; here the nontrivial fixed points are undergoing saddle-node bifurcations, (f) from D to E, (g) L_2; here the nontrivial fixed points are undergoing saddle-node bifurcations, and (h) from G to E. Some of these bifurcation sets may be divided into subsets where the eigenvalues of some fixed points are real or are complex; for simplicity we only show one such possibility for each bifurcation set.

other bifurcation sets emerging from F correspond to local bifurcations and were described above.

Now consider points A and B. At these points the Hopf and pitchfork bifurcations of the trivial fixed point coincide, giving double zero eigenvalues. However, these differ from the double zero bifurcation at point F because the dynamics about the trivial state are equivariant with respect to the Z_2 symmetry. Thus, it is appropriate to unfold these bifurcations while preserving this symmetry. Following §7.3 of [40] we consider the unfolding

after rescaling given by

$$\dot{x} = y, \tag{E.6}$$

$$\dot{y} = \mu_1 x + \mu_2 y + a_3 x^3 - x^2 y, \tag{E.7}$$

where $a_3 = \pm 1$. The cases $a_3 = 1$ and $a_3 = -1$ are distinct, and to determine which case applies it is necessary to put the equations into normal form. We undertake this normal form calculation for point A for which $(\lambda, \omega) = (0, -f)$. Letting

$$\begin{pmatrix} z_r \\ z_i \end{pmatrix} = \begin{pmatrix} f & 1 \\ -f & 0 \end{pmatrix} \begin{pmatrix} \tilde{x} \\ \tilde{y} \end{pmatrix}, \tag{E.8}$$

where $z = z_r + i z_i$, we find that the vector field at A is

$$\dot{\tilde{x}} = \tilde{y} + 2f^2(a-b)\tilde{x}^3 + 2f(a-2b)\tilde{x}^2\tilde{y} + (a-3b)\tilde{x}\tilde{y}^2 - \frac{b}{f}\tilde{y}^3, \tag{E.9}$$

$$\dot{\tilde{y}} = 4f^3 b\tilde{x}^3 + 2f^2(a+3b)\tilde{x}^2\tilde{y} + 2f(a+2b)\tilde{x}\tilde{y}^2 + (a+b)\tilde{y}^3. \tag{E.10}$$

Now make the near-identity coordinate transformation

$$x' = \tilde{x} + d_1\tilde{x}^3 + e_1\tilde{x}^2\tilde{y} + f_1\tilde{x}\tilde{y}^2 + g_1\tilde{y}^3 + \mathcal{O}(5),$$

$$y' = \tilde{y} + d_2\tilde{x}^3 + e_2\tilde{x}^2\tilde{y} + f_2\tilde{x}\tilde{y}^2 + g_2\tilde{y}^3 + \mathcal{O}(5),$$

and choose, for example,

$$d_1 = \frac{1}{3}(2fb - 3fa), \qquad e_1 = -a + b, \qquad f_1 = 0, \qquad g_1 = 0, \tag{E.11}$$

$$d_2 = 2f^2(a-b), \qquad e_2 = -f(2b+a), \qquad f_2 = -a - b, \qquad g_2 = -\frac{b}{f}. \tag{E.12}$$

This gives the normal form for the vector field at the point A (cf. [221])

$$\dot{x'} = y' + \mathcal{O}(5),$$

$$\dot{y'} = 4f^3 b(x')^3 + 8f^2 a(x')^2 y' + \mathcal{O}(5).$$

These equations can be rescaled with the transformation

$$t' = -\frac{2a}{bf}\, t, \qquad x' = \frac{1}{4a}\sqrt{\frac{b}{f}}\, x, \qquad y' = -\frac{b^{3/2} f^{1/2}}{8a^2}\, y,$$

to give the cubic truncation

$$\begin{aligned} \dot{x} &= y, \\ \dot{y} &= x^3 - x^2 y. \end{aligned}$$

This corresponds to the choice $a_3 = 1$ in equation (E.7). (Here we have assumed that $b > 0$. This is true without loss of generality by letting $z \to \bar{z}$ in equation (E.1) if necessary). The dynamics near point A are summarized in Figures 7.3.4 and 7.3.5 of [40]. We conclude that the bifurcation set given by the line from A to C gives the condition for a heteroclinic bifurcation involving two nontrivial fixed points (see Figure E.3(b)). A similar calculation shows that point B corresponds to the choice $a_3 = -1$ in equation (E.7); the dynamics near point B are summarized in Figures 7.3.7 and 7.3.9 of [40]. We conclude that the bifurcation set given by the line from B to E gives the condition for a saddle-node bifurcation of periodic orbits (see Figure E.3(c)), while the line from B to G gives the condition for a gluing bifurcation (see Figure E.3(d)). The other bifurcation sets emerging from points A and B correspond to local bifurcations and were described above.

E.3.2 Other Codimension Two Bifurcations

At the points H and I the saddle-node bifurcation of the nontrivial fixed points coincides with the pitchfork bifurcation of the trivial fixed point. At these points equations (E.2) and (E.5) hold simultaneously, implying that $\lambda a + \omega b = 0$. From equation (E.4) this

corresponds to a degenerate pitchfork bifurcation: it would be necessary to keep higher order terms to determine if the bifurcation is forward or backward at these points in parameter space.

Point C is a heteroclinic analog of the homoclinic saddle-node bifurcation considered in [222] (also see Appendix C of [106]). Here the nontrivial fixed points have a zero eigenvalue and (without loss of generality) a negative eigenvalue, and the *center* manifold of a nontrivial fixed point coincides with the stable manifold of the symmetry-related nontrivial fixed point. From above, the bifurcation set from C to H gives the condition for a saddle-node bifurcation of the nontrivial fixed points; also, the bifurcation set from C to A gives the condition for a heteroclinic bifurcation (see Figure E.3(b)). The other bifurcation set emerging from C (labeled L_1 in Figure E.1) gives the condition for a *simultaneous* saddle-node bifurcation of and heteroclinic connection between the nontrivial fixed points (see Figure E.3(e)). The behavior near point D is similar to that near point C. From above, the bifurcation set from D to I gives the condition for a saddle-node bifurcation of the nontrivial fixed points. The bifurcation set from D to E gives the condition for the heteroclinic connection shown in Figure E.3(f). Finally, the bifurcation set labeled L_2 in Figure E.1(a) gives the condition for a *simultaneous* saddle-node bifurcation of and heteroclinic connection between the nontrivial fixed points (see Figure E.3(g)).

Now consider point G. From above, the bifurcation set from G to B gives the condition for a gluing bifurcation (see Figure E.3(d)), and the bifurcation set from G to F gives the condition for the existence of two symmetry-related homoclinic bifurcations (see Figure E.3(a)). At G, the gluing bifurcation is occurring while the trivial fixed point is also

undergoing a pitchfork bifurcation. We find that the bifurcation set given by the line from G to E gives the condition for a heteroclinic orbit as shown in Figure E.3(h) (see Appendix C of [106]).

The final codimension two point is point E. Here the heteroclinic connection shown in Figure E.3(f) is undergoing a saddle-node bifurcation. The bifurcation sets emerging from E have been previously mentioned (see Figure E.3(c,g,h)).

E.4 Relation to a Codimension Three Bifurcation

Now we extend the normal form calculation for the vector field at point A to fifth order. Equations (E.9,E.10) are unchanged, and the near-identity transformation is now taken to be

$$\begin{aligned} x' = \tilde{x} \quad &+ \quad d_1\tilde{x}^3 + e_1\tilde{x}^2\tilde{y} + f_1\tilde{x}\tilde{y}^2 + g_1\tilde{y}^3 + h_1\tilde{x}^5 + j_1\tilde{x}^4\tilde{y} \\ &+ \quad k_1\tilde{x}^3\tilde{y}^2 + l_1\tilde{x}^2\tilde{y}^3 + m_1\tilde{x}\tilde{y}^4 + n_1\tilde{y}^5 + \mathcal{O}(7), \qquad \text{(E.13)} \\ y' = \tilde{y} \quad &+ \quad d_2\tilde{x}^3 + e_2\tilde{x}^2\tilde{y} + f_2\tilde{x}\tilde{y}^2 + g_2\tilde{y}^3 + h_2\tilde{x}^5 + j_2\tilde{x}^4\tilde{y} \\ &+ \quad k_2\tilde{x}^3\tilde{y}^2 + l_2\tilde{x}^2\tilde{y}^3 + m_2\tilde{x}\tilde{y}^4 + n_2\tilde{y}^5 + \mathcal{O}(7). \qquad \text{(E.14)} \end{aligned}$$

Taking $d_1, e_1, f_1, g_1, d_2, e_2, f_2$, and g_2 from equations (E.11,E.12), and

$$\begin{aligned} h_1 &= \frac{f^2}{10}(10b^2 - 12ab + 15a^2), \\ j_1 &= f(3b^2 - 4ab + 3a^2), \\ k_1 &= \frac{1}{6}(21b^2 - 16ab + 9a^2), \\ l_1 &= \frac{2b^2}{f}, \\ m_1 &= 0, \end{aligned}$$

$$
\begin{aligned}
n_1 &= 0, \\
h_2 &= 6f^3(b-a)a, \\
j_2 &= -\frac{f^2}{2}(2b^2 - 28ab + 9a^2), \\
k_2 &= f(2b^2 + 5ab + 3a^2), \\
l_2 &= \frac{1}{2}(7b^2 + 6ab + 3a^2), \\
m_2 &= \frac{2b(a+b)}{f}, \\
n_2 &= 0,
\end{aligned}
$$

we obtain the normal form equations

$$\dot{x}' = \quad y' + \mathcal{O}(7), \tag{E.15}$$

$$\dot{y}' = \quad 4f^3b(x')^3 + 8f^2a(x')^2y' - 4f^4(a^2+b^2)(x')^5 - \frac{32}{3}f^3ab(x')^4y' + \mathcal{O}(7). \tag{E.16}$$

For $b = 0$ the $(x')^3$ and $(x')^4y'$ terms in equation (E.16) vanish, and equations (E.15,E.16) are equivalent to equation (11) of [219]. The dynamics near the codimension three point $(\lambda, \omega, b) = (0, -f, 0)$ may then be obtained from the unfolding given in equation (11a) of [219]. In fact, the analysis of this codimension three bifurcation captures *all* possible dynamics for equation (E.1), even for the "large" value $b = 5.0$ used in the example in §E.2 (compare Figure E.1 with Figures 1 and 2 of [219]). However, the relation between the unfolding parameters α, β, γ in [219] and the coefficients λ, ω, b is apparently not linear, so the *details* of the bifurcation sets look different.

Choosing $a = b = 0$ makes both cubic terms and both fifth order terms in equation (E.16) vanish. This degeneracy of the fifth order terms is removed by adding a fifth order

term to equation (E.1):

$$\dot{z} = (\lambda + i\omega)z + f\bar{z} + (a + ib)|z|^2 z + (c + id)|z|^4 z. \tag{E.17}$$

The normal form at the codimension four point $(\lambda, \omega, a, b) = (0, -f, 0, 0)$ for equation (E.17) is then expected to be (cf. [221])

$$\dot{x}' = y', \qquad \dot{y}' = C(x')^5 + D(x')^4 y',$$

where C and D are nonzero coefficients. The dynamics near this codimension four point are obtained from the unfolding given in equation (4) of [220]. This implies that there will be many regions in which the dynamics of equation (E.17) will be distinct from the possible dynamics found for equation (E.1). Also, a new type of heteroclinic connection (the "triple loop") may exist. A more detailed analysis of equation (E.17) has not yet been attempted.

Index

Arnol'd tongues, 43, 156

asymptotically stable, 22

attractor, 21

attractor, strange, 29

autonomous, 20

bifurcation, 20

bifurcation, double zero, 39, 44, 146, 223

bifurcation, global, 44

bifurcation, gluing, 47, 148

bifurcation, Hopf, 37

bifurcation, Hopf with D_4 symmetry, 55

bifurcation, Hopf with O(2) symmetry, 52

bifurcation, local, 35

bifurcation, Naimark-Sacker, 41

bifurcation, period-doubling, 40

bifurcation, pitchfork, 36, 40

bifurcation, planar homoclinic, 44

bifurcation, saddle-node, 36, 40

bifurcation, Shil'nikov, 47

bifurcation, supergluing, 148, 165

bifurcation, transcritical, 36, 40

blinking state, 95, 98, 105

Boussinesq approximation, 6

burst mechanism, 83

burst mechanism, robustness to higher order terms, 127

bursts, Kolmogorov flow, 175

bursts, large aspect-ratio binary fluid convection, 65, 138

bursts, neural systems, 184

bursts, shear flows, 171

bursts, Taylor-Couette system, 178

bursts, turbulent boundary layer, 169

center manifold theorem, 29

chaos, 12, 15, 25, 39, 41, 45, 48, 106, 127, 129, 154, 157, 160

convection, binary fluid, 61

convection, Rayleigh-Bénard, 5

crisis, 158, 160, 182

dynamic range, 65, 66

dynamical system, 19

equivariance, 17

equivariant branching lemma, 51

equivariant Hopf bifurcation theorem, 51

fixed point, 22

fixed point subspace, 51

forced symmetry-breaking, 1, 58, 67, 140

heteroclinic connections to infinity, 173

heteroclinic cycle, 85, 170

heteroclinic network, 90

heteroclinic orbit, 44

homoclinic explosion, 47, 102

homoclinic orbit, 44

horseshoe map, 26

intermittency, 160, 163, 181

isotropy subgroup, 50

Liapunov exponent, 28

Liapunov stable, 22

logistic map, 41

Lorenz equations, 10, 31

Navier-Stokes equations, 3

normal forms, 33, 140

parameter symmetry, 74, 198

period-doubling cascade, 41, 105, 108

periodic orbit, 23

Poincaré map, 23

quasiperiodic orbit, 25

Shil'nikov-like behavior, 90

Soret effect, 62

spontaneous symmetry-breaking, 51

structural stability, 20

subcritical, 39

supercritical, 38

topological equivalence, 20

topologically transitive, 21

universal unfolding, 58

winking state, 96, 98

Bibliography

[1] G. Dangelmayr and E. Knobloch. On the Hopf bifurcation with broken O(2) symmetry, in *The Physics of Structure Formation*, ed. W. Güttinger and G. Dangelmayr. Springer-Verlag, New York, pp. 387–393, 1987.

[2] G. Dangelmayr and E. Knobloch. Hopf bifurcation with broken circular symmetry. *Nonlinearity*, 4:399–427, 1991.

[3] R. Lauterbach and M. Roberts. Heteroclinic cycles in dynamical systems with broken spherical symmetry. *J. Diff Eq.*, 100:22–48, 1992.

[4] E. Knobloch. System symmetry breaking and Shil'nikov dynamics, in *Pattern Formation: Symmetry Methods and Applications*, ed. J. Chadam, M. Golubitsky, W. Langford and B. Wetton. American Mathematical Society, Providence, pp. 271–279, 1996.

[5] P. Hirschberg and E. Knobloch. Complex dynamics in the Hopf bifurcation with broken translation symmetry. *Physica D*, 92:56–78, 1996.

[6] A. S. Landsberg and E. Knobloch. Oscillatory bifurcation with broken translation symmetry. *Phys. Rev. E*, 53:3579–3600, 1996.

[7] G. K. Batchelor. *An Introduction to Fluid Dynamics.* Cambridge University Press, Cambridge, 1967.

[8] R. L. Panton. *Incompressible Flow, 2nd Edition.* John Wiley & Sons, New York, 1996.

[9] S. Chandrasekhar. *Hydrodynamic and Hydromagnetic Stability.* Dover, New York, 1961.

[10] P. G. Drazin and W. H. Reid. *Hydrodynamic Stability.* Cambridge University Press, Cambridge, 1981.

[11] E. L. Koschmieder. *Bénard Cells and Taylor Vortices.* Cambridge University Press, Cambridge, 1993.

[12] A. V. Getling. *Rayleigh-Bénard Convection: Structures and Dynamics.* World Scientific, Singapore, 1998.

[13] E. Bodenschatz, W. Pesch, and G. Ahlers. Recent Developments in Rayleigh-Bénard Convection. *Annu. Rev. Fluid Mech.*, 32:709-778, 2000.

[14] H. Bénard. Les tourbillons celleulaires dans une nappe liquide. *Rev. Gén. Sciences Pure Appl.*, 11:1261–1271 and 11:1309-1328, 1900.

[15] Lord Rayleigh. On convection currents in a horizontal layer of fluid when the higher temperature is on the under side. *Phil. Mag.*, 32:529–546, 1916.

[16] J. Boussinesq. *Théorie Analytique de la Chaleur*, Vol. 2. Gauthier-Villars, Paris, 1903, p. 172; also, see A. Oberbeck. Über die Wärmeleitung der Flüssigkeiten bei

Berücksichtigung der Strömungen infloge von Temperaturdifferenzen. *Ann. Phys. Chem.*, 7:272–292, 1879.

[17] E. A. Spiegel and G. Veronis. On the Boussinesq approximation for a compressible fluid. *Astrophys. J.*, 131:442–447, 1960.

[18] G. Veronis. The magnitude of the dissipation terms in the Boussinesq approximation. *Astrophys. J.*, 135:655–656, 1962.

[19] J. M. Mihaljan. A rigorous exposition of the Boussinesq approximations applicable to a thin fluid layer. *Astrophys. J.*, 136:1126–1133, 1962.

[20] P. Manneville. *Dissipative Structures and Weak Turbulence.* Academic Press, San Diego, 1990.

[21] M. C. Cross and P. C. Hohenberg. Pattern formation out of equilibrium. *Rev. Mod. Phys.*, 65:851–1112, 1993.

[22] M. J. Block. Surface tension as the cause of Bénard cells and surface deformation in a liquid film. *Nature*, 178:650–651, 1956.

[23] J. R. A. Pearson. On convection cells induced by surface tension. *J. Fluid Mech.*, 4:489–500, 1958.

[24] E. N. Lorenz. Deterministic nonperiodic flow. *J. Atmos. Sci.*, 20:130–141, 1963.

[25] J. H. Curry, J. R. Herring, J. Loncaric, and S. A. Orszag. Order and disorder in two- and three-dimensional Bénard convection. *J. Fluid Mech.*, 147:1–38, 1984.

[26] E. Zienicke, N. Seehafer, and F. Feudel. Bifurcations in two-dimensional Rayleigh-Bénard convection. *Phys. Rev. E*, 57:428–435, 1998.

[27] E. J. Hinch. *Perturbation Methods*. Cambridge University Press, Cambridge, 1991.

[28] G. Ahlers. Low-temperature studies of the Rayleigh-Bénard instability and turbulence. *Phys. Rev. Lett.*, 33:1185–1188, 1974.

[29] A. Libchaber and J. Maurer. A Rayleigh-Bénard experiment: helium in a small box, in *Nonlinear Phenomena at Phase Transitions and Instabilities*, ed. T. Riste. Plenum, New York, pp.259–286, 1982. Reprinted in *Universality in Chaos*, ed. P. Cvitanović. Adam Hilger, Bristol, 1984.

[30] I. Goldhirsch, R. B. Pelz, and S. A. Orszag. Numerical simulation of thermal convection in a two-dimensional finite box. *J. Fluid Mech.*, 199:1–28, 1989.

[31] J. Prat, J. M. Massaguer, and I. Mercader. Large-scale flows and resonances in 2-D thermal convection. *Phys. Fluids*, 7:121–134, 1995.

[32] A. M. Rucklidge. Chaos in models of double convection. *J. Fluid Mech.*, 237:209–229, 1992.

[33] J. D. Crawford, M. Golubitsky, M. G. M. Gomes, E. Knobloch, and I. N. Stewart. Boundary conditions as symmetry constraints, in *Singularity Theory and its Applications, Warwick 1989, Part II*, ed. M. Roberts and I. Stewart. Springer-Verlag, New York, pp. 63–79, 1991.

[34] J. D. Crawford and E. Knobloch. Symmetry and symmetry-breaking bifurcations in fluid mechanics. *Ann. Rev. Fluid Mech.*, 23:601–639, 1991.

[35] M. Golubitsky, I. Stewart, and D. G. Shaeffer. *Singularities and Groups in Bifurcation Theory, Volume II.* Springer-Verlag, New York, 1988.

[36] J. S. Lomont. *Applications of Finite Groups.* Dover, New York, 1959.

[37] T. K. Callahan and E. Knobloch. Symmetry-breaking bifurcations on cubic lattices. *Nonlinearity*, 10:1179–1216, 1997.

[38] V. I. Arnol'd. *Ordinary Differential Equations, 3rd edition.* Springer-Verlag, New York, 1992.

[39] M. W. Hirsch and S. Smale. *Differential Equations, Dynamical Systems, and Linear Algebra.* Academic Press, New York, 1974.

[40] J. Guckenheimer and P. Holmes. *Nonlinear Oscillations, Dynamical Systems, and Bifurcations of Vector Fields.* Springer-Verlag, New York, 1983.

[41] S. Wiggins. *Introduction to Applied Nonlinear Dynamical Systems and Chaos.* Springer-Verlag, New York, 1990.

[42] J. D. Crawford. Introduction to bifurcation theory. *Rev. Mod. Phys.*, 63:991–1037, 1991.

[43] P. Glendinning. *Stability, Instability, and Chaos.* Cambridge University Press, Cambridge, 1994.

[44] Y. A. Kuznetsov. *Elements of Applied Bifurcation Theory, 2nd Edition*, Springer-Verlag, New York, 1998.

[45] S. Wiggins. *Chaotic Transport in Dynamical Systems.* Springer-Verlag, New York, 1992.

[46] R. L. Devaney. *An Introduction to Chaotic Dynamical Systems.* Benjamin/Cummings: Menlo Park, California, 1986.

[47] S. Smale. Differentiable dynamical systems. *Bull. Amer. Math. Soc.*, 73:747–817, 1967.

[48] E. Ott. *Chaos in Dynamical Systems.* Cambridge University Press, Cambridge, 1993.

[49] C. Grebogi, E. Ott, S. Pelikan, and J. A. Yorke. Strange attractors that are not chaotic. *Physica D*, 13:261–268, 1984.

[50] J. E. Marsden and M. McCracken. *The Hopf Bifurcation and Its Applications.* Vol. 19 of Springer Series in Appl. Math. Sci. Springer-Verlag, New York, 1976.

[51] G. Gaeta. Poincaré renormalized forms. *Ann. Inst. Henri Poincaré Physique Théorique*, 70:461–514, 1999.

[52] G. Cicogna and G. Gaeta. *Symmetry and perturbation theory in nonlinear dynamics.* Springer-Verlag, New York, 1999.

[53] C. Elphick, E. Tirapegui, M. E. Brachet, P. Coullet, and G. Iooss. A simple global characterization for normal forms of singular vector fields. *Physica D*, 29:95–127, 1987. Addendum. *Physica D* 32:488, 1988.

[54] F. Takens. Singularities of vector fields. *Publ. Math. IHES*, 43:47–100, 1974.

[55] R. I. Bogdanov. Versal deformations of a singular point on the plane in the case of zero eigenvalues. *Functional Anal. Appl.*, 9(2):144-145, 1975.

[56] S.-N. Chow, C. Li, and D. Wang. *Normal Forms and Bifurcation of Planar Vector Fields.* Cambridge University Press, Cambridge, 1994.

[57] A. Arnéodo, P. H. Coullet, and E. A. Spiegel. The dynamics of triple convection. *Geophys. Astrophys. Fluid Dyn.*, 31:1–48, 1985.

[58] E. Knobloch, A. S. Landsberg, and J. Moehlis. Chaotic direction-reversing waves. *Phys. Lett. A*, 255:287–293, 1999.

[59] M. J. Feigenbaum. Quantitative universality for a class of nonlinear transformations. *J. Stat. Phys.*, 19:25–52, 1978.

[60] P. Cvitanović, ed. *Universality in Chaos.* Adam Hilger, Bristol, 1984.

[61] D. G. Aronson, M. A. Chory, G. R. Hall, and R. P. McGehee. Bifurcations from an invariant circle for two-parameter families of maps of the plane: a computer-assisted study. *Commun. Math. Phys.*, 83:303–354, 1982; see also D. G. Aronson, M. A. Chory, G. R. Hall, and R. P. McGehee. A discrete dynamical system with subtly wild behavior, in *New Approaches to Nonlinear Problems in Dynamics*, ed. P. J. Holmes. Society for Industrial and Applied Mathematics, Philadelphia, pp. 339–359, 1980.

[62] V. I. Arnold. *Geometrical Methods in the Theory of Ordinary Differential Equations.* Springer-Verlag, New York, 1983.

[63] S. Wiggins. *Global Bifurcations and Chaos: Analytic Methods.* Springer-Verlag, New York, 1988.

[64] P. Glendinning. Global bifurcations in flows, in *New Directions in Dynamical Systems*, ed. T. Bedford and J. Swift. Cambridge University Press, Cambridge, pp. 120–149, 1988.

[65] C. Sparrow. *The Lorenz Equations: Bifurcations, Chaos, and Strange Attractors.* Springer-Verlag, New York, 1982.

[66] A. Arnéodo, P. Coullet, and C. Tresser. A possible new mechanism for the onset of turbulence. *Phys. Lett. A*, 81:197–201, 1981.

[67] C. Tresser. About some theorems by L. P. Silnikov. *Ann. Inst. H. Poincaré*, 40:440–461, 1984.

[68] P. Glendinning and C. Sparrow. Local and global behavior near homoclinic orbits. *J. Statist. Phys.*, 35:645–696, 1984.

[69] L. P. Shil'nikov. A case of the existence of a denumerable set of periodic motions. *Sov. Math. Dokl.*, 6:163–166, 1965.

[70] P. Hirschberg and E. Knobloch. Shil'nikov-Hopf bifurcation. *Physica D*, 62:202–216, 1993.

[71] J. W. Swift. Hopf bifurcation with the symmetry of the square. *Nonlinearity*, 1:333-377, 1988.

[72] M. Golubitsky and D. G. Shaeffer. *Singularities and Groups in Bifurcation Theory, Volume I.* Springer-Verlag, New York, 1985.

[73] S. P. Frankel. Elementary derivation of thermal diffusion. *Phys. Rev.*, 57:661, 1940.

[74] H. R. Brand, P. C. Hohenberg, and V. Steinberg. Codimension-two bifurcations for binary fluid mixtures. *Phys. Rev. A.*, 3-:2548–2561, 1984.

[75] T. Clune and E. Knobloch. Mean flow suppression by endwalls in oscillatory binary fluid convection. *Physica D*, 61:106–112, 1992.

[76] T. S. Sullivan and G. Ahlers. Nonperiodic time dependence at the onset of convection in a binary liquid mixture. *Phys. Rev. A*, 38:3143–3146, 1988.

[77] O. Batiste, I. Mercader, M. Net, and E. Knobloch. Onset of oscillatory binary fluid convection in finite containers. *Phys. Rev. E*, 59:6730–6741, 1999.

[78] P. Hirschberg and E. Knobloch. Mode interactions in large aspect ratio convection. *J. Nonlinear Sci.*, 7:537–556, 1997.

[79] M. C. Cross. Traveling and standing waves in binary-fluid convection in finite geometries. *Phys. Rev. Lett.*, 57:2943–2946, 1986.

[80] J. Moehlis and E. Knobloch. Forced symmetry breaking as a mechanism for bursting. *Phys. Rev. Lett.*, 80:5329–5332, 1998.

[81] E. Knobloch and J. Moehlis. Bursts, in *IUTAM Symposium on New Applications of Nonlinear and Chaotic dynamics in Mechanics*, ed. F. C. Moon. Kluwer, Dordrecht, pp. 51–60, 1999.

[82] J. Moehlis and E. Knobloch. Bursts in oscillatory systems with broken D_4 symmetry. *Physica D*, 135:263–304, 2000.

[83] S. A. van Gils and M. Silber. On the uniqueness of invariant tori in $D_4 \times S^1$ symmetric systems. *Nonlinearity*, 8:615–628, 1995.

[84] T. Clune and E. Knobloch. Pattern selection in three-dimensional magnetoconvection. *Physica D*, 74:151–176, 1994.

[85] I. Melbourne, P. Chossat and M. Golubitsky. Heteroclinic cycles involving periodic solutions in mode interactions with O(2) symmetry. *Proc. R. Soc. Edinburgh A*, 113:315–345, 1989.

[86] J. W. Swift and K. Wiesenfeld. Suppression of period doubling in symmetric systems. *Phys. Rev. Lett.*, 52:705–708, 1984.

[87] E. Knobloch and N. O. Weiss. Bifurcations in a model of double-diffusion convection. *Phys. Lett. A*, 85:127–130, 1981.

[88] E. Kaplan, E. Kuznetsov, and V. Steinberg. Burst and collapse in traveling-wave convection of a binary fluid. *Phys. Rev. E*, 50:3712–3722, 1994.

[89] A. Back, J. Guckenheimer, M. R. Myers, F. J. Wicklin, and P. A. Worfolk. *dstool*: Computer assisted exploration of dynamical systems. *Not. Amer. Math. Soc.*, 39:303–309, 1992.

[90] E. Doedel, A. Champneys, T. Fairgrieve, Y. Kuznetsov, B. Sandstede, and X. Wang.

AUTO 97: Continuation and bifurcation software for ordinary differential equations. Available via FTP from directory pub/doedel/auto at ftp.cs.concordia.ca, 1997.

[91] P. Kolodner, C. M. Surko, and H. Williams. Dynamics of traveling waves near the onset of convection in binary fluid mixtures. *Physica D*, 37:319–333, 1989.

[92] V. Steinberg, J. Fineberg, E. Moses, and I. Rehberg. Pattern selection and transition to turbulence in propagating waves. *Physica D*, 37:359–383, 1989.

[93] A. A. Predtechensky, W. D. McCormick, J. B. Swift, A. G. Rossberg, and H. L. Swinney. Traveling wave instability in sustained double-diffusive convection. *Phys. Fluids*, 6:3923–3935, 1994.

[94] P. Chossat and M. Golubitsky. Symmetry-increasing bifurcation of chaotic attractors. *Physica D*, 32:423–436, 1988.

[95] J. D. Rodriguez and M. Schell. Global bifurcations into chaos in systems with SO(2) symmetry. *Phys. Lett. A*, 146:25–31, 1990.

[96] C. D. Andereck, S. S. Liu, and H. L. Swinney. Flow regimes in a circular Couette system with independently rotating cylinders. *J. Fluid Mech.*, 164:155–183, 1986.

[97] R. D. Pierce and E. Knobloch. Spiral vortices in finite cylinders, in *Ordered and Turbulent Patterns in Taylor-Couette Flow*, ed. C. D. Andereck and F. Hayot. NATO ASI Series B 297, Plenum, New York, pp. 83–90, 1992.

[98] A. D. D. Craik and I. M. Moroz. Temporal evolution of interaction waves in non-conservative systems: some exact solutions. *Wave Motion*, 10:443–452, 1988.

[99] O. Batiste, I. Mercader, M. Net, and E. Knobloch. Repeated transients and blinking states in binary fluid convection in finite containers, in preparation.

[100] T. L. Clune. Pattern Selection in Convecting Systems. Ph.D. Dissertation, Univ. California at Berkeley, 1993.

[101] A. S. Landsberg and E. Knobloch. Oscillatory doubly diffusive convection in a finite container. *Phys. Rev. E*, 53:3601–3609, 1996.

[102] C. Elphick, G. Iooss, and E. Tirapegui. Normal form reduction for time-periodically driven differential equations. *Phys. Lett. A*, 120:459–463, 1987.

[103] A. K. Bajaj. Resonant parametric perturbations of the Hopf bifurcation. *J. Math. Anal. Appl.*, 115:214–224, 1986.

[104] N. S. Namachchivaya and S. T. Ariaratnam. Periodically perturbed Hopf bifurcation. *SIAM J. Appl. Math.*, 47:15–39, 1987.

[105] J. M. Gambaudo. Perturbation of a Hopf bifurcation by an external time-periodic forcing. *J. Differ. Equations*, 57:172–199, 1985.

[106] W. Vance and J. Ross. A detailed study of a forced chemical oscillator: Arnol'd tongues and bifurcation sets. *J. Chem. Phys.*, 91:7654–7670, 1989.

[107] H. Riecke, M. Silber, and L. Kramer. Temporal forcing of small-amplitude waves in anisotropic systems. *Phys. Rev. E*, 49:4100–4113, 1994.

[108] A. Steindl and H. Troger. One and two-parameter bifurcations to divergence and

flutter in the three-dimensional motions of a fluid conveying viscoelastic tube with D_4 symmetry. *Nonlinear Dynam.*, 8:161–178, 1995.

[109] A. K. Bajaj and C. N. Folley. Three-dimensional dynamics of a continuous cantilever tube conveying a pulsatile flow. *Z. Angew. Math. Mech.*, 76 (no. 2, suppl.):547–550, 1996.

[110] Z. C. Feng and P. R. Sethna. Symmetry-breaking bifurcations in resonant surface waves. *J. Fluid Mech.*, 199:494–518, 1989.

[111] F. Simonelli and J. P. Gollub. Surface wave mode interactions: effects of symmetry and degeneracy. *J. Fluid Mech.*, 199:471–494, 1989.

[112] M. Silber and E. Knobloch. Parametrically excited surface waves in square geometry. *Phys. Lett. A*, 137:349–354, 1989.

[113] M. Nagata. Nonlinear Faraday resonance in a box with a square base. *J. Fluid Mech.*, 209:265–284, 1989.

[114] M. Nagata. Chaotic behaviour of parametrically excited surface waves in square geometry. *Eur. J. Mech. B/Fluids*, 10(no.2, suppl.):61–66, 1991.

[115] A. M. Rucklidge. Global bifurcations in the Takens-Bogdanov normal form with D_4 symmetry near the O(2) limit. Preprint, 2000.

[116] K. Matthies. A subshift of finite type in the Bogdanov-Takens bifurcation with D_3 symmetry. *Doc. Math. J. DMV*, 4:463–485, 1999.

[117] J. P. Gollub and S. V. Benson. Many routes to turbulent convection. *J. Fluid Mech.*, 100:449–470, 1980.

[118] P. Bergé, Y. Pomeau, and C. Vidal. *Order Within Chaos: Towards a Deterministic Approach to Turbulence*. John Wiley & Sons, New York, 1984.

[119] R. E. Ecke and I. G. Kevrekidis. Interactions of resonances and global bifurcations in Rayleigh-Bénard convection. *Phys. Lett. A*, 131:344–352, 1988.

[120] I. G. Kevrekidis, R. Rico-Martinez, R. E. Ecke, R. M. Farber, A. S. Lapedes. Global bifurcations in Rayleigh-Bénard convection. Experiments, empirical maps and numerical bifurcation analysis. *Physica D*, 71:342–362, 1994.

[121] I. Schreiber and M. Marek. Transition to chaos via two-torus in coupled reaction-diffusion cells. *Phys. Lett. A*, 91:263–266, 1982.

[122] V. Franceschini and C. Tebaldi. Breaking and disappearance of tori. *Commun. Math. Phys.*, 94:317–329, 1984.

[123] J. Curry and J. Yorke. A transition from Hopf bifurcation to chaos: computer experiments on maps in $\mathbb{R}^2$. The structure of attractors in dynamical systems, in *Lecture Notes in Mathematics* Vol. 668. Springer-Verlag, New York, pp. 48–68, 1978.

[124] A. Ben-Mizrachi and I. Procaccia. Wrinkling of mode-locked tori in the transition to chaos. *Phys. Rev. A*, 31:3990–3992, 1985.

[125] Y. Pomeau and P. Manneville. Intermittent transition to turbulence in dissipative dynamical systems. *Commun. Math. Phys.*, 74:189–197, 1980.

[126] H. Riecke, J. D. Crawford, and E. Knobloch. Time-modulated oscillatory convection. *Phys. Rev. Lett.*, 61:1942–1945, 1988.

[127] D. Walgraef. External forcing of spatio-temporal patterns. *Europhys. Lett.*, 7:485–491, 1988.

[128] A. M. Rucklidge and P. C. Matthews. Analysis of the shearing instability in nonlinear convection and magnetoconvection. *Nonlinearity*, 9:311–351, 1996.

[129] E. Knobloch and J. Moehlis. Bursting Mechanisms for Hydrodynamical Systems, in *Pattern Formation in Continuous and Coupled Systems: A Survey Volume*, ed. M. Golubitsky, D. Luss, and S. H. Strogatz. Series: IMA Volumes in Mathematics and its Applications, vol. 115, Springer-Verlag, New York, pp. 157–174, 1999.

[130] E. Knobloch and J. Moehlis. Burst Mechanisms in Hydrodynamics, in Nonlinear Instability, Chaos, and Turbulence, Vol. II, ed. L. Debnath and D. Riahi. Computational Mechanics Publications, Southampton, pp. 237–287, 2000.

[131] S. K. Robinson. Coherent motions in the turbulent boundary layer. *Ann. Rev. Fluid Mech.*, 23:601–639, 1991.

[132] *Self-Sustaining Mechanisms of Wall Turbulence*, ed. R.L. Panton. Computational Mechanics Publications, Southampton, 1997.

[133] N. Aubry, P. Holmes, J. L. Lumley, and E. Stone. The dynamics of coherent structures in the wall region of a turbulent boundary layer. *J. Fluid Mech.*, 192:115–173, 1988.

[134] P. Holmes, J. L. Lumley, and G. Berkooz. *Turbulence, Coherent Structures, Dynamical Systems and Symmetry*. Cambridge University Press, Cambridge, 1996.

[135] P. J. Holmes, J. L. Lumley, G. Berkooz, J. C. Mattingly, and R. W. Wittenberg. Low-dimensional models of coherent structures in turbulence. *Phys. Rep.*, 287:337–384, 1997.

[136] F. H. Busse. Transition to turbulence via the statistical limit cycle route, in *Turbulence and Chaotic Phenomena in Fluids*, ed. T. Tatsumi. Elsevier, Amsterdam, pp. 197–202, 1984.

[137] D. Armbruster, J. Guckenheimer, and P. Holmes. Heteroclinic cycles and modulated traveling waves in systems with O(2) symmetry. *Physica D*, 29:257–282, 1988.

[138] M. R. E. Proctor and C. A. Jones. The interaction of two spatially resonant patterns in thermal convection. Part 1. Exact 2:1 resonance. *J. Fluid Mech.*, 188:301–335, 1988.

[139] A. Steindl and H. Troger. Heteroclinic cycles in the three-dimensional postbifurcation motion of O(2)-symmetric fluid conveying tubes. *Appl. Math. Comp.*, 78:269–277, 1996.

[140] M. Krupa. Robust heteroclinic cycles. *J. Nonlin. Sci.*, 7:129–176, 1997.

[141] P. Hirschberg and E. Knobloch. A robust heteroclinic cycle in an $O(2)\times Z_2$ steady-state mode interaction. *Nonlinearity*, 11:89–104, 1998.

[142] J. S. Baggett and L. N. Trefethen. Low-dimensional models of subcritical transition to turbulence, *Phys. Fluids*, 9:1043–1053, 1997.

[143] F. Daviaud, J. Hegseth, and P. Bergé. Subcritical transition to turbulence in plane Couette flow. *Phys. Rev. Lett.*, 69:2511–2514, 1992.

[144] S. Bottin, O. Dauchot, and F. Daviaud. Intermittency in a locally forced plane Couette flow. *Phys. Rev. Lett.*, 79:4377–4380, 1997.

[145] F. Waleffe. Hydrodynamic stability and turbulence: beyond transients to a self-sustaining process. *Stud. Appl. Math.*, 95:319–343, 1995.

[146] F. Waleffe. Transition in shear flows. Nonlinear normality versus non-normal linearity. *Phys. Fluids*, 7:3060–3066, 1995.

[147] F. Waleffe. On a self-sustaining process in shear flows. *Phys. Fluids*, 9:883–900, 1997.

[148] F. Waleffe. How streamwise rolls and streaks self-sustain in a shear flow, in *Self-Sustaining Mechanisms of Wall Turbulence*, ed. R. L. Panton. Computational Mechanics Publications, Southampton, pp. 309–332, 1997.

[149] O. Dauchot and P. Manneville. Local versus global concepts in hydrodynamic stability theory. *J. Phys. II*, 7:371–389, 1997.

[150] J. Guckenheimer, R. Harris-Warrick, J. Peck, and A. Willms. Bifurcation, bursting, and spike frequency adaptation. *J. Comp. Neuroscience*, 4:257–277, 1997.

[151] T. Gebhardt and S. Grossmann. Chaos transition despite linear stability. *Phys. Rev. E*, 50:3705–3711, 1994.

[152] J. S. Baggett, T. A. Driscoll, and L. N. Trefethen. A mostly linear model of transition to turbulence. *Phys. Fluids*, 7:833–838, 1995.

[153] A. C. Newell, D. A. Rand, and D. Russell. Turbulent dissipation rates and the random occurrence of coherent events. *Phys. Lett. A*, 132:112–123, 1988.

[154] A. C. Newell, D. A. Rand, and D. Russell. Turbulent transport and the random occurrence of coherent events. *Physica D*, 33:281–303, 1988.

[155] G. F. Carnevale, J. C. McWilliams, Y. Pomeau, J. B. Weiss, and W. R. Young. Evolution of vortex statistics in two-dimensional turbulence. *Phys. Rev. Lett.*, 66:2735–2737, 1991.

[156] J. B. Weiss and J. C. McWilliams. Temporal scaling behavior of decaying two-dimensional turbulence. *Phys. Fluids A*, 5:608–621, 1993.

[157] C. S. Bretherton and E. A. Spiegel. Intermittency through modulational instability. *Phys. Lett. A*, 96:152–156, 1983.

[158] A. S. Makarenko, M. N. Moskalkov, and S. P. Levkov. On blow-up solutions in turbulence, *Phys. Lett. A*, 235:391–397, 1997.

[159] Z. S. She. Large-scale dynamics and transition to turbulence in the two-dimensional Kolmogorov flow, in *Current Trends in Turbulence Research*, ed. H. Branover, M. Mond, and Y. Unger. AIAA, Washington, pp. 374–396, 1988.

[160] B. Nicolaenko and Z. S. She. Symmetry-breaking homoclinic chaos in Kolmogorov flows, in *Nonlinear World, Int. Workshop on Nonlinear and Turbulent Processes in Physics, Kiev 1989*, ed. V. G. Bar'yakhtar, V. M. Chernousenko, N. S. Erokhin, A. G. Sitenko, and V. E. Zakharov. World Scientific, Singapore, pp. 602–618, 1990.

[161] B. Nicolaenko and Z. S. She. Coherent structures, homoclinic cycles and vorticity explosions in Navier-Stokes flows, in *Topological Fluid Mechanics*, ed. H.K. Moffatt. Cambridge University Press, Cambridge, pp. 265–277, 1990.

[162] B. Nicolaenko and Z. S. She. Symmetry-breaking homoclinic chaos and vorticity bursts in periodic Navier-Stokes flows. *Eur. J. Mech. B/Fluids*, 10(no.2, suppl.):67–74, 1991.

[163] B. Nicolaenko and Z. S. She. Turbulent bursts, inertial sets and symmetry-breaking homoclinic cycles in periodic Navier-Stokes flows, in *Turbulence in Fluid Flows: a Dynamical Systems Approach*, ed. G. R. Sell, C. Foias, and R. Temam. Springer-Verlag, New York, pp. 123–136, 1993.

[164] D. Armbruster, R. Heiland, E. J. Kostelich, and B. Nicolaenko. Phase-space analysis of bursting behavior in Kolmogorov flow. *Physica D*, 58:392–401, 1992.

[165] D. Armbruster, B. Nicolaenko, N. Smaoui, and P. Chossat. Analyzing bifurcations in the Kolmogorov flow equations, in *Dynamics, Bifurcation and Symmetry*, ed. P. Chossat. Kluwer, Dordrecht, pp. 11–34, 1994.

[166] D. Armbruster, B. Nicolaenko, N. Smaoui, and P. Chossat. Symmetries and dynamics for 2-D Navier-Stokes flow. *Physica D*, 95:81–93, 1996.

[167] L. D. Meshalkin and Ia.G. Sinai. Investigation of the stability of a stationary solution of a system of equations for the plane movement of an incompressible viscous fluid. *J. Appl. Math. Mech.*, 25:1700–1705, 1961.

[168] J. S. A. Green. Two-dimensional turbulence near the viscous limit. *J. Fluid Mech.*, 62:273–287, 1974.

[169] C. Marchioro. An example of absence of turbulence for any Reynolds number. *Commun. Math. Phys.*, 105:99–106, 1986.

[170] N. Platt, L. Sirovich, and N. Fitzmaurice. An investigation of chaotic Kolmogorov flows. *Phys. Fluids A*, 3:681–696, 1991.

[171] H. A. Posch and W. G. Hoover. Simulation of two-dimensional Kolmogorov flow with smooth particle applied mechanics. *Physica A*, 240:286–296, 1997.

[172] E. Knobloch. Symmetry and instability in rotating hydrodynamic and magnetohydrodynamic flows. *Phys. Fluids*, 8:1446–1454, 1996.

[173] S. Xin, P. Le Quéré, and L. S. Tuckerman. Bifurcation analysis of double-diffusive convection with opposing thermal and solutal gradients. *Phys. Fluids*, 10:850–858, 1998.

[174] A. M. Rucklidge, N. O. Weiss, D. P. Brownjohn, P. C. Matthews, and M. R. E. Proctor. Compressible magnetoconvection in three dimensions: pattern formation in a strongly stratified layer, preprint, 1999.

[175] R. Tagg. The Couette-Taylor problem. *Nonlinear Science Today.* 4:1–25, 1994.

[176] C. F. Hamill. Turbulent Bursting in the Couette-Taylor System, MA Thesis, Univ. Texas at Austin, 1995.

[177] K. Coughlin and P. S. Marcus. Turbulent bursts in Couette-Taylor flow. *Phys. Rev. Lett.*, 77:2214–2217, 1996.

[178] K. Coughlin, C. F. Hamill, P. S. Marcus, and H. L. Swinney. Turbulent bursts in Couette-Taylor flow, preprint, 1999.

[179] M. Renardy. A note on bifurcation problems in large containers. *Fluid Dyn. Research*, 24:189–199, 1999.

[180] P. Bergé, M. Dubois, P. Manneville, and Y. Pomeau. Intermittency in Rayleigh-Bénard convection. *J. Phys. (Paris)*, 41:L341–345, 1980.

[181] M. Dubois, M. A. Rubio, and P. Bergé. Experimental evidence of intermittencies associated with a subharmonic bifurcation. *Phys. Rev. Lett.*, 51:1446–1449, 1983.

[182] E. Ringuet, C. Rozé, and G. Gouesbet. Experimental observation of type-II intermittency in a hydrodynamical system. *Phys. Rev. E*, 47:1405–1407, 1993.

[183] T. J. Price and T. Mullin. An experimental observation of a new type of intermittency. *Physica D*, 48:29–52, 1991.

[184] M. Bauer, S. Habip, D. R. He, and W. Martienssen. New type of intermittency in discontinuous maps. *Phys. Rev. Lett.*, 68:1625–1628, 1992.

[185] D. R. He, M. Bauer, S. Habip, U. Krueger, W. Martienssen, and B. H. Wang. Type V intermittency. *Phys. Lett. A*, 171:61–65, 1992.

[186] C. Grebogi, E. Ott, and J. A. Yorke. Chaotic attractors in crisis. *Phys. Rev. Lett.*, 48:1507–1510, 1982.

[187] C. Grebogi, E. Ott, and J. A. Yorke. Crises, sudden changes in chaotic attractors, and transient chaos. *Physica D*, 7:181–200, 1983.

[188] C. Grebogi, E. Ott, F. Romeiras, and J. A. Yorke. Critical exponents for crisis-induced intermittency. *Phys. Rev. A*, 36:5365–5380, 1987.

[189] E. Ott and J. C. Sommerer. Blowout bifurcations: the occurrence of riddled basins and on-off intermittency. *Phys. Lett. A*, 188:39–47, 1994.

[190] N. Platt, E. A. Spiegel, and C. Tresser. On-Off intermittency: a mechanism for bursting. *Phys. Rev. Lett.*, 70:279–282, 1993.

[191] P. Ashwin, E. Covas, and R. Tavakol. Transverse instability for non-normal parameters. *Nonlinearity*, 12:563–577, 1999.

[192] S. C. Venkataramani, T. M. Antonsen Jr., E. Ott, and J. C. Sommerer. Characterization of on-off intermittent time series. *Phys. Lett. A*, 207:173–179, 1995.

[193] P. Ashwin and A. M. Rucklidge. Cycling chaos: its creation, persistence and loss of stability in a model on nonlinear magnetoconvection. *Physica D*, 122:134–154, 1998.

[194] E. Covas, R. Tavakol, P. Ashwin, A. Tworkowski, and J. M. Brooke. In-out intermittency in PDE and ODE models of axisymmetric mean-field dynamos, preprint, 1998.

[195] P. Ashwin, J. Buescu, and I. Stewart. Bubbling of attractors and synchronisation of chaotic oscillators. *Phys. Lett. A*, 193:126–139, 1994.

[196] S. C. Venkataramani, B. R. Hunt, E. Ott, D. J. Gauthier, and J. C. Bienfang. Transitions to bubbling of chaotic systems. *Phys. Rev. Lett.*, 77:5361–5364, 1996.

[197] S. C. Venkataramani, B. R. Hunt, and E. Ott. Bubbling transition. *Phys. Rev. E*, 54:1346–1360, 1996.

[198] J. Rinzel. A formal classification of bursting mechanisms in excitable systems, in *Proceedings of the International Congress of Mathematicians*, ed. A.M. Gleason. American Mathematical Society, Providence, pp. 1578–1594, 1987.

[199] J. Rinzel. A formal classification of bursting mechanisms in excitable systems, in *Mathematical Topics in Population Biology, Morphogenesis and Neurosciences*, ed. E. Teramoto and M. Yamaguti. Lecture Notes in Biomathematics Vol. 71, Springer-Verlag, Berlin, pp. 267–281, 1987.

[200] R. Bertram, M. J. Butte, T. Kiemel, and A. Sherman. Topological and phenomenological classification of bursting oscillations. *Bull. Math. Biology*, 57:413–439, 1995.

[201] X. J. Wang and J. Rinzel. Oscillatory and bursting properties of neurons, in *The Handbook of Brain Theory and Neural Networks*, ed. M. Arbib. MIT Press, Cambridge, pp. 686–691, 1995.

[202] E. Knobloch and D. R. Moore. Minimal model of binary fluid convection. *Phys. Rev. A*, 42:4693–4709, 1990.

[203] E. Knobloch and D. R. Moore. Chaotic travelling wave convection. *Eur. J. Mech. B/Fluids*, 10(2,suppl.):37–42, 1991.

[204] D. Armbruster, D. Codimension 2 bifurcation in binary convection with square symmetry, in *Nonlinear Evolution of Spatio-Temporal Structures in Dissipative Continu-*

ous Systems, ed. F. H. Busse and L. Kramer. Plenum Press, New York, pp. 385–398, 1990.

[205] D. Armbruster. Square and almost square symmetry in binary convection. *Eur. J. Mech. B/Fluids*, 10(no.2, suppl.):7–12, 1991.

[206] P. Ashwin and Z. Mei. Normal form for Hopf bifurcation of partial differential equations on the square. *Nonlinearity*, 8:715–734, 1995.

[207] M. Silber, H. Riecke and L. Kramer. Symmetry-breaking Hopf bifurcation in anisotropic systems. *Physica D*, 61:260–278, 1992.

[208] T. Peacock, private communication.

[209] Q. Feng, J. V. Moloney and A. C. Newell. Transverse patterns in lasers. *Phys. Rev. A*, 50:R3601–3604, 1994.

[210] M. Golubitsky and I. N. Stewart. Hopf bifurcation with dihedral group symmetry, in *Multiparameter Bifurcation Theory, Contemporary Maths Vol. 56*, ed. M. Golubitsky and J. Guckenheimer. American Mathematical Society, pp. 131–173, 1986.

[211] P. Ashwin and P. Stork. Permissible symmetries of coupled cell networks. *Math. Proc. Camb. Phil. Soc.*, 116:27–36, 1994.

[212] E. Knobloch and A. S. Landsberg. A new model of the solar cycle. *Mon. Not. R. Astr. Soc.*, 278:294–302, 1996.

[213] E. Knobloch, S. M. Tobias and N. O. Weiss. Modulation and symmetry changes in stellar dynamos. *Mon. Not. R. Astr. Soc.*, 297:1123–1138, 1998.

[214] E. Stone and P. Holmes. Noise induced intermittency in a model of a turbulent boundary layer. *Physica D*, 37:20–32, 1989.

[215] E. Stone and P. Holmes. Random perturbations of heteroclinic attractors. *SIAM J. Appl. Math.*, 50:726–743, 1990.

[216] P. Ashwin, G. Dangelmayr, I. Stewart, and M. Wegelin. Oscillator networks with the symmetry of the unit quaternion group, in *Dynamics, Bifurcation and Symmetry*, ed. P. Chossat. Kluwer, Dordrecht, pp. 35–48, 1994.

[217] J. Guckenheimer and P. Holmes. Structurally stable heteroclinic cycles. *Math. Proc. Camb. Phil. Soc.*, 103:189–192, 1988.

[218] J. H. P. Dawes. The transition between steady and oscillatory motion in three-dimensional rotating convection, preprint, 2000.

[219] G. Dangelmayr, D. Armbruster, and M. Neveling. A codimension three bifurcation for the laser with saturable adsorber. *Z. Phys. B*, 59:365–370, 1985.

[220] G. Dangelmayr, M. Neveling, and D. Armbruster. Structurally stable phase portraits for the five-dimensional Lorenz equations. *Z. Phys. B*, 64:491–501, 1986.

[221] E. Knobloch. Normal forms for bifurcations at a double zero eigenvalue. *Phys. Lett. A*, 115:199–201, 1986.

[222] S. Schecter. The saddle-node separatrix-loop bifurcation. *SIAM J. Math. Anal.*, 18:1142–1156, 1987.